THESIS

GREAT PLAINS DROUGHT IN SIMULATIONS OF THE TWENTIETH CENTURY

Submitted by

Rachel Rose McCrary

Department of Atmospheric Science

In partial fulfillment of the requirements

For the Degree of Masters of Science

Colorado State University

Fort Collins, Colorado

Fall 2008

COLORADO STATE UNIVERSITY

September 9, 2008

WE HEREBY RECOMMEND THAT THE THESIS PREPARED UNDER OUR SUPERVISION BY RACHEL ROSE MCCRARY ENTITLED GREAT PLAINS DROUGHT IN SIMULATIONS OF THE TWENTIETH CENTURY BE ACCEPTED AS FULFILLING IN PART REQUIREMENTS FOR THE DEGREE OF MASTER OF SCIENCE.

Committee on Graduate Work

_____

Jorge A. Ramirez

_____

A. Scott Denning

_____

Advisor: David A. Randall

_____

Department Head: Richard H. Johnson

ABSTRACT OF THESIS

GREAT PLAINS DROUGHT IN SIMULATIONS

OF THE TWENTIETH CENTURY

The Great Plains region of the United States experienced a number of multi-year droughts during the twentieth century. Most notable were the "Dust Bowl" drought of the 1930s and the Great Plains drought of the 1950s. This study evaluates the ability of the Coupled Global Climate Models (CGCMs) that participated in the Intergovernmental Panel on Climate Change's (IPCC's) Fourth Assessment Report (AR4) to simulate Great Plains drought with the same frequency and intensity as was observed during the twentieth century. In particular, simulations from three IPCC models are analyzed in this study: the Geophysical Fluid Dynamics Laboratory (GFDL) Coupled Model version 2.0 (CM2.0), the NCAR Community Climate System Model version 3 (CCSM3), and the Hadley Centre Coupled Atmosphere-Ocean General Circulation Model version 3 (HadCM3).

The results show that the models have some difficulty capturing the climatology of the hydrologic cycle of the Great Plains. The magnitude of the seasonal variations in the hydrologic cycle are too extreme in CM 2.0 and HadCM3, where both models overestimate the amplitude of the annual cycles of precipitation, evapotranspiration and runoff. CCSM3 does not accurately capture the timing of the climatology of the

hydrologic cycle of the Great Plains, as precipitation, evapotranspiration and runoff all experience unrealistic decreases between the months of July and August.

Results indicate that all three models do simulate at least one long-term drought period for the Great Plains region during their representations of 20th Century Climate. Also, multi-year droughts produced by the models exhibit similar magnitudes and spatial scales as was observed during the twentieth century.

This study also investigates the relative roles of external forcing from the tropical Pacific and local feedbacks between the land surface and the atmosphere in the initiation and perpetuation of Great Plains drought in each model. Cool, La Nina-like conditions in the tropical Pacific are found to be associated with long-term drought conditions over the Great Plains in CM 2.0 and HadCM3. There appears to be no systematic relationship between tropical Pacific SST variability and Great Plains drought in CCSM3.

In CCSM3, local contributions to precipitation via evapotranspiration dominate the variability of precipitation over the Great Plains. Land-atmosphere feedbacks may cause precipitation anomalies to lock into place in this model, thereby perpetuating drought conditions. On the other hand, in HadCM3, the land surface and the atmosphere are relatively decoupled such that large-scale forcing mechanisms are what lead to persistent drought conditions in this model.

Rachel Rose McCrary
Atmospheric Science Department
Colorado State University
Fort Collins, CO 80523
Fall 2008

ACKNOWLEDGEMENTS

I would like to thank my advisor, Dr. David Randall, for his support and enthusiasm. Without his constant faith in my abilities and his never ending patience, this thesis would not have been possible. I would also like to thank my committee members, Dr. Scott Denning and Dr. Jorge Ramirez for taking the time to read and review this thesis.

Special thanks owed to the entire Randall research group, but in particular Jim Benedict and Brian Medeiros, for their invaluable scientific discussions. Thank you to Ross Heikes for reminding me to go home every once and a while. Thank you to Melissa Burt and Kate Thayer-Calder, my office mates, for the endless hours you have spent listening to me ramble over the past few years. And thank you to Anna Harper, Nick Parazoo and Michelle Harrold for helping to keep me sane throughout this process and providing me with hours of necessary distraction and laughter.

To my parents, my sister, and my best friend Erika, your willingness to believe in me, when I haven't been able to believe in myself, has made me the person I am today and I am forever grateful. Your love and support has allowed me to succeed beyond my wildest dreams and without you I would not be here today. Thank you.

I wish to thank Kostas Andreadis at the University of Washington for providing me with the historical hydrologic model data set used in this thesis. I would also like to

acknowledge the modeling groups, the Program for Climate Model Diagnosis and Intercomparison (PCMDI) and the World Climate Research Programme's (WCRP's) Working Group on Coupled Modelling (WGCM) for their roles in making available the WCRP Coupled Model Intercomparison Project phase 3 (CMIP3) multi-model dataset. Support of this dataset is provided by the Office of Science, U.S. Department of Energy.

This research was supported by the National Science Foundation Science and Technology Center for Multi-Scale Modeling of Atmospheric Processes, managed by Colorado State University under cooperative agreement No. ATM-0425247.

TABLE OF CONTENTS

Chapter 1: Introduction 1

Chapter 2: Causes of Long-Term Drought over the Great Plains 9

2.1 Forcing by the Tropical Pacific.....9

2.2 Land-Atmosphere Interactions.....14

Chapter 3: Data and Methodology.....19

3.1 Models 19

3.2 Data Sets used for Model Evaluation 23

3.2.1 CRU TS 2.1..... 24

3.2.2 VIC 26

3.2.3 NCEP/NCAR Reanalysis..... 28

3.2.4 HadISST 29

3.3 Methodology 30

3.3.1 Long-term Drought, a Definition 31

3.3.2 Regression and Correlation Analysis 32

3.3.3 Skewness 34

3.3.4 Power Spectrum Analysis 35

Chapter 4: Climatology 37

4.1 The Observed Seasonal Cycle Over the Great Plains 37

4.2 The Modeled Seasonal Cycle Over the Great Plains 49

4.2.1 850 hPa Winds 49

4.2.2 Precipitation 51

4.2.3 Evapotranspiration 55

4.2.4 P-E 58

4.2.5 Soil Moisture 60

4.2.6 Runoff 63
4.3 Summary 64
Chapter 5: Great Plains Precipitation Variability 67
5.1 Variability of Precipitation 69
5.1.1 Variability of Monthly Mean Precipitation Anomalies 69
5.1.2 Variability of Annual, Wet Season, and Dry Season Precipitation ..74
5.2 Extreme Precipitation Events 76
5.2.1 The Distribution of Annual Precipitation Anomalies 79
5.2.2 The Distribution of Mean Wet Season Precipitation Anomalies 84
5.2.3 The Distribution of Mean Dry Season Precipitation Anomalies 85
5.3 Persistence of anomalies 87
5.4 Summary 100
Chapter 6: Long-Term Drought 102
6.1 Identifying Long-Term Great Plains Drought 103
6.2 Seasonality of Long-Term Precipitation Variations 113
6.3 Atmospheric Conditions Associated with Dry and Wet Conditions
over the Great Plains 116
6.3.1 Observations 117
6.3.1 Models 120
6.4 Variability in Tropical Pacific SSTs and Great Plains Drought 134
6.4.1 El Niño Southern Oscillation (ENSO) and U.S. Precipitation 135
6.4.2. SST Anomalies and Long-Term Great Plains Drought 139
6.4.2a CM 2.0 and HadCM3 141
6.4.2b CCSM3 142
6.5 Land-Atmosphere Interactions 156
6.5.1 Precipitation and Evapotranspiration 157
6.5.2 Soil Moisture and Evapotranspiration 160
6.5.3 Precipitation and Soil Moisture 162
6.5.4 Discussion of Land-Atmosphere Interactions 165

6.7 Summary 167
Chapter 7: Conclusions 171
Appendix A : ENSO Variability in the Models.....177
References.....186

Chapter 1

Introduction

Drought is one of the most devastating natural disasters that impacts North America. Reduced precipitation rates act to diminish surface- and ground-water supplies and can have harmful impacts on water quality, crop productivity, hydroelectric power generation, riparian ecosystems, and recreational activity (IPCC, 2008). Until Hurricane Katrina in 2005, droughts were the most economically costly and environmentally damaging climate related disasters that influenced the United States (Cook et al., 2007). Because of the social, economic, and environmental problems associated with long-term droughts, water planners, who manage the allocation of water between agriculture, municipalities and natural ecosystems, are often concerned about the future state of water. This concern is particularly strong in the western part of the United States (west of 95ºW) where water is always in high demand, the climate is arid and drought is a naturally reoccurring phenomena (National Assessment Synthesis Team, 2001).

During the twentieth century, drought was particularly devastating to the Great Plains region of the western United States (105-95ºW, 30-50ºN). During this time period, the Great Plains region was influenced by two severe, long-lasting droughts that occurred during the 1930s and the 1950s. The first of these droughts extended from

approximately 1929-1940 and is historically known as the "Dust Bowl" drought, so named after the severe dust storms that hit the Central Plains during this time period (Mattice, 1935a, 1935b). The Dust Bowl drought has been immortalized by authors such as John Steinbeck and Timothy Egan, who remind us of the political, social, and economic devastation that is often associated with long-term drought. The second of these droughts extended from 1947-1956 and is still to this day considered one of the worst droughts on record in southern Texas (Hughes, 1976). Following these long-term droughts, the Great Plains also experienced two short, but intense dry periods: one during the late 1980s and a second in the late 1990s/early 2000s (Trenberth and Branstator, 1992; Seager, 2007b).

The history of Great Plains drought for the the past hundreds to ten thousands of years has been studied using paleoclimate data proxies such as historical documents, tree rings, lake sediments, archeological remains, and geomorphic data (Stockton and Meko, 1975; Lawson and Stockton, 1981; Fritts, 1991; Bradley and Jones, 1992; Woodhouse and Overpeck, 1998; Cook et al., 1999; Jones et al., 1999; Stahel et al., 2000; Fye et al., 2003, Cook et al., 2004; Herweijer et al., 2006). These studies place the Great Plains droughts of the twentieth century into a broader historical context, and indicate that the Dust Bowl drought of the 1930s and the 1950s drought may have in fact been mild compared to what has happened in the past. Woodhouse and Overpeck (1998) show evidence for two multidecadal "megadroughts" that impacted the Central United States within the past 2000 years. The first of these occurred in the late 13th century and persisted for almost 40 years (Figure 1.1). The second drought occurred during the 16th

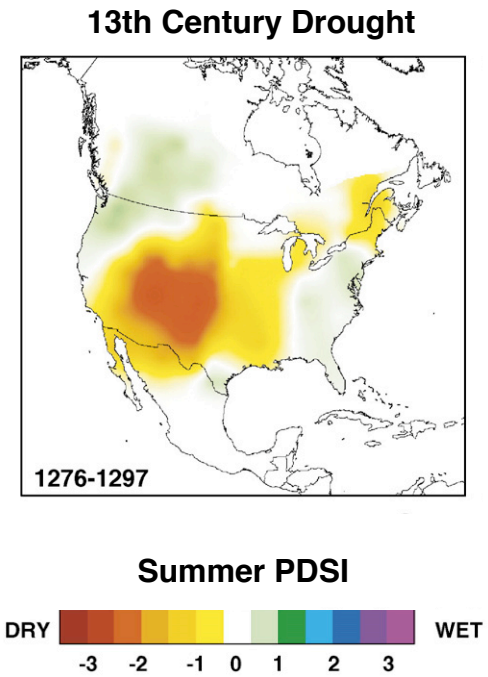


Figure 1.1. *From Cook et al. (2007). Palmer Drought Severity Index (PDSI) values from the reconstruction of the 13th Century "megadrought". The PDSI is a non-dimensional index that ranges from -4 to 4 where negative values represent dry conditions and positive values represent wet conditions*

century, and persisted for 20 years. The megadrought of the 13 century coincided with the abandonment of Anasazi settlements in the Southwest and is believed to have been a major contributing factor in the demise of this ancient civilization (Benson et al., 2007).

More recent paleoclimate records suggest that two long-term droughts also occurred during the 19th century. One that occurred during the United Sates Civil war era (Figure 1.2), and a second that occurred from 1890-1896 (Herweijer et al., 2006; Cook et al., 2007).

Considerable research has been focused on understanding the causes of long-term drought over the Great Plains. Examples include the studies by Namias (1955, 1960, 1983), Borchert (1950, 1971), Oglesby (1991), Ting and Wang (1997), Ropelewski and Halpert (1986), Trenberth and Branstator (1992), and Livezey and Smith (1999). These

studies, and many others, highlight potentially important features that coincide with dry conditions over the Great Plains and include, but are not limited to: variations in Sea Surface Temperature (SST) patterns in the North Pacific, North Atlantic, and Tropical Pacific, changes in the storm tracks, changes in the position and strength of the Bermuda High and feedbacks between the land surface and the atmosphere above.

While these studies discuss many important factors that may contribute to dryness over the Great Plains, recent modeling and observational studies indicate that two primary mechanisms cause Great Plains precipitation anomalies to persist for long periods of time (Schubert et al., 2004; Seager et al., 2003; Seager et al., 2005a; Seager et al., 2005b; Herweijer et al., 2006; Cook et al., 2007; Seager et al., 2007b; Herweijer and Seager, 2008). These two mechanisms are: 1) an external forcing from low-frequency variability in Tropical Pacific SSTs, and 2) local coupling between the land surface and

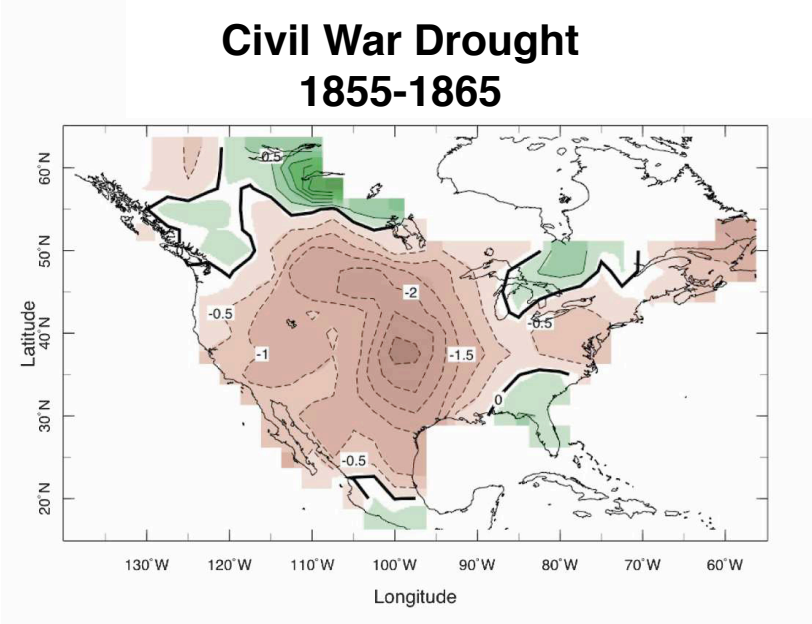


Figure 1.2. *From Herweijer et al. (2007). Palmer Drought Severity Index values from the Civil War drought.*

the atmosphere involving feedbacks between soil moisture concentrations and precipitation. These two mechanisms are described in detail in Chapter 2.

The Great Plains region of the United States has a semi-arid climate, and, as described above, has been plagued by drought throughout history. The impact of drought on this region will be exacerbated in the future as the demand for water increases due to enhanced agricultural production and growing populations (National Assessment Synthesis Team, 2001). A recent study by Seager et al. (2007a, henceforth S07) also shows that western part of the United States is expected to become increasingly more arid in the future due to rising greenhouse gas concentrations in the atmosphere. This study also provides some evidence that this transition to a more arid climate is already well on its way.

The climate models that participated in the Fourth Assessment Report (AR4) of the Intergovernmental Panel on Climate Change (IPCC) (IPCC, 2008), S07 show that changes in the Hadley Circulation associated with increasing greenhouse gas concentrations in the atmosphere will result in the poleward expansion of the subtropical dry zones, thereby increasing the rate of subsidence over the American West and reducing precipitation rates. Reductions in mean precipitation over the western part of the United States are expected to be comparable to those seen during the 1930s and 1950s droughts, indicating a potential regime shift in precipitation over the Great Plains to more arid conditions. The mechanisms that will cause the mean state of precipitation over the Great Plains to decrease in the future are different from those which are thought to have caused the long-term droughts of the 1930s and 1950s (see Chapter 2 for more information on

the causes of long-term drought) and S07 speculates that any long-term droughts to hit the western U.S. in the future will be acting on a base state that is much dryer than that of the twentieth century. They argue that it is possible that the western United States will face droughts comparable to those of the 13th and 16th centuries in the future.

Unfortunately, one issue that was not discussed by S07 was the ability of the AR4 IPCC climate models to accurately capture the variability of precipitation over the Great Plains, as observed during the twentieth century. Studies by Ruiz-Barradas and Nigam (2006 a, b) have shown that some of the IPCC model have difficulty capturing the climatology of summertime precipitation over the Great Plains region, and that precipitation variability in this region differs widely among the models. But, as of yet, no studies have assessed whether or not the IPCC models are capable of capturing twentieth-century Great Plains drought with the same frequency, duration and intensity as observed.

The goal of this thesis is to evaluate the ability of three of the Coupled Global Climate Models (CGCMs) used in the Fourth Assessment Report of the IPCC to reproduce the variability of precipitation over the Great Plains of the United States that was observed during the Twentieth Century. This will require examining the climatology as well as the variability (i.e. deviations from the climatology) of the hydrologic cycle of the Great Plains region as simulated in these models. We will also investigate whether or not the models are capable of simulating long-term drought over the Great Plains region and look to see if the mechanisms responsible for causing the observed droughts of the twentieth century are active in the models. The ultimate goal is to assess whether or not

the models should be used to look at the future state of precipitation over the Great Plains. The main questions we will attempt to answer in this thesis include:

1) Do the models simulate the climatology of the hydrologic cycle of the Great Plains?
2) Do the models simulate the observed variability in Great Plains precipitation?
3) Do the models simulate long-term droughts over the Great Plains region of the United States?
4) Tropical Pacific SSTs influence Great Plains precipitation on long timescales, does this happen in the models?
5) Land-Atmosphere interactions play an important role in influencing the variability in Great Plains precipitation. Are the land surface and the atmosphere coupled in these models?
6) Are the AR4 IPCC climate models credible for use in future drought assessment studies?
7) What could the models do differently to better simulate drought?

In Chapter 2 of this thesis we review some of the leading theories about the causes of long-term drought over the Great Plains, and the factors that lead to persistence in precipitation anomalies over the region. In Chapter 3 we discuss the models and the observational data sets used in this study. In Chapter 4 we compare the climatology of the hydrologic cycle of the Great Plains in the models with observations. In Chapter 5 we discuss the general characteristics of the variability in Great Plains precipitation, including the frequency of occurrence of extreme wet and dry events, and persistence in

precipitation anomalies. Finally, in Chapter 6 we investigate whether or not the models produce long-term drought over the Great Plains, and if they do, we look to see whether or not these droughts occur for the same reasons in the models as they do in the observations. Chapter 7 offers a discussion and conclusions on the main findings this thesis and suggests ideas for future work. We also provide an analysis of the El Nino - Southern Oscillation (ENSO) in Appendix A.

Chapter 2

Causes of Long-Term Drought Over the Great Plains

Large-scale forcing from the tropical Pacific, combined with interactions between soil moisture and precipitation appear to be the primary mechanisms leading to negative precipitation anomalies over the Great Plains, that can persist for long periods of time (Seager et al., 2005b). In the first part of this chapter, we discuss the ways in which changes in tropical Pacific Sea Surface Temperature (SST) patterns can influence Great Plains precipitation. In the second part, we discuss how feedbacks between soil moisture, evapotranspiration and precipitation can cause drought conditions to lock into place over the Great Plains region resulting in persistent dry periods.

2.1 Forcing by the Tropical Pacific

Recent studies have implicated cool, La Niña-like SST patterns in the tropical Pacific as the primary cause of Great Plains drought during the twentieth century (Figure 2.1) (Horeling and Kumar, 2003; Schubert et al., 2004a,b; Seager et al., 2005b; Herwijer et al., 2006; Cook et al., 2007; Seager et al., 2007b; Cook et al., 2008; Herweijer and Seager, 2008; Seager et al., 2008). These studies also indicate that dry conditions over the Great Plains fit into a broader global pattern of mid-latitude drought that has both zonal and hemispheric symmetry (Figure 2.2). This means that when the Great Plains

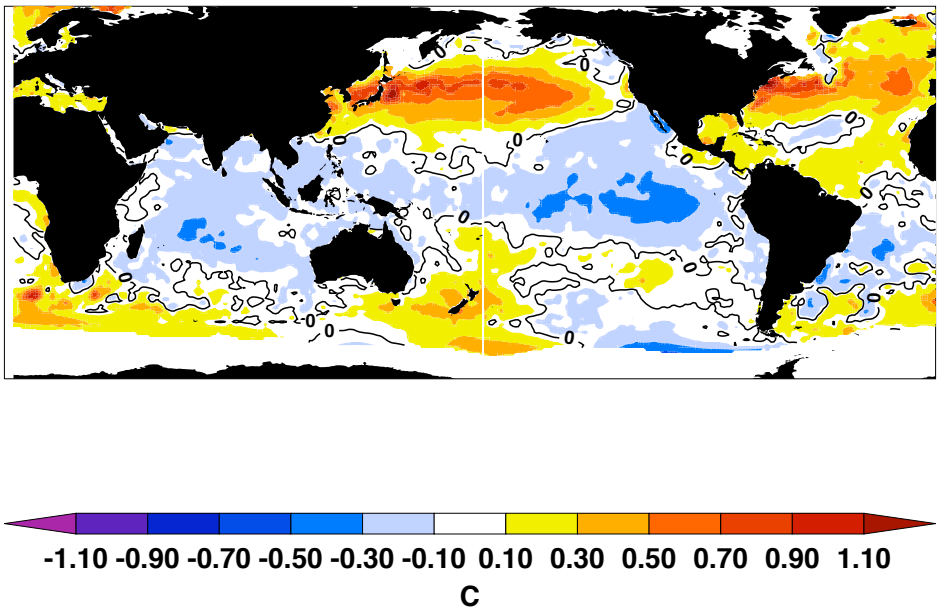


Figure 2.1. *SST anomalies for the period 1947-1956 from the HadISST data set. Anomalies are taken from the 1870-2002 mean. Map similar to Figure 4b in Seager et al. (2005a).*

experiences a long-term dry period, often other mid-latitude regions in both the Southern and Northern hemispheres experience dryness as well.

The six long-term droughts that have occurred over the Great Plains during the past 150 years have been linked to low-frequency variability in tropical Pacific SST patterns. Modeling experiments in which Atmospheric General Circulation Models (AGCMs) are forced with the history of global SSTs have been able to reproduce the timing and spatial variability of Great Plains drought over the past 150 years (Schubert et al 2004a, b; Seager et al., 2005a; Cook et al., 2007; Herwijer and Seager, 2008). These studies indicate that approximately 20-30% of the variability in Great Plains precipitation is forced by changes in global SST patterns. Similar patterns in Great Plains precipitation are found when the AGCMS are forced with the history of tropical Pacific SSTs alone, thus indicating that changes in tropical Pacific SST patterns strongly influence Great Plains precipitation.

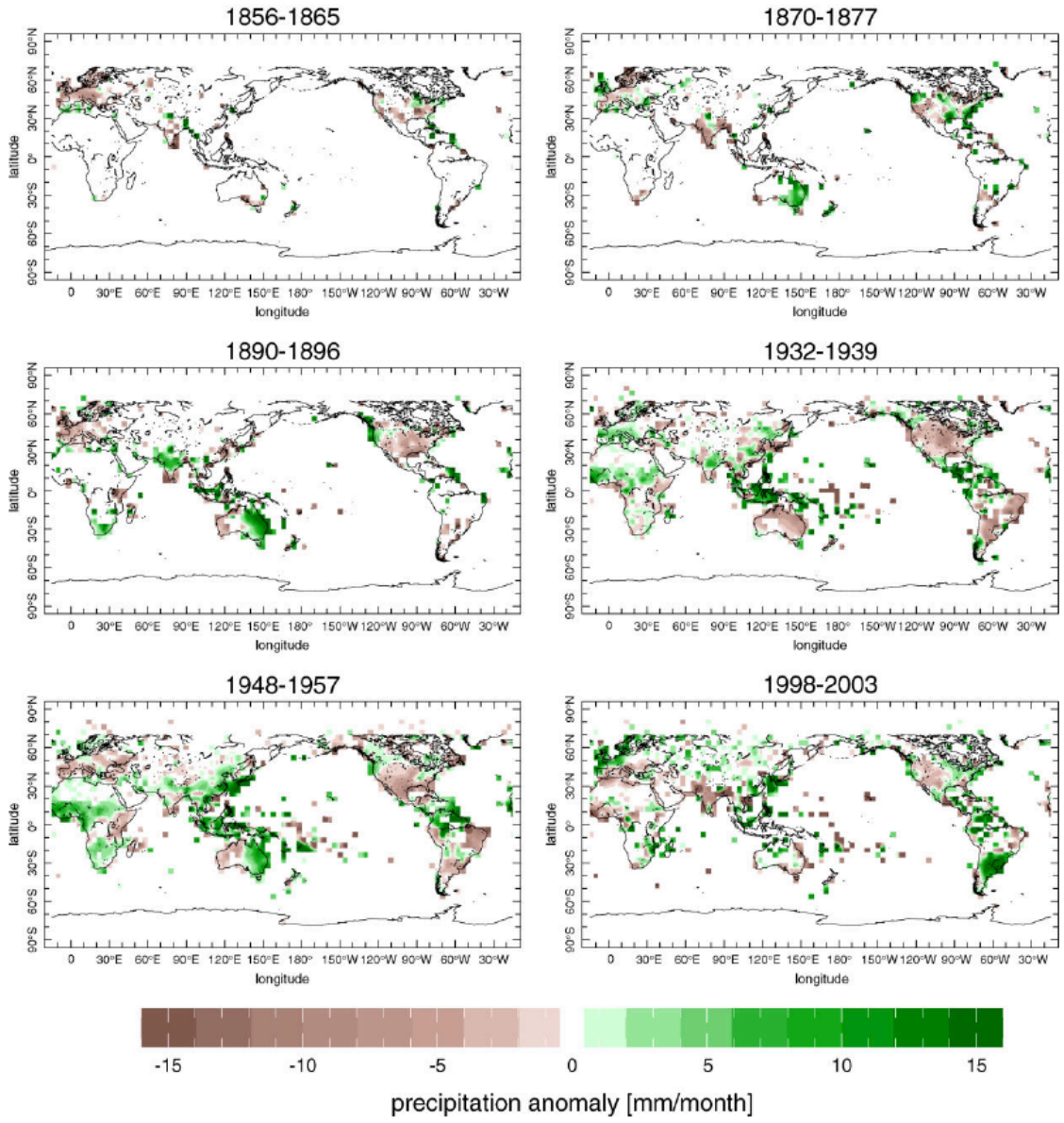


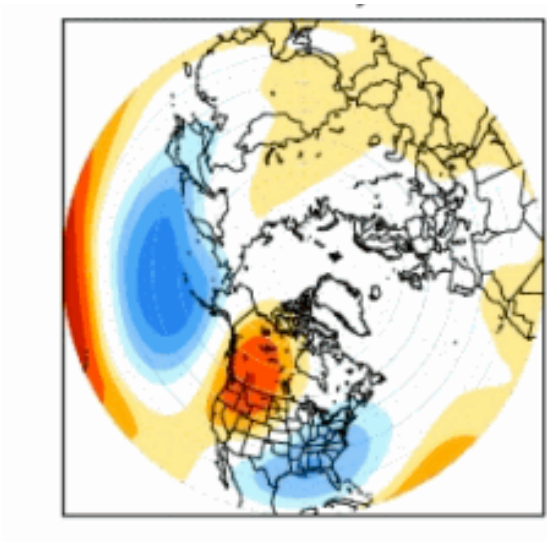
Figure 2.2. *Global land surface precipitation anomalies (mm month $^{-1}$) selected for major North American drought regimes of the instrumental period. Figure taken from Herweijer and Seager 2008. Data is from the observed Global Historical Climatological Network (GHCN)*

The primary mechanism through which anomalously cool conditions in the central and eastern tropical Pacific can influence mid-latitude precipitation in both the Southern and Northern hemispheres has been described in Seager et al. (2003, 2005a, b), Cook et al. (2007), and Seager et al. (2008). To briefly summarize, these studies show

that anomalously cool conditions in the tropical Pacific tend to correspond with a weakening of the subtropical jets. Changes in the position and strength of the subtropical jets impact the propagation of transient eddies and, in this case, cause an anomalously poleward eddy flux of zonal momentum. The meridional divergence of eddy momentum flux in the mid-latitudes must be balanced by the Coriolis force, and by continuity leads to descent in the midlatitudes. The end result is that anomalously cool SSTs in the tropical pacific result in anomalous descent in the mid-latitudes. This descent acts to inhibit precipitation over the Great Plains, thereby causing drought. The descent also occurs in the mid-latitude region of the Southern Hemisphere.

Regional variations in mid-latitude precipitation anomalies have also been associated with stationary Rossby waves that propagate out of the tropical Pacific and are excited by the precipitation anomalies in the tropics associated with the tropical SST anomalies. These "teleconnection patterns" have been described by (Horel and Wallace, 1981; Hoskins and Karoly, 1981; Hoerling et al., 1997; Threnberth et al., 1998; Hoerling and Kumar, 2002; Alexander et al, 2002). La Niña conditions in the central and eastern Tropical Pacific are associated with an upper level anticyclone over the eastern North Pacific, a cyclone over western Canada, and another anti-cyclone over the southern United States. This pattern is some times described as the Pacific-North America (PNA) pattern and is shown in Figure 2.3 (note, the pattern in Figure 2.3 is actually what occurs during El Niño events, the pattern just described for La Niña events is of opposite sign that what is seen in the figures). The teleconnection patters are strongest, and have the largest influence on U.S. precipitation during the winter season, when SSTs and

a)



b)

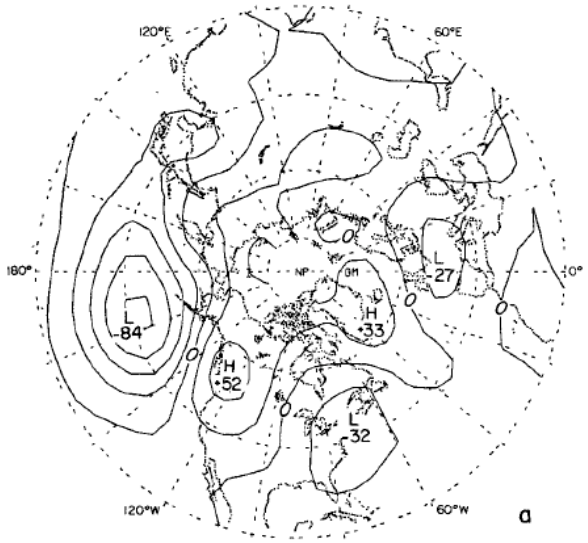


Figure 2.3. *Examples of the Pacific North America (PNA) Pattern from (a) the Climate Prediction center website (http://www.cpc.noaa.gov/data/teledoc/pna.shtml) and (b) Wallace and Gutzler (1981). These patterns represent the positive phase of the PNA pattern which is often associated with El Niño events. La Niña events are typically associated with the negative phase of the PNA and so are of opposite sign.*

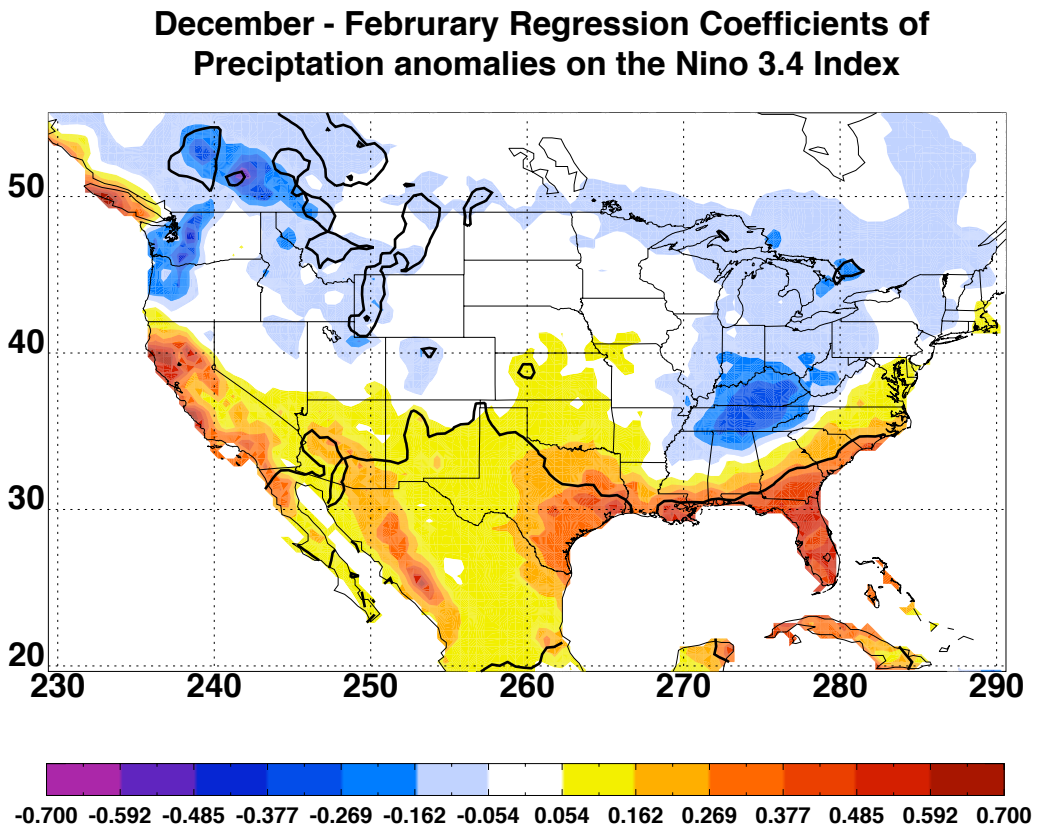


Figure 2.4. *United States precipitation anomalies regressed onto the standardized Niño 3.4 index. Precipitation anomalies created with the CRU TS. 2.1 data set. The Niño 2.4 index was created using the HadISST data set. Black curve delineates where the relationship is statistically significant at the 99% confidence level.*

precipitation anomalies are largest in the tropics (Rasmusson and Carpenter, 1982; Trenberth, 1997). It has also been shown that the relationship between the El Niño - Southern Oscillation (ENSO) and Great Plains precipitation tends to be largest in the southern portion of the region. The relationship between ENSO and Great Plains precipitation can be seen in the linear regression map of the winter Niño 3.4 index and winter United States precipitation (Figure 2.4).

2.2 Land-Atmosphere Interactions

As mentioned in the previous section, changes in global SST patterns have been shown to account for 20-30% of the variability in Great Plains precipitation. Also, the

mechanisms (eddy-mean flow interaction and Rossby wave propagation), by which tropical Pacific SST anomalies influence Great Plains precipitation have the strongest influence on winter time precipitation, but it is the precipitation anomalies that occur during the summer part of the year that have the largest, and most detrimental impacts on the Great Plains. So, although the tropical Pacific does greatly influence Great Plains precipitation, some mechanism must be active during the summer season to help perpetuate harmful, long-term drought conditions.

Studies indicate that land-atmosphere interactions may account for a large portion of the remaining variability in Great Plains precipitation (Schubert et al., 2004a). Interactions between the land surface and the atmosphere involve feedbacks between soil moisture, evapotranspiration and precipitation. These hydrologic parameters have been shown to be tightly coupled during the summer months over the Great Plains region of the United States (Koster et al., 2004). Schubert et al. (2004a), a study that forced AGCMs with the history of global SSTs, also did a model experiment in which the effects of the soil moisture - precipitation feedback were turned off by fixing the evaporation efficiency (the ratio of evaporation to potential evaporation) of the land-surface to its seasonal climatology. In doing this, the variance of precipitation over the Great Plains was reduced by a factor of 5. This supports the findings from other studies that coupling between the land surface and the atmosphere is an important part of Great Plains precipitation variability. Some studies have also indicated that soil moisture feedbacks may act as a bridging mechanism that can extend winter precipitation anomalies into the summer months (Pal and Eltahir, 2001; Seager et al., 2005b).

It has long been thought that land-atmosphere interactions promote the persistence of precipitation anomalies over the Great Plains (Holzman, 1937; Jensen, 1935, Hornton 1943). Although these early studies do discuss a potential relationship between land surface conditions and local precipitation, it was not until the modeling studies performed by Charney (1975) and Charney et al. (1977) that possible mechanisms were identified. Recent observational and modeling studies by Brubaker and Entekhabi (1996) and Eltahir (1998) have been able to elaborate and clarify the results of Charney. These results are summarized as follows.

Although the specific details on feedbacks between soil moisture conditions and precipitation rates are complicated, the basic premise is fairly simple. Over continental regions, such as the Great Plains, the atmospheric initiation of a hydrologic anomaly at the surface, caused by large-scale subsidence or reduced moisture convergence, will result in large-scale changes in soil moisture conditions. Negative soil moisture anomalies then cause latent heat fluxes (evapotranspiration) to decrease. During the summer months, local evapotranspiration is an important source of water vapor to the atmosphere above the Great Plains. By restricting the flux of water from the surface to the atmosphere, reduced soil moisture concentrations cause precipitation rates to remain anomalously low. Also, decreasing latent heat fluxes at the surface must be offset by increasing sensible heat fluxes. Positive sensible heat flux anomalies result in a warming of the surface which acts to reinforce the original atmospheric forcing anomaly by intensify the 500 hPa anticyclone that resides over the Great Plains. This series of events describes the positive feedback that can exist between soil moisture and precipitation

over the Great Plains region. The atmospheric anomaly is reinforced and persists with even greater intensity as long as soil moisture content and evapotranspiration rates remain low. Some studies indicate that drought conditions will persist over the Great Plains until large-scale or synoptic factors are strong enough to overcome the positive feedback, i.e. it must rain enough for soil moisture concentrations to increase significantly.

Studies have shown that negative winter precipitation anomalies cause the surface to be unusually dry at the start of the summer season. This can cause summertime evapotranspiration rates to be abnormally low, thereby helping to reduced precipitation rates. In this way, soil moisture - rainfall feedbacks can act as a bridging mechanism between winter and summer precipitation over the Great Plains. As long as anomalously cool conditions persist in the tropical Pacific, wintertime Great Plains precipitation rates will remain abnormally low. Coupling between the land surface and the atmosphere will then cause reductions in summer time precipitation. Until the tropical Pacific transitions to an anomalous warm state, the Great Plains regions will face potentially devastating long-term drought conditions (Figure 2.5).

This discussion implies that both land-atmosphere interactions and large scale forcing from the tropical Pacific can work together to initiate and perpetuate drought conditions over the Great Plains region. Other factors such as the position of the Bermuda High in the Atlantic Ocean and large-scale synoptic activity can also influence Great Plains drought. These factors will be discussed in more detail later.

In Chapter 6 of this thesis we will look to see whether forcing from the tropical Pacific and land-atmosphere interactions are important in the initiation and perpetuation

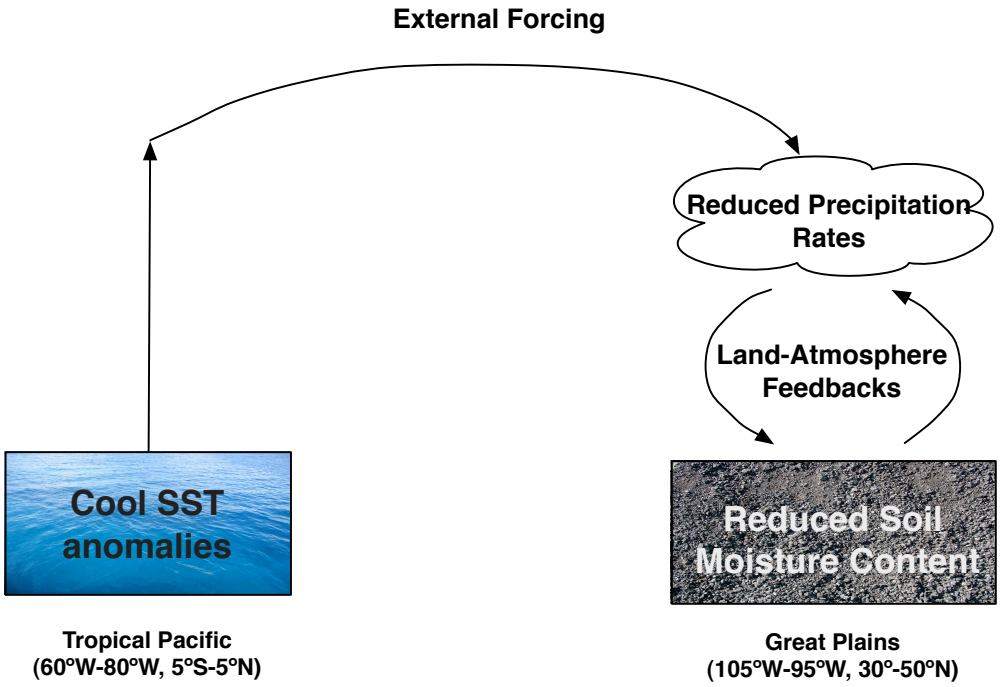


Figure 2.5. *A simple schematic diagram that describes how the external forcing from the tropical Pacific and local land- atmosphere interactions can induce drought conditions over the Great Plains. Cool conditions in the tropical Pacific act as an external forcing of Great Plains precipitation by inducing subsidence over the region via changes in eddy-mean flow interactions and Rossby Wave propagation. Enhanced subsidence over the Great Plains results in clear skies and reduced precipitation rates. Reductions in rainfall cause soil moisture concentrations in the Great Plains region to lower. During the wet season, interactions between the land surface and the the atmosphere via evapotranspiration will result in soil moisture - rainfall feedbacks that can perpetuate drought conditions.*

of long-term drought over the Great Plains region in three Global Climate Models (GCMs). In order to accurately represent drought over this region, the models must be able to accurately capture the variability in tropical Pacific SSTs as well as coupling between the land surface and the atmosphere over the Great Plains.

Chapter Three

Data and Methodology

The following includes a discussion of the models and observational data sets, used in this study, our definition for long-term drought, and a description of the statistical techniques used to process these data.

3.1 Models

This study utilizes the Climate of the 20th Century integrations performed by three of the coupled global climate models (CGCMs) that were used in the Fourth Assessment Report (AR4) of the Intergovernmental Panel on Climate Change (IPCC, IPCC, 2007). These simulations were obtained from the World Climate Research Programme's (WCRP's) Coupled Model Intercomparison Project Phase 3 (CMIP3, Meehl, 2007) multimodel dataset. This data set was made available by the Program for Climate Model Diagnosis and Intercomparison (PDMDI) and can be found online at http://www-pcmdi.llnl.gov. Although simulations of twentieth-century climate are available from 21 different modeling groups, in this study we chose to restrict our analysis of drought over the Great Plains to only three models; the Geophysical Fluid Dynamics Laboratory (GFDL) Climate Model - version 2.0 (CM2.0), the National Center for Atmospheric Research (NCAR) Community Climate System Model - version 3.0

Table 3.1. *Climate models whose twentieth-century climate simulations were used in this study.*

Model Name	Center/Country	Horizontal Resolution	Number of Levels	Number of Simulations	Key Reference
CM 2.0	Geophysical Fluid Dynamics Laboratory (GFDL)/United States	2.0º lat x 2.5º lon	24	3	Dellworth et al. (2006)
CCSM	National Center for Atmospheric Research (NCAR)/United States	T85 (~1.4º lat x 1.4º lon)	26	8	Collins et al. (2004, 2006)
HadCM3	Met office/ United Kingdom	2.5º lat x 3.75º lon	19	2	Gordon et al. (2000)

(CCSM3), and the United Kingdom Met Office (UKMO) Hadley Center Climate Model - Version 3 (HadCM3). Table 3.1 summarizes these models.

The twentieth century climate simulations produced for the AR4 IPCC report were initialized from preindustrial control runs for which the atmospheric content of trace gases and the solar irradiance were representative of the late nineteenth century. The simulations also made use of historical time series of observed 20th Century atmospheric greenhouse gas concentrations, sulfate aerosol direct effects, and volcanic and solar forcings. Multiple integrations of twentieth century climate were performed with each of the three models and differ only in their initial conditions as determined by the preindustrial control run of each model (see Table 3.1 for the number of 20th Century Climate integrations performed with each model). Although each simulation represents the Climate of the Twentieth century, specifications for actual length of the simulations was not giving by the IPCC and therefore the lengths of the integrations performed by each modeling group is somewhat different (Figure 3.1). Output from the models is

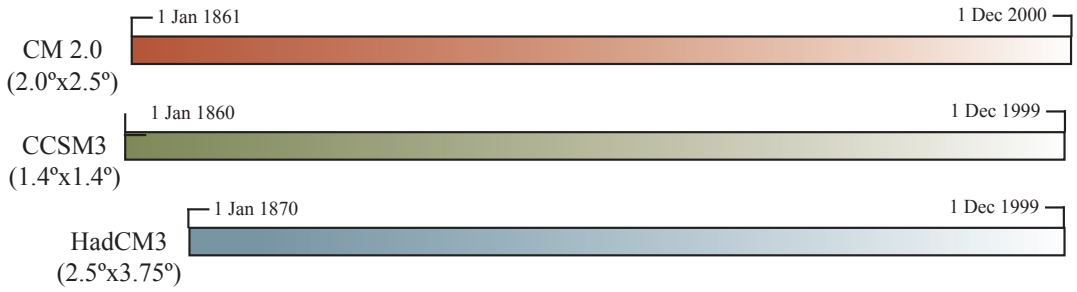


Figure 3.1. *Visual representation of the length of each model simulation.*

provided in a monthly mean format, higher time resolution is not available for the entire 20th Century.

The ability of the models to simulate long-term drought over the Great Plains of the United States depends on how well the models represent the various factors that influence precipitation over the Great Plains. Specifically, differences between the simulated droughts will be determined by how each model represents the dynamics of SST variability in the tropical Pacific, the interactions between the Tropics and the Midlatitudes, and interactions between the land surface and the atmosphere. Also important are the methods by which each model parameterizes precipitation.

These models are fully coupled GCMs and as such are comprised of four different physical components that represent the atmosphere, ocean, land surface and sea ice. The physical components of the models are then connected via a coupler that exchanges information between them. Tables 3.2, 3.3, and 3.4 summarize the main differences in model resolution, numerical schemes, and physical parameterizations between the atmospheric, oceanic, and land-surface components of each model.

GCM Name	CM 2.0	CCSM3	HadCM3
Name of Atmospheric Component	GFDL global atmopshepre model, Version 2 (AM2)	Community Atmosphere Model, Version 3 (CAM3)	UK Hadley Centre atmospheric model (HadAM3)
Key Reference	GFDL GAMDT (2004)	Collins et al. (2004, 2006 a,b)	Pope et al. (2000)
Horizontal Resolution	2.0º x 2.5º	~1.4º x 1.4º (T85 Spectral Resolution)	2.75º x 3.75º
Dynamical Core	Finite-difference model, using the Arakawa B-gird, with an Eulerian advection scheme	Eulerian spectral dynamical core with semi-Lagrangian advection scheme	Finite-difference model, using the Arakawa B-gird, with an Eulerian advection scheme
Number of Levels	24	26	19
Vertical Coordinate	Hybrid sigma-pressure coordinate	Pure sigma coordinate in lowest levels, pure pressure coordinate above 83mb and a hybrid sigma-pressure coordinate inbetween	Hybrid sigma-pressure coordinate
Cloud Parameterizations	Cloud microphysics from Rotstayn (2000) and microphysics from Tiedtke (1993)	Prognostic condensate based on Rash and Kristjason (1998), Zhang et al. (2003) and Boville et al. (2005)	cloud water and ice parameterizations based on Smith (1990) and modified by Gregory and Morris (1996)
Convective Parameterizations	Relaxed Arakawa-Schubert scheme from Moorthi and Suarez (1992)	Deep convection parameterized using a simplified Arakawa-Schubert (1974) scheme developed by Zhang and McFarlane (1995). Parameterization of shallow convection uses Hack (1994)	Bulk mass flux scheme from Gregory and Rowntree (1990) and improved by Gregory et al. (1997)
Boundary Layer Parameterizations	K-profile scheme with prescribed entrainment for convective layers from Lock et al. (2000)	Non-local boundary layer scheme from Holstag and Boville (1993) and Boville and Bretherton (2003)	First order turbulent mixing scheme developed by Smith (1990, 1993)
Radiation Parameterization	Shortwave parameterizations follow Freidenreich and Ramaswamy (1999), longwave parameterizations follow Schwarzkoph and Ramaswamy (1999), both have been modified by (GFDL GAMDT, 2004)	Parameterization of shortwave and longwave radiation is described in Collins (2001) and Collins et al. (2004)	Shortwave and longwave radiation parameterized using Edwards and Slingo (1996)

Table 3.2. *Summary of the Atmospheric component of each model. Table includes information about model resolution, the numerical representation scheme used in each model, and key atmospheric parameterizations that describe cloud formation, convection, boundary layer processes and radiative transfer schemes.*

GCM Name	CM 2.0	CCSM3	HadCM3
Name of Ocean Component	GFDL ocean model, Version 3 (OM3.0)	Parallel Ocean Program, Version 1.4.3 (POP 1.4.3)	UK Hadley Centre ocean model
Key Reference	Griffies et al. (2003, 2005)	Smith and Gent (2002)	Gordon et al. (2000)
Horizontal Resolution	1.0º x 1.0º with enhanced equatorial resolution of 1/3º	1.0º x 1.0º	1.25º x 1.25º
Mixed Layer Treatment	KPP Boundary Layer mixing (Large et al., 1994)	KPP Boundary Layer mixing (Large et al., 1994) with modifications described in Danabasoglu et al. (2005)	Kraus-Turner (1967) and K-theory scheme (Pacanowski and Philander 1981) for momentum
Eddy Parameterizations	Isopycnal mixing of tracers and layer thickness (Gent-McWilliams, 1990; Griffies et al., 1998; Griffies, 1998)	Gent-McWilliams (1990)	Gent-Mcwilliams (1990) with a variable thickness diffusion parameterizations (Wright, 1997; Visbeck et al. 1997)

Table 3.3. *Summary of the Ocean component of each model. Table includes information about model resolution, and parameterizations that involve the treatment of the mixed layer and the effects of eddy transport.*

In general, differences in model physics, parameterizations and resolution will influence their representations of the 20th century climate. Specific discussion of all of these differences is beyond the scope of this research, but when applicable differences in model physics or parameterizations will be highlighted. Variability in tropical Pacific SSTs plays a key role in influencing Great Plains drought (See Chapter 2). In Appendix A of this thesis we provide discussion of the ability of the models to simulate the El Nino - Southern Oscillation (ENSO) phenomenon and its associated teleconnection patterns that influence the North American hydroclimate.

3.2 Data Sets Used for Model Evaluation

The data sets used to evaluate the CGCM output are summarized in Table 3.5. Detailed descriptions of each data set are given in the following four sections.

GCM Name	CM 2.0	CCSM3	HadCM3
Name of Land Component	GFDL global land model, Version 2 (LM2)	Community Land Model, Version 3 (CLM3)	Met Office Surface Exchange Scheme (MOSES)
Key Reference	Milly and Shmakin (2002)	Bonan et al. (20002 a,b)	Cox et al. (1999)
Tiling?	No, single surface type for each grid box (i.e. same vegetation cover and soil type defined at each grid box)	Yes, grid cells are composed of multiple land units, snow/soil columns and plant functional types.	No, single surface type for each grid box (i.e. same vegetation cover and soil type defined at each grid box)
Soil Layers	10	10	4
Surface and Subsurface Runoff	Frozen and liquid water overflow are routed directly to the ocean	Modification of TOPMODEL (Beven and Kirkby, 1979) is used to parameterize runoff. The River Transport model of Bransetetter (2001) and Bransetetter and Famigliett (1999) is used to transport runoff from the land to the ocean.	Overflow water from the surface and sub-surface drainage is instantaneously routed to the corresponding river mouth.
Surface Albedo	Snow-free surface albedo is a function of vegetation type and soil color.	Radiative transfer within vegetative canopies is calculated from the two stream approximation, soil albedos are determined from soil color	All-band surface albedo. Prescribed snow-free albedo based on vegetation cover and soil color
Vegetation Cover	9 vegetation types are considered, global distribution is determined from Matthews (1983)	Land cover types include: glacier, lake, wetland, and vegetation. Vegetated land units can be divided into 4 of 16 plant functional types which are specified by satellite data	surface vegetation cover is set to one of the 23 classes defined in the Wilson and Henderson-Sellers (1985) land cover archive
Transpiration	Bulk Stomatal resistance is included in evapotranspiration terms	Transpiration fluxes are predicted using a coupled canopy conductance-photosynthesis scheme.	Evaporation from transpiring vegetation is controlled by canopy conductance, calculated by a photosynthesis model (Cox et al. 1998, Cox, 2001).

Table 3.4. *Summary of the Land Surface Component of each model. Table includes information about surface tiling, soil layers, runoff (both surface and subsurface drainage), surface albedo, vegetation, and the treatment of transpiration in each model.*

3.2.1 CRU TS 2.1

Simulated precipitation and surface temperature are compared with the CRU TS 2.1 observational data set produced by the Climate Research Unit (CRU) at the University of East Anglia, United Kingdom (Mitchell and Jones 2005). CRU TS 2.1 (from now on just CRU) is a gridded data set that covers the global land surface at a 0.5

	CRU TS 2.1	VIC	NCEP	HadISST
Origin	Station data	Hydrologic Model forced with observed precipitation and surface meterology	Observations and model forecasts	Observations
Horizontal resolution	0.5º x 0.5º	0.5º x 0.5º	2.5º x 2.5º	1º x 1º
Horizontal domain	global land surface (except Antarctica)	land surface of continuous United States	global	global ocean surface
Period	1901-2002	1920-2003	1948-present	1870-present
Variables	Precipitation, temperature	Precipitation, evapotranspiration, runoff, soil moisture	850 hPa winds, precipitable water, specific humidity, short wave forcing geopotential height	Sea Surface Temperature
Source	Climate Research Unit of the University of East Anglia (Mitchelle and Jones 2005)	Variable Infiltration Capacity Macroscopic Hydrologic Model from the University of Washington (Andreadis et al. 2005)	National centers for Environmental Prediction/National Center for Atmospheric Research reanalysis project (Kalnay et al. 1996)	United Kingdom Met Office Hadley Centre Sea Ice and SST data set (Rayner et al. 2003)

Table 3.5. *Specifications of the data sets used to evaluate the CGCMS in this study.*

degree resolution for the period 1901-2002. In our study we utilize the monthly total precipitation and monthly mean surface air temperature fields from CRU.

The CRU data set is developed from observational station data of monthly total precipitation and monthly mean surface temperature. The data set was created using the techniques outlined in New et al. (1999, 2000) and Mitchell and Jones (2005). A brief description of the general methodology is as follows. First the 1961-1990 station climate normals (or monthly mean climatology) were created for each station. Then the station normals were interpolated onto a 0.5º x 0.5º uniform grid using thin-plate spline

techniques that take into consideration the latitude, longitude, and elevation dependence of each variable. Next, each station time series was converted to anomalies relative to the station (1961-1990) normals. The anomalies were then interpolated onto the same 0.5º x 0.5º grid as the climatology, but this time angular distance-weighted techniques were employed. Finally, the interpolated anomaly fields for each month between 1901-2002 were combined with the 1961-1990 gridded monthly mean climatology field, According to New et al. (1999), interpolating anomalies rather than absolute values (anomalies + means) is advantageous because anomalies tend to be a function of large-scale circulation patterns therefore a less extensive network can be used to describe month-to-month departures from the mean climate.

3.2.2 VIC

Observations of hydrologic variables such as soil moisture and evapotranspiration are scarce over the United States. It is particularly difficult to find long-term data records (i.e. records longer than a few decades) for these variables over the Great Plains region (Robock et al., 2000). Without observations, it is not possible to make direct estimates of the relationships between precipitation, evapotranspiration and soil moisture over the Great Plains region during the two most devastating droughts of the 20th century (the 1930s and 1950s). As a consequence of the lack of long-term, large-scale observations, many hydroclimatology studies use land surface and hydrologic models forced with observed precipitation and near surface meteorology to estimate soil moisture and evapotranspiration fields (Road et al., 1994; Shao and Henderson-Sellers, 1996; Huang et al., 1996; Dirmeyer et al. 1999; Georgakakos and Smith 2001).

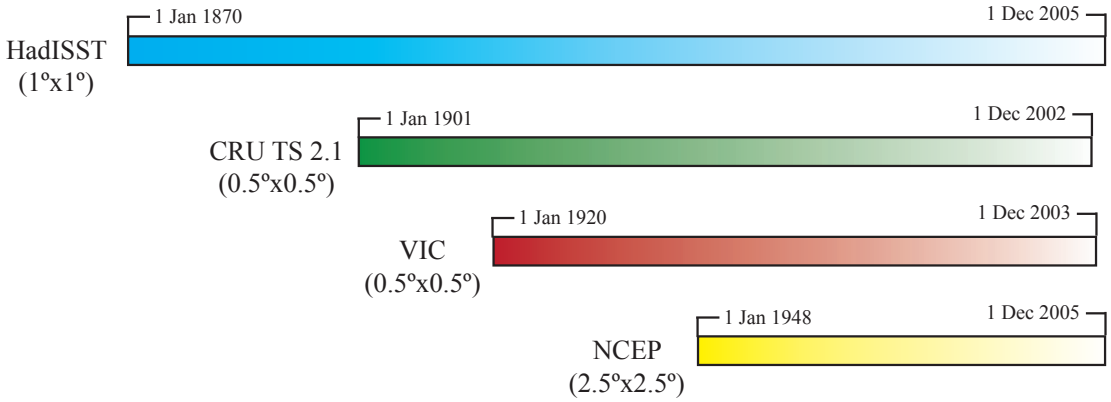


Figure 3.2. *Visual representation of date ranges for the evaluation data sets.*

In this study we compare the simulated soil moisture, evapotranspiration and runoff fields from the CGCMs with results from a hydrologic modeling study performed by Andreadis et al. (2005; hereafter, AEA). AEA simulated historical soil moisture, evapotranspiration and runoff over the contiguous United States for the period 1920-2003 at a 0.5º spatial resolution, using the Variable Infiltration Capacity (VIC) Macroscopic Hydrologic Model (Liang et al., 1994,1996; Cherkauer and Lettenmaier, 2003). The VIC model balances energy and moisture fluxes at the grid scale level. The model includes a soil-vegetation atmosphere transfer scheme (SVAT) to represent the controls that vegetation and soil moisture have on the fluxes of energy and moisture between the land surface and the atmosphere. Also included in VIC are parameterizations that allow subgrid scale spatial variability in soils, topography and vegetation to influence grid scale fluxes of moisture and energy (Maurer et al., 2002).

In the AEA study, the VIC model used a one-day timestep, and was forced with observed daily minimum, maximum and mean air temperature, wind speed, precipitation and other near-surface meteorological parameters. Output from the model includes

evapotranspiration, soil moisture in three subsurface layers, surface runoff from the uppermost soil layer, and subsurface runoff (baseflow) from the two deeper layers. The soil layers vary in thickness and range from 0.1 to 0.5 m for the upper layer, 0.2 to 2.4 m for the middle layer and from 0.1 to 2.5 m for the lower layer.

For completeness, the monthly precipitation and temperature fields used as inputs into the VIC model are also compared with output from the the twentieth century integrations of the CCGMs and the CRU observational data set. The gridded observational precipitation and temperature data sets used by AEA in their study were derived from the Cooperative Observer station meteorological daily data sets DSI-3206 and DSI-3200 maintained by the NCDC. The COOP station data sets were spatially interpolated by AEA onto the 0.5º spatial resolution of the VIC model, using the techniques outlines by Maurer et al. (2002). For more information about interpolation methods and the creation of the precipitation and temperature data sets see (Maurer et al., 2002; Mitchell et al., 2004).

3.2.3 NCEP/NCAR Reanalysis

Data from the National Centers for Environmental Prediction/National Center for Atmospheric Research (NCEP/NCAR) reanalysis project obtained from the NOAA CDC website (http://www.cdc.noaa.gov/cdc/reanalysis/reanalysis.shtml) are also used in this study. The NCEP/NCAR reanalysis (from now on NCEP reanalysis) extends from January 1948 - present and has global coverage with horizontal resolution of 2.5ºx2.5º latitude/longitude with data available on 17 levels. This data set will be used to compare

fields such as geopotential height, 805 hPa winds, and downwelling shortwave radiation with the observations.

The NCEP reanalysis data set is constructed with techniques that combine observations with data assimilation and model forecasts (Kalnay et al., 1996). The observations used in the reanalysis process come from land surface, ship, rawindsonde, aircraft, satellite, and other data sources. The variables from the NCEP reanalysis data set have been separated into four categories, based on the relative influence of the observations versus the model on analysis values. Class A variables, such as geopotential height and u and v winds, are strongly influenced by observations and are considered the most reliable analysis values. Class B variables are influenced by both the observations and the model and include precipitable water, specific humidity and surface temperature. Class C variables are derived solely from the model and are not influenced directly by observed data. They include precipitation and radiative fluxes. Finally, Class D variables are derived from climatological fields, with no influence from data assimilation. Examples of Class D variables include surface roughness and the land-sea mask. Our study primarily uses Class A and B variables from the reanalysis data set, although downwelling short wave radiation at the surface is considered a Class C variable and is used in the climatology chapter of this thesis.

3.2.4 HadISST

For Sea Surface Temperature (SST) data analysis, we use the United Kingdom Met Office (UKMO) Hadley Centre Sea Ice and SST data set (HadISST; Rayner et al. 2003) which has 1º horizontal resolution and spans from 1870 – present. The SST data

used to develop this data set are taken from the Met Office Marine Data Bank (MDB) and include in situ SST measurements from ships and buoys and satellite derived SST after 1982. The Comprehensive Ocean-Atmosphere Data Set (COADS) is also incorporated into the HadISST data set, to help enhance data coverage for the period 1871-1995. The gridded SST data set is then constructed using a two-stage reduced-space optimal interpolation procedure.

3.3 Methodology

Our analysis investigates drought over the Great Plains of the United States. We define the Great Plains region as the area between 30º-50ºN and 95º-105ºW (Figure 3.3, red box). This is similar to the definition used in Schubert et al. (2004). Any time series analysis in this thesis references area-weighted averages calculated for each variable over this domain.

Chapter 4 of this thesis discusses the average climatology of the Great Plains for the CGCMs and the validation data sets. For each model and each validation data set, climatological values were computed for the entire time period of the data record as seen in Tables 3.1, 3.5. and Figures 3.1 and 3.2. For the models, the climatological values were created by averaging over all of the simulations available for each model and therefore represent the ensemble mean climatology.

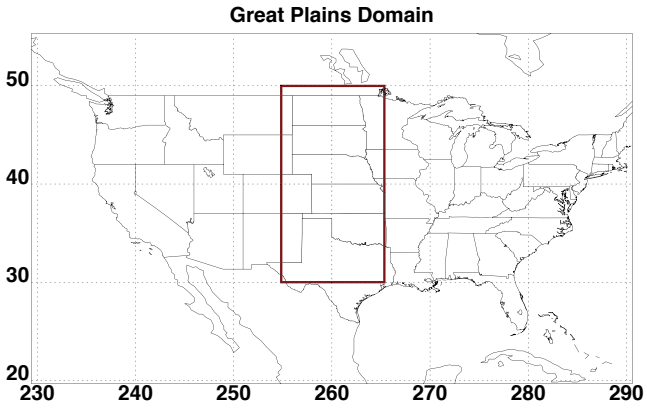


Figure 3.3 *Great Plains region of the United States defined as the area between 95º-105º W and 30º-50ºN*

Anomalies were then calculated by removing the seasonal cycle from the time series. Individual runs will have more variability than the ensemble mean and will be used in our analysis of long-term drought.

3.3.1 Long-Term Drought, a Definition

One of the more interesting challenges that we face in this thesis is settling on a definition for what we mean by "long-term" drought. In the scientific literature there are a number of different definitions for drought. Some are based only on precipitation deficits, some on the supply of surface and subsurface water, others look at sustained soil moisture deficits, and still others take into account the overall health of the surface vegetation cover (Heim, 2002). Since drought can influence the amount of water available for human consumption, food production and the generation of electricity it is also possible to define drought in terms of how deficits in precipitation, soil moisture and runoff impact human societies both socially and economically.

A multitude of different drought indices have been developed to help characterize drought intensity, duration and severity. Some of these include the Palmer Drought Severity Index (PSDI, Palmer 1965), the Standardized Precipitation Index (SPI, Mckee et al., 1993; Guttman, 1999), the Crop Moisture Index (CMI, Palmer, 1968) the Satellite Vegetation Health Index and the Severity-area-duration analysis (SAD, Andreadis et al, 2005). Common to all of these drought definitions and indices is the fact that droughts originate from a deficiency in precipitation. For this reason we have chosen to define long-term drought simply in terms of sustained precipitation deficits.

Specifically, we define a long-term drought as a period of time in which annual precipitation is abnormally low for 80 percent of years during a minimum of seven years (i.e anomalously low precipitation during 6 out of 7 years, 7 out of 8 years, 8 out of 9 years etc). Also, any time period exhibiting 6 or more consecutive years of anomalously low precipitation will be considered a long-term drought. We further require that any positive precipitation anomalies that occur during the long-term drought period must not exceed one standard deviation away from the mean.

We fully acknowledge that there are many different ways to formulate such a definition for long-term drought, but this simple definition does capture both the 1930s and 1950s droughts from the annual time series of Great Plains precipitation (Figure 1.3, drought periods are shaded in blue). Details about these droughts will be given in Chapter 6 of this thesis.

In our exploration of long-term drought over the Great Plains for both the observations and the models we employed we use statistical tools such as regression/ correlation analyses, skewness and power spectrum analysis. The remainder of this section describes these techniques in greater detail.

3.3.2 Regression and Correlation Analysis

We use univariate linear regression analysis to describe the linear relationship between two variables using the following equation:

$$\hat{y}(t) = a_0 + a_1 x(t), \tag{3.1}$$

where *x(t)* is an independent variable and $\hat{y}(t)$ is the estimate of the observed *y(t)*. Linear regression determines the slope of the line that produces the smallest error in estimating the observed data *y(t)*. The most common method of determining the error is the least squares method which minimizes the sum of the squared error (y- $\hat{y}$) at each time step. Using the least squares method, the regression coefficient a_1 is given as:

$$a_1 = \frac{\overline{x'y'}}{\overline{x'^2}}, \tag{3.2}$$

where the prime denotes the deviation from the mean and the overbar represents the mean. If the independent variable *x(t)* is standardized then the regression coefficient will have units of change in *y(t)* per one standard deviation change in *x(t)*.

Correlation analysis is a useful tool for determining the statistical significance of the linear relationship between *x(t)* and *y(t)*. In the linear case described above, the correlation coefficient r can be calculated as a function of regression coefficient:

$$r = a_1 \frac{\sqrt{\overline{x'^2}}}{\sqrt{\overline{y'^2}}}, \tag{3.3}$$

The square of *r* indicates what fraction of the total variance in *y(t)* is explained by the linear relationship with *x(t)*. The statistical significance of all correlation coefficients is assessed using the t-statistic defined as:

$$t = \frac{r\sqrt{N_{eff} - 2}}{\sqrt{1 - r^2}}, \tag{3.4}$$

where r is the correlation coefficient and N_{eff} is the effective sample size. The effective sample size accounts for the persistence in the data. If the data exhibit substantial persistence, then say each sample may not be independent from the previous sample and the number of independent samples will not be equal to N. Assuming the data follows a first order auto regressive process, Bretherton et al. (2002) outlined a method for determining the effective sample size N_{eff} as:

$$N_{eff} = N\left[\frac{1 - r_1 r_2}{1 + r_1 r_2}\right], \tag{3.5}$$

where N is the sample size; and r_1 and r_2 are the lag-one autocorrelations of the time series being autocorrelated. Note that as the persistence increases in the time series, effective sample size decreases.

3.3.3 Skewness

Skewness is a third moment coefficient that indicates the degree of asymmetry of the distribution about its mean. The skewness, s, of a distribution can be calculated as:

$$s = \frac{1}{N}\sum_{j=0}^{N-1}\left(\frac{x_j - \bar{x}}{\sqrt{\overline{x'^2}}}\right)^3 \tag{3.6}$$

If s is positive, then the distribution has a longer tail on the positive side of the distribution maximum, and vice versa.

3.3.4 Power Spectrum Analysis

We used Discrete Fourier transform methods to determine at which periods or frequencies a time series, y_t, exhibits the most power. Using these methods, we interpret our time series as a summation of contributions for a series of harmonic functions. The discrete Fourier transform of y_t is described by two equations:

$$A_k = \frac{2}{n}\sum_{t=1}^{n} y_t \cos\left(\frac{2\pi kt}{n}\right) \tag{3.7a}$$

$$B_k = \frac{2}{n}\sum_{t=1}^{n} y_t \sin\left(\frac{2\pi kt}{n}\right) \tag{3.7b}$$

where k is the wave number, t is time time, and n is the total length of the time series y_t. We can then use A_k and B_k to define $\frac{C_k^2}{2}$, the power spectrum (or line spectrum), as:

$$\frac{C_k^2}{2} = \frac{1}{2}\left(A_k^2 + B_k^2\right) \quad . \tag{3.8}$$

We then smooth $\frac{C_k^2}{2}$ by applying a running mean. $\frac{C_k^2}{2}$ can be plotted against, wave number (k), angular frequency (w), frequency (f), or period (p) where:

$$f_k = \frac{k}{n} = \frac{\omega_k}{2\pi} = \frac{1}{p} \; . \tag{3.9}$$

To test the significance of the power spectrum we calculate the red noise power spectrum from our data R as:

$$R = \frac{2T}{1 + T^2\omega^2} \,. \tag{3.10}$$

where T is the e-folding time of our time series y_t.

Chapter 4

Climatology

The first step to assessing the usefulness of these models is to investigate how well they represent the climatology of the hydrologic cycle of the Great Plains. If the models do not accurately capture the annual cycle of variables such as precipitation and evaporation over the Great Plains, they should not be used in studies that require an investigation of the variability of these about the seasonal mean. This chapter begins with a discussion of the observed hydroclimate of the Great Plains region, followed by an evaluation of the models abilities to represent the observed climatology of the hydrologic cycle of the Great Plains.

4.1 The Observed Seasonal Cycle Over the Great Plains

The seasonal cycle of precipitation over the Great Plains can largely be explained by the seasonal transitions of the dominant air masses that influence the region throughout the year. During winter (December – February, DJF), the Great Plains are primarily influenced by a cold, dry arctic air mass from the north (Figure 4.1a). This air mass brings with it very little moisture, and so winter over the Great Plains tends to be associated with low precipitation rates (Figure 4.2a-b). During spring (March – May,

MAM), the Great Plains are often influenced by two different air masses; a cold, dry arctic air mass from the north and a warm, moist, tropical air mass that flows into the region from the Gulf of Mexico (Figure 4.1b). The mixing of these two air masses results in increased precipitation rates characteristic of spring (Figure 4.2c-d). During summer, the Great Plains are highly influenced by the warm, Tropical air mass that flows in to the region from the Gulf of Mexico (Figure 4.1c). This air mass is associated with the westward shift of the Bermuda High (also called the North Atlantic subtropical high) which allows for greater moisture transport into the Great Plains region via a phenomenon known as the "Great Plains nocturnal low-level jet" (Bonner 1968; Helfand

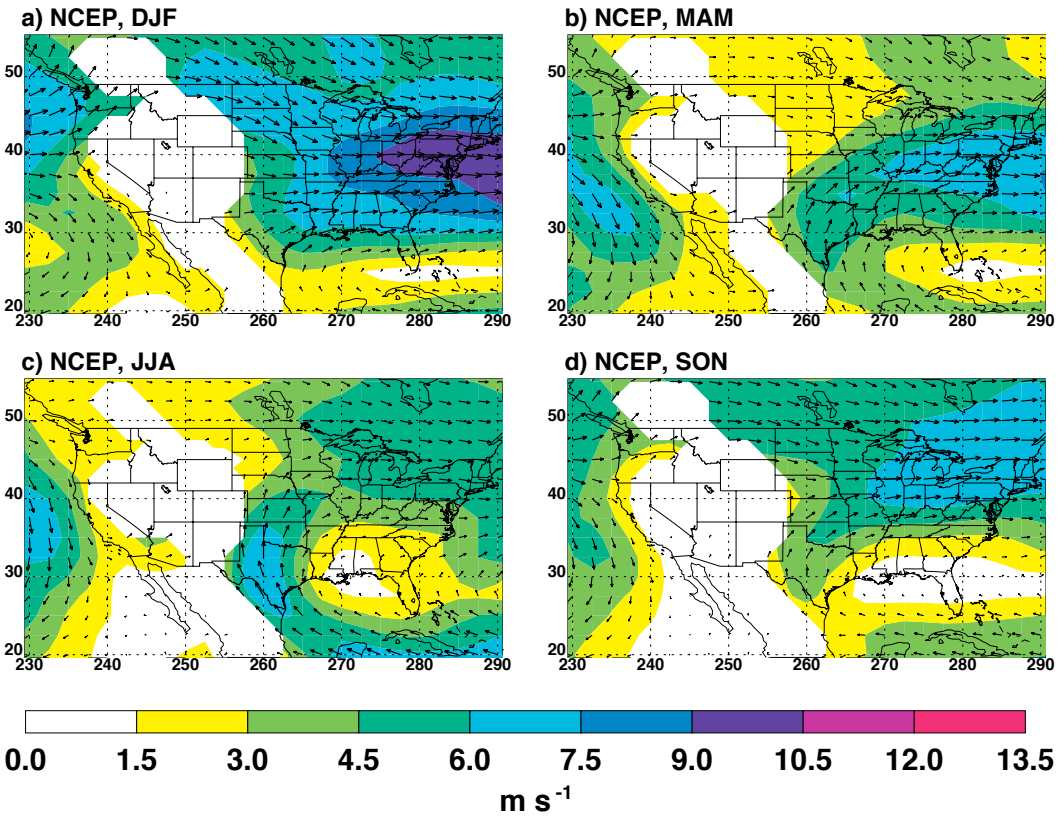


Figure 4.1. *Climatology of 850 hPa winds for DJF (a), MAM (b), JJA (c), and SON (d) from NCEP. Shading indicates wind speed and arrows give wind direction.*

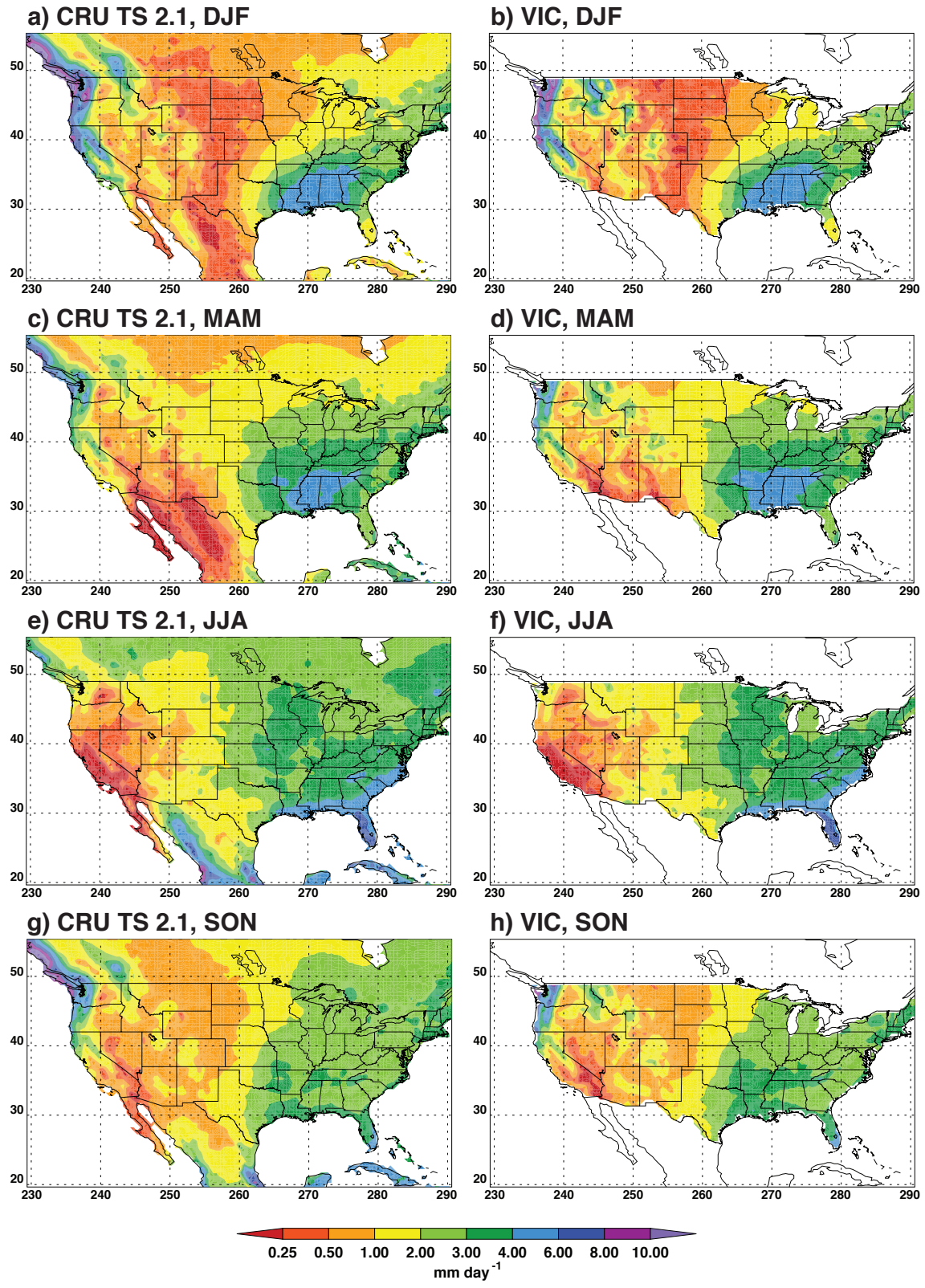


Figure 4.2. *Climatological precipitation rates in mm day^{-1} over the United States from CRU TS 2.1 (left column) and VIC (right column) for DJF (a-b), MAM (c-d), JJA(e-f), SON(g-h).*

and Schubert 1995; Higgins et al. 1997). The intrusion of this warm, moist air mass into the Central United States causes precipitation rates over the Great Plains to increase significantly (Figure 4.2e-f). Local evapotranspiration also plays an important role in influencing summertime precipitation over the Great Plains and will be discussed later in this chapter. During fall, precipitation rates over the Great Plains decrease (Figure 4.2g-h) when the region is primarily influenced by an air mass that flows in from the Pacific (Figure 4.1d). This air mass tends to be dry, because much of the moisture is precipitated out of the air as it passes over the Rocky Mountains. (See also: Bryson, 1966; Bryson and Hare, 1974; Doesken and Stanton, 1992; Helfand and Schubert, 1995; Hirschboeck, 1991; Mock, 1996; Woodhouse and Overpeck, 1997)

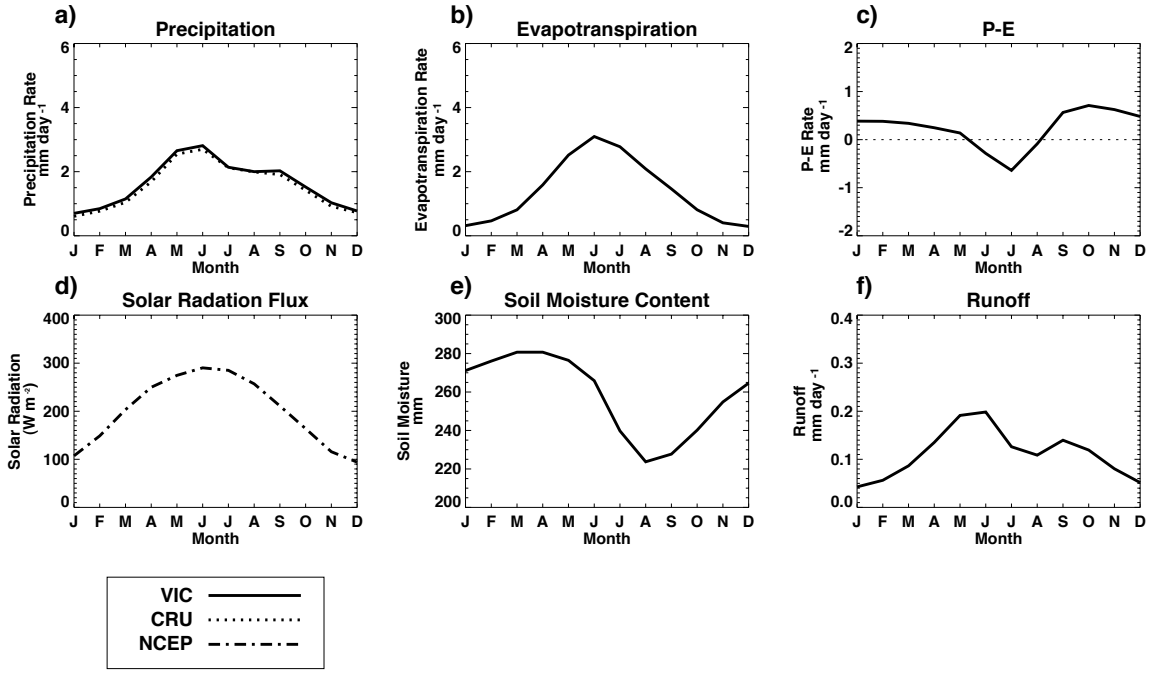


Figure 4.3. *Time series plots of multiple climatological variables averaged over the Great Plains region. The variables include: precipitation rates from CRU TS 2.1 and VIC in mm day^{-1}(a), evapotranspiration rate from VIC in mm day^{-1} (b), P-E from VIC in mm day^{-1} (c), downwelling solar radiation flux at the surface in W m^{-2} from NCEP (d), total column soil moisture content in mm from VIC (e), and runoff (surface+subsurface) in mm day^{-1} from VIC (f).*

The climatology of precipitation averaged over the entire Great Plains region is consistent with the above explanation of the seasonal cycle (Figure 4.3a). Average precipitation rates for the Great Plains region are the lowest in January at approximately 0.6 mm day^{-1}. Precipitation rates then ramp up during spring reaching a maximum in June of 2.7 mm day^{-1}. In July they drop off slightly to about 2 mm day^{-1} where they remain fairly constant until September when they drop off again. Precipitation rates first dip below 1 mm day^{-1} in November and remain low until March. The overall pattern that emerges from this time series is that the Great Plains are dry during fall and winter (October – March) and wet during spring and summer (April – September). In Chapter 5 and Chapter 6 of this thesis, we divide the year into two distinct seasons, the wet season which extends from April - September, and the dry season which extends from October-March, however for the remainder of this Chapter we focus on the traditional four season year.

The time series of climatological precipitation from each of the two observational data sets (VIC and CRU TS 2.1) are almost identical because they are based on the same meteorological station data. The spatial maps of climatological precipitation over the United States are also strongly correlated between the two data sets (Figure 4.2) although, some discrepancies do occur over the Rocky Mountains due to differences in interpolation methods.

When compared to the rest of the United States (Figure 4.2), it becomes clear that the seasonal cycle of precipitation over the Great Plains region is unique. While the Great Plains experiences strong seasonal differences in precipitation, especially between

summer and winter months, the Eastern United States experiences little seasonal change in precipitation rates. In fact, over much of the Southeastern United States precipitation rates only fluctuate by approximately 0.7 mm day^{-1} between seasons. The West Coast region of the United States, much like the Great Plains region, also experiences strong seasonal differences in average precipitation rates, but over the West Coast, it is the winter months that are wet and the summer months that are dry. This implies that assessing the timing of drought and the mechanisms that cause drought will be unique to the Great Plains region of the United States.

Evapotranspiration can also play an important role in influencing precipitation rates over the Great Plains, especially during the summer. Evapotranspiration rates are typically influenced by surface water availability, surface energy availability and the photosynthesis rates of the plants. Water availability at the surface is typically related to precipitation rates while energy availability at the surface is directly related to the amount of short-wave radiation being fluxed to the surface from the sun. The rate of evapotranspiration is further complicated by the fact that photosynthesis is connected to the amount of water available in the "root zone" of the underlying soils and the amount of visible light received by the plants. This indicates that both precipitation and downwelling solar radiation not only influence evaporation rates, but also influence photosynthesis rates.

Figure 4.3b shows the climatology of evapotranspiration averaged over the Great Plains region from the VIC soil moisture model. Evapotranspiration rates are low from October through March when they are typically less than 1 mm day^{-1}. During this time

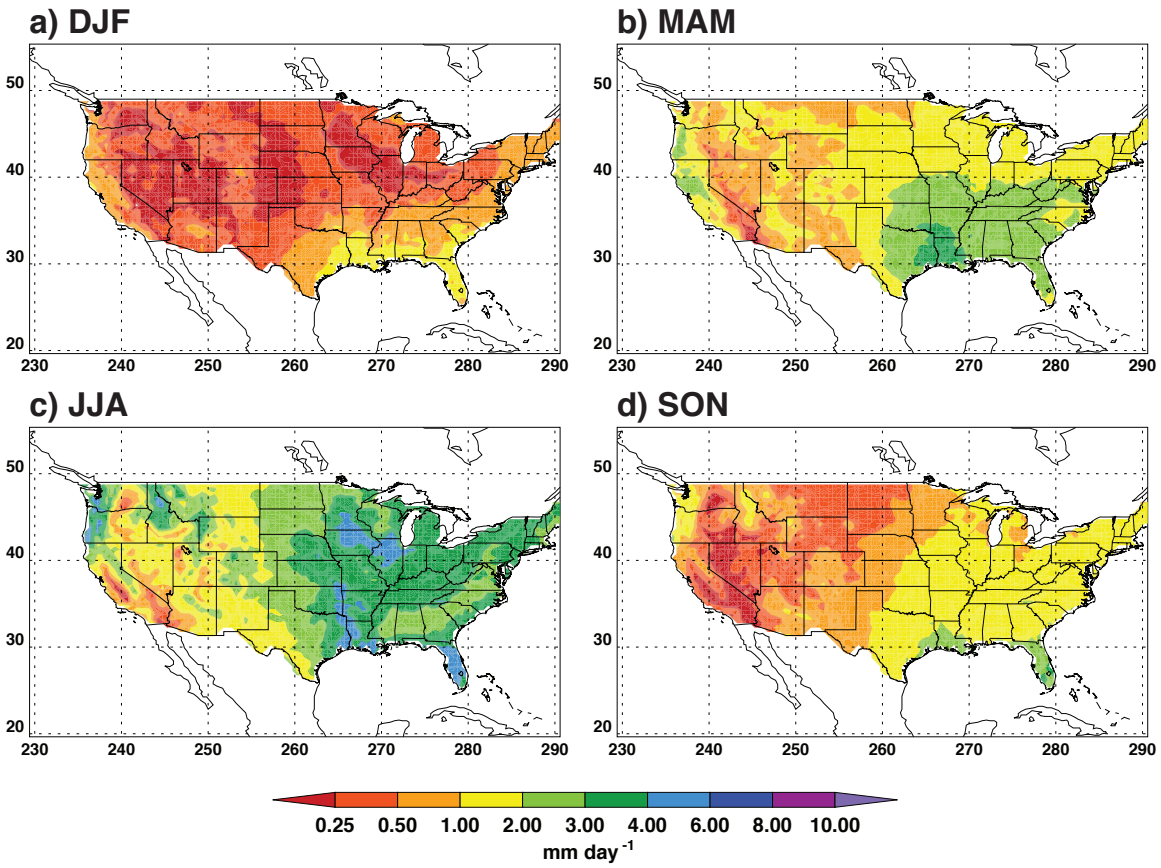


Figure 4.4. *Climatology of evapotranspiration rates in mm day^{-1} over the United States from VIC for DJF (a), MAM (b), JJA (c), SON (d).*

both precipitation rates and downwelling solar radiation are also low (Figure 4.3a and 4.3d). Photosynthesis rates are also expected to be low at this time, since much of the vegetation covering the Great Plains region is either dead or covered with snow. During spring, evapotranspiration rates increase dramatically to reach a maximum in June of 3.2 mm day^{-1}. This maximum also coincides with maximums in both precipitation and downwelling solar radiation over the region. Since spring is the time when plants in the Great Plains tend to grow, it is expected that transpiration rates from plants would also be high at this time. Following the June maximum, the evapotranspiration rates over the Great Plains begin to steadily decline until they reach a minimum in fall. Much like precipitation, evapotranspiration also shows marked seasonality, with high

evapotranspiration rates in the spring and summer and much lower rates in the fall and winter.

Figure 4.4 shows the spatial patterns for the climatology of evapotranspiration over the United States. The first important factor that stands out in this figure is that evapotranspiration is low over the entire U.S. during the winter (DJF). Over the Great Plains, both a lack of moisture and energy at the surface inhibit evapotranspiration rates during DJF, but over the Pacific Northwest region of the United States precipitation rates are at an all time high during DJF, therefore only surface energy availability must be limiting evapotranspiration (see Figure 4.5 for the spatial patterns of the climatology of downwelling short-wave radiation at the surface). During the remaining three seasons of the year, evapotranspiration rates exhibit similar patterns to precipitation, thereby indicating that over much of the United States, water availability at the surface greatly influences evapotranspiration rates.

Overall, evapotranspiration is important for the Great Plains region because it provides a secondary source of water vapor to the atmosphere, with convergence of moisture into the region by the winds the primary source. In the literature, "precipitation recycling" is the term commonly used to describe the contribution of local evapotranspiration to local precipitation (Brubaker et al., 1993). Previous studies have shown that up to 34% of summertime precipitation is supplied by local evapotranspiration over the Central United States (Entekhabi et al., 1996). Therefore, over the Great Plains, precipitation influences evapotranspiration rates by providing a source of water at the surface, and evapotranspiration influences precipitation rates by

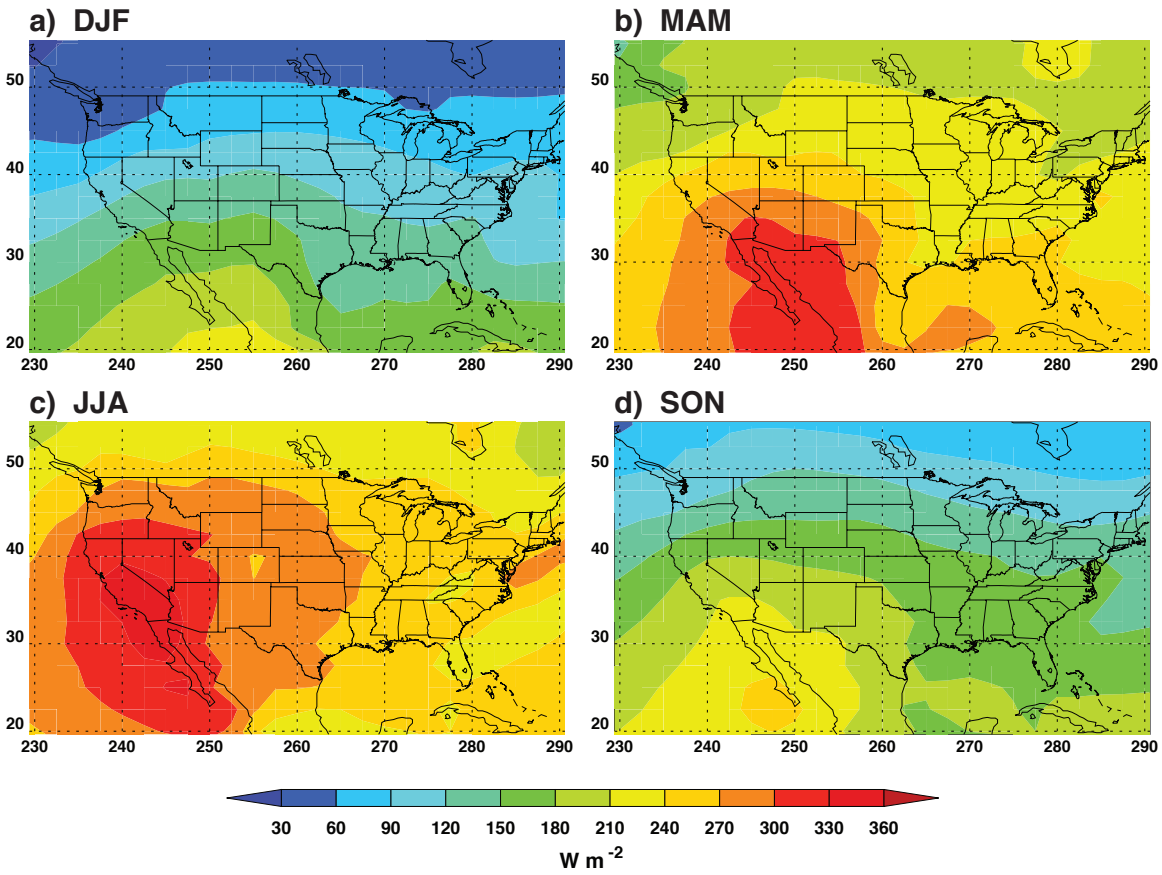


Figure 4.5. *Climatology of downwelling shortwave radiation in W m^{-2} rates in mm day^{-1} over the United States from NCEP for DJF (a), MAM (b), JJA (c), SON (d)*

fluxing water vapor into the atmosphere above.

The difference between precipitation and evapotranspiration (P-E) provides insight into the different roles that moisture flux convergence and evapotranspiration play in influencing the climatology of precipitation over the Great Plains. Figure 4.3c shows the seasonal cycle of P-E averaged over the Great Plains region from the VIC soil moisture model. From May through August, P-E is less than zero when evapotranspiration rates are greater than precipitation rates. At this time the excess of evapotranspiration over precipitation must be supplied by the moisture stored in the surface and subsurface soils. The moisture stored within the upper layer of the soils will primarily be depleted via

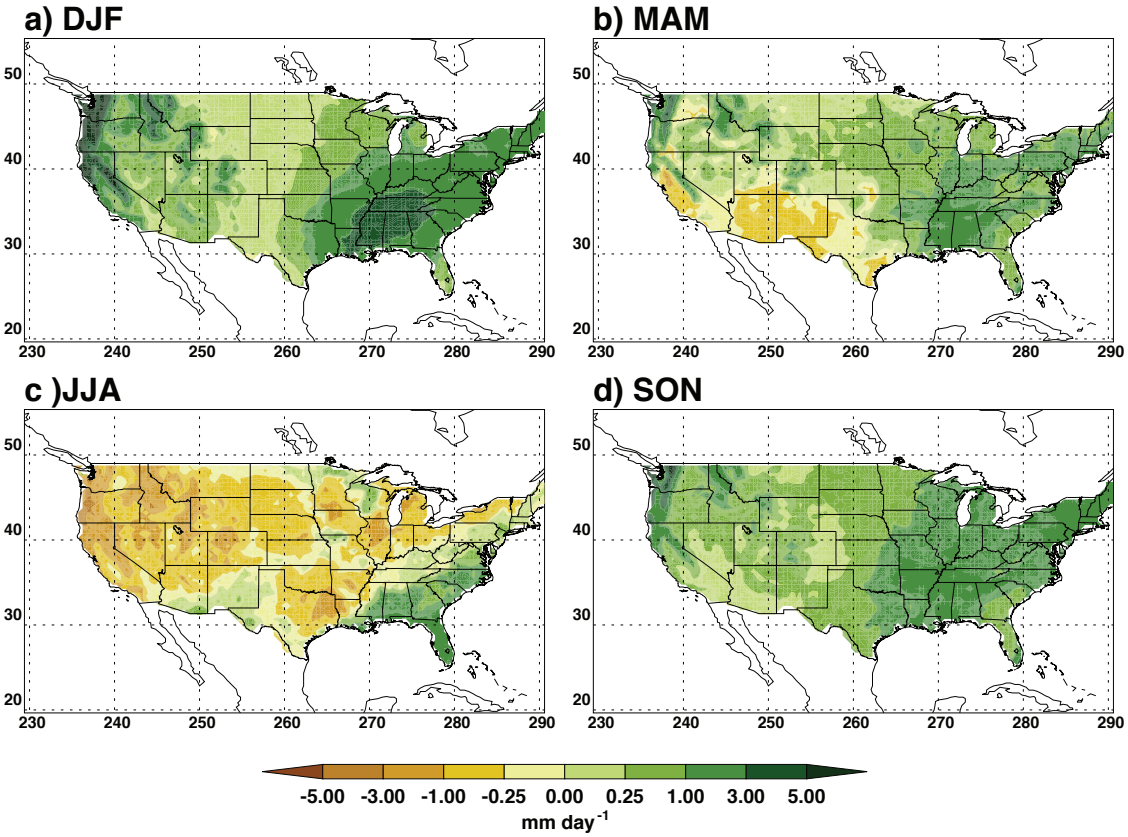


Figure 4.6. *Climatology of P-E in mm day^{-1} over the United States from VIC for DJF (a), MAM (b), JJA (c), SON (d)*

evaporation while subsurface soil moisture stores will be depleted by the plants as they take up water through their roots to help drive photosynthesis. Figure 4.3e shows that soil moisture stores are depleted from May through August, when the total column soil moisture content drops by over 60 mm. It is interesting to note that, while the minimum of P-E occurs in July, soil moisture stores continue to be depleted as long as E is greater than P, thus the minimum in soil moisture content does not occur until August. During the remainder of the year (September - April) precipitation exceeds evapotranspiration (P-E >0) and moisture flux convergence supplies this excess water. At the surface, the excess water that does not evaporate either recharges the soil moisture stores or flows out of the Great Plains region as runoff. From Figure 4.3f it is apparent that surface runoff is

low over this region compared to P, E, and P-E. Not surprisingly, runoff rates for the Great Plains region exhibit a similar seasonal cycle to both precipitation and evapotranspiration. When precipitation is low in the winter, runoff tends to be low and when precipitation rates increase in summer and early fall, runoff rates tend also to be large.

The spatial patterns for the climatology of P-E over the United States can be seen in Figure 4.6. P-E is generally greater than zero over most of the land surface of the United States throughout the annual cycle (with the exception of JJA). This implies that moisture must be supplied to the land surface from the oceans by the winds. During the summer (JJA), evapotranspiration tends to be greater than precipitation over much of the United States indicating that moisture is actually being fluxed from the land surface to the oceans.

Figure 4.7 shows the spatial patterns associated with the seasonal cycle of U.S. soil moisture content. Soil moisture content is spatially variable over the United States because it depends on both the soil type and the overall depth of the soil layers being considered and both of these parameters turn out to be highly heterogeneous over the United States. Seasonal variations in soil moisture content tend to be in phase with each other over the United States, with the soils typically drying out during the summer when evapotranspiration exceeds precipitation, and moistening during the winter when precipitation exceeds evapotranspiration. Over the Great Plains region of the United States, soils tend to be particularly dry during all months of the year at the intersection of Wyoming, Colorado and Nebraska.

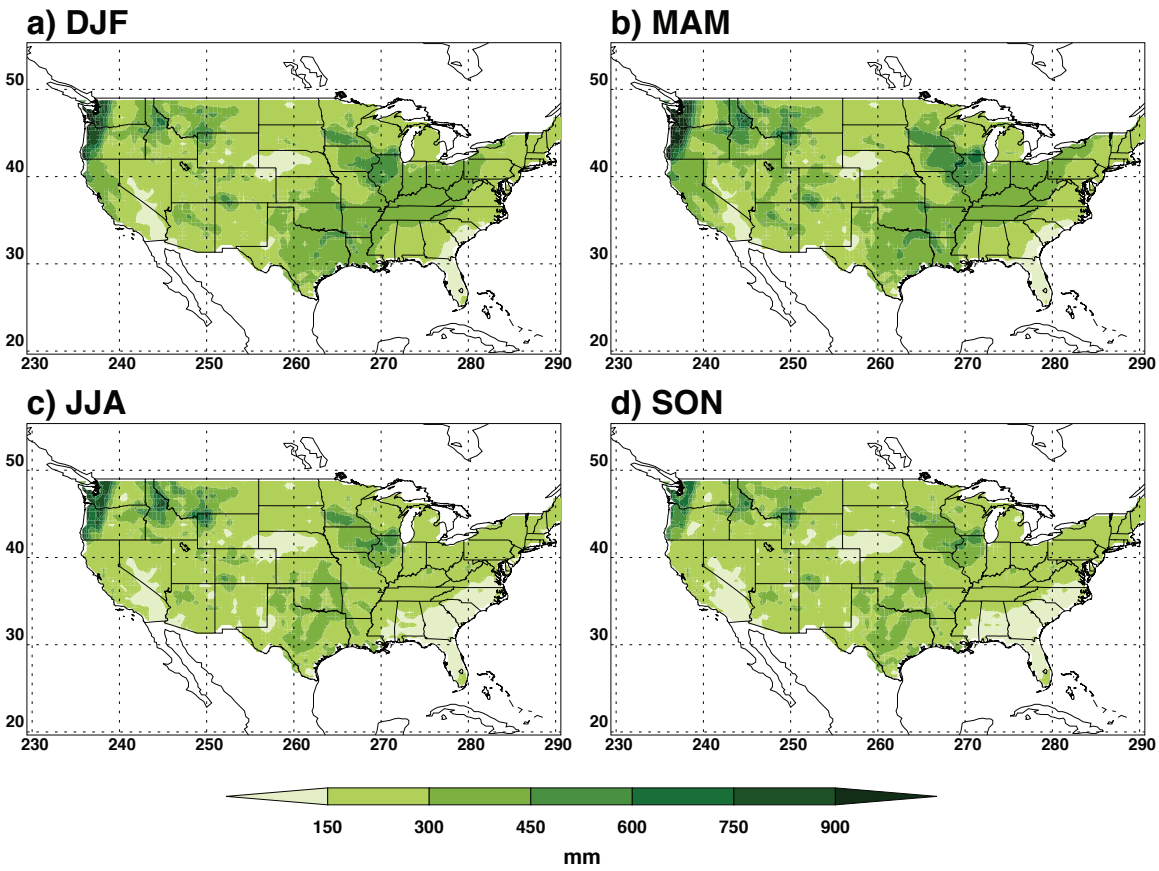


Figure 4.7. *Climatology of total column soil moisture content in mm over the United States from VIC for DJF (a), MAM (b), JJA (c), SON (d)*

From the above analysis it is apparent that precipitation, evapotranspiration and soil moisture content are closely related in the seasonal cycle, which is to be expected. In the following section, the relationships between these variables will be evaluated in the three CGCMs. The ultimate question that needs to be answered is whether or not the models accurately capture the seasonal cycle of these important hydrologic variables over the Great Plains. Before the variability of precipitation about the climatology can be investigated, the climatology itself must be well simulated. In order to test the validity of these models, the simulated climatologies of the 850 hPa winds, precipitation, evapotranspiration, P-E, soil moisture content, runoff and shortwave radiation will be compared with the observations.

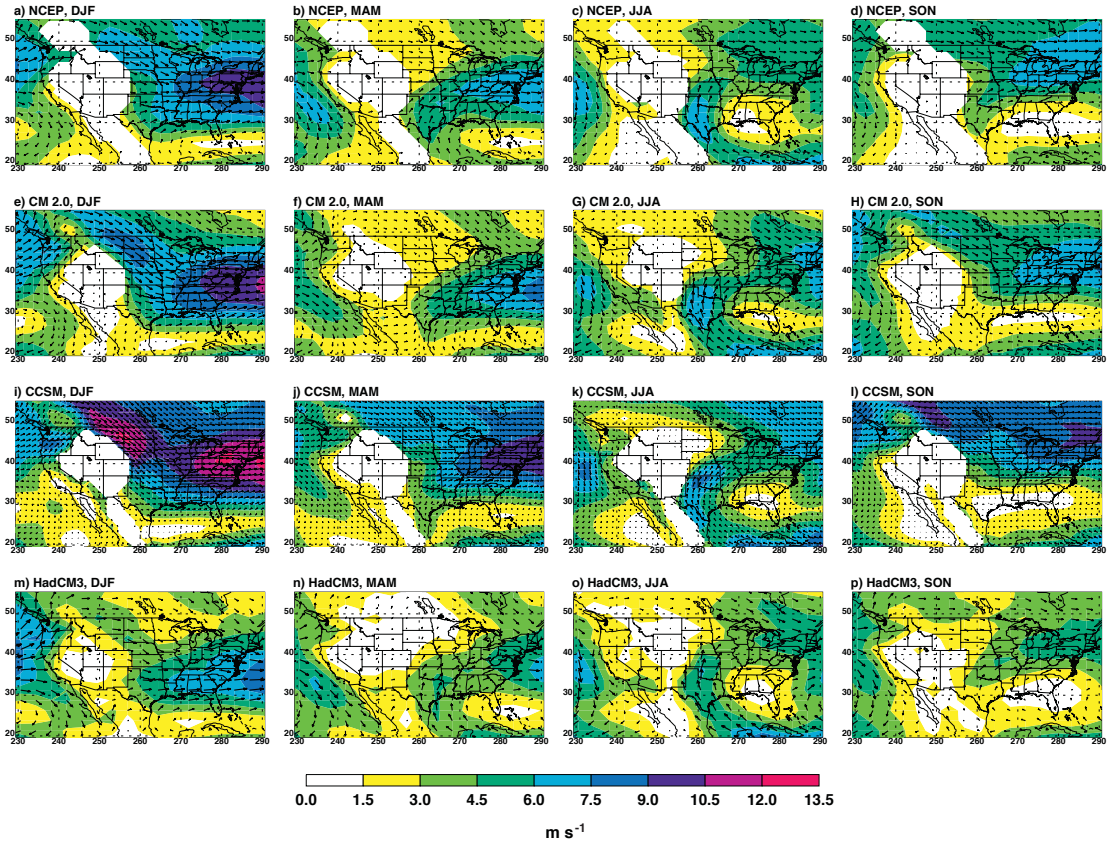


Figure 4.8. *850 hPa climatological winds over the United States for DJF(left most column), MAM (left center column), JJA (right center column) and SON (right most column), from NCEP reanalysis (a-d), CM 2.0 (e-h), CCSM3 (i-l) and HadCM3 (m-p).*

4.2 The Modeled Seasonal Cyle Over the Great Plains

4.2.1 850 hPa Winds

The climatolgies of the 850 hPa winds over the United States from NCEP, CM 2.0, CCSM3 and HadCM3 are shown in Figure 4.8. During DJF, much like the observations, in all three models, the Great Plains region is heavily influenced by a cold, dry arctic air mass that flows into the region from the Northwest. In CM 2.0 and CCSM3, this air mass appears to penetrate farther south into the Great Plains region that it does in the observations, but in HadCM3, this same air mass appears to have less of an impact on the region because the winds from the north are weaker (Figure 4.8 a, e, i and n). By

MAM, in NCEP, the Bermuda high starts to transition westward and the Great Plains region begins to be influenced by moisture transport from the Gulf of Mexico (Figure 4.8b). At this same time, the winds from the northwest begin to die down, although the Great Plains are still somewhat influenced by winds from the Arctic (Figure 4.8b). A similar transition of the Bermuda High also occurs in the three models, thus allowing the Great Plains region in each of the models to be influenced by the warm moist Tropical air mass that flows in from the Gulf of Mexico. The strength of the winds into the Great Plains from the Gulf of Mexico is the strongest in the CCSM3 model and slightly weaker in the CM 2.0 and HadCM3 models (Figure 4.8f, j and n). In contrast to the observations, during spring, the Great Plains region in CCSM3 is overly influenced by the Arctic air mass that flows in from the north (Figure 4.8 j), while in the HadCM3 model, the winds from the north do not even enter the Great Plains (Figure 4.8 n). In the summer (JJA) all three models and the observations are strongly influenced by the air mass that flows in from the Gulf of Mexico (Figure 4.8 c, g, o and s). This air mass brings with it lots of moisture, so precipitation rates are expected to be high during JJA in the models. Finally, in Fall (SON), as with the observations, the Great Plains region in all three models, is primarily influenced by an air mass that flows into the region from the Pacific (Figures 4.8d, h, l, and p). The seasonal transitions in the dominant air masses that influence the Great Plains regions in all three GCMs are similar to what has been observed. The next question to be answered is, how well do the models capture the seasonal cycle of precipitation over the Great Plains, remembering that the large-scale winds are not the only factor that influence precipitation rates over the Great Plains, but they are also

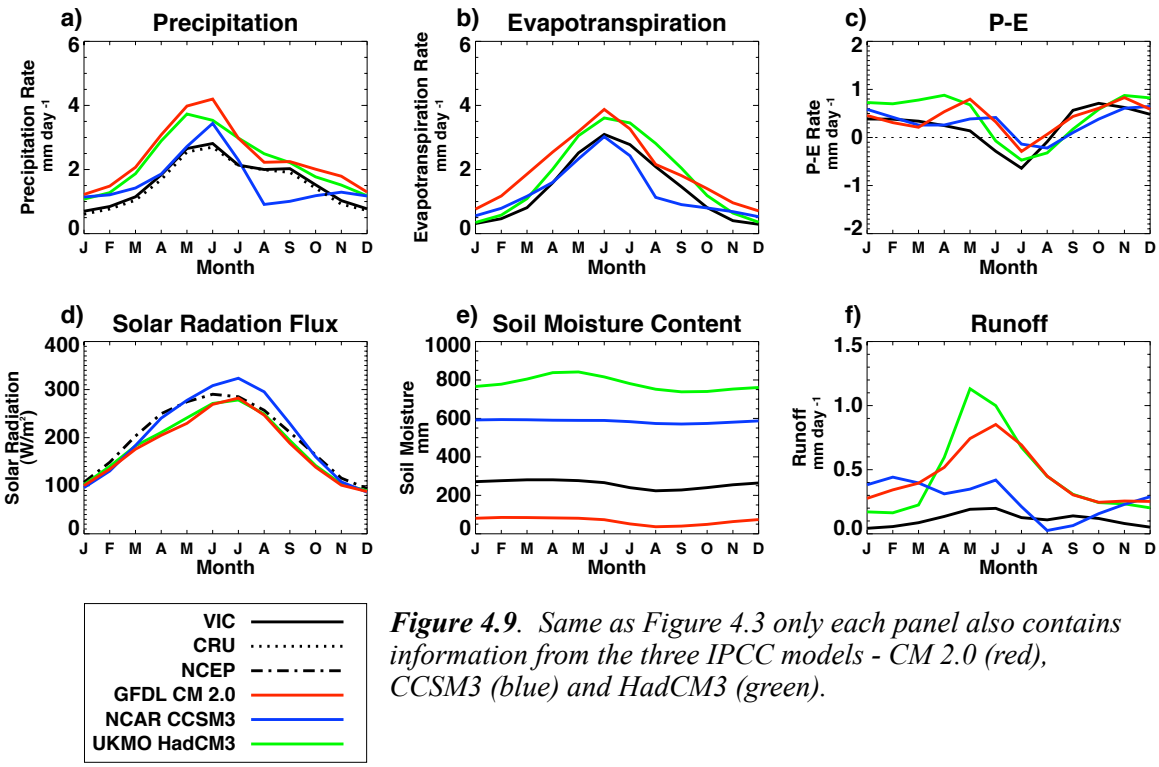


Figure 4.9. *Same as Figure 4.3 only each panel also contains information from the three IPCC models - CM 2.0 (red), CCSM3 (blue) and HadCM3 (green).*

influenced by evaporation.

4.2.2 Precipitation

Precipitation is generally a difficult variable for climate models to simulate because most precipitation occurs on spatial scales that are smaller than the gridboxes used in the models (Airey and Hulme, 1995). Also, precipitation rates are often influenced by fine-scale local topography that global circulation models with coarse (multi-degree) resolution are unable to resolve (Hughes, 2007). Figure 4.9a shows the time series for precipitation averaged over the Great Plains region from CRU TS 2.1, VIC, CM 2.0, CCSM3, and HadCM3 and Figure 4.10 shows the spatial patterns of the climatology of precipitation over the United States for all four seasons from the same data sets.

The seasonal cycle of precipitation averaged over the Great Plains as simulated by the three models, is somewhat similar to the observed seasonal cycle (Figure 4.9). Much

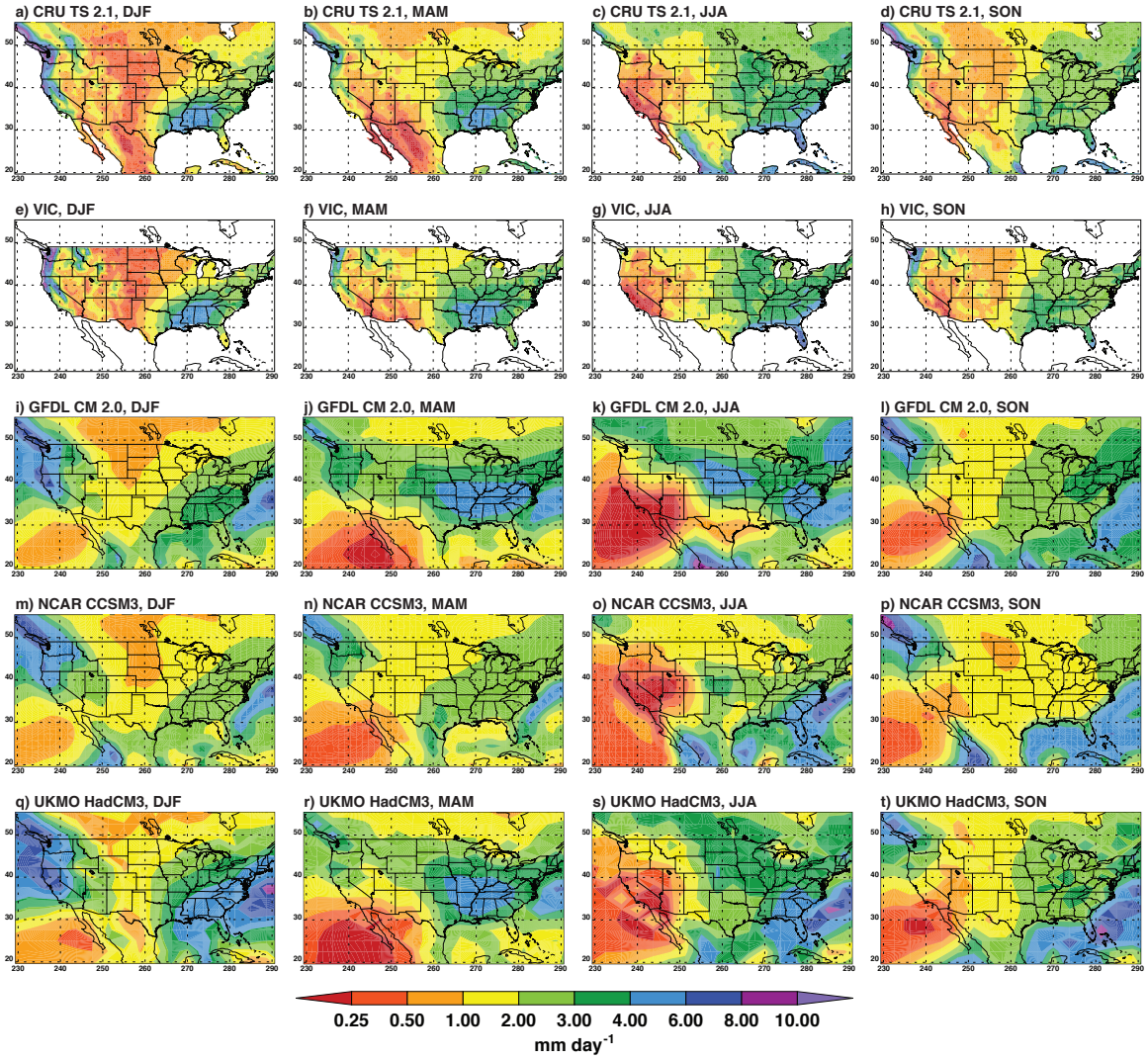


Figure 4.10. *Climatology of precipitation over the United States for DJF(left most column), MAM (left center column), JJA (right center column) and SON (right most column), from CRU TS 2.1(a-d), VIC (e-h), CM 2.0 (i-l) and CCSM3 (m-p) and HadCM3 (q-t).*

like the observations, all three models show marked seasonality throughout the year, with high precipitation rates in spring and summer and low precipitation rates in fall and winter. Unfortunately, each model does experience some difficulty in representing the exact timing and magnitude of the variations in the seasonal cycle of precipitation over the Great Plains.

All three models overestimate precipitation rates for the Great Plains in late fall, winter and early spring (November – March) (Figures 4.9a and 4.10). This because the models do not capture the magnitude of the topography of the mountain ranges to the west of the Great Plains and so the "rainshadow" effect of the Rocky Mountains tends to be poorly represented by the models. When the Great Plains are influenced by winds from the west, precipitation rates should drop over the region because most of the moisture is precipitated out of the air as it passes over the mountains. In each model, precipitation rates do drop off significantly during the dry months, but they do not get as low as in the observations. Poor resolution of the topography of the United States also explains why the models tend to underestimate precipitation rates over the Pacific Northwest sector of the U.S. during DJF (Figure 4.10 a, e, i, m and q). In this region, precipitation is typically orographically induced when moist air is forced up the windward side of a mountain thus causing the air to cool, water vapor in the air to condense, and precipitation to fall to the surface. To first order, orographic precipitation can be considered a function of the slope of the local topography (Hughes, 2007). Since the climate models used in this study do not accurately represent the slope and elevation of the topography in the Pacific Coast Range, precipitation rates in this region tend to be less than observed.

Over the Great Plains, both CM 2.0 and HadCM3 also overestimate precipitation rates throughout the remainder of the seasonal cycle (April-October). In fact, the maximum in precipitation that occurs in CM 2.0 is almost twice what is observed for the region in CRU TS 2.1 (Figure 4.9). From Figure 4.10 j, k, r, and s it is apparent that

precipitation rates in both CM 2.0 and HadCM3 tend to be too large in the northern part of the Great Plains. These anomalies dominate the magnitude of the average precipitation rates for the entire region in the spring and early summer. It is possible that precipitation rates in these models are too large in the spring because too much moisture is being fluxed into the region by the winds (Figure 4.8). Interestingly, HadCM3 also misrepresents the timing of the maximum in precipitation in this region, showing that it occurs in May rather than June (Figure 4.9a).

CCSM3 has difficulty capturing the timing of the seasonal cycle of precipitation. In this model, a dramatic drop in precipitation occurs between July and August. In this case, precipitation rates fall below 1 mm day^{-1} in August and remain significantly less than the observed until November. Abnormally low precipitation rates in SON are not unique to the Great Plains region of CCSM3. Figure 4.10p shows that precipitation rates are also low over the Midwestern and Eastern parts of the United States during the fall season. It is possible that mesoscale convective complexes, which typically cause late summer precipitation over the Great Plains, are not well parametrized in this model.

In summary, it appears that both CM 2.0 and HadCM3 tend to overestimate Great Plains precipitation during all months of the year, while CCSM3 misrepresents the timing of the seasonal cycle of Great Plains precipitation. In the next section the seasonal cycle of evapotranspiration over the Great Plains is evaluated in the models. Remember that precipitation and evapotranspiration tend to be tightly coupled over this region so we expect the models to exhibit similar problems.

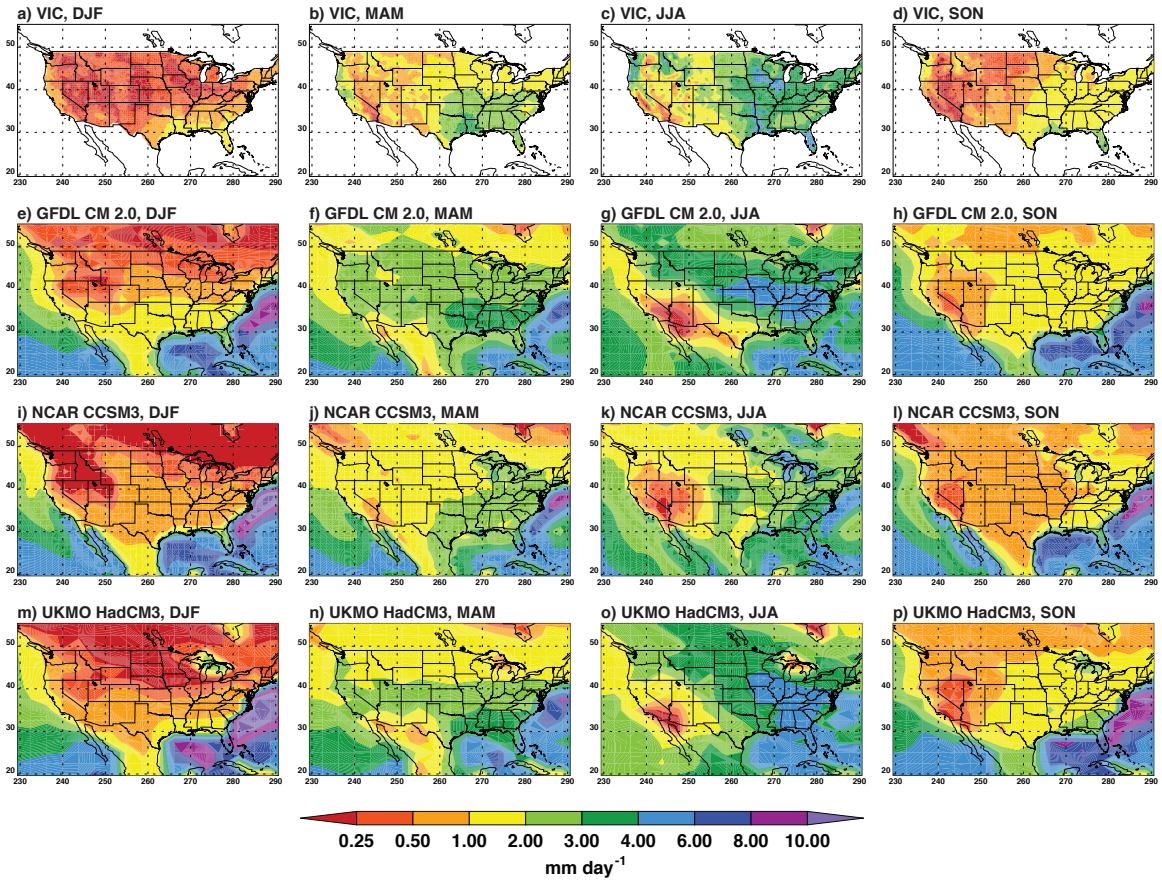


Figure 4.11. *Climatology of evapotranspiration over the United States for DJF(left most column), MAM (left center column), JJA (right center column) and SON (right most column), from, VIC (a-d), CM 2.0 (e-h) and CCSM3 (i-l) and HadCM3 (n-p).*

4.2.3 Evapotranspiration

Much like precipitation, evapotranspiration from the land surface is a difficult variable for climate models to simulate accurately. Part of the problem is that we still lack sufficient knowledge about the physical processes involved with evaporation and transpiration at the surface. But a more significant problem that the models face is that the land surface is very heterogeneous and evapotranspiration rates are highly dependent on differences in vegetation cover and soil moisture that occur on spatial scales that are much smaller than the average GCM grid box (Hostetler, 1994). In this section, evapotranspiration rates, as simulated by the three CGCMs, are compared with results

from the VIC soil moisture model. It is important to note that although the VIC model has a much finer spatial resolution than the CGCMs, it is still a model, and many of the microscopic processes that are associated with evaporation and transpiration must be still be parameterized. Unfortunately, evapotranspiration rates are also difficult to measure in the real world, thus the VIC soil moisture model is the closest representation we have to "observed" evapotranspiration rates.

Figure 4.9b shows the time series for evapotranspiration averaged over the Great Plains region from VIC, CM 2.0, CCSM3, and HadCM3 while Figure 4.11 shows the

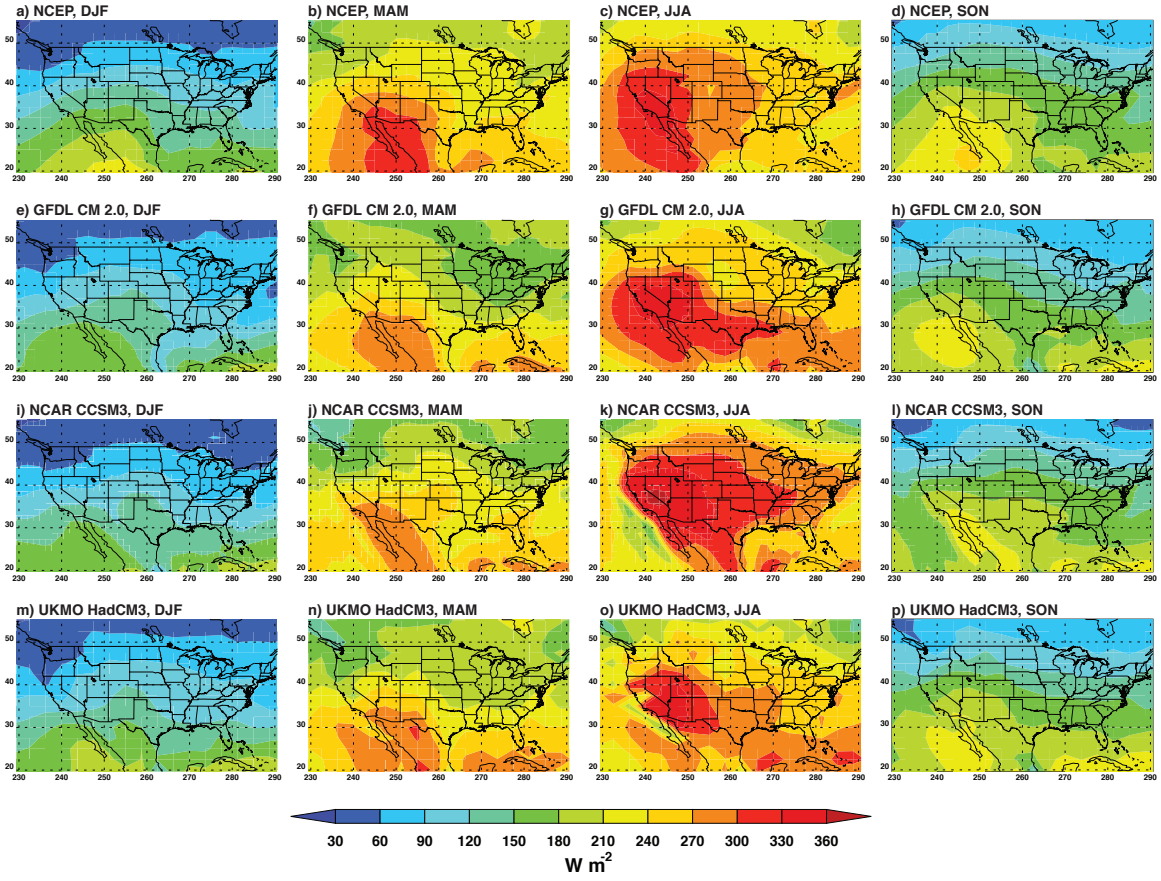


Figure 4.12. *Climatology of downwelling shortwave radiation over the United States for DJF(left most column), MAM (left center column), JJA (right center column) and SON (right most column), from NCAR (a-d), CM 2.0 (e-h) and CCSM3 (i-l) and HadCM3 (n-p).*

spatial patterns of the climatology of evapotranspiration over the United States from the same data sets. Evapotranspiration rates in the VIC model and the three CGCMs exhibit a similar seasonal cycle to precipitation over the Great Plains, with high evapotranspiration rates occurring in spring and summer and lower evapotranspiration rates occurring in fall and winter (Figure 4.9b). Remember that evapotranspiration rates are influenced by surface moisture content, energy availability and photosynthesis thus it makes sense that evapotranspiration rates are largest in spring and summer when both precipitation rates (Figure 4.9a) and downwelling solar radiation flux at the surface are high (Figure 4.9d). Unfortunately, the models also have difficulty accurately capturing the timing and magnitude of the seasonal cycle evapotranspiration, much like they did with precipitation.

CM 2.0 overestimates evapotranspiration rates over the Great Plains in all months of the annual cycle (Figure 4.9b). During DJF, CM 2.0 appears to overestimate evapotranspiration rates in the southern Great Plains region (Figure 4.11e). This may be due, in part, to too much short wave radiation reaching the surface (Figure 4.12e). In MAM, JJA and SON, CM 2.0 overestimate evapotranspiration in regions where precipitation rates are also too high (Figures 4.10 f-h and 4.11 f-h). For example in MAM and JJA, over the Great Plains, regions of enhanced evapotranspiration correspond exactly with regions of enhanced precipitation. Although it is difficult to determine causality between changes in precipitation and evapotranspiration, it is apparent that two variables are closely related in this model.

HadCM3 also overestimates evapotranspiration rates throughout most of the seasonal cycle, except in December and January, when evapotranspiration rates in HadCM3 dip down as low as the evapotranspiration rates simulated by the VIC model (Figure 4.9). Evapotranspiration rates in HadCM3 tend to be excessively large in summer between June and September. Much like in CM 2.0, excessive evapotranspiration rates in HadCM3 correspond with regions that experience excessively high precipitation rates.

CCSM3 experiences a large drop in evapotranspiration between the months of June – August (Figure 4.9b). As discussed in section 4.2.2, decreases in evapotranspiration correspond with similar drops in precipitation rates over the Great Plains. It is possible that this drop in evapotranspiration causes precipitation rates over the Great Plains to plummet, but it is also possible that decreases in precipitation over the region reduce surface moisture availability and cause evapotranspiration rates to decrease. The relationship between precipitation and evapotranspiration will be further discusses in the next section by looking at the difference between precipitation and evapotranspiration over the Great Plains throughout the seasonal cycle.

4.2.4 P-E

The difference between precipitation and evapotranspiration over the Great Plains indicates whether moisture is being converged into the region by the winds (P-E > 0) or if moisture is being diverged or transported out of the region by the winds (P-E <0). Comparing the climatology of P-E in the models indicates when abnormal moisture flux convergence occurs over the Great Plains during the modeled seasonal cycles.

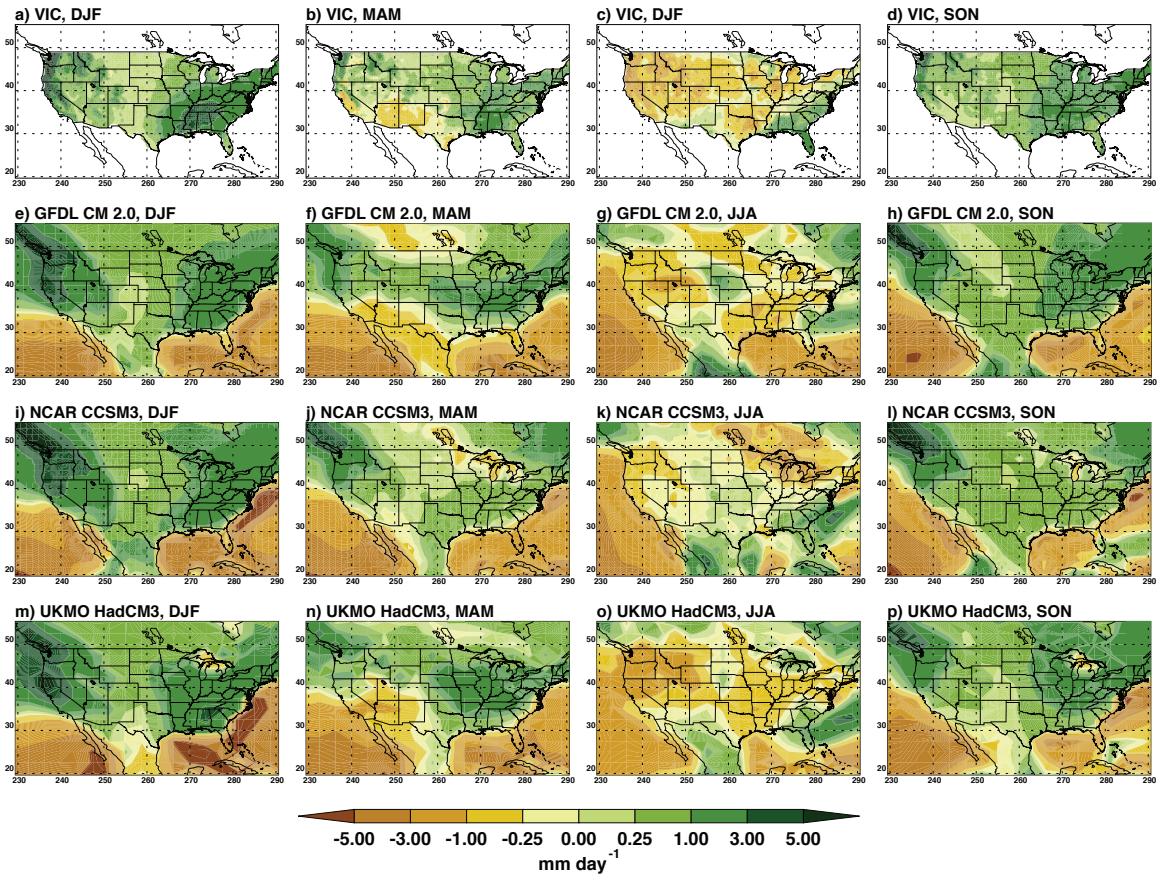


Figure 4.13. *Climatology of P-E over the United States for DJF(left most column), MAM (left center column), JJA (right center column) and SON (right most column), from VIC (a-d), CM 2.0 (e-h) and CCSM3 (i-l) and HadCM3 (n-p).*

Figure 4.9c shows the time series for P-E averaged over the Great Plains region from VIC, CM 2.0, CCSM3, and HadCM3 while Figure 4.13 shows the spatial patterns of the climatology of P-E over the United States from the same data sets.

Overall the models capture the general pattern of the seasonal cycle of P-E over the Great Plains, but much like precipitation and evapotranspiration themselves, the models have some difficulty reproducing the exact time series and spatial variability of the climatology of P-E.

Both CCSM3 and HadCM3 overestimate how much larger P is than E during the winter (DJF). HadCM3 also overestimates the difference between P and E during the

spring (MAM). P-E is well captured during DJF in CM 2.0, but abnormal growth of P over E occurs in HadCM3 during MAM. In fact, in the observations, P-E first drops below zero in May, while P-E actually experiences a maximum in May in CM 2.0.

In the VIC model, E is greater than P from May-August, when surface moisture and energy availability are both high. Although all three models also experience negative values of P-E during the summer, the exact timing and extent of the surplus of E over P is different in each model. For example CM 2.0 only experiences negative vales of P-E in July and this minimum in P-E over the Great Plains is half that seen in the VIC soil moisture model. Anomalous convergence of moisture over the Central Great Plains (Figure 4.13 h and g) is most likely to blame for the problems CM 2.0 has in representing the seasonal cycle of P-E during spring and summer. During fall and early winter, the models are in general agreement with each other as as precipitation rates gradually overtake evapotranspiration rates over the Great Plains. When reading the following sections keep in mind that the difference between precipitation and evapotranspiration is closely tied to changes in soil moisture content and runoff throughout the annual cycle.

4.2.5 Soil Moisture

Total column soil moisture content is an ambiguously defined variable which represents the total amount of water stored within the entire column of soil below the surface. Total column soil moisture (or from now on just soil moisture content) is highly dependent on a number of factors, which include but are not limited to; the soil type, the porosity of the soil, the ratio of soil infiltration to runoff, and the total depth of the soil column being considered. Soil moisture content can also be influenced by vegetation

cover of a region and the intensity of the precipitation that falls over the region. These parameters are prescribed in the models, and it has proven difficult to determine exactly how they vary among the different models.

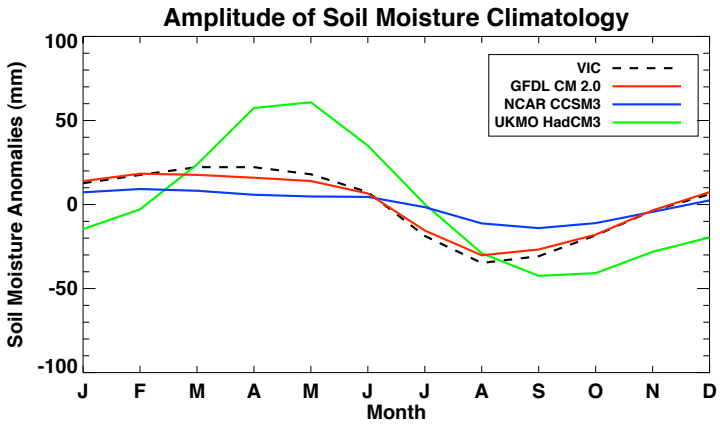


Figure 4.14. *Climatological anomalies in soil moisture content averaged over the Great Plains in mm from, VIC (black dashed), CM 2.0 (red), NCAR CCSM 3 (blue), UKMO HadCM (green).*

From Figure 4.9e it is apparent that the VIC soil model, CM 2.0, CCSM3 and HadCM3 all treat soil moisture differently. For example over the Great Plains, in the VIC model, average soil moisture concentrations are approximately 270 mm, while in the CGCMs, average soil moisture content ranges from up to 750 mm in HadCM3 down to only 180 mm in CM 2.0. Unfortunately reliable in situ measurements of soil moisture content are hard to come by, so it is difficult to determine which of the models most accurately represents the average soil moisture content over the Great Plains.

Putting aside these differences, what we actually want to compare between the models is the magnitude and the timing of the variations in soil moisture content throughout the seasonal cycle. To do this, the time mean of the climatology of soil moisture is removed from the seasonal cycle of each model. This leaves only the changes in soil moisture content that occur throughout the annual cycle. The time series plots for the anomalies in soil moisture content that occur throughout the seasonal cycle are shown

in Figure 4.14. Remember that soil moisture is typically depleted when evapotranspiration is greater than precipitation and soil moisture is replenished when precipitation is greater than evapotranspiration.

The variability of soil moisture content over the Great Plains in the seasonal cycle is largest in the HadCM3 model. In this model, a there is 100 mm change in soil moisture content between its maximum in May of 840 mm and its minimum in September of 740. The CCSM3 model, on the other hand, experiences the least amount of variability in the seasonal cycle of soil moisture content over the Great Plains. In this model, the amplitude of the seasonal cycle of precipitation only varies by 15 mm. Although the CM 2.0 model has some difficulty accurately capturing the climatology of P-E over the Great Plains, this model most accurately captures the timing and the magnitude of the changes in soil moisture content when compared to the VIC model. It is possible that surface runoff can explain the discrepancies between P-E and soil moisture in this model, and will be discussed in the next section.

Spatial maps for the seasonal cycle of soil moisture content for the United States are shown in Figure 4.15. Note the differences in the magnitudes of soil moisture content in each of the figures. The general patterns in the spatial variability of soil moisture over the United States are similar in the models compared to VIC. As expected, the Pacific North West region tents to exhibit high soil moisture concentrations, the Great Basin and the Central United States tends to have low soil moisture concentrations, and then soil moisture concentrations are high again over the Eastern United States in New England and the South. Of the three models, on CCSM3 represents the low soil moisture

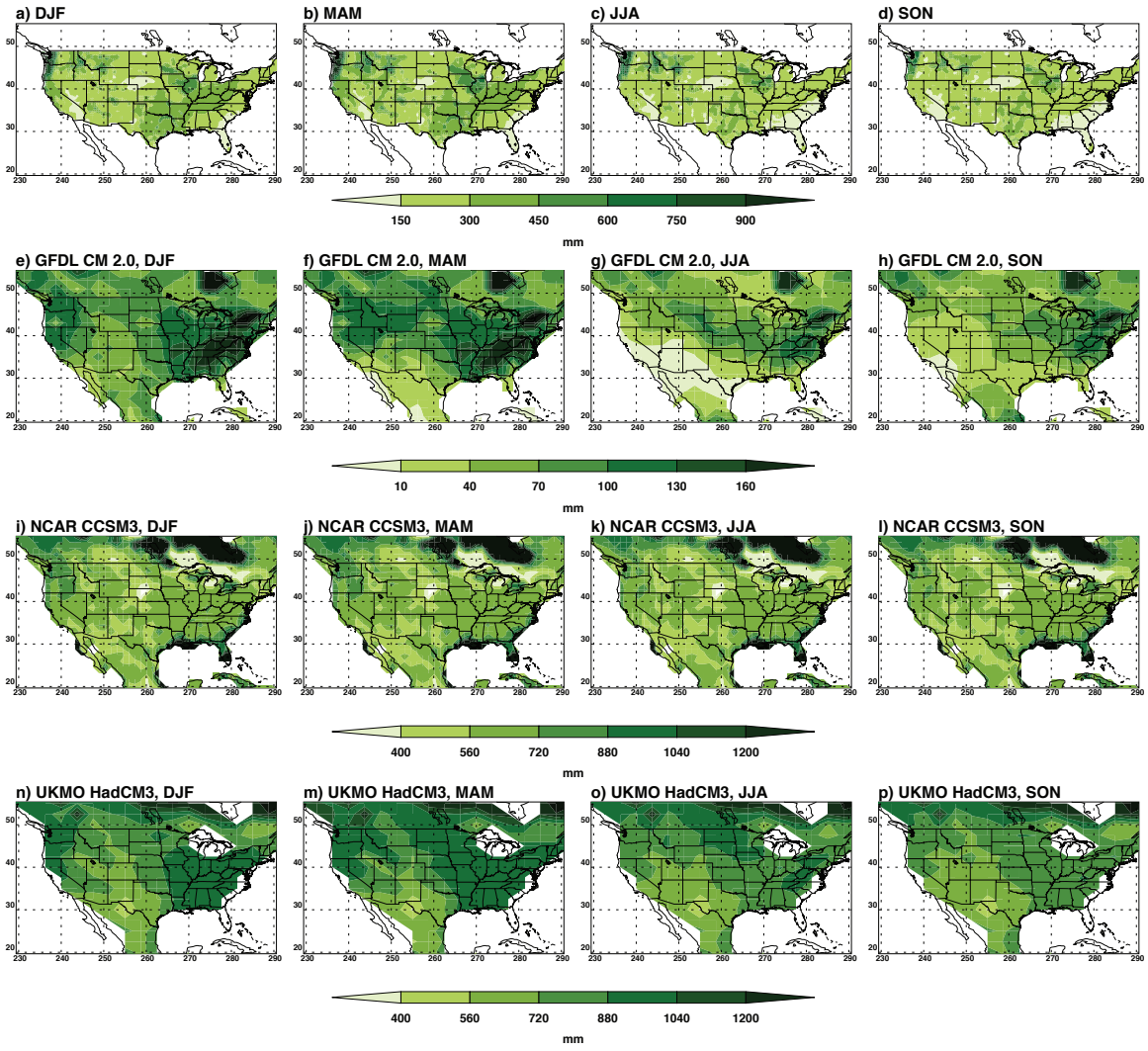


Figure 4.15. *Climatology of total column soil moisture content over the United States for DJF(left most column), MAM (left center column), JJA (right center column) and SON (right most column), from VIC (a-d), CM 2.0 (e-h) and CCSM3 (i-l) and HadCM3 (n-p).*

conditions that occur in the Central Great plains over Nebraska. Throughout the annual cycle, the spatial variability in soil moisture remains similar in the modes, but the soils do tend to dry out during summer when evapotranspiration is greater than precipitation, and the soils moisten in spring when P is greater than E.

4.2.6 Runoff

As with the observations, runoff (which includes both surface runoff and

subsurface drainage) in the models exhibits a similar seasonal cycle to precipitation and evapotranspiration. In the spring when precipitation generally exceeds evapotranspiration, moisture is being converged in the Great Plains region by the winds, and snow at the surface beings to melt, runoff out of the Great Plains is high. In the summer and early fall, when evapotranspiration over takes precipitation and moisture is generally fluxed out of the Great Plains region by the winds, runoff tens to be low. Both CM 2.0 and HadCM3 greatly overestimate the amplitude of the seasonal cycle of runoff, which is especially large in the spring in these models. In CCSM3, runoff also exhibits an unrealistic drop of in late summer, similar to the decreases seen in precipitation and evapotranspiration in this model.

4.3 Summary

In this chapter we have compared the simulated climatology of the hydrologic cycle of the Great Plains from the models with observations. We argue that the models must first be able to represent the seasonal cycle of precipitation over the Great Plains, before they should used in studies involving drought. The main findings from this chapter are as follows.

- The models all capture the broad features of the hydrologic cycle of the Great Plains. In the models and the observations, the annual cycle of precipitation can be divided in to two distinct seasons, a wet season that extends from approximately April through September and a dry season that extends from October through March.

- The models accurately represent the seasonally varying climatology of the 850 hPa winds over the United States. Much like in the observations, the Great Plains region in the models is influenced by a cold dry arctic air mass during the winter and a warm moist tropical air mass that flows in from the Gulf of Mexico during the summer. The 850 hPa winds are generally to strong in CCSM3 and to weak in HadCM3 which may influence the flux of moisture into the Great Plains region in both of these models.
- The magnitude of the seasonal variations in the hydrologic cycle are too extreme in CM 2.0 and HadCM3. Both, CM 2.0 and HadCM3 overestimate the amplitude of the annual cycles of precipitation, evapotranspiration and runoff. HadCM3 also over estimates the amplitude of the annual cycle of soil moisture. The strength hydrologic cycle of the Great Plains appears to be much larger in these models compared to what has been observed.
- In CCSM3 the hydrologic cycle of the Great Plains crashes in late summer when precipitation, evapotranspiration and runoff all experience unrealistically large decreases between the months of July and August. Diagnosing this problem will require further research and other model experiments. This may influence the variability of Great Plains precipitation during the late summer and early fall.
- All of the models overestimate winter precipitation rates because the rainshadow effect of the Rocky Mountains is not well reproduced in the models.
- Total Column Soil Moisture content differs significantly between the three models and from the VIC soil moisture model. Differences in the total depth of the soil

column in each model as well as the theoretical holding capacity of water in the soils may impact total column soil moisture content calculations.

Although the models do have some trouble capturing the details of the hydrologic cycle of the Great Plains, we argue that they do a reasonably good job representing the broad features of annual cycle and so, therefore, can be used in studies involving the variability about the seasonal mean. In the next chapter we discuss the model's abilities to represent the observed variability of Great Plains precipitation that occurred during the 20th century. Its important to keep in mind that CM 2.0 and HadCM3 overestimate mean precipitation rates over the Great Plains during all months of the year, and that CCSM3 does not maintain high precipitation rates throughout the course of the summer.

Chapter 5

Great Plains Precipitation Variability

The goal of this chapter is to evaluate the ability of the models to represent the general characteristics of Great Plains precipitation variability. The chapter begins with a discussion of the temporal variability of precipitation by examining the time series of monthly mean precipitation anomalies, annual mean precipitation anomalies, wet season mean precipitation anomalies, and dry season mean precipitation anomalies. This is followed by an evaluation of the distribution of precipitation over the Great Plains and a discussion of the occurrence of extreme wet and dry events. The chapter ends with a discussion of the lengths of wet and dry events and touches on the idea of persistence in the precipitation time series. We chose to examine the results from each individual model integration, rather than the ensemble mean. This is because we are looking at fully coupled integrations that are only constrained by historical time series of 20th Century Green House Gas emissions and volcanic eruptions. Averaging over all model integrations would remove most of the variability we are trying to investigate.

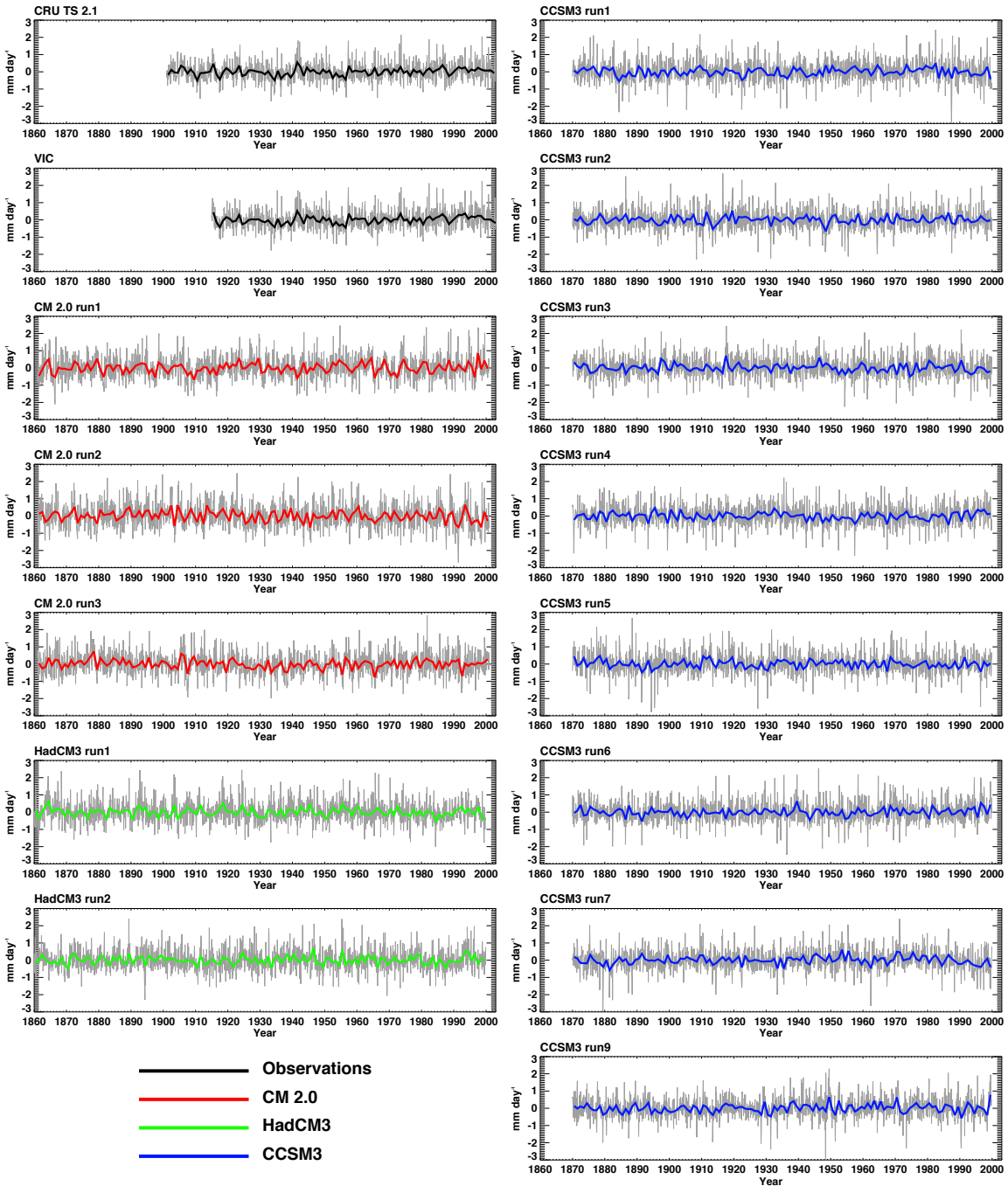


Figure 5.1. *Time series of monthly mean precipitation anomalies (grey curves) and annual mean precipitation anomalies (colored curves) averaged over the Great Plains. Results are from from the two observational data sets used in this study (black) and the models: CM 2.0 (red), HadCM3 (green), CCSM3 (blue). Monthly mean precipitation anomalies were created by removing the seasonal mean from the time series. Annual mean precipitation anomalies were created by averaging precipitation over each year and then removing the arithmetic mean. Units for all precipitation anomalies are in mm day^{-1}.*

5.1 Variability of Precipitation

5.1.1 Variability of Monthly Mean Precipitation Anomalies

Monthly mean precipitation averaged over the Great Plains region is highly variable. This variability can be seen graphically in the time series plots shown in Figure 5.1 (gray lines) and numerically by the standard deviations given in Table 5.1. We use the standard deviation or the root mean square (RMS) deviation of the precipitation anomalies as a measure of variability because the standard deviation measures how widely spread the anomalies are from the mean. The monthly mean precipitation anomalies discussed in this section were created by removing the seasonal cycle of precipitation from the time series. Therefore in this section we are primarily discussing the variability of precipitation about the annual cycle.

Figure 5.1 and Table 5.1 show that the models tend to overestimate the variability in monthly mean precipitation for the Great Plains. This is especially true for CM 2.0. While in the observations the standard deviation of monthly mean precipitation ranges from 0.518 - 0.536 mm day $^{-1}$, depending on the data set, in CM 2.0 standard deviations range from 0.614 - 0.675 mm day $^{-1}$, depending on the model integration. CCSM3 and HadCM3 also over estimate the variability of precipitation, but to a lesser extent than CM 2.0.

The overall magnitude of the precipitation anomalies in the time series can also provide some insight into the variability of precipitation about the seasonal mean. We evaluate the magnitude of the precipitation anomalies in two different ways. First we compare the overall amplitude of the precipitation anomalies by calculating the difference

Data Set		Standard Deviation	Range (min - max)	Amplitude	mean negative anomaly	mean postive anomaly
CRU TS 2.1		0.518	-1.709 - 2.147	3.856	-0.360	0.428
VIC		0.536	-1.772 - 2.242	4.014	-0.382	0.443
CM 2.0	run 1	0.614	-2.107 - 2.457	4.564	-0.470	0.528
	run 2	0.675	-2.692 - 2.486	5.178	-0.498	0.551
	run 3	0.622	-1.980 - 2.832	4.812	-0.467	0.506
CCSM3	run 1	0.609	-2.979 - 2.424	5.403	-0.432	0.501
	run 2	0.587	-2.305 - 2.697	5.002	-0.420	0.480
	run 3	0.595	-2.254 - 2.438	4.692	-0.431	0.505
	run 4	0.592	-2.306 - 2.216	4.522	-0.438	0.482
	run 5	0.604	-2.785 - 2.666	5.451	-0.425	0.490
	run 6	0.594	-2.477 - 2.529	5.006	-0.424	0.490
	run 7	0.590	-2.945 - 2.400	5.345	-0.432	0.459
	run 9	0.594	-3.104 - 2.296	5.400	-0.424	0.488
HadCM3	run 1	0.601	-2.001 - 2.452	4.453	-0.431	0.484
	run 2	0.590	-2.294 - 2.410	4.704	-0.412	0.503

Table 5.1. *Table of statistical values used to measure the variability of the time series of monthly mean precipitation anomalies. Variables shown include: the standard deviation (second column), the range of maximum to minimum precipitation anomalies (third column), the amplitude of total precipitation anomalies (fourth column), the average deviation of negative anomalies from the mean (fourth column), and the average deviation of positive anomalies from the mean(fifth column). Units of all statistical variables is in mm day^{-1}.*

between the minimum precipitation anomaly and maximum precipitation anomaly in each time series. Second, we look at the average deviation of the negative and positive anomalies from the mean in each time series. Values for the amplitude, range and the average deviations can also be found in Table 5.1.

In the observations, precipitation anomalies range from -1.709 - 2.147 mm day $^{-1}$ for a total amplitude of 3.856 mm day $^{-1}$. The average deviation of the negative anomalies from the mean is approximately -0.360 mm day $^{-1}$ while positive anomalies are on average approximately 0.428 mm day^{-1} away from the mean. These results indicate that positive anomalies tend to be larger than negative anomalies in the observations which can be expected given that precipitation has a lower limit of zero and has no upper limit.

In all of the simulations performed with the three models, the magnitude of the

monthly mean precipitation anomalies for the Great Plains is overestimated. Also, all of the simulations overestimate the mean of the negative anomalies, the mean of the positive anomalies and the overall range of possible anomalies. This is especially true for CCSM3 Run 5, in which the precipitation anomalies range from -2.785 - 2.666 mm day $^{-1}$ with an amplitude that is 1.6 mm day $^{-1}$ larger than the observations. The magnitude of the negative anomalies simulated in these models appears to be especially large. This may be due to the fact that the magnitude of negative anomalies is proportional to the mean and mean precipitation tends to be larger in the models than the observations (Chapter 3).

In general, the models overestimate the dispersion of the monthly precipitation time series. Therefore, we can expect precipitation anomalies to be more extreme in the CGCM representations of the 20th Century Climate than was observed. Of the three models, CM 2.0 does the worst job in capturing the observed variability of monthly mean precipitation, while HadCM3 does the best job. With its large ensemble size, CCSM3's representation of the variability of Great Plains precipitation lies someplace in between these two models, with some integrations closely capturing the observed variability (Run 3 and Run 4), and others greatly overestimating it (Run 1 and Run 5).

Interestingly, the variability of precipitation turns out to be highly dependent on the time of year, and tends also to be a function of mean precipitation rate. Figure 5.2 shows the seasonal cycle of the standard deviation of precipitation for each month of the year. In the observations, the seasonal cycle of precipitation variability exhibits a

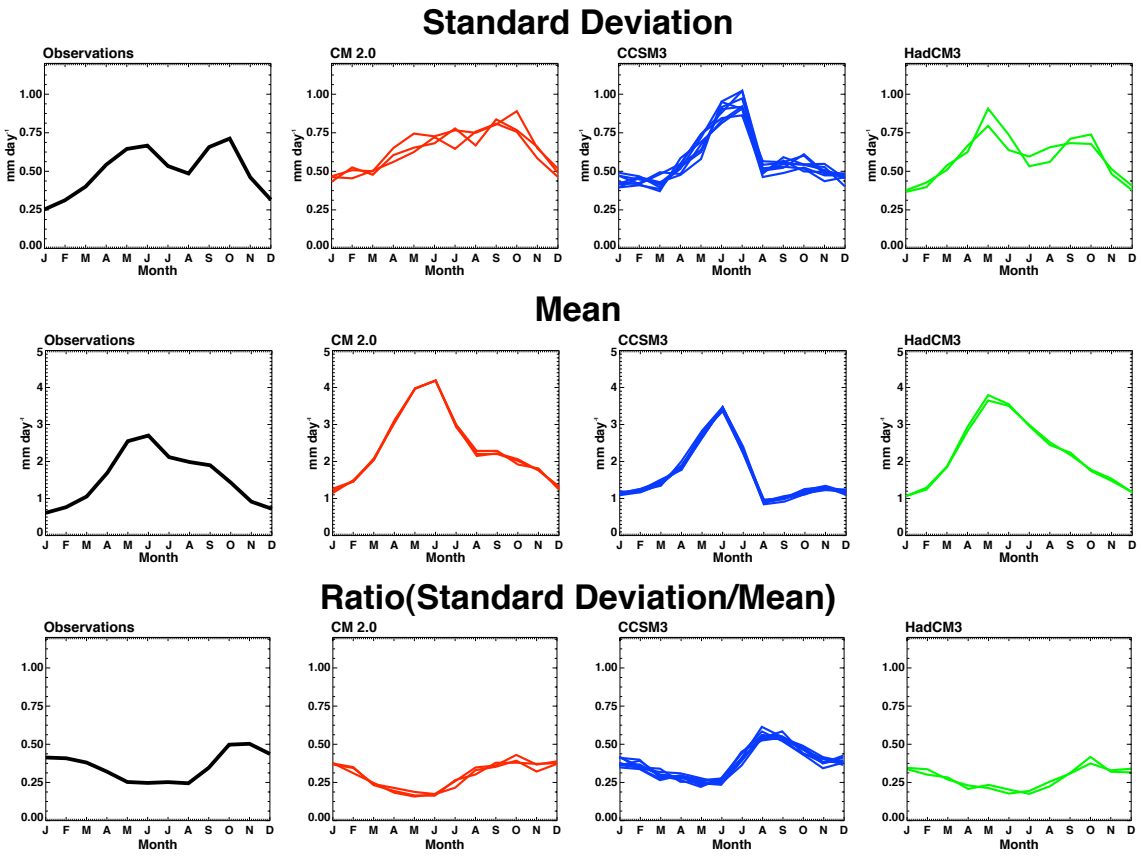


Figure 5.2. *Seasonal Cycle of the standard deviation of monthly precipitation (top row). Seasonal Cycle of monthly mean precipitation (middle row). The seasonal cycle of the ratio of the standard deviation of precipitation tot the mean precipitation for each month. Results are from CRU TS 2.1 (black) and the three models.*

bimodal pattern with maximum variability occurring in May and October and minimum variability occurring in December.

The seasonal cycle for the standard deviation of precipitation looks similar to the seasonal cycle of mean precipitation (Figure 5.2 middle row). Precipitation variability tends to be low when mean precipitation is low in winter, and precipitation variability is large when mean precipitation is high. The maximum peak in the seasonal cycle of precipitation variability occurs in October for the observations. This implies that the Great Plains experiences a large amount of interannual variability in precipitation during the Fall months. The seasonal cycle of the ratio of the standard deviation of precipitation

to the average precipitation for each month of the year is shown in Figure 5.2 (bottom row). The slope of the curve is largest between September and October, indicating that, that relative to the mean, the variance of precipitation is largest in October and smallest in the summer months.

In each of the models, the seasonal cycle of the ratio of the standard deviation of precipitation to the mean precipitation looks similar to the observations. In each model maximum ratios occur in the late Fall and early Winter, while minimum ratios occur during summer. The similarities in the seasonal cycle of the ratio of these variables happens in spite of the fact that the seasonal cycles of mean precipitation and the standard deviation of precipitation for each of the models is fairly different from the observations. This is especially true for CCSM3, which completely misses the secondary maximum in precipitation that occurs in Fall.

In the observations, precipitation is most variable during the transition seasons of Spring and Fall. During the Spring, the Great Plains region transitions from of the cold dry winter season into the warm wet summer season. The opposite occurs during the fall. In both of these seasons, precipitation is not only dependent on the amount of moisture in the Great Plains region, but also on the synoptic scale storm disturbances that travel through the region. Previous studies have shown that the variability of precipitation during October is highly dependent on atmospheric blocking patterns which lead to a stagnation of weather events. This means that during some years, the central United States is persistently under the influence of high pressure systems which inhibits precipitation, while in other years the same region can be persistently influenced by low

pressure systems which tends to dump large amounts of rainfall onto the region. Both CM 2.0 and HadCM3 also show maximum precipitation variability occurring during the transition seasons indicating that synoptic scale disturbances may influence the Great Plains during the Spring and Fall. In CCSM3, however, maximum precipitation variability appears to be only coupled to mean precipitation rates. It is possible that CCSM3 does not accurately represent the influence that synoptic scale disturbances have on precipitation in this region, and that precipitation rates are only a function of moisture supply.

Data Set		annual	wet season	dry season
CRU TS 2.1		0.204	0.313	0.220
VIC		0.207	0.314	0.235
CM 2.0	run 1	0.288	0.419	0.271
	run 2	0.296	0.442	0.295
	run 3	0.260	0.402	0.255
CCSM3	run 1	0.216	0.387	0.197
	run 2	0.204	0.366	0.202
	run 3	0.217	0.356	0.192
	run 4	0.207	0.358	0.209
	run 5	0.216	0.367	0.205
	run 6	0.208	0.350	0.204
	run 7	0.220	0.383	0.186
	run 9	0.239	0.398	0.218
HadCM3	run 1	0.224	0.332	0.243
	run 2	0.230	0.329	0.217

Table 5.2. *Values of the Standard Deviations for the annual mean precipitation time series, wet season mean precipitation time series, and dry season mean precipitation time series. Units are in mm day $^{-1}$.*

5.1.2 Variability of Annual, Wet Season, and Dry Season Precipitation

Not surprisingly, averaging Great Plains precipitation in time greatly reduces its variability. In Figure 5.1, the thick colored lines overlaying the gray lines represent the annual mean precipitation anomalies. After averaging, the overall amplitude of the precipitation anomalies is greatly reduced as is the standard deviation (Table 5.2). The models still tend to overestimate the variability of precipitation, even in the annual mean, although some of the simulations performed with the CCSM3 do accurately capture the observed magnitude of variability in the annual mean time series.

In the observations, the precipitation anomalies associated with the wet season months (April-September) dominate the annual variability. This relationship is also true for the models. This indicates that precipitation is more variable during the wet season months than the dry season months (October - March), and that precipitation anomalies during the wet season tend to be more extreme than during the dry season (Table 5.2). This can also be seen in the plots of the seasonal cycle of the standard deviation of precipitation in Figure 5.2. Since both mean precipitation rates and the variability of precipitation are largest during the wet season months, we expect that reductions in precipitation during the wet season will have the largest impact on the Great Plains. To give a real world consideration, farmers working in the Great Plains region are highly dependent on wet season precipitation to produce their crops. Although, precipitation rates are generally high during the summer, especially in June, there exists a lot of year to year variability of precipitation during this season. Without irrigation, farmers are at the will of nature to produce large yields and quite frequently, precipitation rates may be devastatingly low for crop growth. For this reason, we primarily emphasize the differences between simulated and observed wet season Great Plains precipitation in this model.

Now that we have seen that variability of Great Plains precipitation is generally over estimated in the models, we can begin to investigate the magnitude of extreme wet events verses extreme dry events in the models compared to the observations. The remaining parts of this chapter will focus primarily on the annual mean, wet season mean, and dry season mean time series of precipitation averaged over the Great Plains.

5.2 Extreme Precipitation Events

In this section we compare and contrast the simulated distributions of Great Plains precipitation with the observed distribution. We are primarily interested in looking at how frequently extreme wet and dry precipitation events occur over the Great Plains in the models compared to the observations. We have already shown that the models tend to overestimate the overall variability in Great Plains precipitation, so we know that precipitation extremes tend to be larger in the models than the observations. The question we are trying to answer in this section is, do the models tend to over or under estimate the frequency of occurrence of extreme wet and dry events compared to the observations? We are also want to see if there is a tendency for wet events to be more extreme or to occur more frequently than dry events, or vice versa.

To do this we create Relative Frequency Distribution (RFD) curves for the time series of annual mean, wet season mean and dry season mean precipitation anomalies (von Storch and Zwiers, 2001, p.19). The RFD curves are created by dividing the precipitation time series into discrete, evenly sized bins and then normalizing each by by the total length of the time series (i.e. the number of years in each time series). This results in a value for each bin that represents the "relative frequency" of occurence of precipitation events within that bin size. In Figures 5.5-5.7, the relative frequency values are plotted against standard deviation such that the area under each curve is equal to one.

From the RFD curves we are primarily interested in looking at the frequency of occurrence of extreme wet and dry events. We can used the skewness value of each distribution to determine whether extreme dry or wet events occur more frequently over

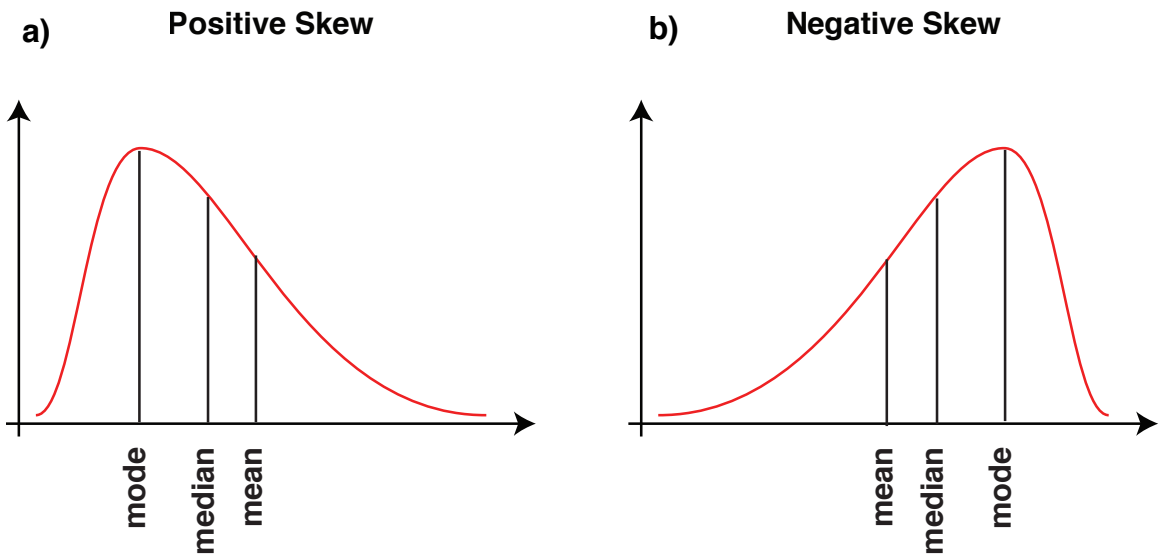


Figure 5.3. *Idealized frequency distribution curves representing the difference between a distribution that exhibits positive skewness (a) versus negative skewness (b). Positive skewness indicates the distribution is skewed the the right, with a longer tail to the right of the distribution maximum. The opposite is true for a negatively skewed distribution curve.*

the Great Plains region in the models relative to the observations. The skewness of each RFD curve determines whether a distribution is symmetric about its maximum. Positive skewness indicates the distribution is skewed to the right, with a longer tail to the right of the distribution maximum and negative skewness indicates the distribution is skewed to the left, with a longer tail to the left of the distribution maximum (Figure 5.3). In a positively skewed distribution, positive (wet) precipitation anomalies tend to be more extreme or occur more frequently that negative (dry) precipitation anomalies. The opposite is true for a negatively skewed distribution. A distribution curve that is symmetric about its maximum has an equal number of events that lie on either side of its maximum peak, and positive and negative anomalies tend to exhibit similar extremes.

We use Monte Carlo methods to determine how large skewness values need to be for them to be significantly different from zero (Livesey and Chen, 1983; van den Dool, 1983; Bretherton et al., 1999; von Storch and Zwiers, 2001, p.104). To do this we first

generate 10,000 normally distributed data arrays that are all 100 elements in length (the approximate length of our Great Plains precipitation time series). Next we calculate the skewness of all 10,000 arrays. We can then create a Relative Frequency Distribution curve for the skewness of our normally distributed arrays (See Figure 5.4). From Figure 5.4 we see that the distribution curve for the skewness values is approximately equal to the normal distribution and has a mean of -0.001 a median value of 0.0007, skewness of 0.004 and standard deviation of 0.23. Since over 65% of all skewness values in our distribution curve fall within ± 1 standard deviation away from the mean, we argue that only skewness values greater than ± 0.23 are significantly different from zero. Any distribution curve that exhibits a skewness value that is less than ± 0.23 can be considered symmetric about its maximum peak.

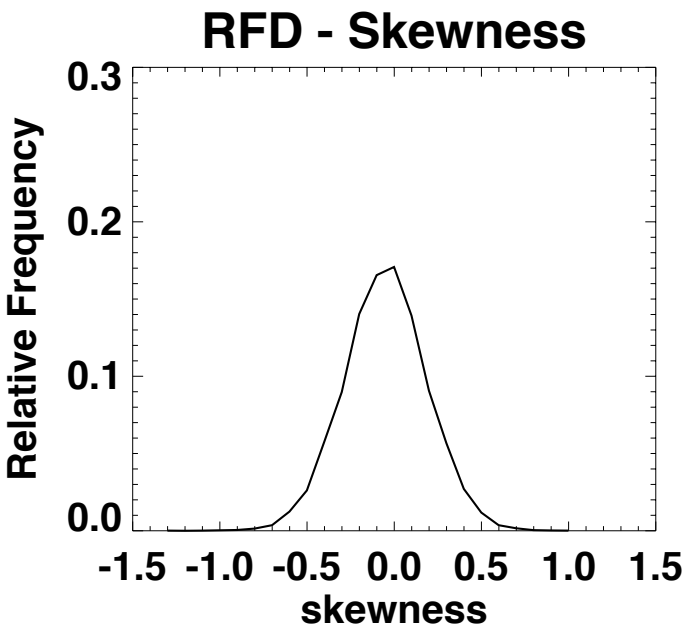


Figure 5.4. *Relative Frequency Density curve for skewness values of 10,000 normally distributed data arrays all 100 elements in length. Over 65% of all skewness values fall within ± 1 standard deviation from the mean, therefore we argue that only skewness values larger than ±0.23 are significantly different from zero.*

In this section we also want to look at the relative magnitudes of the extreme wet and dry events that occur over the Great Plains in the models compared to the observations. We are primarily interested in looking at the most rare, extreme anomalies

that make up less than 10% of the total distribution. Therefore, in the following analysis we define extreme dry precipitation events as the anomalies that lie within the bottom 5th percentile of the relative frequency distribution curve and we define extreme wet precipitation events as the anomalies that lie within the top 95th percentile of the distribution curve. In a positively skewed distribution we expect wet precipitation anomalies to exhibit larger extremes than dry precipitation anomalies. The opposite is expected for a distribution that is negatively skewed.

5.2.1 The Distribution of Annual Precipitation Anomalies

The Relative Frequency Distribution Curves for the time series of annual mean Great Plains precipitation anomalies from the models and the observations are shown in Figure 5.5. The skewness values as well as the average of the extreme negative and postive anomalies of each distribution are shown in Table 5.3.

The observed distributions from CRU and VIC are both negatively skewed indicating that in the annual mean precipitation time series, negative precipitation anomalies tend to be more extreme than positive precipitation anomalies, although it should be noted that the skewness values for these distributions are relatively small, such that the observed distribution curves are practically symmetric about their maximum. For CRU TS 2.1 extreme negative precipitation anomalies average approximately -0.461 mm day $^{-1}$, while the extreme positive precipitation anomalies are on average only 0.425 mm day $^{-1}$.

As a whole, the models do a reasonably good job representing the distribution of annual mean precipitation anomalies for the Great Plains. The skewness of the RFD

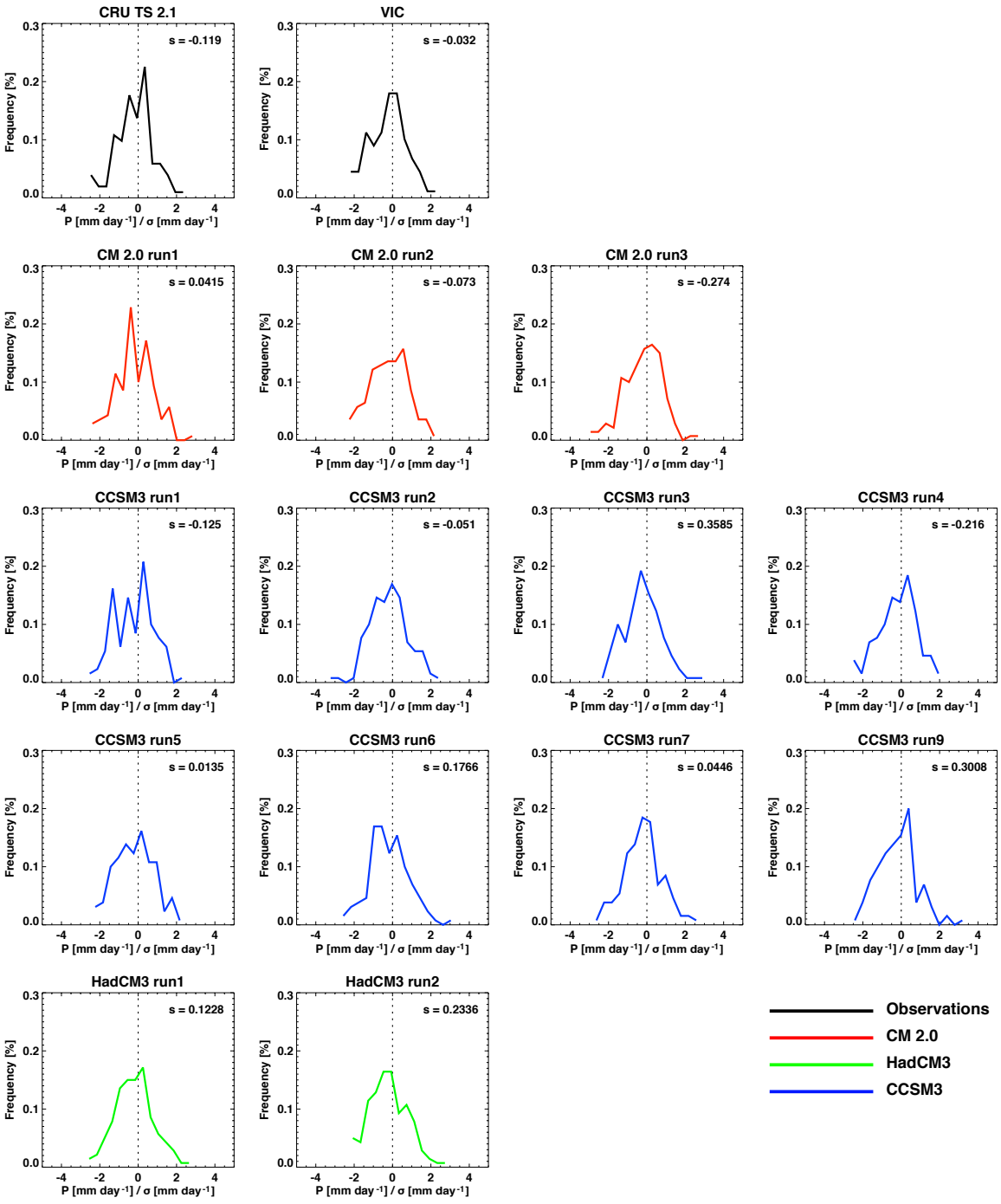


Figure 5.5. *Relative Frequency Distribution (RFD) curves for the time series of annual mean precipitation anomalies. Relative frequency is plotted against normalized precipitation anomalies (precipitation anomalies/the standard deviation (σ)).*

Data Set		Annual			Wet Season			Dry Season		
		Skewness	Average Negative Extreme	Average Postive Extreme	Skewness	Average Negative Extreme	Average Postive Extreme	Skewness	Average Negative Extreme	Average Postive Extreme
CRU TS 2.1		-0.119	-0.461	0.425	0.215	-0.630	0.702	0.446	-0.380	0.521
VIC		-0.032	-0.408	0.412	0.266	-0.600	0.690	0.270	-0.423	0.480
CM 2.0	run 1	0.041	-0.581	0.584	-0.075	-0.897	0.834	-0.090	-0.566	0.546
	run 2	-0.073	-0.585	0.582	-0.294	-0.962	0.798	0.141	-0.540	0.583
	run 3	-0.274	-0.588	0.498	-0.309	-0.916	0.738	0.107	-0.470	0.509
CCSM3	run 1	-0.125	-0.425	0.388	-0.076	-0.786	0.744	0.131	-0.392	0.428
	run 2	-0.051	-0.408	0.411	-0.006	-0.749	0.762	0.279	-0.358	0.430
	run 3	0.359	-0.392	0.492	0.218	-0.683	0.758	0.421	-0.345	0.437
	run 4	-0.216	-0.435	0.391	-0.095	-0.719	0.683	0.155	-0.383	0.441
	run 5	0.014	-0.418	0.433	-0.207	-0.728	0.648	0.364	-0.354	0.443
	run 6	0.177	-0.423	0.449	0.191	-0.652	0.723	0.649	-0.361	0.501
	run 7	0.045	-0.462	0.473	0.013	-0.782	0.800	0.228	-0.338	0.398
	run 9	0.301	-0.431	0.535	0.174	-0.780	0.850	0.802	-0.393	0.517
HadCM3	run 1	0.123	-0.443	0.485	0.182	-0.637	0.714	0.280	-0.450	0.516
	run 2	0.234	-0.439	0.492	0.169	-0.629	0.695	0.304	-0.383	0.476

Table 5.3. *Information regarding the distribution of the annual mean precipitation time series (First three columns), the wet season mean precipitation time series (middle three columns), and the dry season mean precipitation time series (last three columns). For each time series the skewness of the distribution in shown in the left most column, the average of the anomalies that fall in the bottom 5th percentile are shown in the middle column, and the average of the anomalies that fall in the top 95th percentile are in the right most column. Skewness values are non-dimensional, the average extreme values are in units of mm day^{-1}.*

curves tend to be small, with most of the model distributions tending toward the normal distribution. Of the three models, CM 2.0 best captures the observed distribution of annual precipitation. The skewness values for the distributions from Run 1 and Run 2 of this model are small and the RFD curves are essentially normally distributed. In these model integrations extreme positive and negative precipitation anomalies exhibit similar magnitudes and frequency of occurrence. Run 3 from this model, on the other hand, is negatively skewed, with a skewness that is more than twice what is observed. Much like the observations, extreme negative precipitation anomalies tend to be larger than the extreme positive precipitation anomalies with the anomalies in the bottom 5th percentile averaging -0.588 mm day^{-1} while the anomalies in the upper 95th percentile only reach an average 0.498 mm day^{-1}. Remember from section 4.1 that CM 2.0 tends to overestimate

the variability of precipitation over the Great Plains, so, as expected, extreme precipitation events in this model are larger than observed.

The RFD curves from CCSM3 also tend to be fairly normally distributed, although notable exceptions to this do occur. The distribution curve from Run 4 of this model is negatively skewed, with a skewness of -0.216, and looks very similar to the CRU distribution curve. Runs 3 and 9, on the other hand are both strongly positively skewed and have long tails on the right-hand sides of their distributions. These two RFD curves are very different from the observed distributions, since positive precipitation extremes tend to be larger than the negative precipitation extremes in these Runs. For example, in Run 3 extreme positive precipitation anomalies average 0.492 mm day^{-1} while negative precipitation extreme only average -0.392 mm day^{-1}. The larger number of simulations performed by CCSM3 shows us that internal model variability is very important and greatly influences how precipitation is distributed over the Great Plains.

Although the skewness values in the two HadCM3 integrations are relatively small, both distribution curves from this model are positively skewed indicating that extreme positive precipitation events tend to be larger in magnitude than extreme wet precipitation events. This is especially true for Run 2 of this model.

Since mean precipitation rates and the variability of precipitation are both dependent on time of year, it of interest to compare how the distributions of precipitation differ between the average of the wet season months of each year and the average of the dry season months of each year. Figure 5.6 shows the RFD curves for the time series of the mean wet season precipitation anomalies and Figure 5.7 shows the RFD curves for

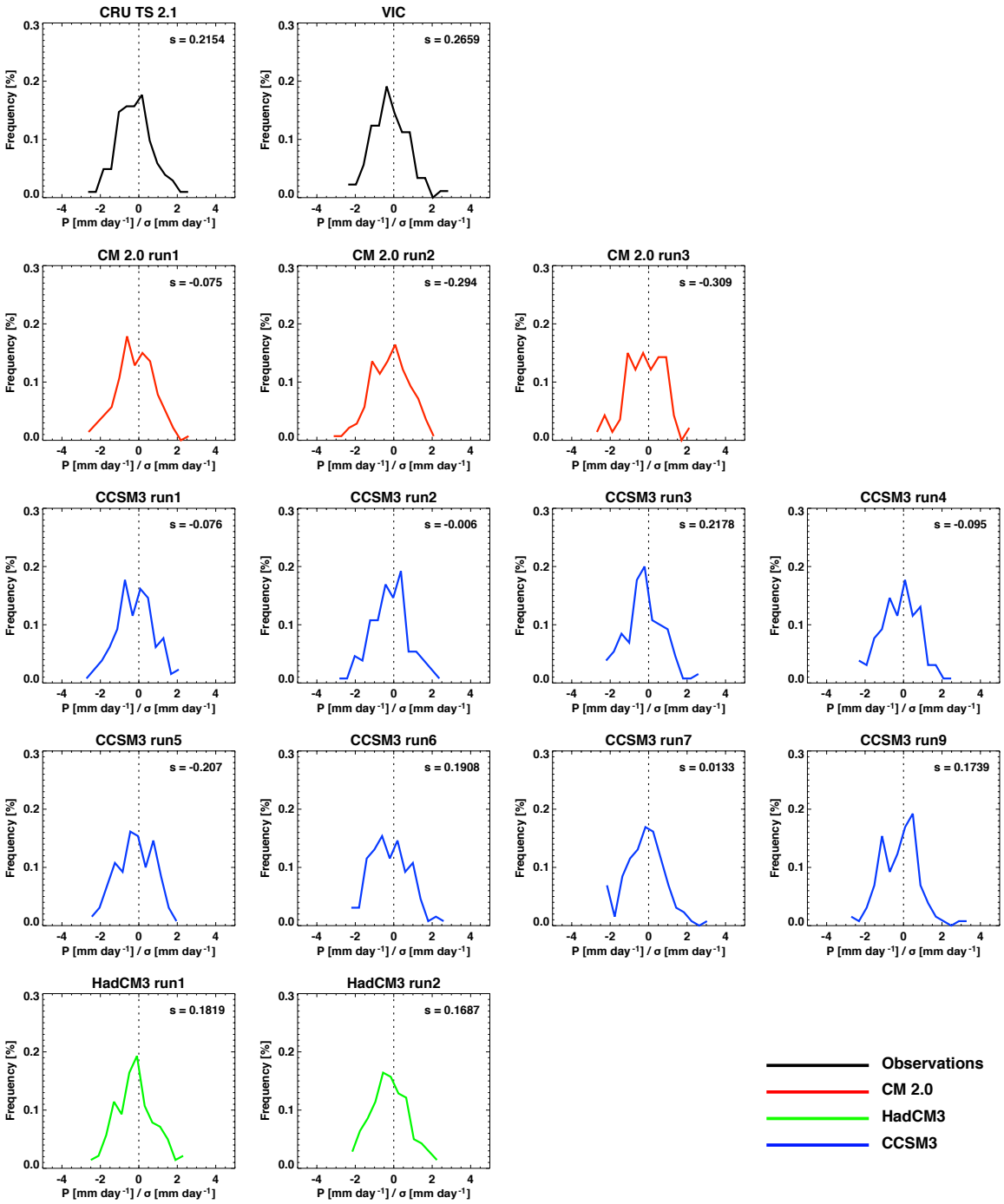


Figure 5.6. *Relative Frequency Distribution (RFD) curves for the time series of wet season mean precipitation anomalies. Relative frequency is plotted against normalized precipitation anomalies (precipitation anomalies/the standard deviation (σ)).*

the mean dry season precipitation anomalies.

5.2.2 The Distribution of Mean Wet Season Precipitation Anomalies

Unlike the distributions for the annual mean precipitation anomalies, the observed wet season distributions are both positively skewed. This implies that positive wet season precipitation anomalies are more extreme than negative wet season precipitation anomalies. Although, once again skewness values are small and close to the normal distribution. In CRU precipitation anomalies in the bottom 5th percentile of the distribution average -0.629 mm day^{-1} while precipitation anomalies in the top 95th percentile average 0.702 mm day^{-1} (Table 5.3). Remember from the previous discussion that variability of wet season precipitation tends to be larger than the variability of annual precipitation, so extreme events in the wet season distribution are also larger. Of the three models, CM 2.0 does the worst job in capturing the observed distribution of wet season precipitation anomalies. All three RFD curves from CM 2.0 are negatively skewed, with the distribution curve from Run 3 exhibiting the largest skewness. In this model, extreme negative precipitation events occur too frequently, and are more extreme than in the observations. CCSM3 also underestimates the positive skewness of the distribution for wet season precipitation anomalies. Wet season precipitation for half of the integrations performed with this model are normally distributed (Runs, 1, 2, 4, and 7), one integration is strongly negatively skewed (Run 5), and three of the integrations closely match the positive skewness seen in the observations (Runs 3, 6, and 9) with run 3 best capturing the observed distribution of wet season precipitation anomalies. Both integrations performed by HadCM3 capture the observed distributions of wet seasons

precipitation anomalies, with positive precipitation anomalies being more extreme and occurring more frequently than negative precipitation extremes. For all three models, average positive precipitation extremes and negative precipitation extremes can be found in Table 5.3. where the extreme values match the skewness of each curve.

5.2.3 The Distribution of Mean Dry Season Precipitation Anomalies

Moving on to the distribution of dry season precipitation anomalies, we see from Figure 5.7 that the observed RFD curves are strongly positively skewed, even more so than the wet season distributions. As mentioned previously in this chapter, mean precipitation in the dry season tends to be fairly low thereby limiting how extreme negative precipitation anomalies can be during this season therefore we expect positive anomalies to be more extreme than negative anomalies. In general CM 2.0 underestimates the the relative magnitude of the positive precipitation anomalies during the dry season, with all three distribution curves exhibiting small positive or negative skewness values. CCSM3 again shows a wide range of in variety of distributions for dry season precipitation. All of the RFD curves for CCSM3 are positively skewed with three of the integrations (Run 1, Run 4 and Run 2) strongly underestimating the observed skewness, three of the models capturing the general features of the observational RFD curves, and two of the integrations (Run 6 and Run 9) greatly overestimating the extreme positive precipitation anomalies. For example, Run 9 of this model exhibits extreme positive skewness with a value of 0.802 with positive precipitation extremes averaging 0.490 mm day^{-1} and negative precipitation extremes only reaching approximately -0.393 mm day^{-1} (Table 5.3). Much like the distribution of wet season precipitation anomalies,

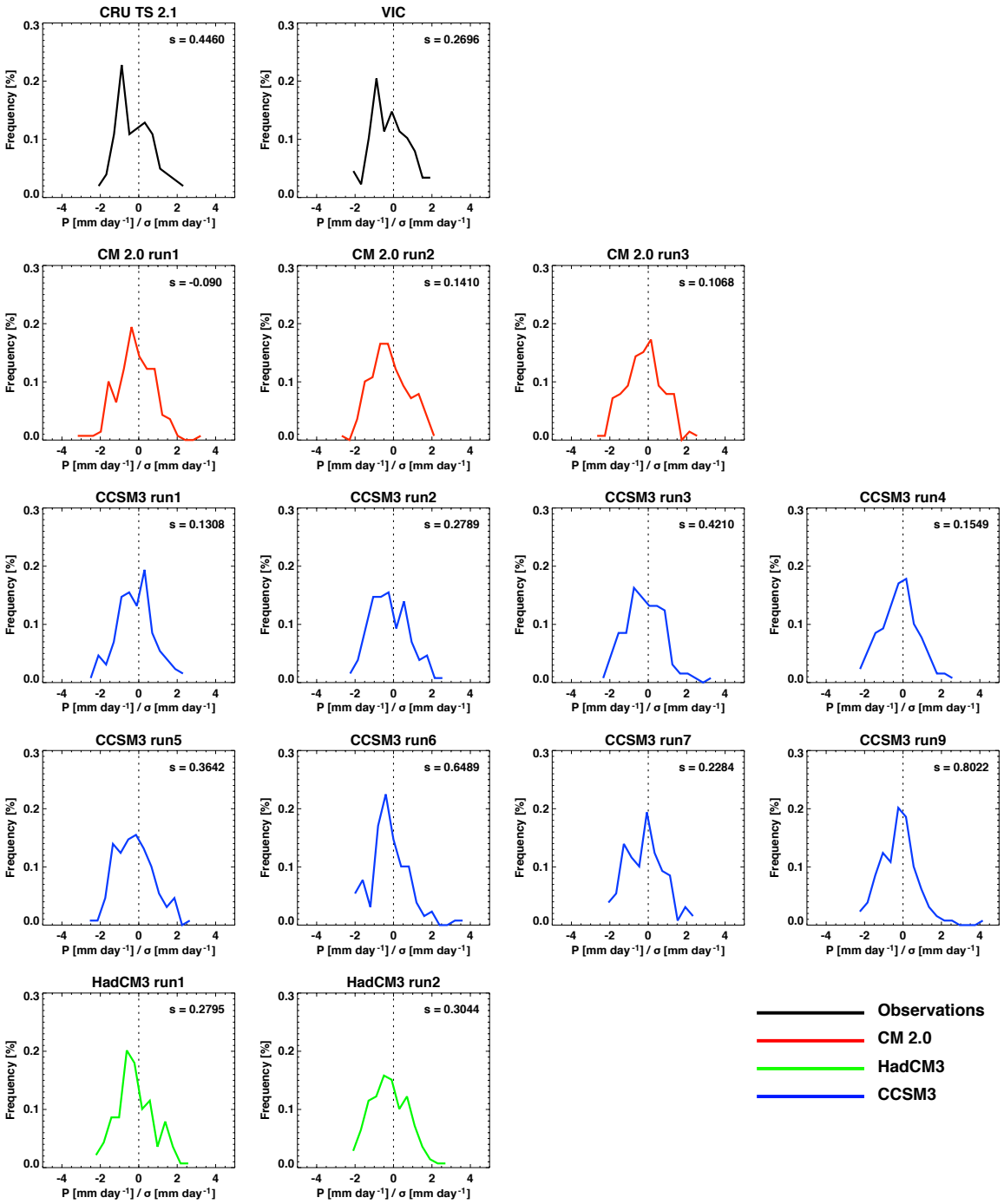


Figure 5.7. *Relative Frequency Distribution (RFD) curves for the time series of dry season mean precipitation anomalies. Relative frequency is plotted against normalized precipitation anomalies (precipitation anomalies/the standard deviation (σ)).*

HadCM3 best captures the observed distribution of dry season precipitation with both integrations exhibiting positive skewness values.

In this section we have seen that CM 2.0 does the best job of the three models in capturing the distribution of annual mean precipitation anomalies, HadCM3 does the best job of representing the distribution of wet season and dry season mean precipitation anomalies, and CCSM3, with its large ensemble size, produces a wide variety of precipitation distributions. Ultimately, we only have on realization of what actually happened in the real world. It appears that reproducing the observed distribution of Great Plains precipitation is difficult. This may, in part, be due to the fact that a number of connected and interacting factors can influence preciptation. Longer time integrations or a larger ensemble size would allow us to see if one distribution curve dominates over the others in each model. Possibly then we could make more accurate comparisons between the simulated and observed distributions of Great Plains precipitation.

While we are interested in determining the models ability to reproduce the observed distribution of precipitation over the Great Plains and the frequency of occurrence of extreme positive and negative precipitation anomalies, we also want to see if the models are able to capture the observed persistence of anomalies in Great Plains precipitation. In the following section we discuss the frequency of occurrence of long lasting dry and wet events over the Great Plains

5.3 Persistence of Anomalies

The extent to which negative or positive precipitation anomalies persist over the Great Plains region has important implications for water management and food

production. Therefore, we want to see not only if the models are able to produce individual severe events with the same frequency and magnitude as the observations, but also if the models are able to represent the persistence of dry and wet events with any accuracy.

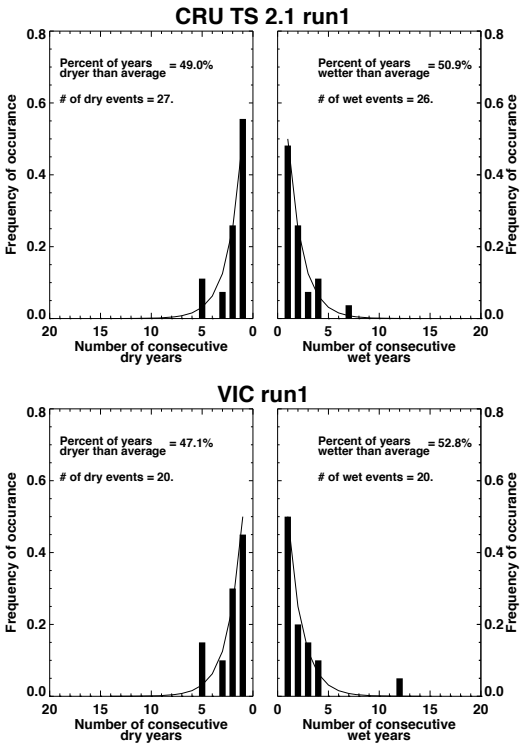


Figure 5.8. *RFD histograms for the length of wet events (right hand side) and dry events (left hand side) in the observations. Idealized PDF shown by the solid curve.*

To investigate the tendency for positive and negative precipitation anomalies to persist for long periods of time over the Great Plains, we first create Relative Frequency Distribution (RFD) histograms for the lengths of wet and dry events in the annual mean precipitation time seres. The RFD histograms are created by first binning precipitation by the number of consecutive years with abnormally low or high precipitation. These bins are then normalized by the total number of dry or wet events that occur during the time series, where an "event" is defined by the time period over which precipitation anomalies persist. The RFD curves for the observations and the models are shown in Figures 5.8-5.11. The thin black curves in these figures will be described later.

By comparing these figures we see that in each annual mean precipitation time series, approximately half of all anomalies are positive and half of all anomalies are

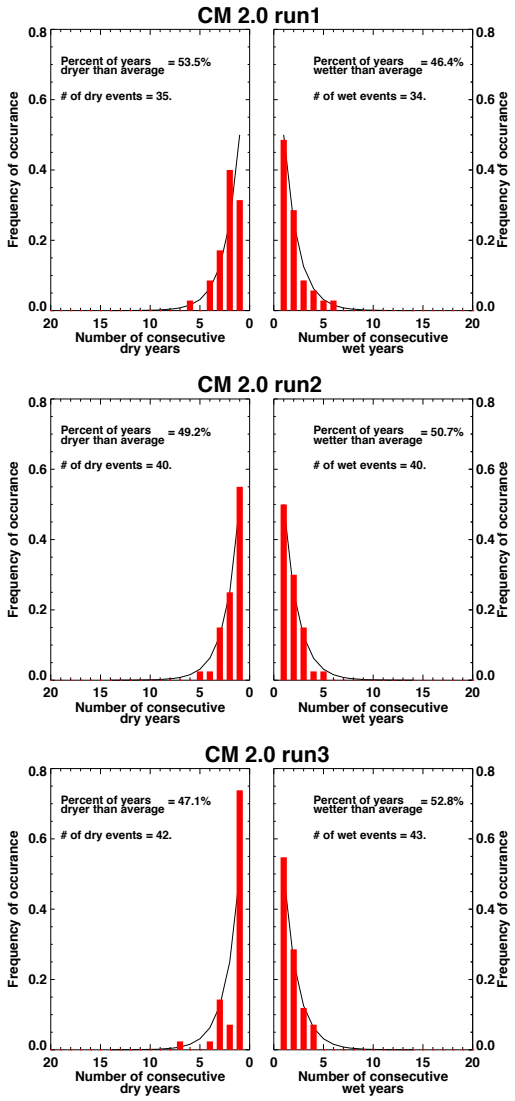


Figure 5.9. *Same as Figure 5.8, but for CM 2.0.*

negative. Also, we see that an equal number of wet and dry events occur in the each time series. Generally, in each time series, approximately 50% of all wet and dry events only persist for one year, approximately 25% of all events persist for 2 years in duration and therefore approximately 25% of all dry and wet events tend to persist for longer than two years.

In the observations (Figure 5.8) three dry events persisted for 5 years, accounting for 11% of the total dry distribution, while one wet event persisted for approximately a decade (7 years in CRU and 12 years in VIC) and accounts for approximately 4% of the total wet distribution. This indicates a tendency for precipitation anomalies to persist over long periods of time in the observations.

Since the models extend over a longer period of time than the observations, a larger number of total wet and dry events do occur (Figures 5.9-5.11). In all of the model integrations, at least one dry event persists for at least 5 years in duration, with some of the models experience dry events that persist on even longer time scales. For example in

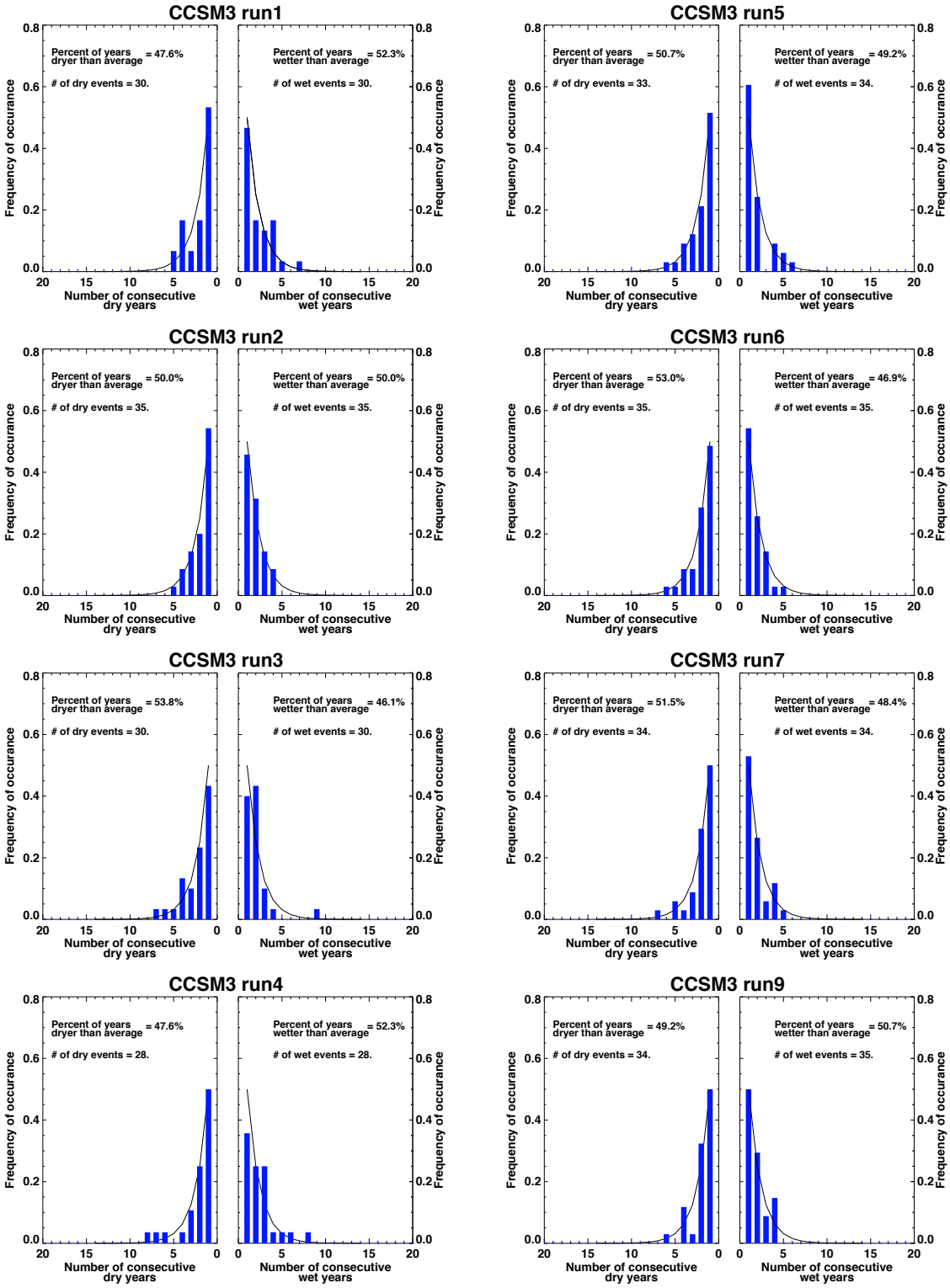


Figure 5.10. *Same as Figure 5.8, but for CCSM3.*

CCSM3 Run 4, one dry precipitation event persisted for 8 years. The models also exhibit persistent wet periods, although there appears to be a tendency for dry precipitation events to persist for longer periods of time than wet precipitation events in the models.

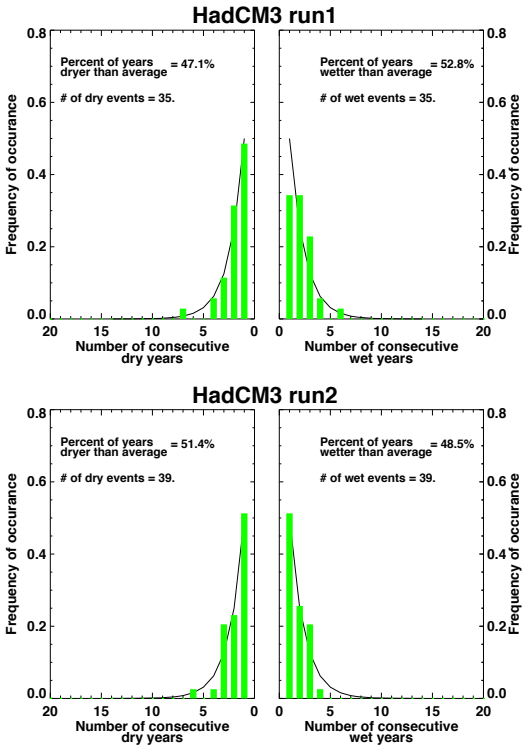


Figure 5.11. *Same as Figure 5.8, but for HadCM3.*

The next question we can ask is, do these dry and wet precipitation events persist for long periods of time just by chance, or is there some external forcing or memory in the system that causes persistence in Great Plains precipitation?

To answer this question, let's first consider an idealized time series of annual mean precipitation anomalies for the Great Plains region that is independent and identically distributed (i.i.d.). In our idealized time series only two outcomes are possible at each time step, precipitation anomalies can either be positive (wetter than average) or negative (dryer than average). In a time series that is i.i.d. there is equal probability of getting a negative or positive value. This means that the occurrence or nonoccurrence of a wetter-than-average year does not affect the probability of occurrence of a dryer-than-average year. This implies that there is no memory in the precipitation time series and that precipitation is not being externally forced by a persistent forcing. Defined in this

way, our precipitation time series can be considered identical to a sequence of coin flips. When flipping a coin, the probability of getting heads is equal to the probably of getting tails, such that:

$$P\{heads\} = P\{tails\} = \frac{1}{2}. \tag{5.1}$$

The same is true in our precipitation time series where the probably of getting a dry year is the same as the probability of getting a wet year. i.e.:

$$P\{wet\} = P\{dry\} = \frac{1}{2}. \tag{5.2}$$

We can now ask the question, what is the probability that two consecutive years will be wetter than average (or dryer than average)? Since the precipitation events that occur in our time series are independent, the likelihood that two consecutive years will be positive (or negative) is equal to:

$$P\{2\ day\} = P^2\{dry\} = \left(\frac{1}{2}\right)^2 = \frac{1}{4}. \tag{5.3}$$

Following this same reasoning, what then is the probability that *l* consecutive years will be positive (or negative)? In this case the probability is simply defined as :

$$P\{l\ day\} = P^l\{dry\} = \left(\frac{1}{2^l}\right). \tag{5.4}$$

Using this idea, we can then use Monte Carlo methods to create idealized Probability Density Functions (PDF) for the length of consecutive dry and wet events (Figure 5.12). The idealized PDFs show us how frequently long-term dry events and long-term wet

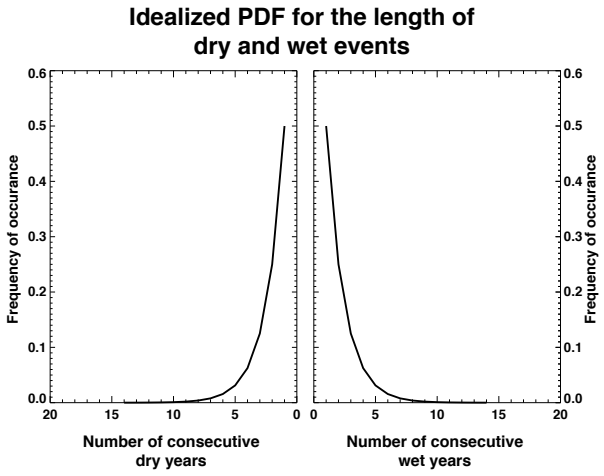


Figure 5.12 . *Idealized PDF for the frequency of occurrence of precipitation events based on the length of duration of consecutive wet and dry periods.*

events are expected to occur by chance. With the idealized PDF, it is expected that 50% of all wet and dry events will only persist for one year, 25% of all wet and dry events will persist for 2 years, 12.5 % will persist for 3 years, 6.25% for 4 years, 3.125% for 5 years, and so on from there. (Figure 5.12).

We can now compare the RFD histograms created from the observations and models with the idealized PDF. The idealized PDF curve shown in Figure 5.12 has been plotted on each RFD histogram for comparison. The RFD histograms show us how precipitation events are organized in the models and the observations while the idealized PDF shows us what is expected from a random series of independent events . Any persistent dry or wet periods in the RFD curves that exceed the idealized curve may indicate some memory or forcing in the system that allows precipitation events to persist over long periods of time.

In the observations (Figure 5.8) we see that, as expected from the idealized PDF, approximately 50% of all wet and dry events only persist for one year and 25% persist for two years. In both data sets, events that persist for three years tend to be under represented compared to the idealized PDF, but events (both wet and dry) that persist for longer than 3 years stand above the idealized curve. During the 100 year sample period

of the observational data sets, three dry periods persisted for five years. It is clear that the frequency of occurrence of these long-term dry events greatly exceeds the expected value from the idealized PDF. In the wet RFD histogram, multiple events last four years in duration, and at least one event persisted for approximately a decade. Again these events that persist for longer than three years, occur more frequently that was expected just by chance. This points to a possible forcing of or feedback with precipitation that locks in droughts and pluvials.

Unlike the observations, the RFD curves for the lengths of dry and wet events in the models tend to follow the idealized PDF much more smoothly. Even the long-term events that the models produce tend to lie under the idealized curve, indicating that it is possible for these long-term events to occur just by chance and not influenced by an external forcing or memory in the system. Exceptions do occur for each model. For CM 2.0, the histograms from Run 1 and Run 2 both generally follow the idealized PDF, but in Run 3, approximately 80% of all dry events persist for only one year therefore exceeding the expected frequency of occurrence from the idealized PDF. Also in CM 2.0 Run 3, one dry precipitation event persisted for seven years, which is longer than expected. In CCSM3 the frequencies of occurrence of wet and dry events exceed the idealized PDF in Runs 1, 3, 4, 7 and 9. For example in Run 4, the precipitation events that lasted for six years and longer all persist for a longer period of time than what is expected just by chance. In the remaining runs from this model, the RFD distributions for the length of wet and dry events matches the idealized PDF almost perfectly. In HadCM3, persistent long-term dry and wet periods fall within the realm of chance, although precipitation

events that persist for only 2-3 years appear to be over represented. It is possible that mechanisms that influence the persistence of precipitation occur too frequently in this model thereby causing precipitation anomalies to persist for shorter periods of time.

In the above test we considered the most simple situation in which precipitation anomalies could only be positive or negative. To make the probability test a little more rigorous we consider a case where precipitation anomalies can fall into one of three categories: dry, wet or normal. Where normal precipitation anomalies are those anomalies that lie close to the mean. To keep things simple, in the idealized case we assume equal probability of getting a dry year, a wet year, or a normal year, such that:

$$P\{dry\} = P\{wet\} = P\{normal\} = \frac{1}{3} \tag{5.5}$$

Following the methods used in the previous test we see that the probability of getting two consecutive years that are dryer than normal, or wetter than normal, or just normal is:

$$P\{2\ day\} = P^2\{dry\} = \left(\frac{1}{3}\right)^2 = \frac{1}{9} \tag{5.6}$$

And finally, the probability that l consecutive years will be dry, wet, or normal is defined as:

$$P\{l\ day\} = P^l\{dry\} = \left(\frac{1}{3^l}\right) \tag{5.7}$$

Once again, using Montel Carlo methods we create an idealized PDF for the lengths of consecutive dry, wet, and normal events (Figure 5.13). In this case it is expected that ~33.3% of all events will persist for only one year, ~11.1% of all events will persist for 2

years, and ~0.4% of all events will persist for 5 years or longer (Figure 5.13).

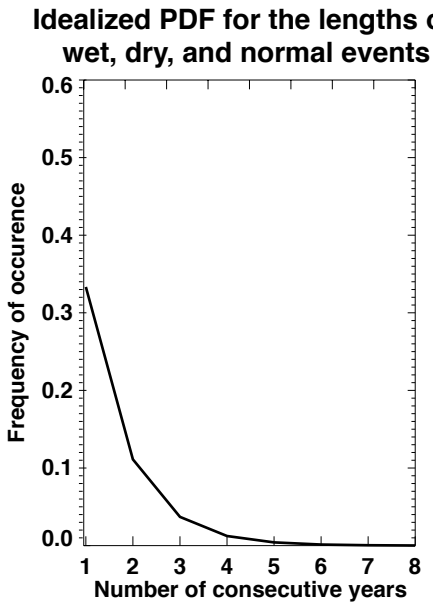


Figure 5.13. *Idealized PDF for the frequency of occurrence of precipitation events based on the length of duration of consecutive dry, wet or normal periods.*

To create the RFD histograms, for this case, for the models and the observations we first divide each precipitation time series into thirds; where the bottom third represents the driest years, the middle third represents those years with normal or close to average precipitation rates, and the upper third represents the wettest years. We then bin each third by the number of consecutive years that experience drier than average precipitation rates, normal precipitation rates, or wetter than average precipitation rates. To determine the relative frequency of occurrence for each event, we normalize each bin by the total number of years that fall within that third of the time series. The RFD histograms for the observations and the models can be seen in Figures 5.14-5.17. We have also included the idealized PDF for this probability test on each diagram.

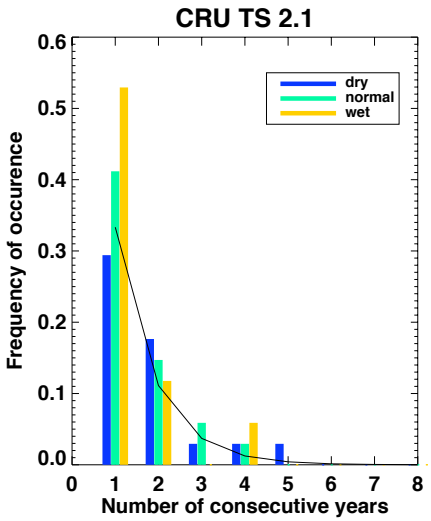


Figure 5.14. *The RFD histogram for the lengths of wet, dry and normal precipitation events from CRU TS 2.1. The black curve represents the idealized PDF from Figure 5.13.*

By including a "normal" range for precipitation anomalies, the RFD histograms for the observed Great Plains precipitation time series

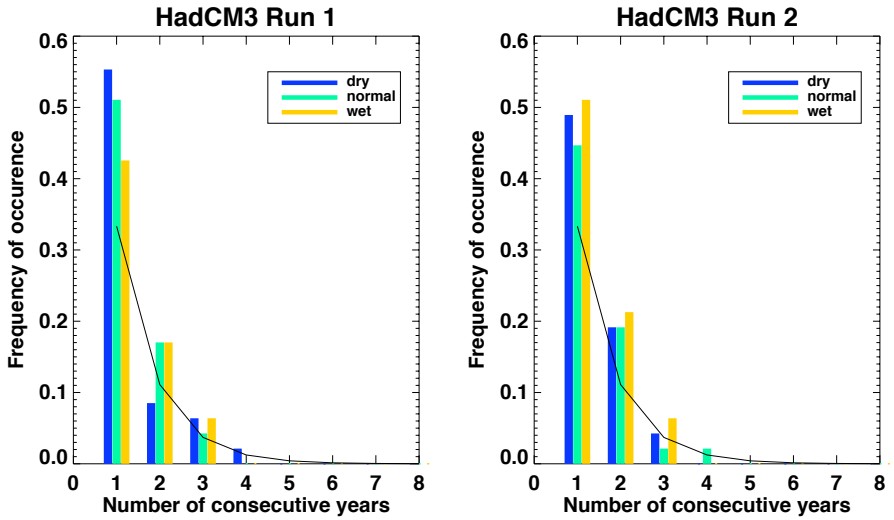


Figure 5.15. *Same as Figure 5.14 but for HadCM3.*

follow the idealized curve much more smoothly than in the previous test where precipitation could only fall into one of two categories. Including this third category reduces the total number of dry periods that persisted for five years in duration from three events down to one. This indicates that in the observations, persistent dry periods are often interrupted by years that exhibit "normal" or close to average precipitation rates. Also, by including a third category for precipitation events, wet events in the observations tend to more frequently persist for short periods of time, with over 50% of all wet events lasting for only one year in duration.

Much like in the previous test, the RFD histograms for HadCM3 follow the idealized curve very smoothly (Figure 5.15). The only real differences is that by including a third category for precipitation events, short-term events that last only one year in duration are overestimated. This is true for all three categories of precipitation.

Adding a normal range for precipitation reduced the number of persistent dry periods that occur in CM 2.0 and CCSM3 (Figures 5.16 and 5.17). In both of these

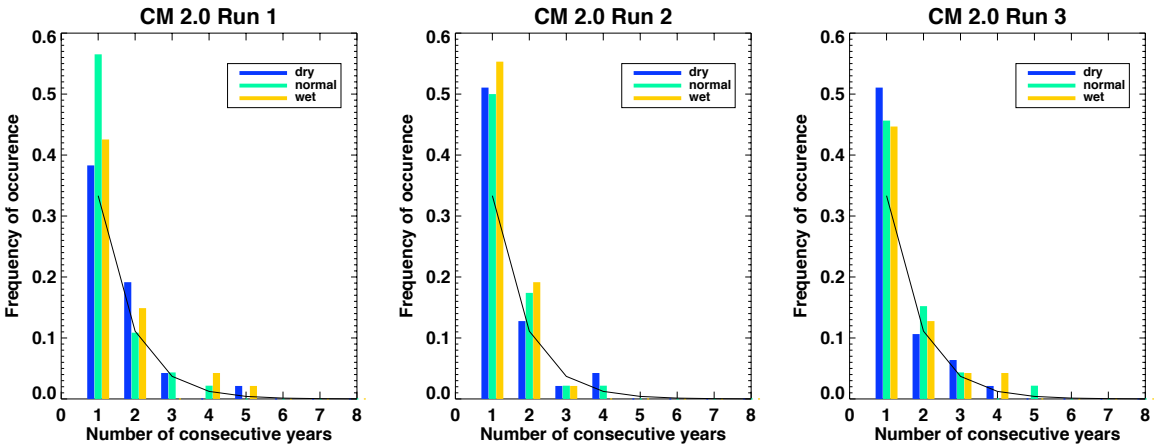


Figure 5.16. *Same as Figure 5.14 but for CM 2.0.*

models, dry events that last for four years are longer occur more frequently than expected in about half of the simulations from these models. Only CCSM3 shows any real tendency for long persistent dry periods to occur over the Great Plains (see Run 1 and Run 4 from CCSM, Figure 5.17). Of course it should be noted that, in CCSM3, precipitation events that fall into the "normal" range also persist for multiple years and beyond what was expected by chance.

Under this more rigorous test, the frequency of occurrence of persistent precipitation events is reduced. In the observations, one dry period does persist for five years and the occurrence of that event exceeds what was expected by chance. Of the models, only CCSM3 exhibits any real persistent dry periods and they only occur in three of the eight simulations from this model.

It seems that in general, the long-term, continuous, precipitation events that do occur in the models appear to fall within the realm of chance, and it is possible that the mechanisms in the observed system that cause precipitation events to persist for long periods do not exist or are too weak in the models. Potentially this is not the case for

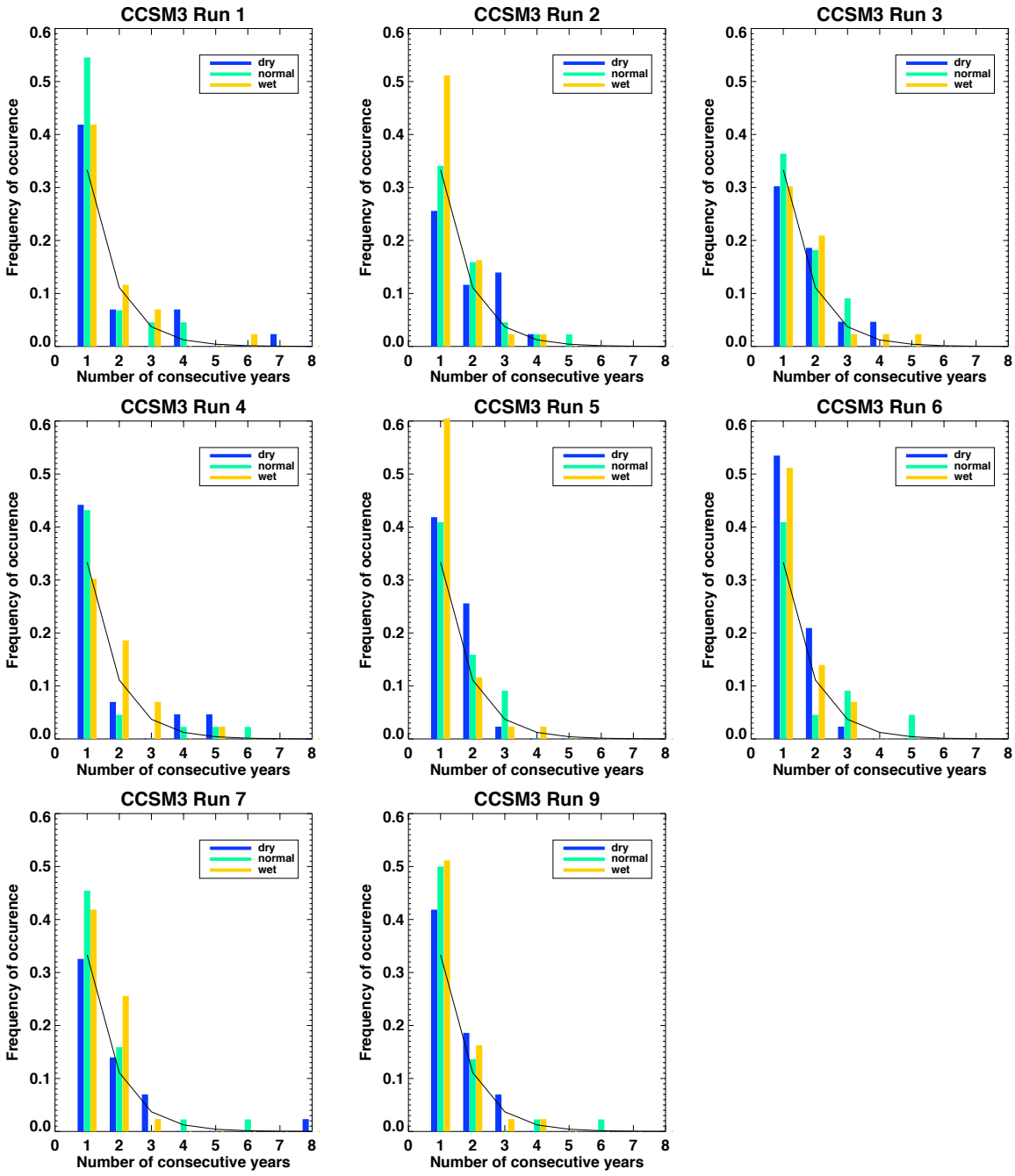


Figure 5.17. *Same as Figure 5.14 but for CCSM3.*

some of the integrations from CCSM3. We investigate some of the mechanisms that potentially cause drought conditions to persist over the Great Plains in the next chapter, and we examine whether these mechanisms influence precipitation in the models.

5.4 Summary

In this chapter we evaluated the ability of the models to represent the variability of Great Plains precipitation including the frequency of occurrence of extreme precipitation events and the tendency for precipitation events to persist over long periods of time. The following is a summary of the main findings of this chapter.

- The models overestimate the variability of Great Plains precipitation. This is especially true for CM 2.0. This indicates that precipitation anomalies will generally be larger in the models than the observations, therefore we expect larger extreme values in the models than the observations.
- Precipitation tends to be a fairly noisy variable over the Great Plains. One explantation for this is that it is influenced by a number of connected and interacting factors. For these reasons it can difficult for the models to capture the observed distribution of the Great Plains precipitation anomalies. With its large ensemble size, CCSM3 exhibits a wide variety of distributions, indicating precipitation variability is not well constrained by the experimental design of these model simulations. Longer time integrations or a larger ensemble size would allow us to see if one distribution curve dominates over the others in CCSM3.
- Simple probably tests indicate that the persistent dry periods (i.e. dry periods that persist for 5 years or longer) simulated by the models could happen just by chance and that large-scale forcing or local lock-in mechanisms may not play a role in the simulated droughts. This is especially true for HadCM3, which does not exhibit

any dry or wet periods that persist for longer than expected. Of the three models, only CCSM3 shows any real tendency for persistent dry periods to occur for longer than expected just by chance.

In the next chapter we will examine the occurrence of multi-year droughts in the models and the observations and investigate some of the possible mechanisms that allow dry conditions to persist in the Great Plains for long periods of time.

Chapter 6

Long-Term Drought

In this chapter we identify and describe the long-term droughts that occurred over the Great Plains in the observed and modeled twentieth centuries. We compare and contrast the temporal and spatial distributions of drought between the models and the observations and then we investigate some of the mechanism that may cause droughts to persist over the Great Plains region for many years. These mechanisms include, large-scale forcing from the tropical Pacific and feedbacks between the land surface and the atmosphere. The ultimate goal of this chapter is to assess the ability of the models to realistically simulate long-term Great Plains drought, and to determine if similar mechanisms force the modeled and observed droughts.

It is important to note that these are fully coupled GCM integrations that are forced only by time series of observed greenhouse gas concentrations, sulfate aerosols, and volcanic eruptions. This implies that for each model integration, not only are the atmospheric conditions different, but so are the oceanic and land surface conditions. Therefore, we do not expect the timing of any long-term droughts in the models to occur during the same time periods as observed. We also expect that the timing of long-term droughts between each individual model integration from the same model will be different. This being said, what we are looking to see is if the characteristics of Great

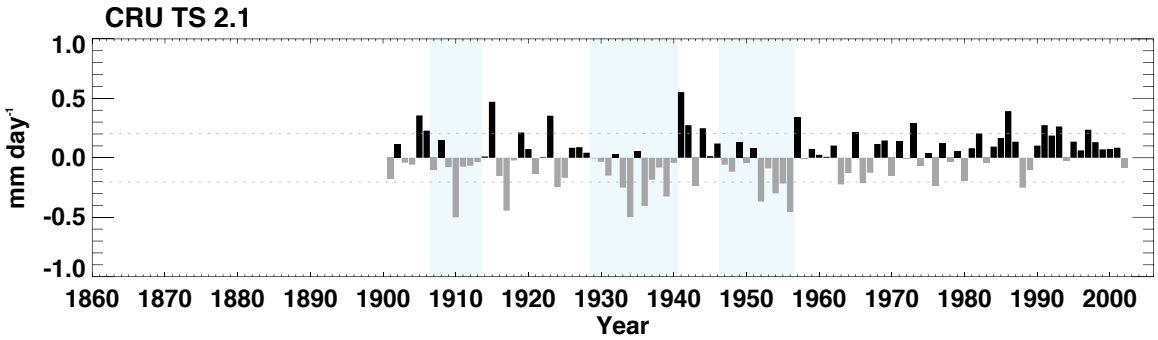


Figure 6.1. *Area-averaged annual Great Plains precipitation anomalies from CRU TS 2.1 (observations) in units of mm day^{-1}. Anomalies are calculated by removing the mean annual precipitation rate calculated from the entire time period (1901-2002) from the time series. Long-term drought periods are shaded in blue. Dashed lines delimitate one standard deviation away from the mean.*

Plains droughts and the mechanisms that cause droughts are similar in the models as in the observations.

6.1 Identifying Long-Term Great Plains Drought

The time series plot in Figure 6.1 shows the area-averaged annual precipitation anomalies for the Great Plains region from the CRU TS 2.1 data set. Remember from Chapter 3 that we define a long-term drought as period of time in which annual precipitation is abnormally low for 80 percent of years during a minimum of seven years (i.e anomalously low precipitation during 6 out of 7 years, 7 out of 8 years, 8 out of 9 years etc). Following this definition we see that the Great Plains region experienced three long-term droughts during the observed 20th Century. The long-term drought periods are shaded in blue on the figure. Details about these droughts can be found in Table 6.1.

The first observed drought occurred from 1907-1913. During this time period, negative precipitation anomalies were most extreme over Southeastern Texas and Oklahoma (Figure 6. 2a). The second drought the Great Plains experienced during the

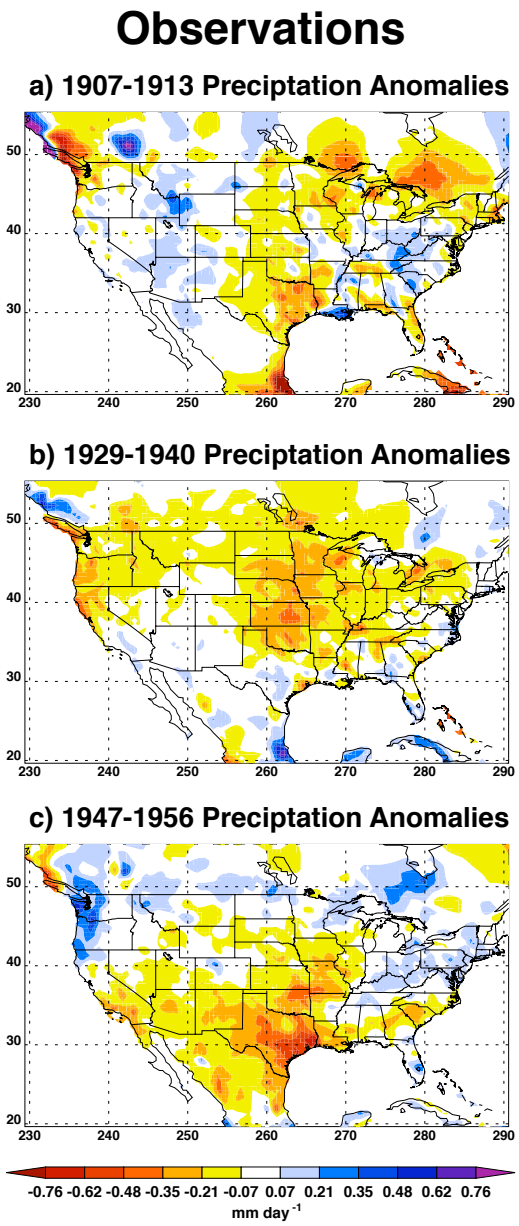


Figure 6.2. *Composite annual precipitation anomalies for the three long-term droughts that occurred during the observed 20th Century from the CRU TS 2.1 data set. Units are in mm day^{-1}*

20th Century extended from 1929-1940. This drought is commonly referred to as the "Dust Bowl" because it was accompanied by severe dust storms. The Central and Northern parts of the Great Plains were most heavily impacted by drought during the 1930s, with the largest anomalies occurring over Kansas (Figure 6.2b). The third and final long-term drought for the observed 20th century occurred during 1947-1956. It had a larger impact on the Southern Great Plains than either of the two previous droughts, and to this day 1956 is still considered the driest year on record for parts of southern Texas (Hughes, 1976) (Figure 6.2c).

Figures 6.3-6.5 show the area-averaged annual precipitation anomalies for the Great Plains region as simulated by each of the three climate models. Once again, long-term dry periods, based on the definition introduced in Chapter 3, are shaded in blue. More information about the droughts produced in each model integration can also be found in Table 6.1. In each simulation of 20th Century climate, the Great Plains

Data Set		Number of Droughts	Length of Drought (years)	Drought Years	Average Anomaly (mm day^{-1})
CRU TS 2.1		3	7	1907-1913	-0.1019
			12	1929-1940	-0.1575
			10	1947-1956	-0.1437
CM 2.0	run 1	2	7	1865-1871	-0.1737
			11	1906-1916	-0.2183
CM 2.0	run 2	1	7	1961-1967	-0.1757
CM 2.0	run 3	1	14	1925-1938	-0.2065
CCSM3	run 1	3	7	1883-1889	-0.2602
			7	1941-1947	-0.1511
			7	1966-1972	-0.0851
CCSM3	run 2	1	7	1892-1898	-0.1270
CCSM3	run 3	3	10	1875-1884	-0.0875
			9	1950-1958	-0.1528
			8	1991-1999	-0.1660
CCSM3	run 4	4	11	1904-1914	-0.1016
			6	1920-1925	-0.1030
			17	1942-1958	-0.1511
			12	1974-1986	-0.1110
CCSM3	run 5	4	20	1881-1900	-0.0992
			8	1923-1930	-0.1992
			6	1972-1977	-0.0551
			11	1980-1990	-0.1157
CCSM3	run6	3	6	1888-1893	-0.1650
			7	1911-1917	-0.0753
			7	1949-1955	-0.1603
CCSM3	run 7	3	12	1877-1888	-0.1607
			8	1924-1931	-0.0481
			11	1988-1999	-0.1900
CCSM3	run9	2	9	1894-1902	-0.1676
			6	1923-1928	-0.1365
HadCM3	run 1	2	7	1925-1931	-0.1368
			10	1980-1989	-0.1600
HadCM3	run 2	3	8	1864-1870	-0.1740
			10	1904-1913	-0.1022
			11	1980-1991	-0.1539

Table 6.1. *Summary of the long-term droughts from the observations and the simulations of the climate of the 20th Century. Table includes the total number of droughts in each realization of the 20th Century, the total length of each drought, the years spanned by each drought, and the average precipitation anomalies associated with each drought.*

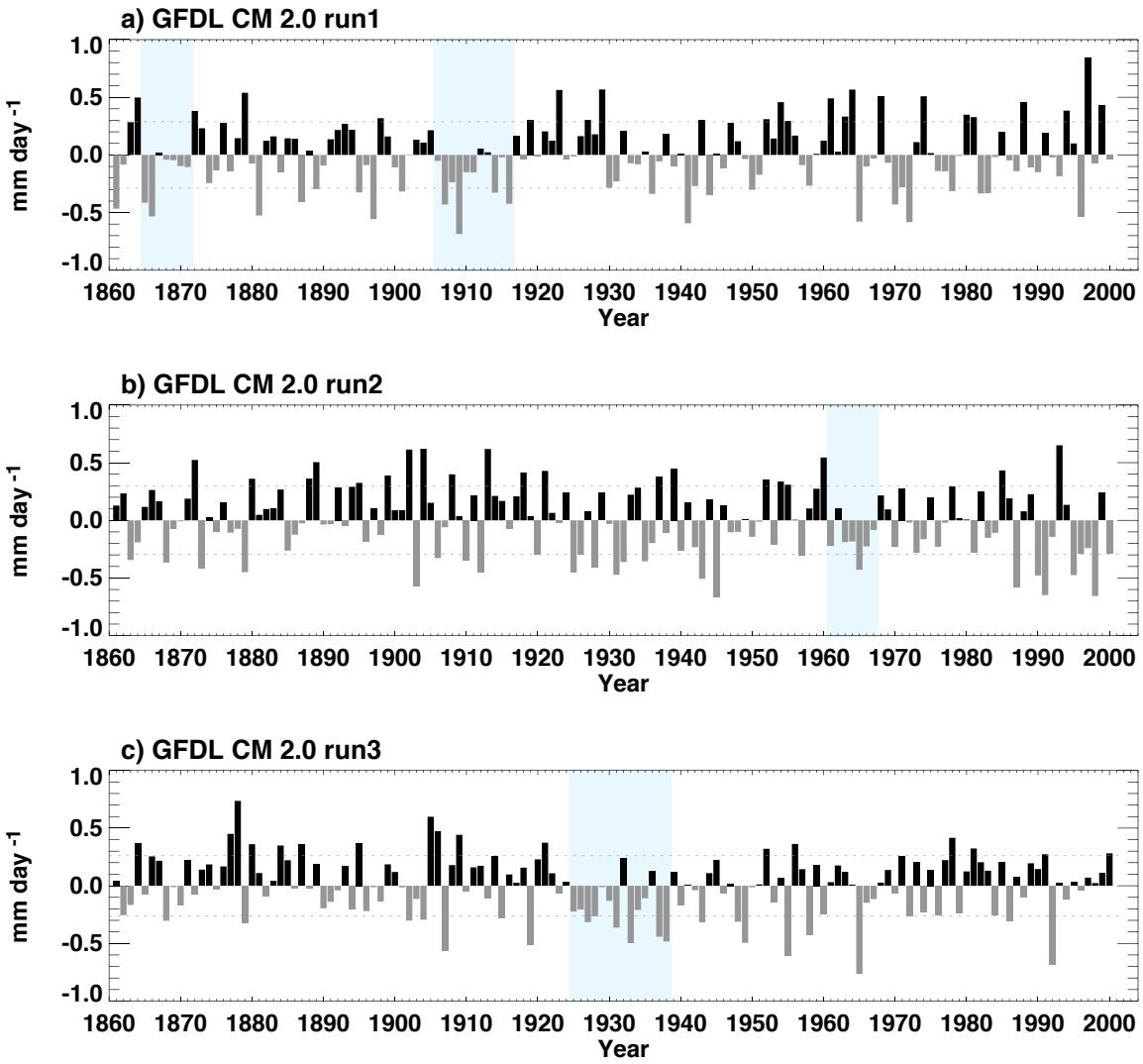


Figure 6.3. *Same as Figure 6.1 only for CM 2.0.*

region experienced at least one long-term drought period, with some integrations having up to three or four long-term droughts impacting the region. From Table 6.1 we see that the simulated long-term droughts lasted from 6 years up to 20 years, with most long-term droughts persisting for 7-11 years. This range is similar to the range seen during the observed 20th century. The longest period with consecutively dry years occurred in CCSM3 Run 4 during the 1942-1958 drought. During the latter part of this drought, the Great Plains region experienced eight consecutive years with abnormally low precipitation rates.

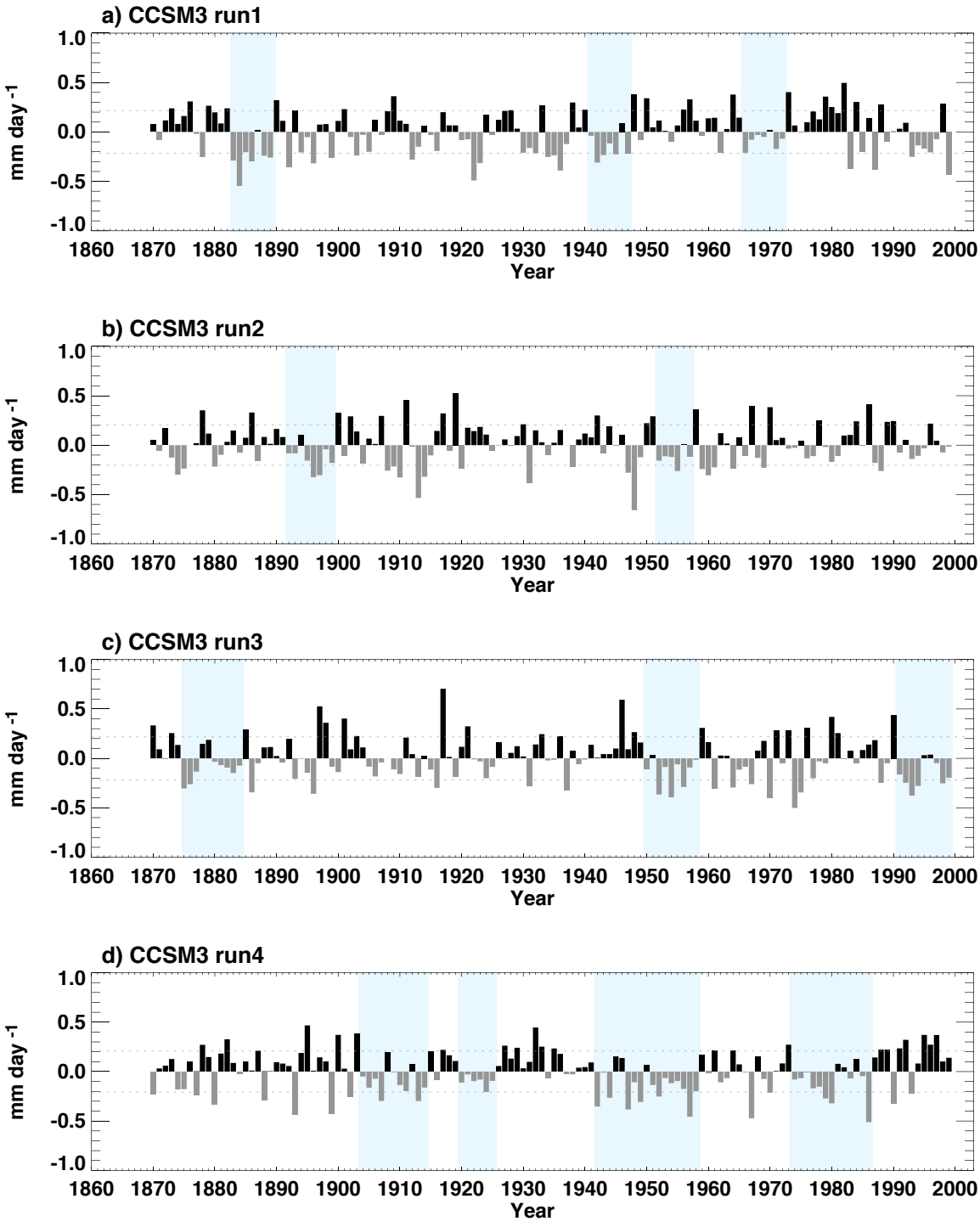


Figure 6.4. *Same as Figure 6.1 only for CCSM3.*

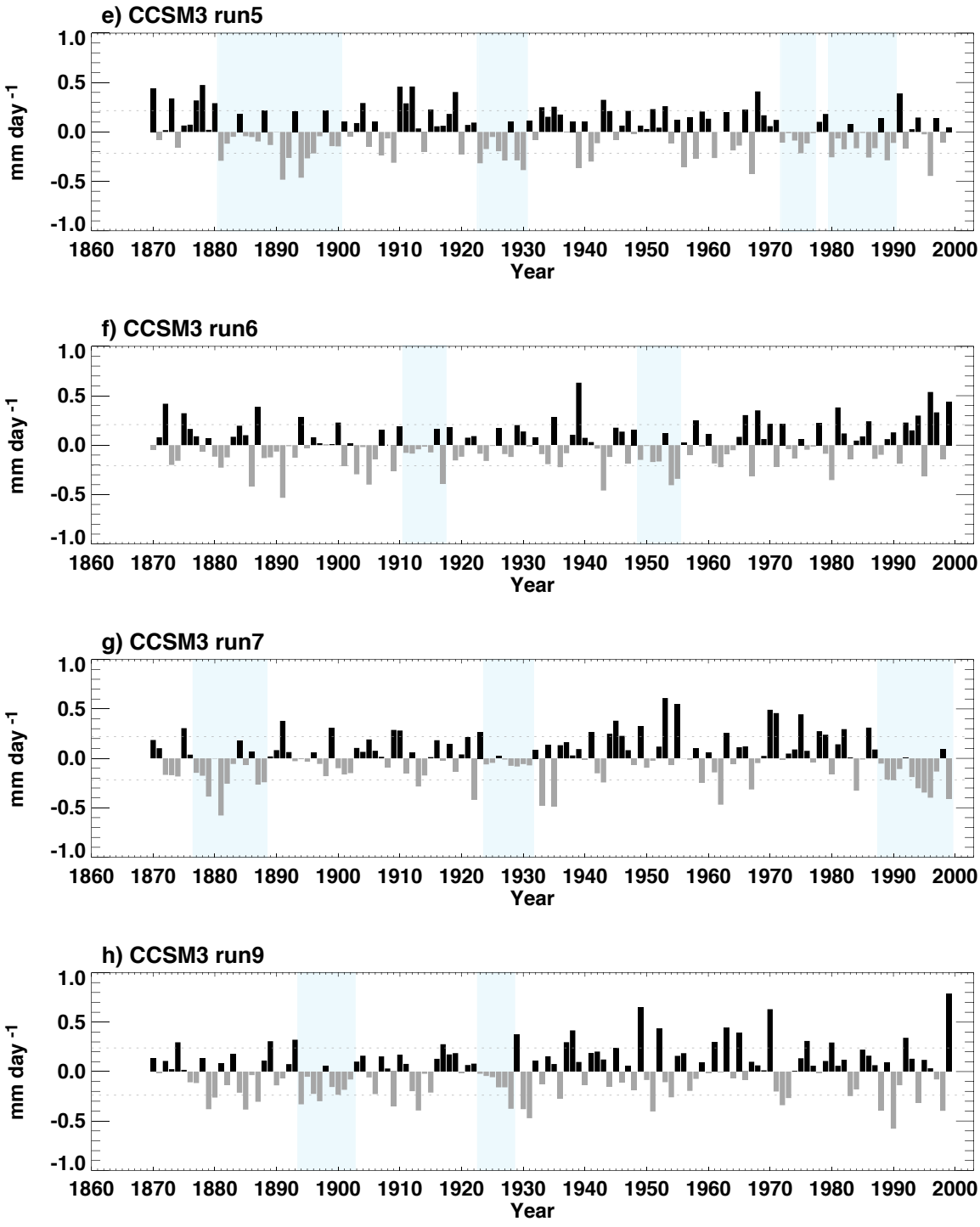


Figure 6.4 continued.

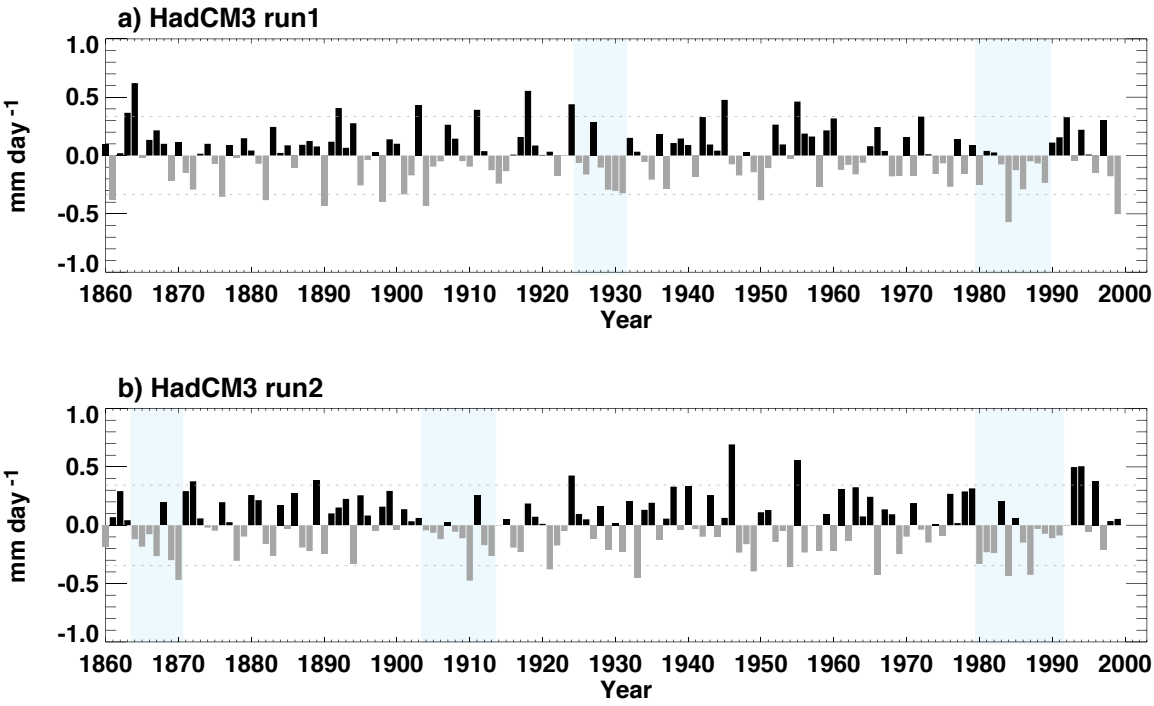


Figure 6.5. *Same as Figure 6.1 only for HadCM3.*

Spatial patterns of the simulated long-term droughts can be see in Figures 6.6-6.9. In general, the simulated droughts exhibit similar spatial patterns as were observed during the 20th Century. The southern half of the Great Plains tends to be more heavily impacted by drought than the northern half. In section 6.4.1 we show that the El Niño - Southern Oscillation (ENSO) has a strong influence on the southern part of the United States, indicating that the tropical Pacific may play a role in influencing Great Plains drought. In some cases, Great Plains drought fits into a broader category of drought that influences most of North America, much like it did during the 1930s "Dust Bowl" drought (see: Figure 6.7a, Figure 6.7j, Figure 6.8e, Figure 6.9b). Other times, drought is restricted to only the Great Plains region, much like it was during the 1907-1913 drought (see: Figure 6.7b, Figure 6.7c, Figure 6.7k, Figure 6.8n, and Figure 9a). In the models,

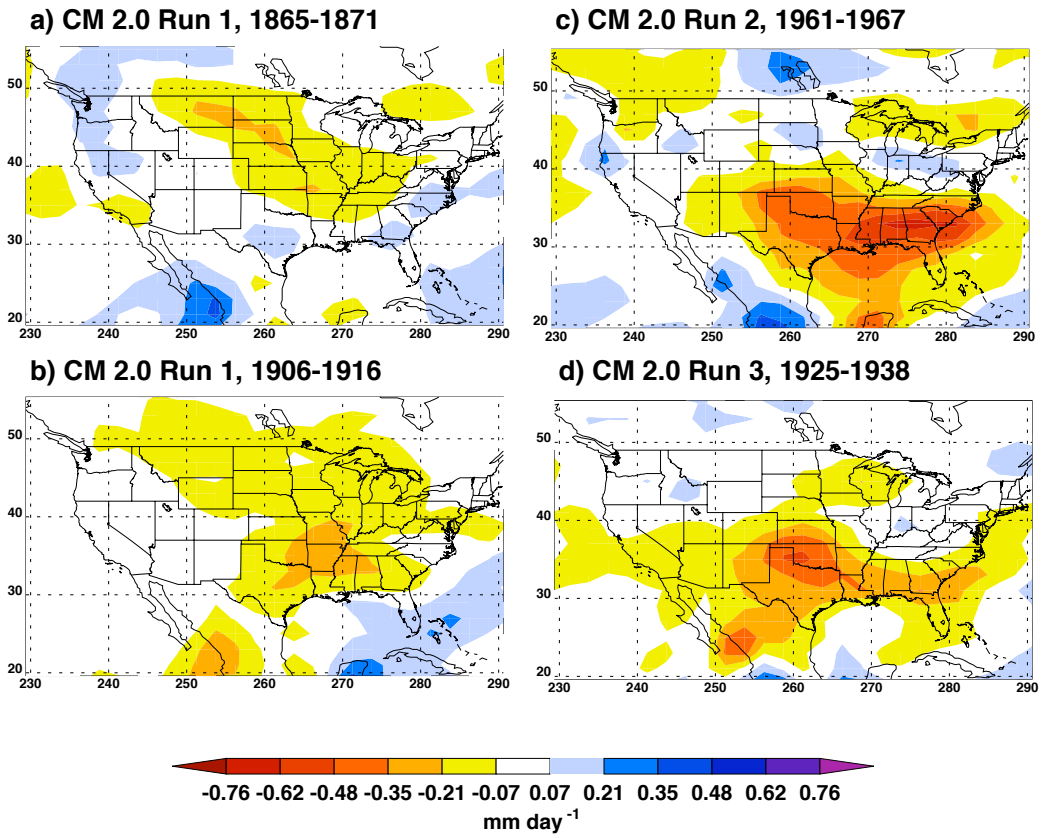


Figure 6.6. *Same as Figure 6.2 only for CM 2..0. Spatial patterns for the long-term droughts simulated with all three CM 2.0 model integrations are show in the figure.*

Great Plains drought is often also associated with dry conditions in the eastern half of the United States, especially the southern portion near the Gulf of Mexico (See: Figure 6.6a, Figure 6.6d, and Figure 6.9b) . As will be shown later in the chapter, drought in this region is often connected to the cold phase of the ENSO, also known as La Niña. Whatever factors are causing these droughts, whether it be large-scale forcing from the tropical Pacific, or local feedbacks between the atmosphere and the land surface, they do not appear to influence just the small area we have defined as the Great Plains, but these factors have implications for precipitation over a broader portion of the United States.

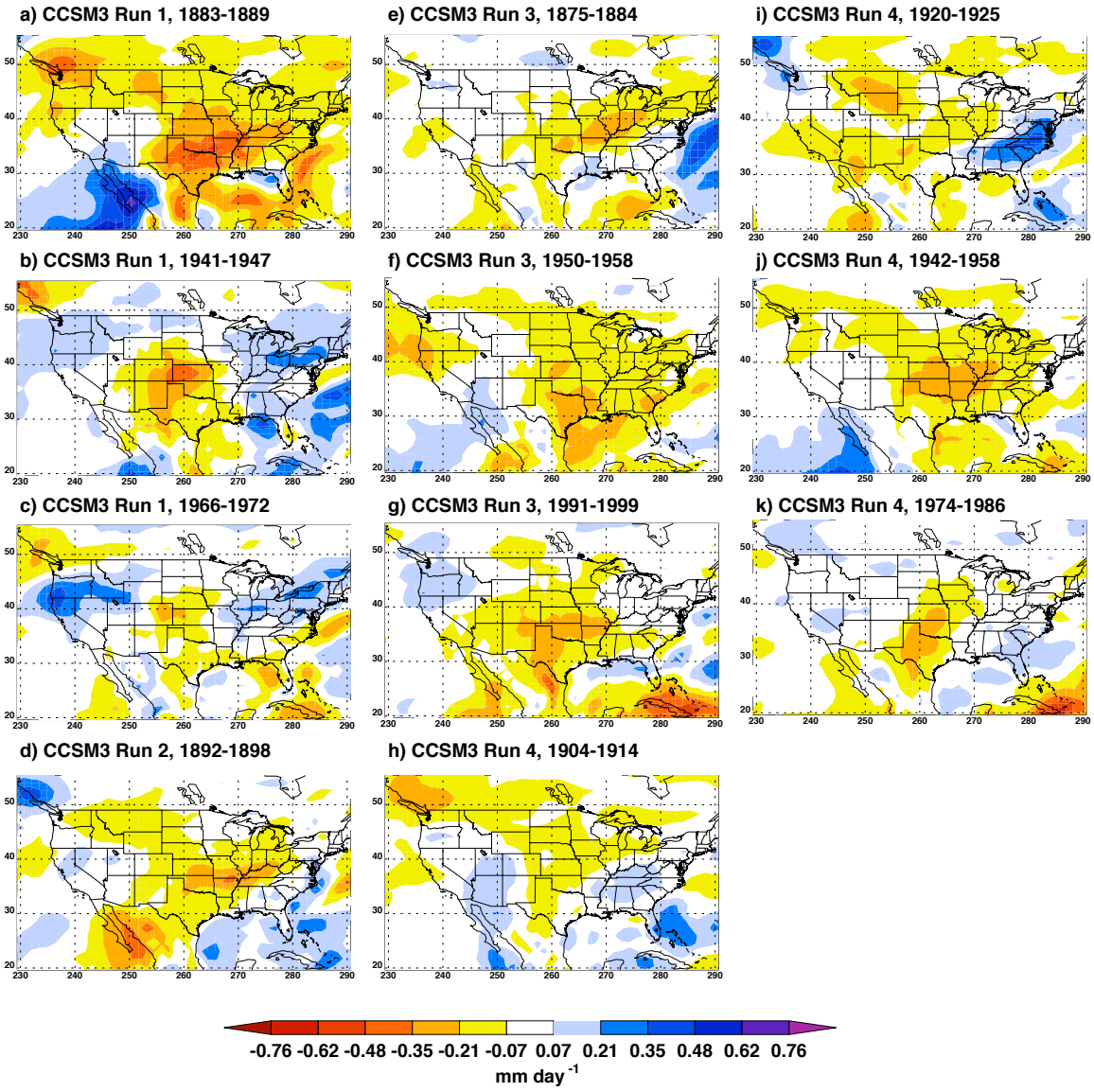


Figure 6.7. *Same as Figure 6.2 only for CCSM3. Spatial patterns for the long-term droughts simulated in Runs 1-4 from CCSM3 are shown in the figure.*

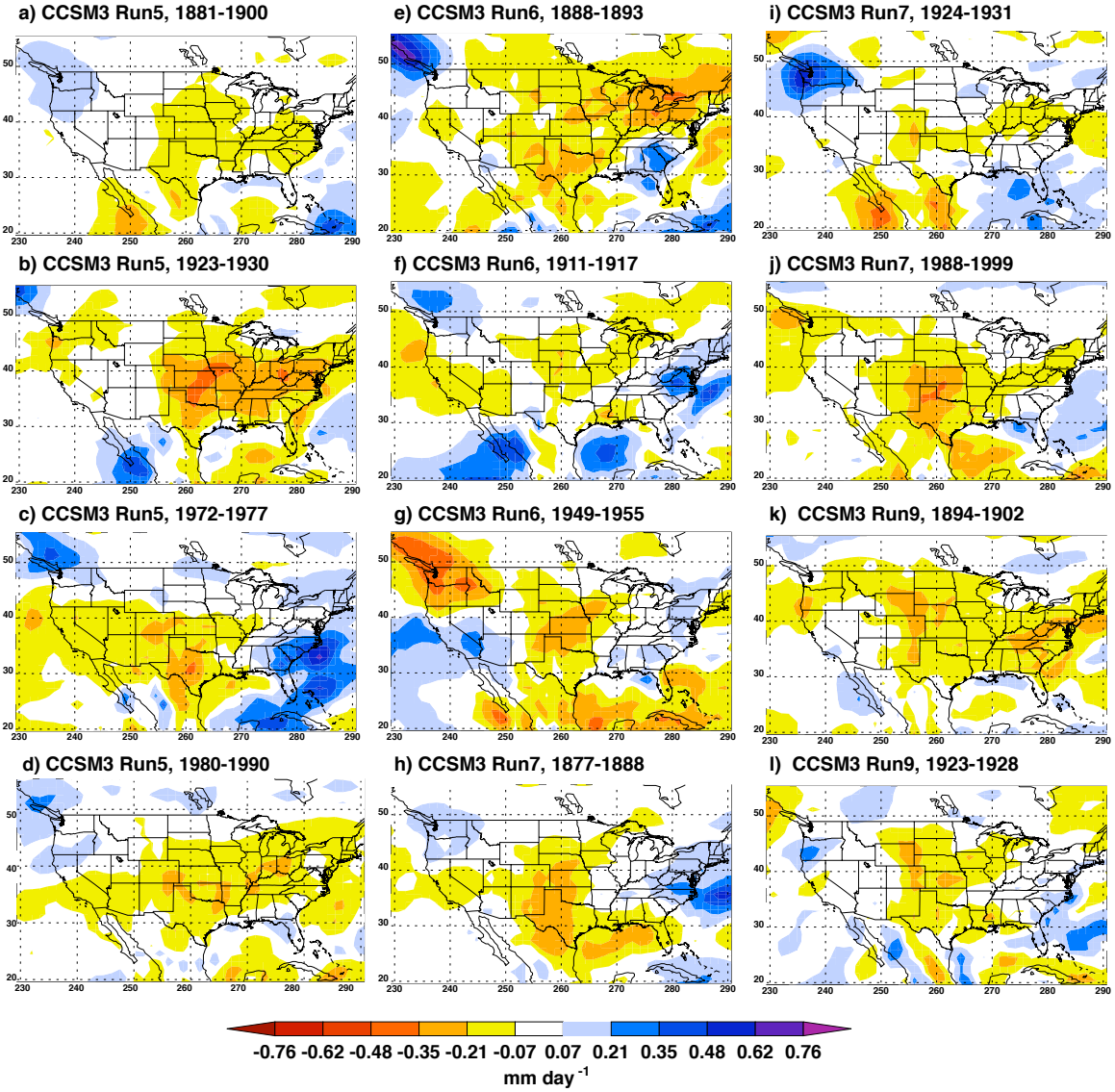


Figure 6.8. *Same as Figure 6.2 only for the CCSM3 integrations. Spatial patterns for the long-term droughts simulated in Runs 5-7 and 9 from CCSM3 are shown in the figure.*

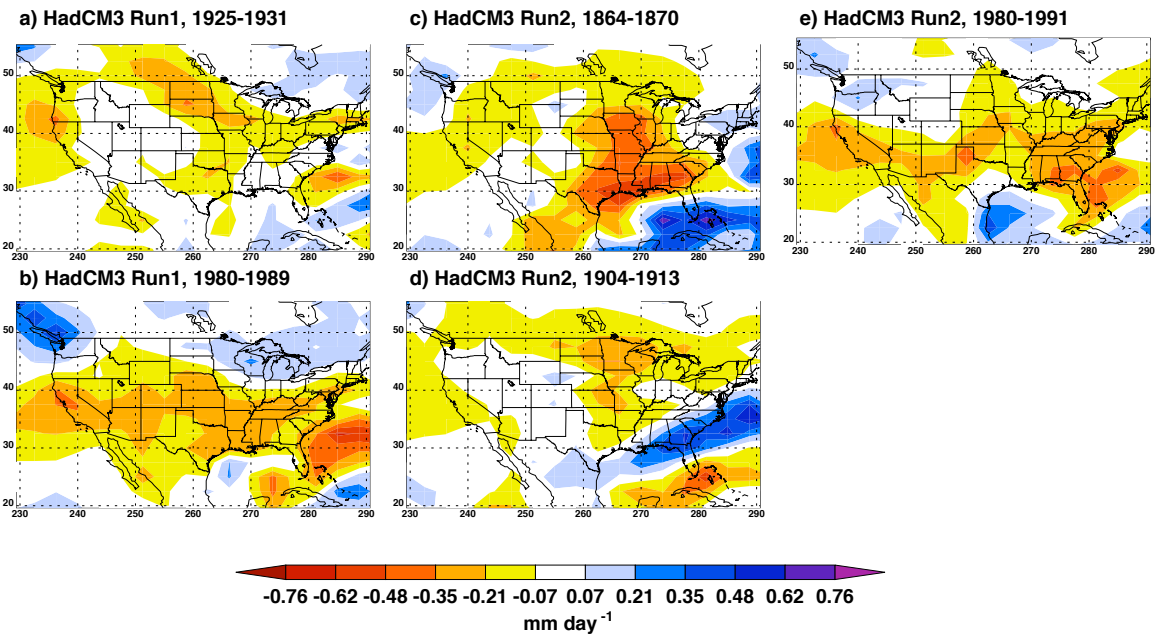


Figure 6.9. *Same as Figure 6.2 only for the HadCM3 integrations. Spatial patterns for the long-term droughts simulated in all the HadCM3 integrations are shown in the figure*

6.2 Seasonality of Long-Term Precipitation Variations

Drought in the Great Plains can occur during any season, but since over 70% of the annual precipitation falls from April through September, droughts that occur during the wet season months have the largest impact on the hydrology of the Great Plains. Figures 6.10 - 6.13 show the wet season and dry season precipitation departures from climatology for each long-term drought period (observed and simulated). From the observations we see that the 1907-1913 and 1929-1940 droughts were primarily caused by reductions in rainfall during the wet season months with dry season anomalies

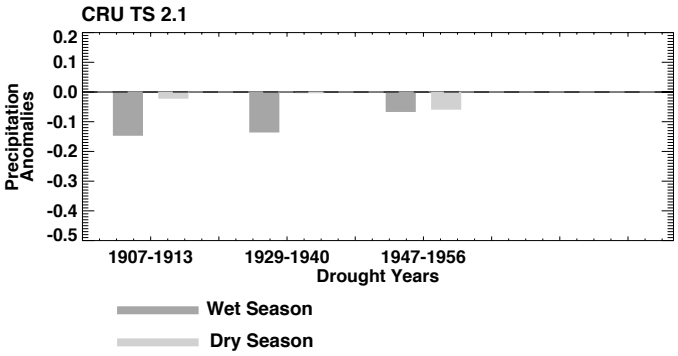


Figure 6.10. *Precipitation anomalies as a function of time of year for the three observed long-term drought periods. The left hand bar is the average wet season precipitation anomalies associated with each drought and the right hand bar is for the averaged dry season precipitation anomalies associated with each drought.*

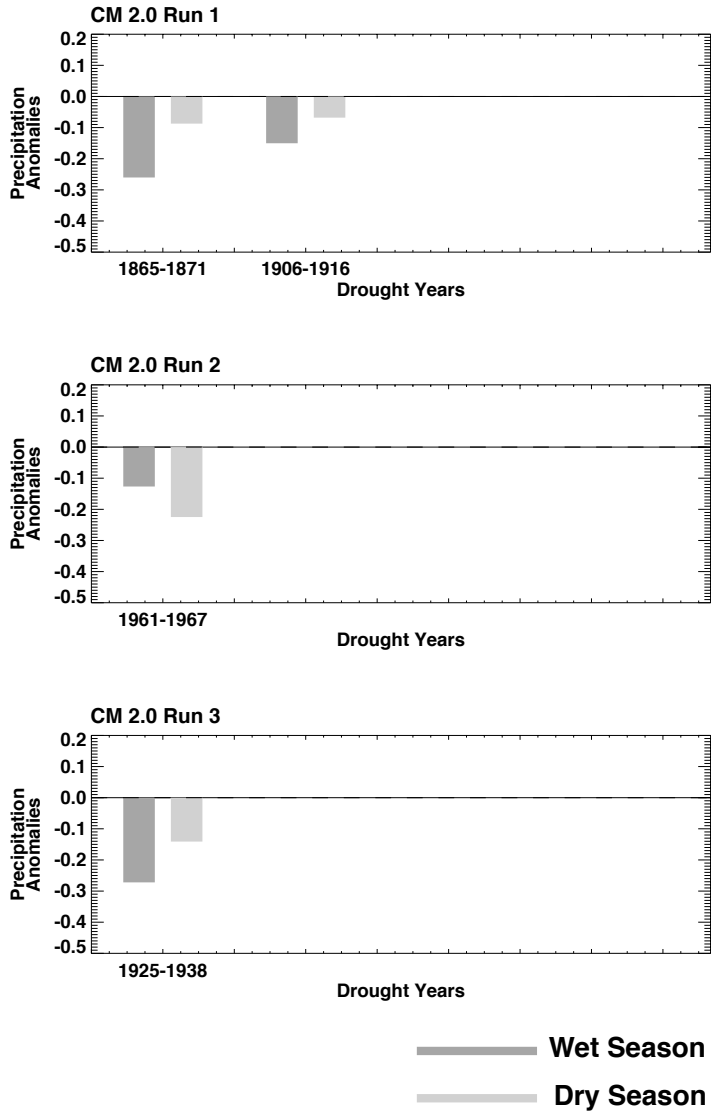


Figure 6.11. *Same as Figure 6.10 only for the long-term drought periods from CM 2.0.*

being only slightly negative and significantly less than the wet season anomalies. In the 1947-1956 drought, on the other hand, precipitation was reduced during both the wet and dry season months (Figure 6.10).

The models also show a tendency for rainfall reductions to be larger in wet season than the dry season, although in general dry-season precipitation anomalies do contribute to the total drought period anomaly. In a few rare cases, dry-season rainfall reductions

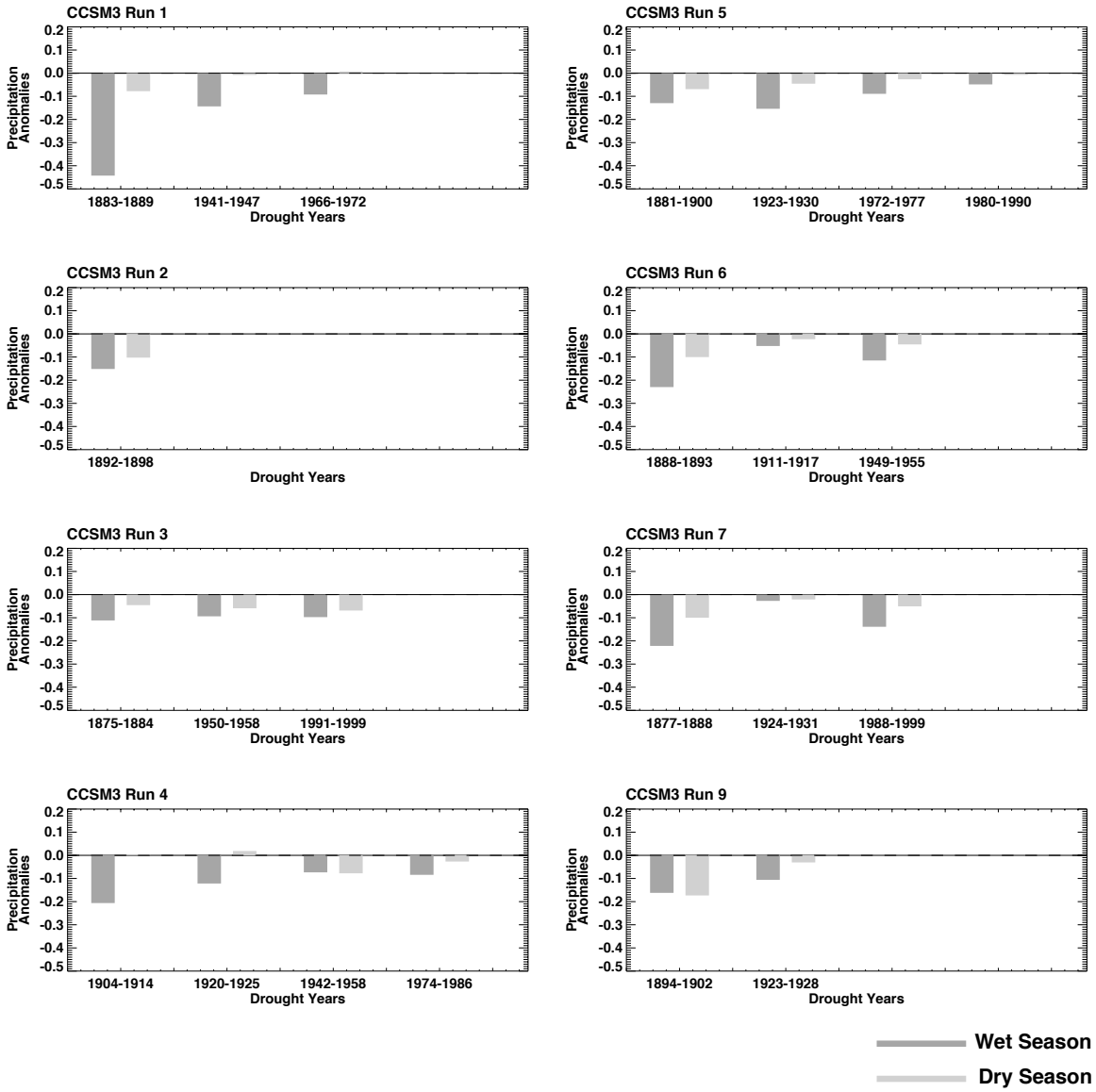


Figure 6.12. *Same as Figure 6.10 only for the long-term drought periods from CCSM3.*

greatly out-weigh the reductions in wet-season precipitation. See CM 2.0 Run 2 (Figure 6.10) and HadCM3 Run 1 (Figure 6.13).

Since reductions in rainfall amount appear to be largest during the wet season months we are primarily concerned with the factors that inhibit wet season precipitation. In the following section we discuss the synoptic scale weather patterns associated with wet and dry conditions over the Great Plains during the wet-season months.

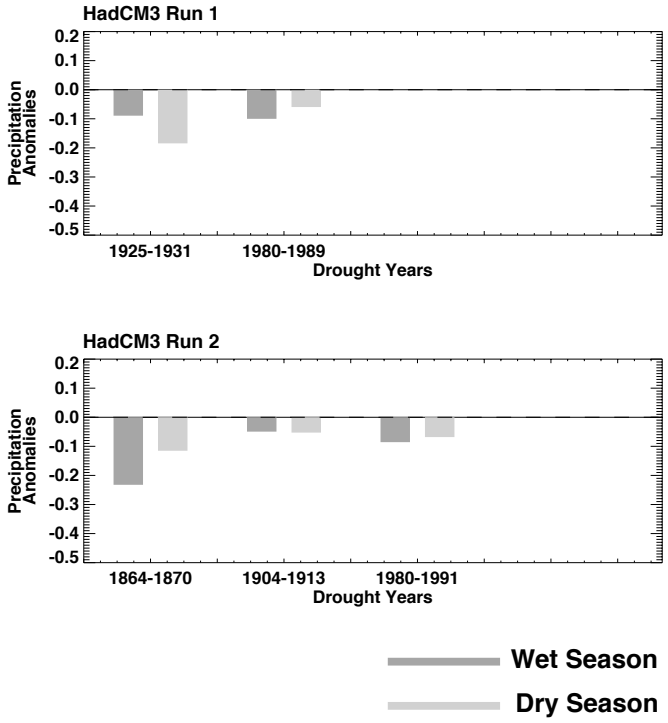


Figure 6.13. *Same as Figure 6.10 only for the long-term drought periods from HadCM3.*

6.3 Atmospheric Conditions Associated with Dry and Wet Conditions Over the Great Plains

In this section, we show composite maps of the time-averaged 500 hPa geopotential height anomalies, surface temperature anomalies, 850 hPa wind anomalies, and precipitation (P) - evapotranspiration (E) anomalies associated with wet and dry conditions over the Great Plains during the wet-season (April-September). In these figures P-E equals both the vertically integrated moisture convergence and the soil moisture tendency plus runoff. Negative P-E anomalies represent anomalous moisture divergence (i.e. moisture flow out of the region) and reduced soil moisture concentrations while positive P-E anomalies represent anomalous moisture convergence into the region and increasing soil moisture concentrations.

6.3.1 Observations

Dry conditions over the Great Plains tend to be characterized by a semipermanent mid- to upper-tropospheric anticyclone over the central United States (Namias 1955, 1983). This feature can be seen in the composite map of the 500 hPa geopotential height anomalies associated with the ten driest wet seasons that occurred between 1948-2002 (the length of the NCEP reanalysis data). Positive height anomalies are associated with large-scale subsidence and anomalous warming of the mid- to upper troposphere. Both of these factors cause the atmosphere above the Great Plains to become more statistically stable, thereby inhibiting convection and reducing precipitation rates. Anomalously high heights and the associated large-scale subsidence also tend to correspond with strong surface warming (Figure 6.14b, contours) and clear skies. The semipermanent ridge centered over the Great Plains also acts to block the flow of moisture into the region from the Gulf of Mexico (Oglesby, 1991). This too causes precipitation rates to decrease over the region (Borchert, 1950). Composite anomalies of 850 hPa winds show that in general, winds tend to be anomalously off shore near the Gulf of Mexico during dry periods (Figure 6.14c). It has also been shown that during anomalously dry periods for the Great Plains, the midlatitude jet stream can shift poleward thereby changing the location of surface fronts and cyclogenesis, although it should be noted that fronts play a limited role in influencing precipitation over the Great Plains during the wet season (Bryson, 1966). In general, the circulation patterns associated with droughts can persist on timescales of months to seasons and are perpetuated or amplified by large-scale subsidence, strong surface heating and low soil moisture concentrations (Figure 6.14b, d)

(Charney, 1975; Naimas, 1983; Oglesby and Erickson, 1989). As discussed in Chapter 2, interactions between soil moisture, evapotranspiration and precipitation can cause precipitation anomalies to persist for long periods of time over the Great Plains. The relationships among these variables are discussed later in this chapter.

In contrast to dry conditions, wet conditions over the Great Plains are characterized by a dipole-like anomaly pattern in the geopotential height field . A composite map of the 500 hPa geopotential height anomalies associated with the ten wettest wet seasons that occurred between 1948-2002 is show in Figure 6.14f. As can be seen in the figure, during wet periods, negative geopotential height anomalies are centered over the western half of the United States, while positive height anomalies reside over the Eastern half. The negative height anomalies over the Great Plains are associated with anomalously unstable atmospheric conditions and large-scale ascent, and therefore represent conditions that are conducive for convection. The flow around the anticyclone centered over the eastern half of the Untied States allows for increased moisture transport into the Great Plains region and enhanced precipitation rates (Figure 6.14g). The added flux of moisture into the region may due, in part, to a strengthening of the Nocturnal Great Plains low-level jet during wet periods (Weaver and Nigam, 2008). Wet conditions over the Great Plains tend also to be associated with positive soil-moisture anomalies, which help to provide added moisture to the atmosphere via evapotranspiration (Figure 6.14h).

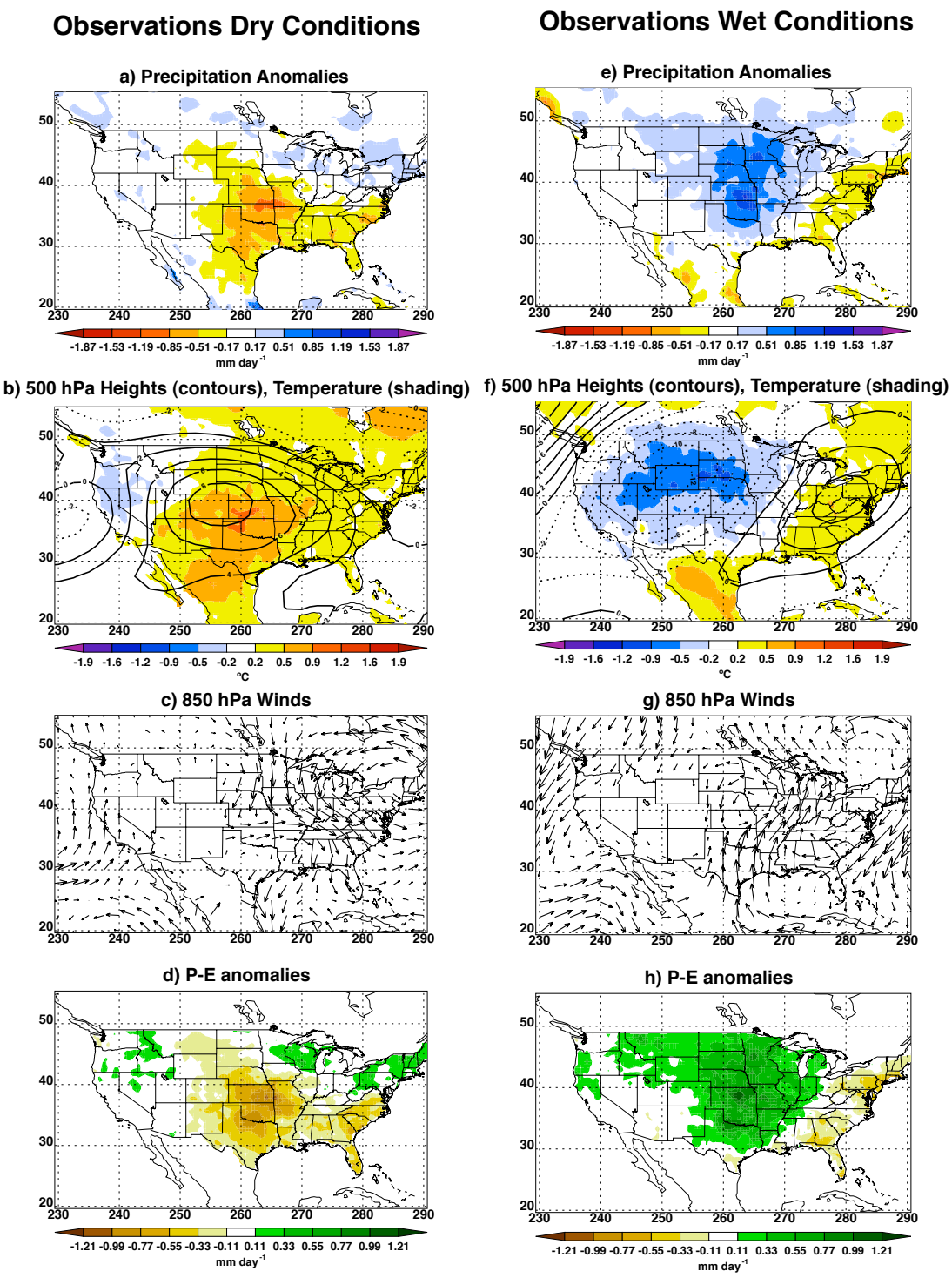


Figure 6.14. *Composite anomalies of precipitation (a, e), 500 hPa geopotential heights and surface temperature (b, f), 850 hPa winds (c, g) and Precipitation (P) - Evapotranspiration (E) from the ten driest wet season (left column) and ten wettest wet seasons (right column) for the Great Plains region for the period 1948-2002. Precipitation and temperature data are from CRU, evapotranspiration is from VIC, 850 hPa winds and 500 hPa geopotential heights are from NCEP.*

The position of the Bermuda High in the Atlantic ocean also plays an important role influencing moisture transport in to the Great Plains region. When the Bermuda High is positioned farther east than normal, moisture is diverted into the eastern corridor of the United States, rather than the Great Plains region (Helfand and Schubert, 1995)

6.3.2 Models

Figures 6.15-6.27 show the anomalous atmospheric conditions associated with the ten driest (left-hand side) and ten wettest (right-hand side) wet seasons from each simulation. As in the observations, dry conditions over the Great Plains in the models are associated with an anomalous mid- to upper-level anti-cyclone that is typically centered over the central United States. This anti-cyclone is associated with anomalous warming of the surface, caused by large scale subsidence, clear skies, and low evapotranspiration rates. Also, P-E is always anomalously low over the Great Plains region during dry periods, indicating anomalous divergence of moisture out of the central United States and reduced soil moisture concentrations. In the models, 850 hPa wind anomalies are generally influenced by low-level pressure anomalies which can be different from the mid- to upper-level disturbances. This means that low-level winds are not always anomalously off shore as was seen in the observations.

In both the models and the observations, maximum precipitation anomalies and surface temperature anomalies tend to occur slightly to the south east of the maximum geopotential height anomaly. This is because downwind from the region of maximum ridging at 500 hPa, you have negative vorticity advection, which by the omega equation will be associated with large-scale subsidence (Holton, p. 166 and p. 178).

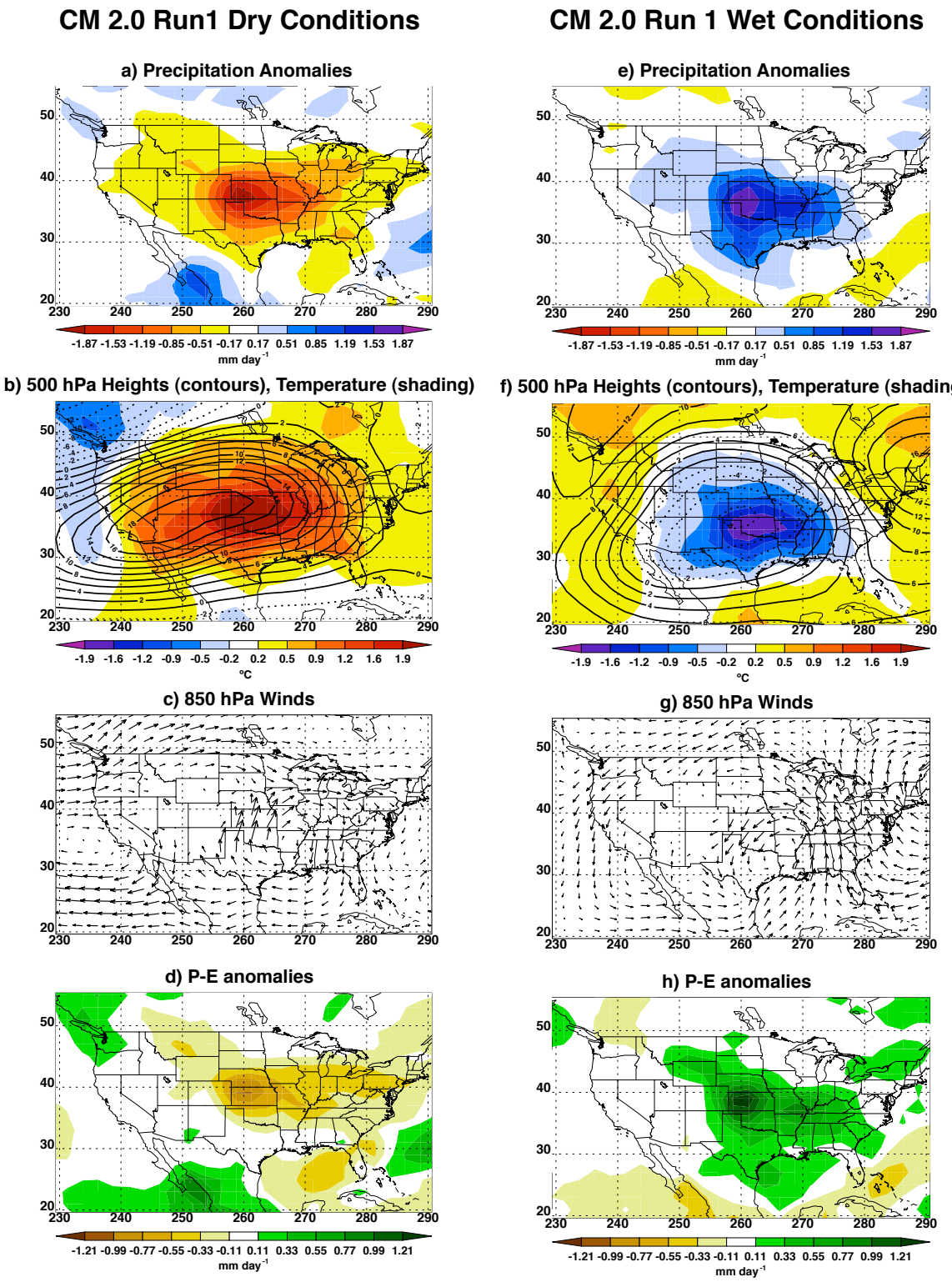


Figure 15. *Same as Figure 14 only for CM 2.0 Run 1*

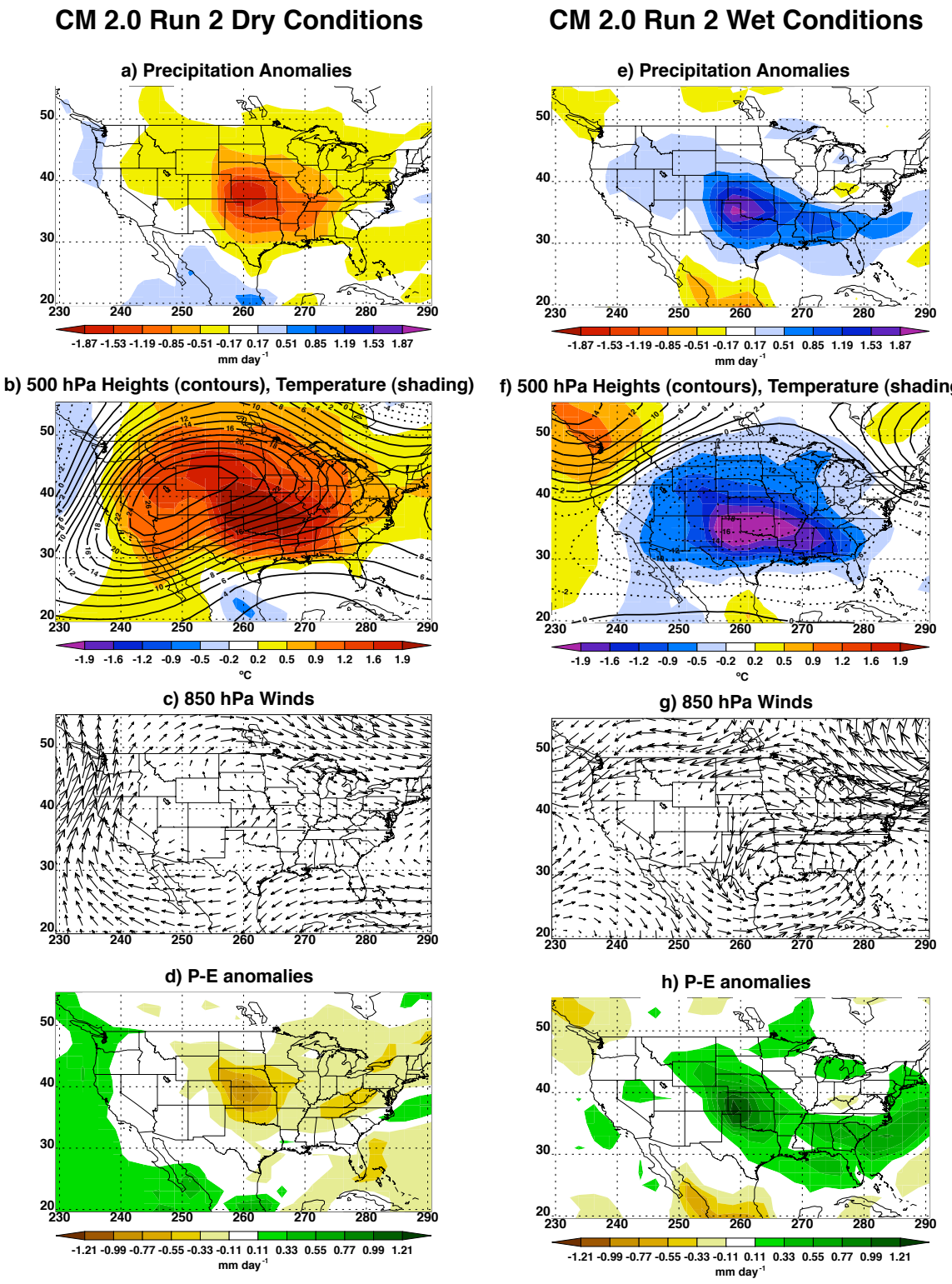


Figure 16. *Same as Figure 14 only for CM 2.0 Run 2*

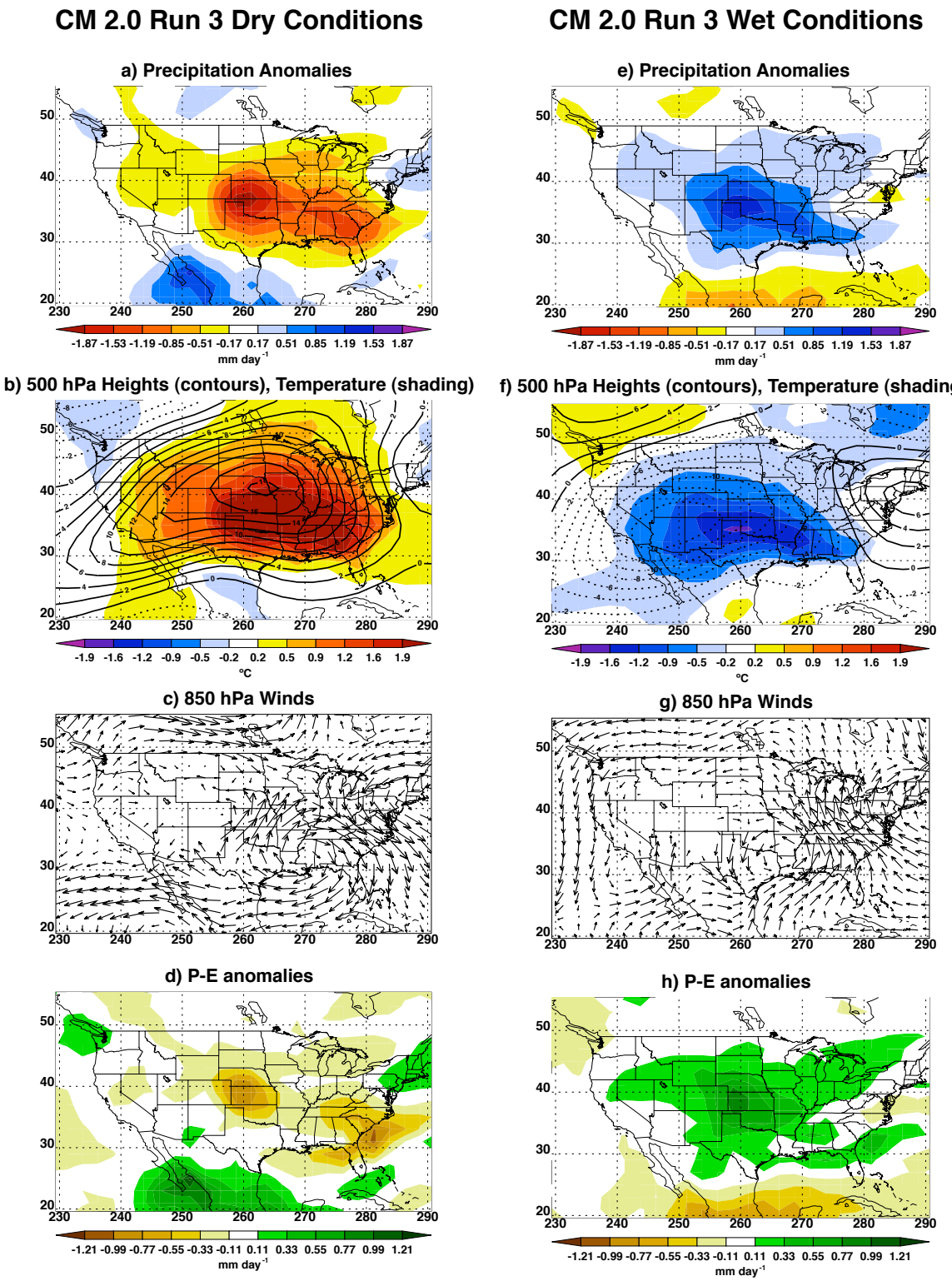


Figure 17. *Same as Figure 14 only for CM 2.0 Run 3*

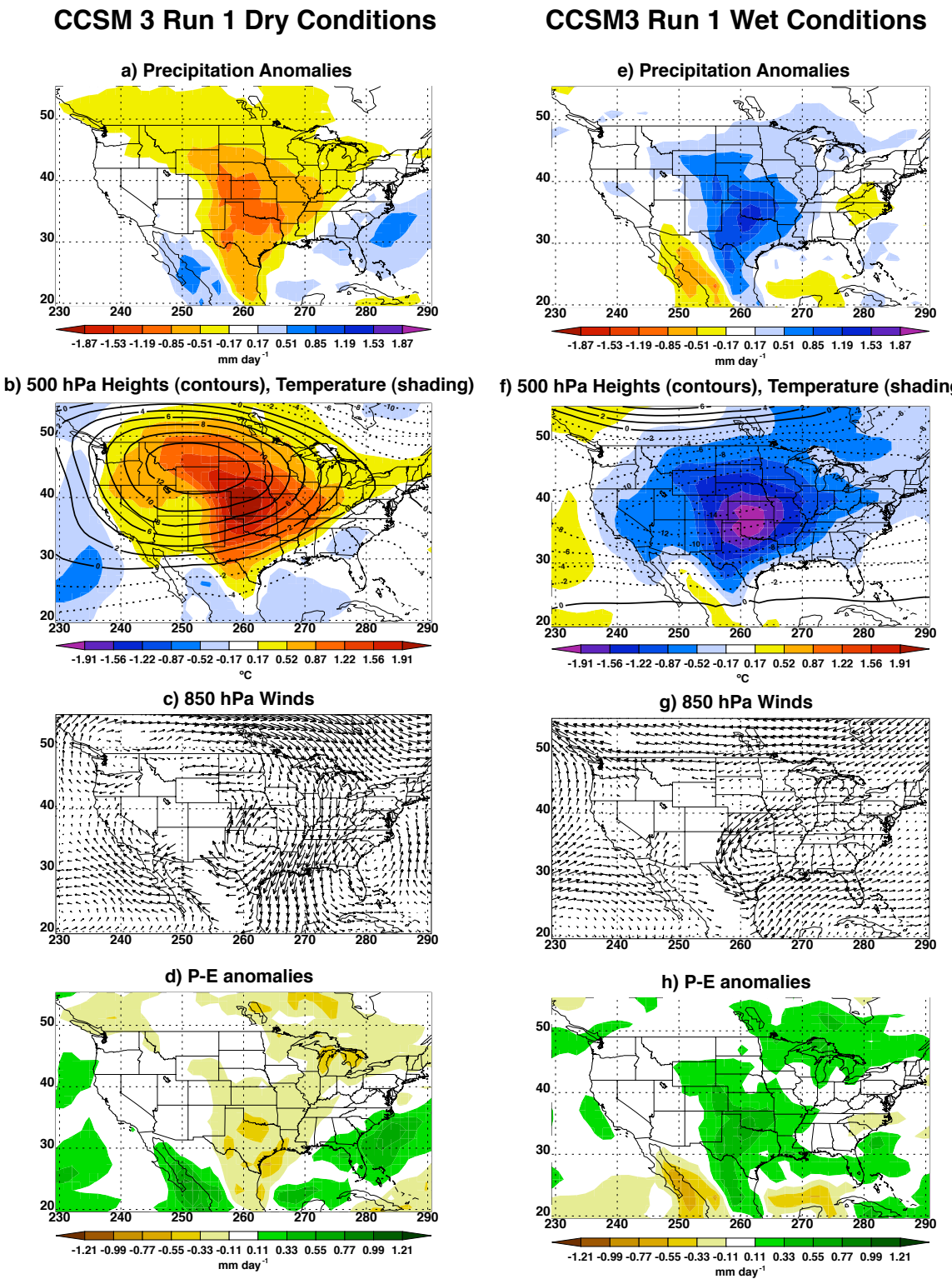


Figure 18. *Same as Figure 14 only for CCSM3 Run 1.*

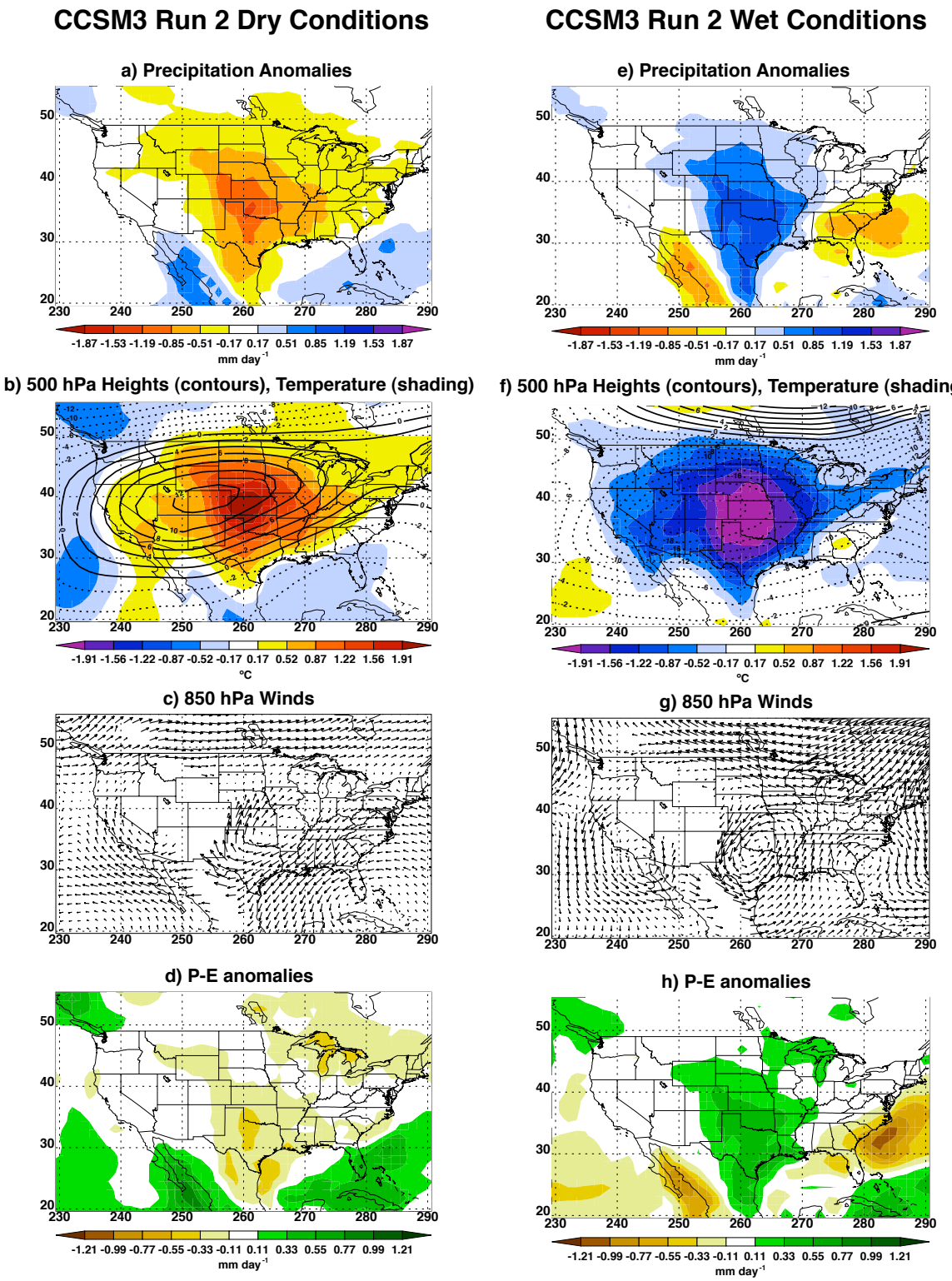


Figure 19. *Same as Figure 14 only for CCSM3 Run 2.*

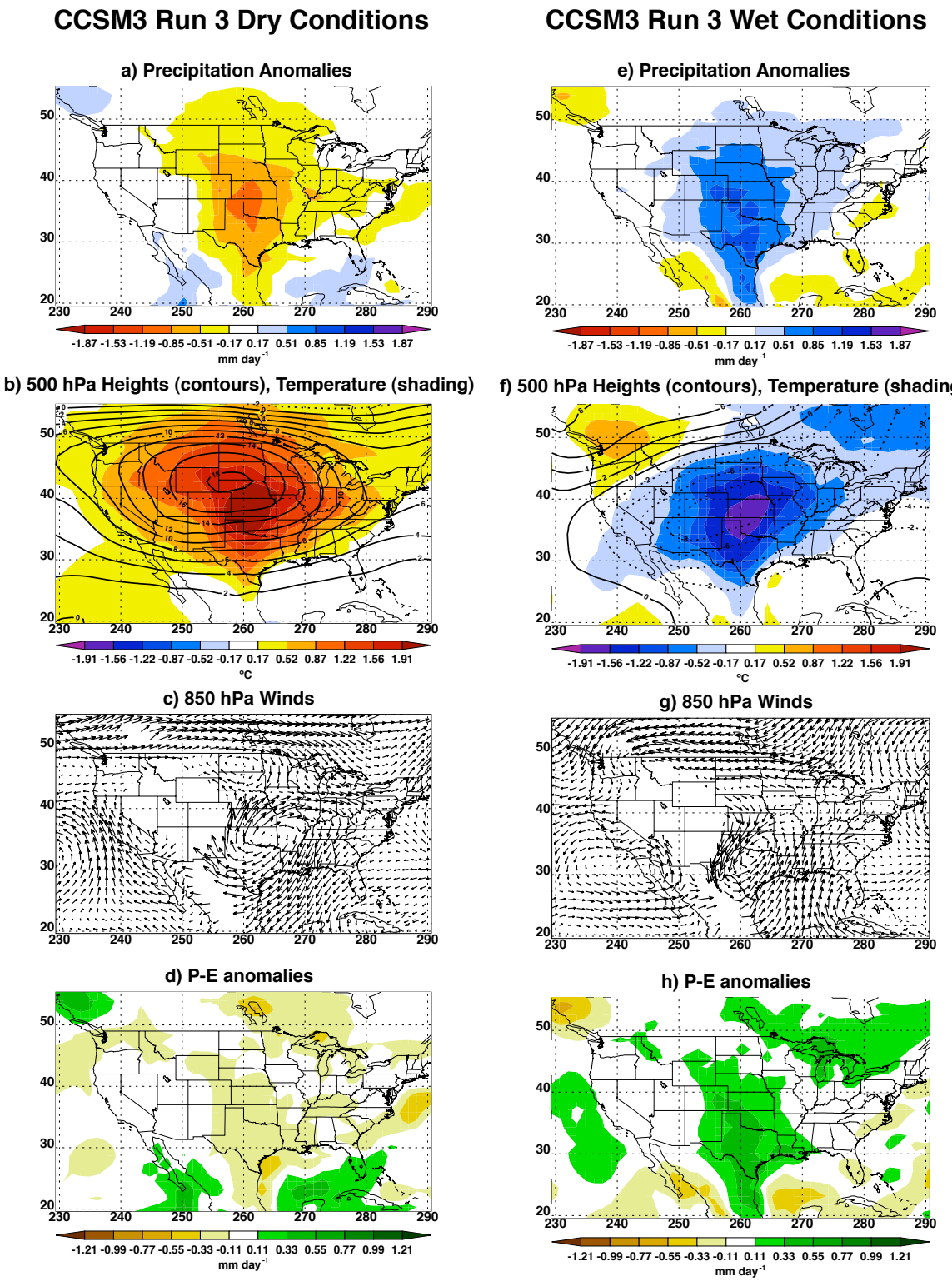


Figure 20. *Same as Figure 14 only for CCSM3 Run 3.*

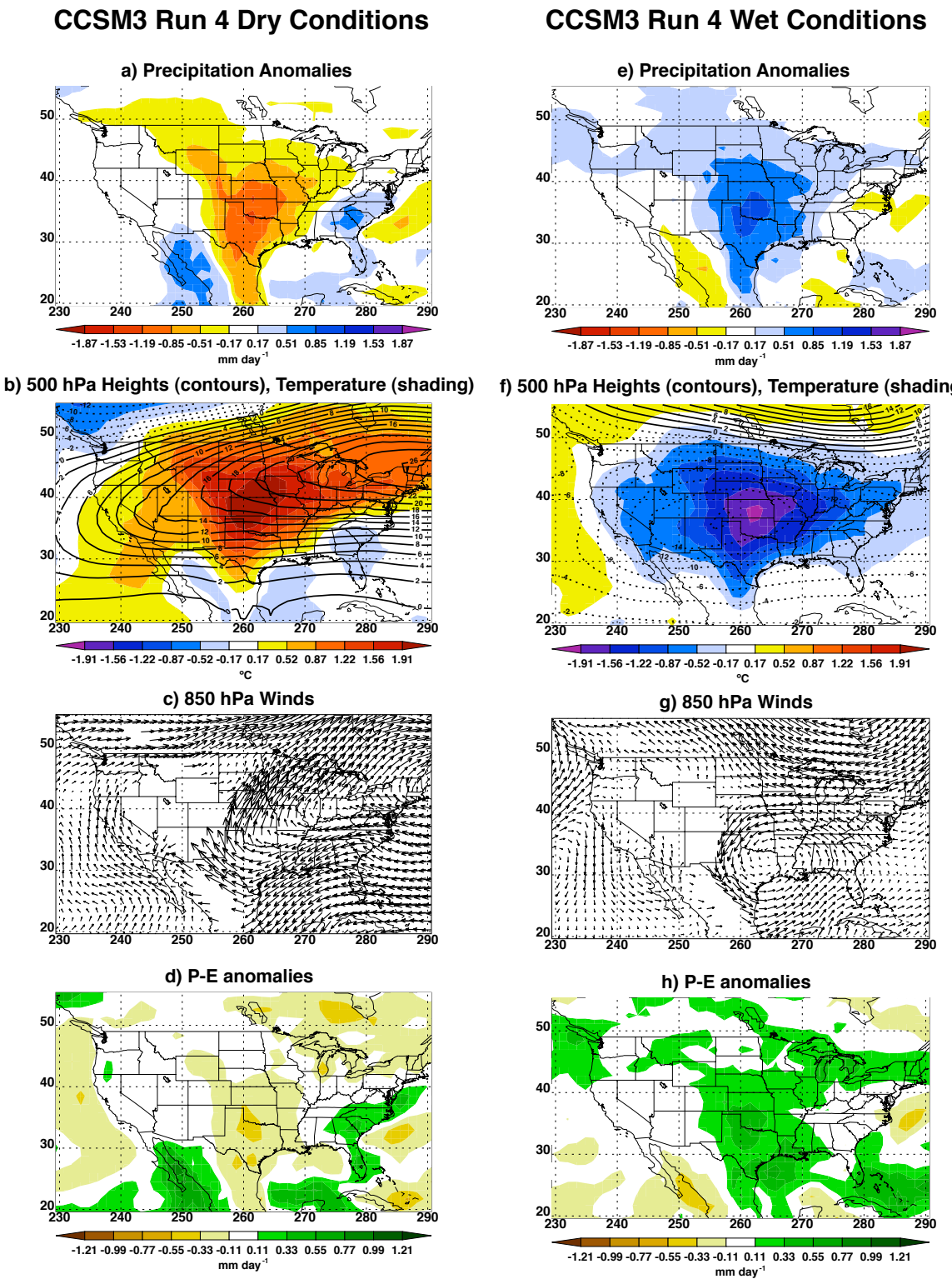


Figure 21. *Same as Figure 14 only for CCSM3 Run 4.*

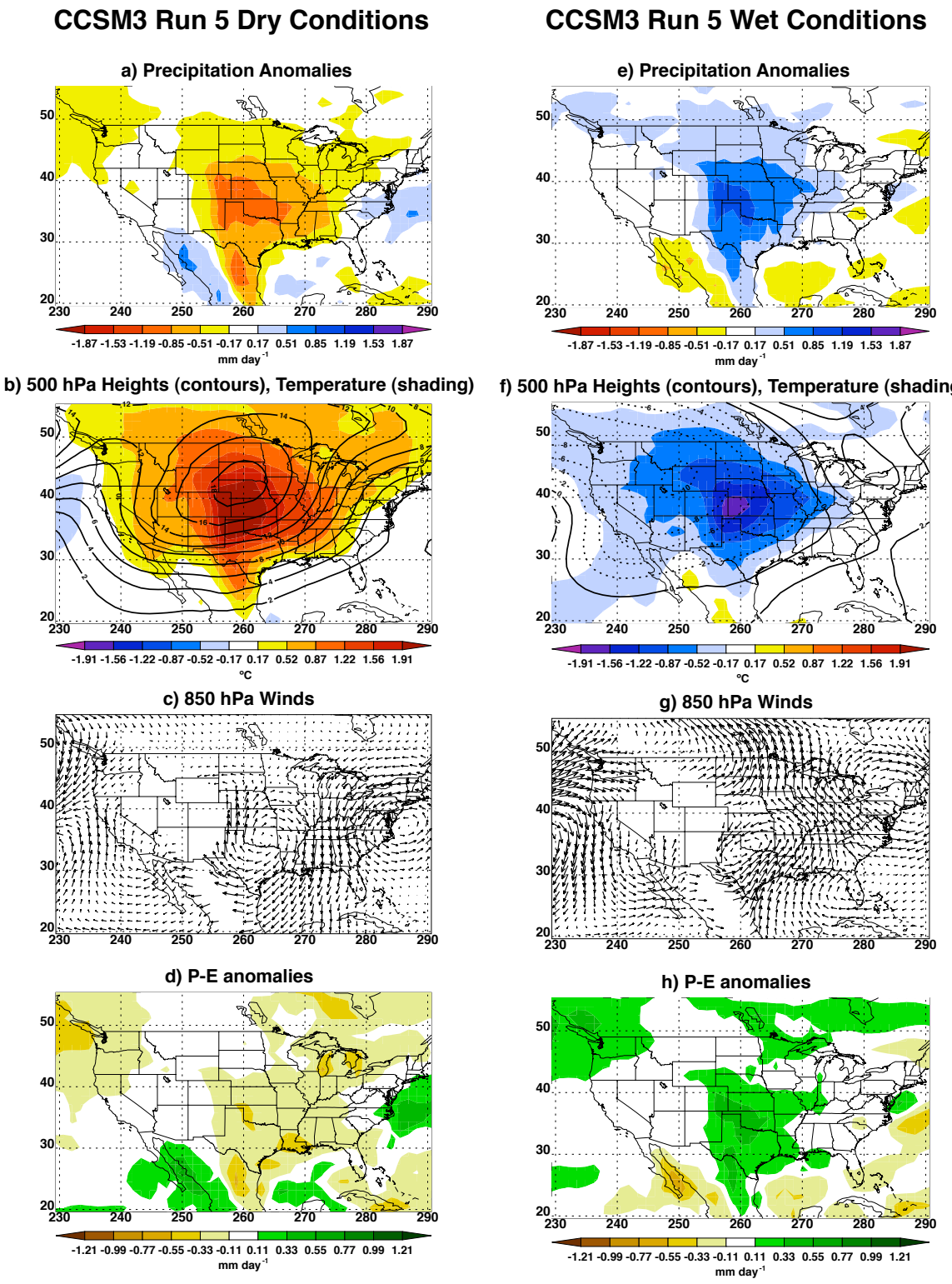


Figure 22. *Same as Figure 14 only for CCSM3 Run 5.*

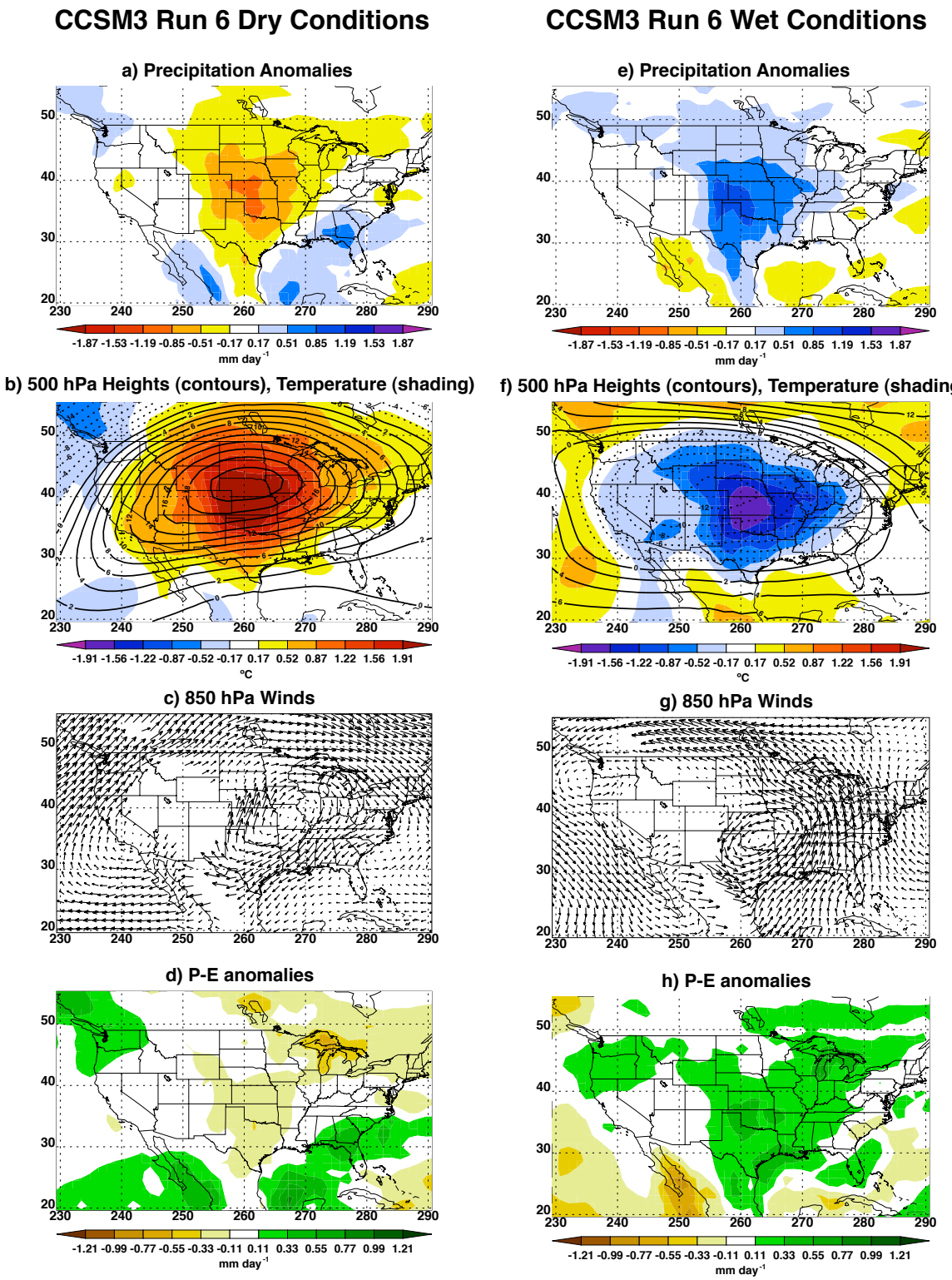


Figure 23. *Same as Figure 14 only for CCSM3 Run 6.*

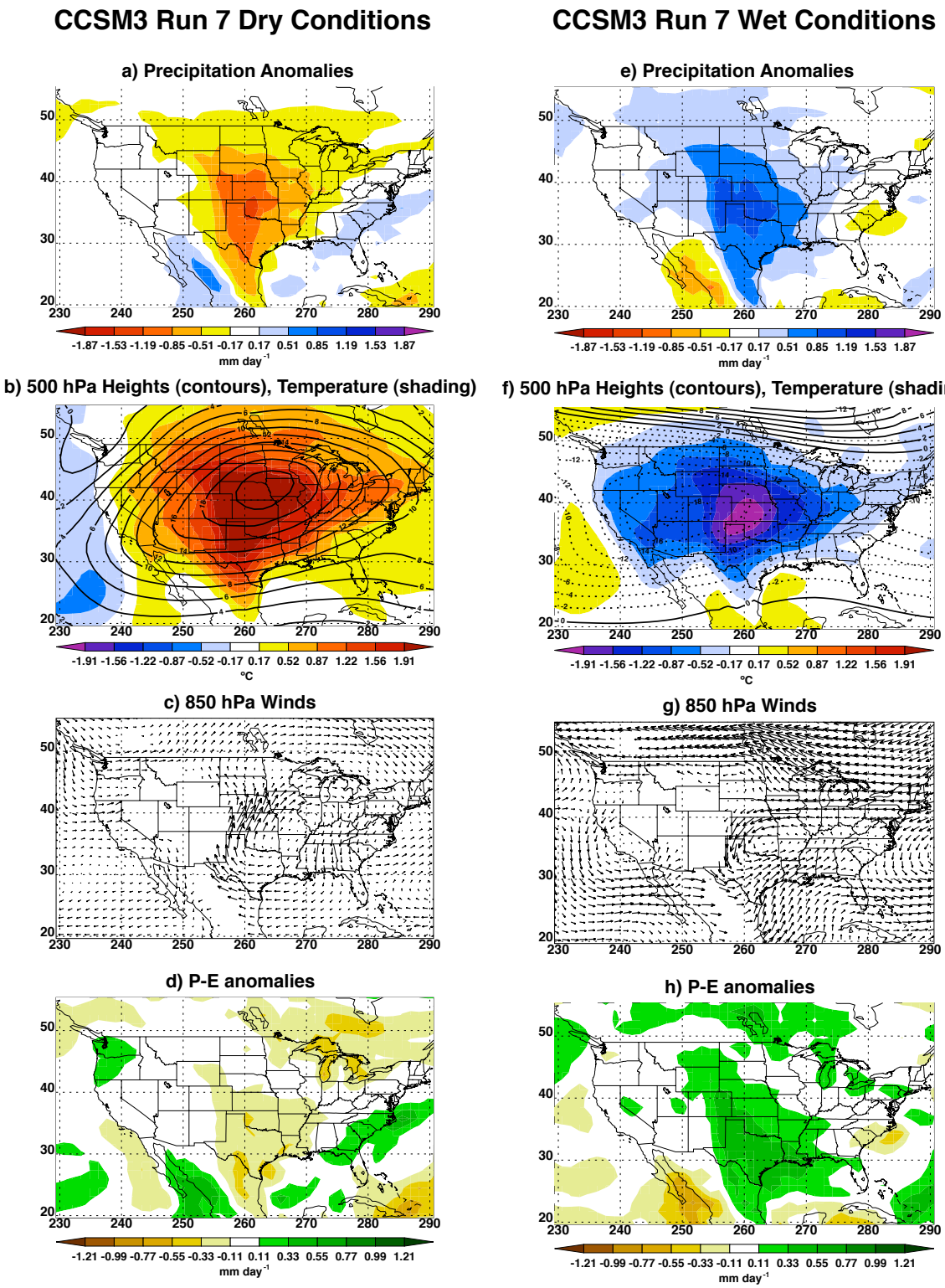


Figure 24. *Same as Figure 14 only for CCSM3 Run 7..*

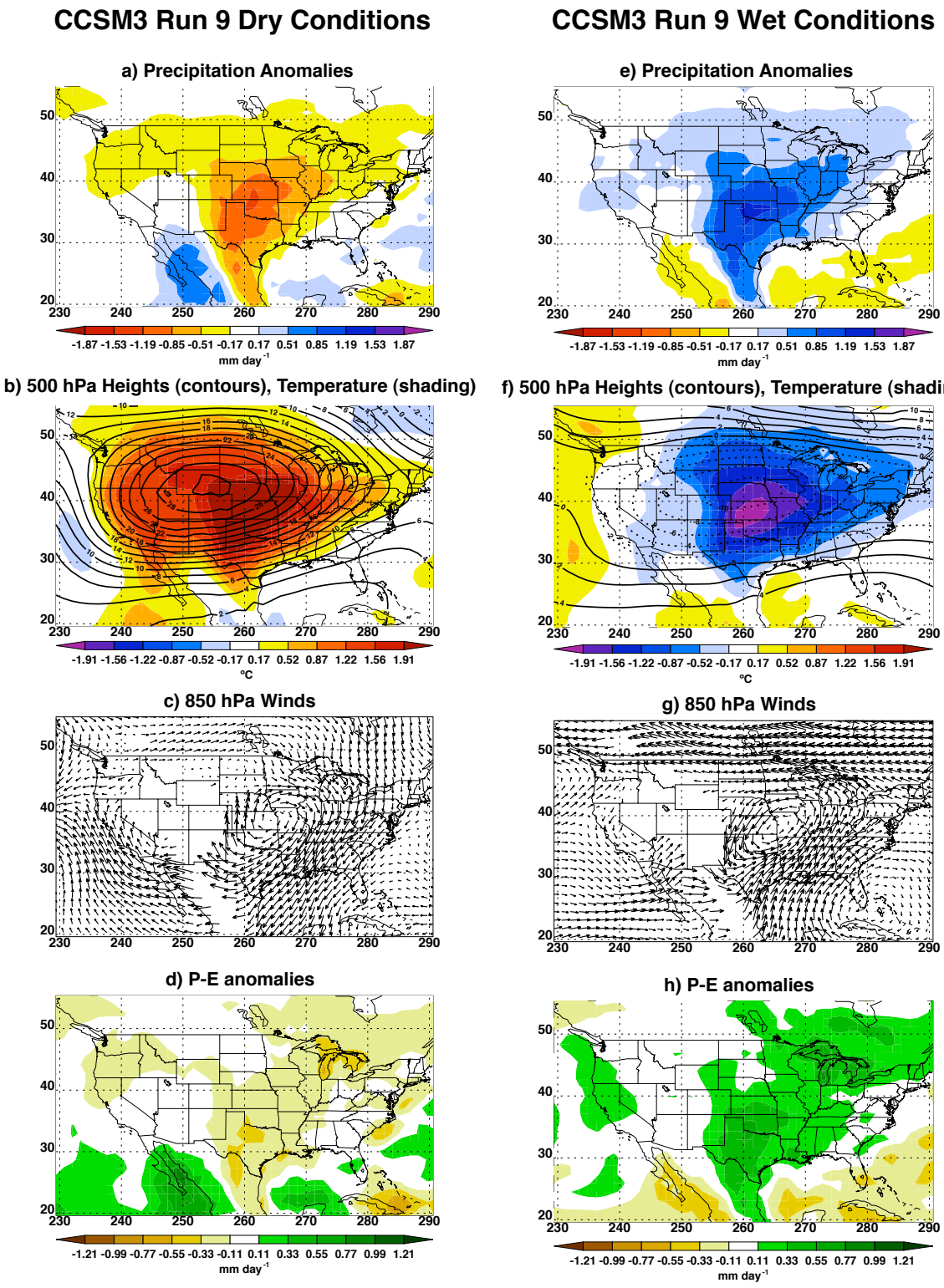


Figure 25. *Same as Figure 14 only for CCSM3 Run 9.*

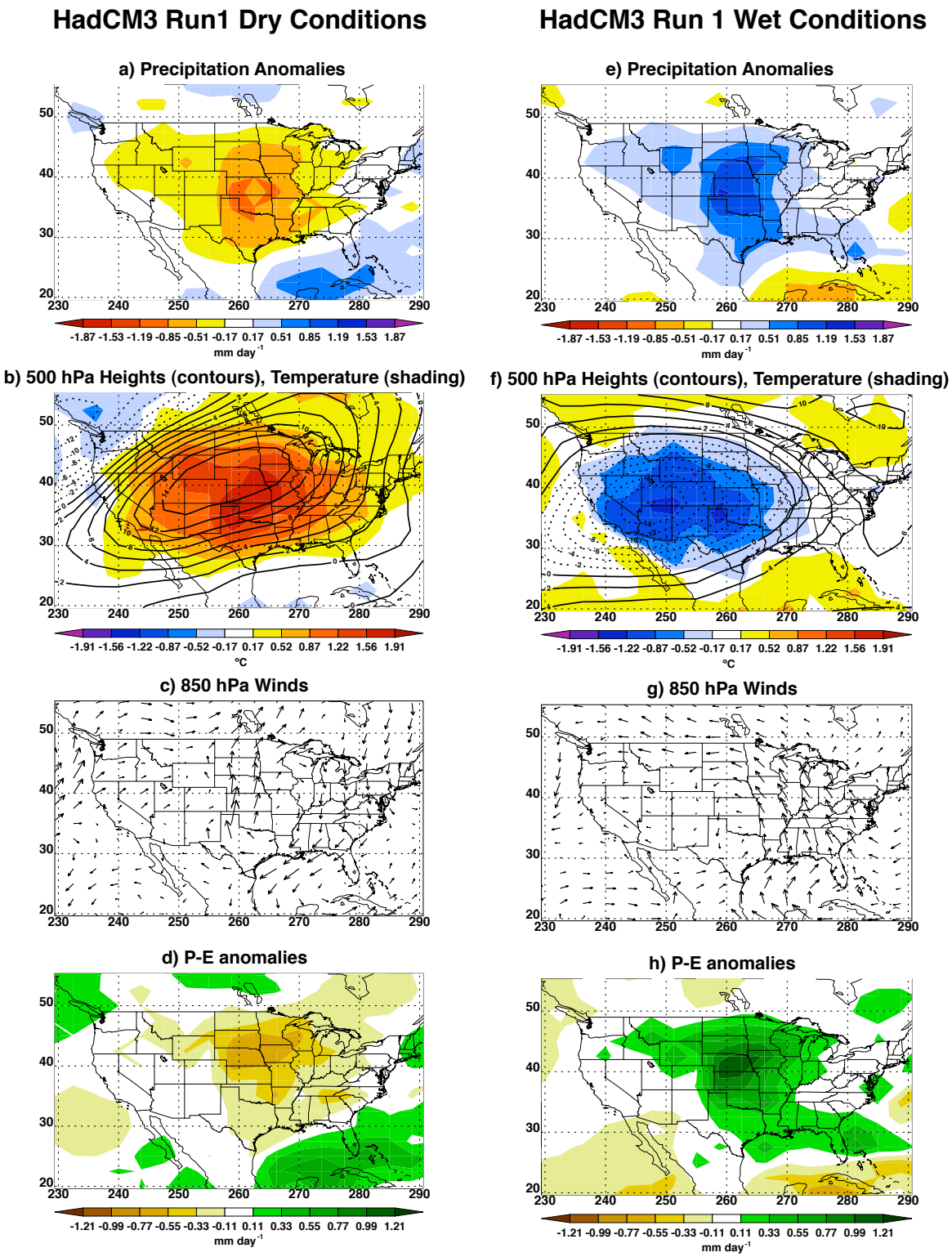


Figure 26. *Same as Figure 14 only for HadCM3 Run 1.*

Wet conditions over the Great Plains in the models are characterized by somewhat different atmospheric conditions than those seen in the observations. While in the observations, the geopotential height anomaly was characterized by a dipole-like pattern with negative heights centered over the western half of the United States and positive heights over the eastern United States, in the models, negative geopotential height anomalies influence the entire United States, and rarely is the eastern portion of the United States under the influence of high pressure. The wet conditions over the Great Plains in the models are also associated with anomalous surface cooling, anomalous moisture flux convergence, and positive soil moisture anomalies. Again, 850 hPa height anomalies tend to be influenced by low level pressure anomalies, so are not always anomalously on shore as was seen in the observations.

Out of all the simulations we argue that HadCM3 Run 2 (Figure 6.27) most accurately captures the the observed atmospheric anomalies that are associated with wet and dry conditions. In HadCM3 Run 2, not only are the geopotential height anomaly fields and surface temperature anomaly fields similar to those observed, but also, the 850 hPa wind fields exhibit similar patterns, with anomalous off shore flow during dry periods and on shore flow during wet periods. The strong flow into the region from the Gulf of Mexico during wet periods, in this model, possibly represent the enhancement of the Great Plains nocturnal low-level jet. Identifying this jet in the model would require data with a finer temporal resolution, on the time scale of hours to a day, and so is not within the scope of this research.

From the above analysis we can conclude that models do capture the atmospheric anomaly patterns associated with dry conditions that occur during wet-season months. The next question we want to answer is, what mechanisms cause negative Great Plains precipitation anomalies to persist for long-periods of time in the simulations? Remember from Chapter 2 that during the observed 20th Century, both large-scale forcing from the tropical Pacific and local feedbacks between the land surface and the atmosphere have been shown to be associated with long-term Great Plains drought. In the following sections we investigate the role that these factors play in influencing the simulated droughts.

6.4 Variability in Tropical Pacific SSTs and Great Plains Drought

In Chapter 2 we discussed how cool conditions in the tropical Pacific can induce drought conditions over the Great Plains region via two main mechanisms, 1)eddy-mean-flow interactions that induce subsidence over the mid-latitude regions of both the southern and northern hemispheres, and 2) stationary Rossby wave patterns that emanate out of the Tropics and result in an anomalous high over the southern portion of the United States.

In this section we investigate the relationship between tropical Pacific SST variability and Great Plains precipitation. To do this, we first look at the relationship that exists between the El Niño Southern Oscillation (ENSO), the leading pattern of interannual SST variability in the tropical Pacific, and U.S. precipitation in the models compared to the observations. Then we compare the global SST patterns that are associated with each of the Great Plains droughts simulated by the models with the SST

patterns that are associated with the observed Great Plains droughts. The ability of the models to simulate ENSO is examined in Appendix A.

6.4.1 El Niño Southern Oscillation (ENSO) and U. S. Precipitation

The observed linear relationship between the El Niño Southern Oscillation (ENSO) and U. S. precipitation is illustrated in Figure 6.28. This figure shows the regression values of U. S. precipitation anomalies regressed onto the Niño 3.4 index for dry season months (Figure 6.28a) and wet season months (Figure 6.28b) over the time period of 1901-2002. In these figures, positive regression coefficients indicate that U.S. precipitation is in phase with ENSO. This means that warm conditions in the equatorial Pacific correspond with increased precipitation rates while cool conditions in the equatorial Pacific correspond with decreased precipitation rates. Negative regression coefficients indicate where U.S. precipitation and ENSO are out of phase with each other. The linear relationships that are significant at the 95% confidence level using a two tailed t-test are

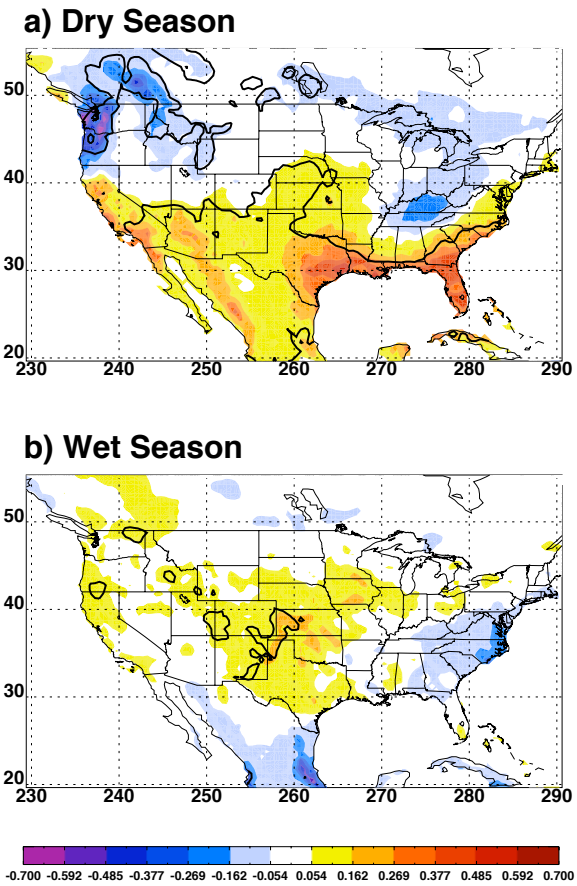


Figure 6.28. *Regression values of U. S. precipitation regressed on to the standardized Niño 3.4 index in units of mm/day. (a) Dry season (October-March) precipitation regressed onto October-March Niño 3.4 values, and (b) Wet season (April-September) precipitation regressed onto April - September Niño 3.4 values. Black curves delineate regression values that are significant at the 95% confidence level.*

delineated by the black curves. To test the robustness of these patterns we also subdivided the data into two 50 year blocks and found similar results (not shown).

From the figures we see that there exists a positive relationship between precipitation and ENSO over much of the southern portion of the United States. This relationship is particularly strong over the eastern half of Texas, the Gulf Coast region, and Florida. Over the Great Plains, ENSO influences precipitation from Texas up to Nebraska. North of Nebraska, ENSO has no significant influence on precipitation.

ENSO and precipitation tend to be out of phase in the Pacific Northwest region of the United States and in portions of the South including Tennessee and Kentucky. The relationship between ENSO and precipitation is strongest during the dry season months (October - March), when Rossby wave propagation out of the tropics is most prominent (Rasmusson and Carpenter, 1982; Trenberth, 1997). During the wet season, ENSO's influence on the Great Plains is minimal and primarily centered over the Central Plains in Kansas and the panhandle of Oklahoma. Interestingly, over Mexico, during dry season months, precipitation tends to be in phase with ENSO, while during wet season months precipitation over Mexico tends to be out of phase with ENSO.

Figures 6.29 and 6.30 show the relationships between ENSO and U. S. precipitation from each simulation for dry season months and wet season months respectively. In CM 2.0 and HadCM3, the simulated relationships between ENSO and U.S. precipitation are similar to the observations. In these models the southern portion of the United States is in phase with ENSO while the Pacific Northwest region is out of phase with ENSO. Both models do, however, overestimate the linear relationship

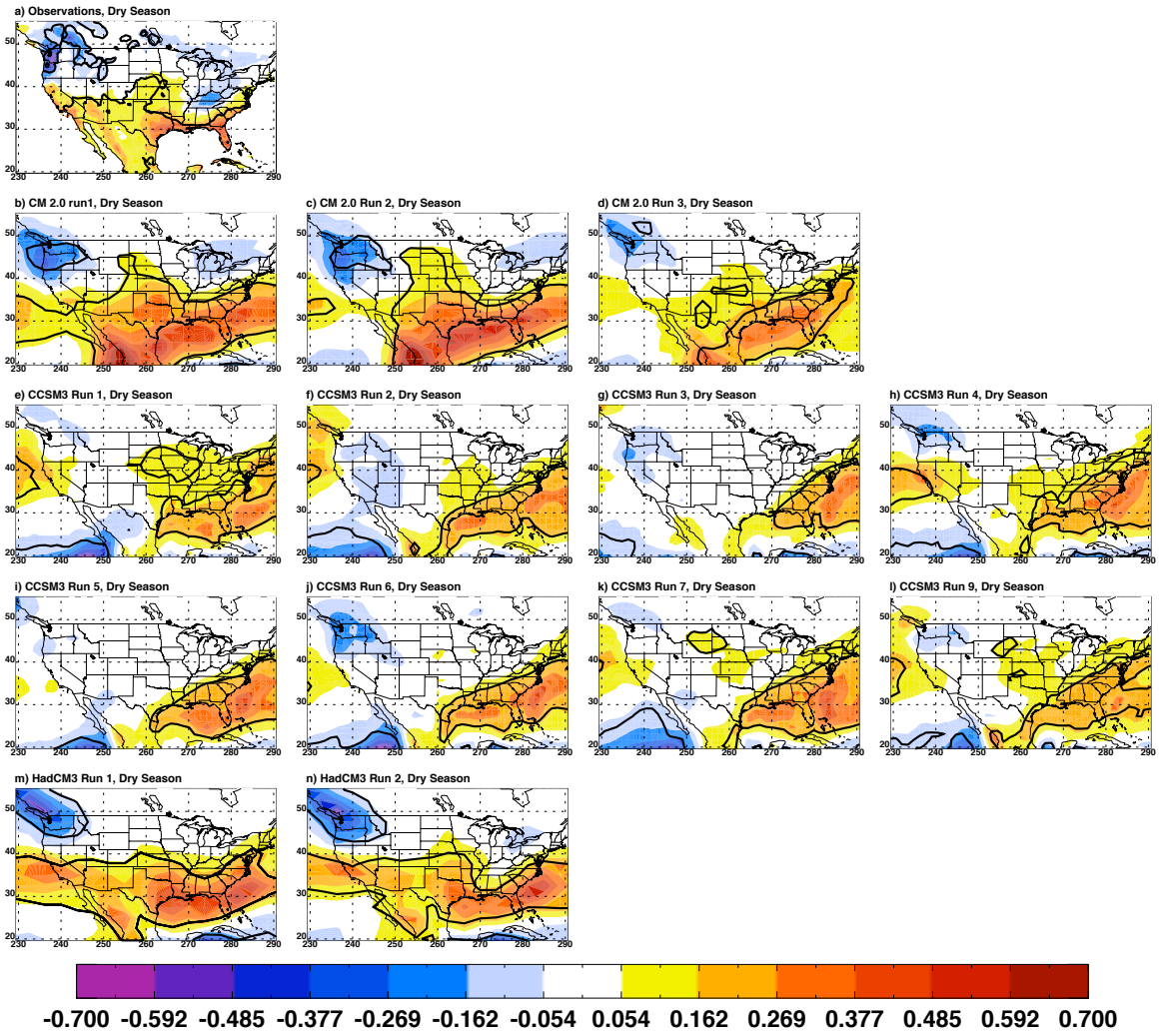


Figure 6.29. *Regression values of dry season (October - March) precipitation regressed onto October-March Niño 3.4 values from the observations (a), CM 2.0 (b-d), CCSM3 (e-l) and HadCM3 (m-n). Black curves delineate regression values that are significant at the 95% confidence level.*

between ENSO and U.S. precipitation in the dry and wet seasons. For example, during the wet season, regression coefficients are significantly larger over the Great Plains region in both CM 2.0 and HadCM3 than were observed. In CCSM3, on the other hand, the relationship between ENSO and U. S. precipitation is somewhat different than what was observed. In this model, precipitation over the eastern half of the United States is in phase with ENSO while precipitation over the western half of the country is out of phase

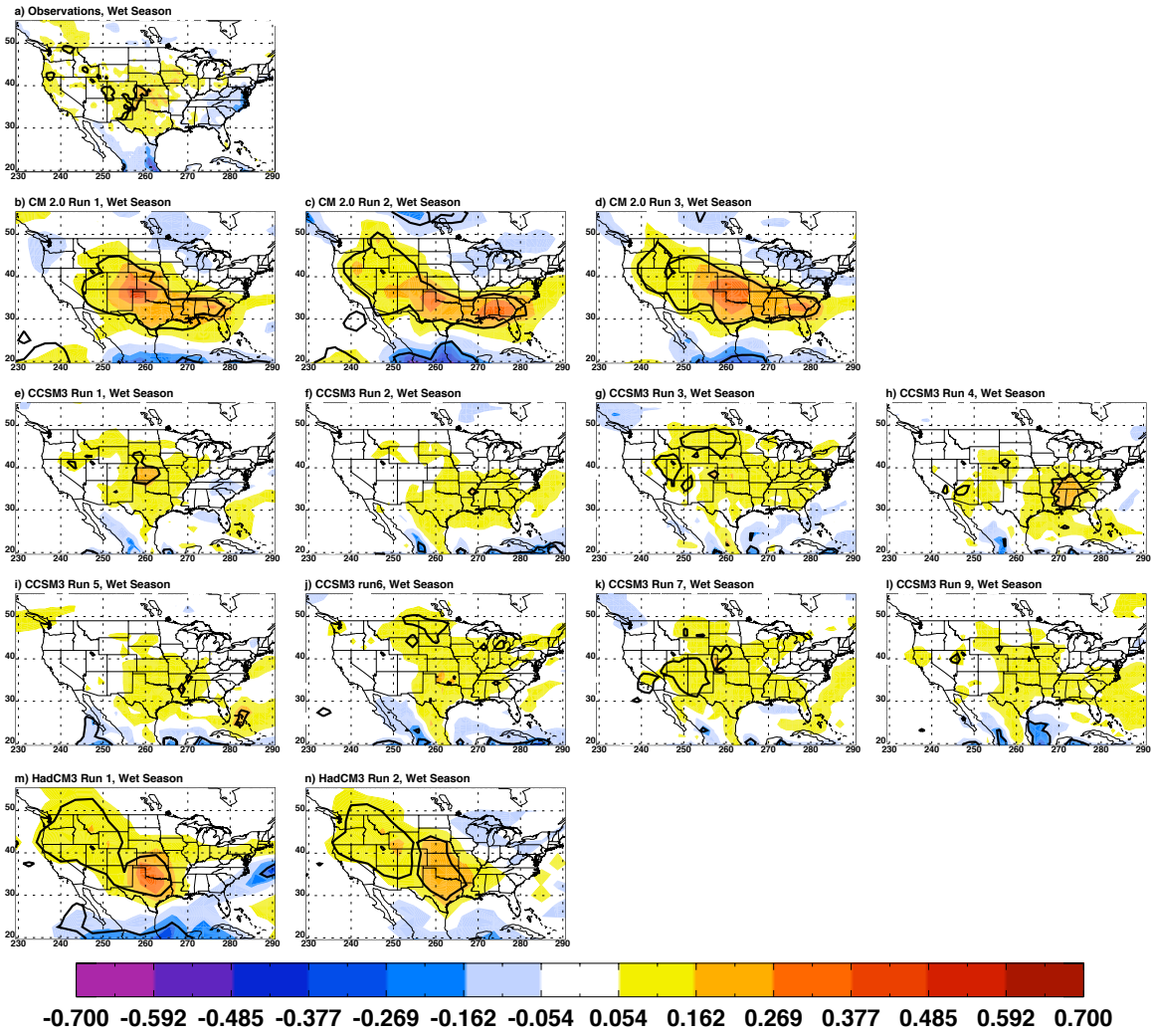


Figure 6.30. *Same as Figure 6.29 only for wet season months (April - September).*

with ENSO. Also, during dry season months, there is very little relationships between ENSO and precipitation over the Great Plains region. It appears that the teleconnection patterns that extend from the from the equatorial Pacific are slightly shifted to the East in the CCSM compared to what has been observed. Since ENSO appears to have very little influence on Great Plains precipitation in CCSM3, other factors such as land-atmosphere interactions and synoptic scale features such as the position of the Bermuda High must influence Great Plains precipitation in this model.

From these results we might expect cool conditions to occur in the tropical Pacific during the long-term drought periods simulated by CM 2.0 and HadCM3. In both of these models, there exists a positive relationship between ENSO and Great Plains precipitation during both the dry and wet season. In CCSM3, on the other hand, the relationship between Great Plains precipitation and SST anomalies in the tropical Pacific is less clear. In this model, there appears to exist almost no relationship between Great Plains precipitation and ENSO. In the next section we look at the global SST anomalies associated with the long-term drought periods from the models and the observations.

6.4.2 SST Anomalies and Long-Term Great Plains Drought

As mentioned in Chapter 2, cool La Niña-like conditions in the tropical Pacific are associated with long-term, Great Plains drought. In this section we diagnose the SST anomalies associated with long-term drought conditions in the models to determine if cool conditions in the tropical Pacific are associated with the simulated droughts.

Figures 6.31d-f show the composite SST anomalies associated with the three long-term drought periods identified in our observational record. During the 1907-1913 drought, anomalously cool conditions persisted in all ocean basins throughout the drought period. Negative anomalies were particularly large along the Pacific coast of North America, in the central equatorial Pacific, and in the Atlantic Ocean. Slight positive anomalies did exist during this time period in the midlatitude regions of the North and South Pacific (Figure 6.31d). During the "Dust Bowl" drought, SST anomalies were strikingly different, with moderately cool conditions in the central and eastern Tropical Pacific, cool conditions in the North Pacific and along the Pacific coast of North

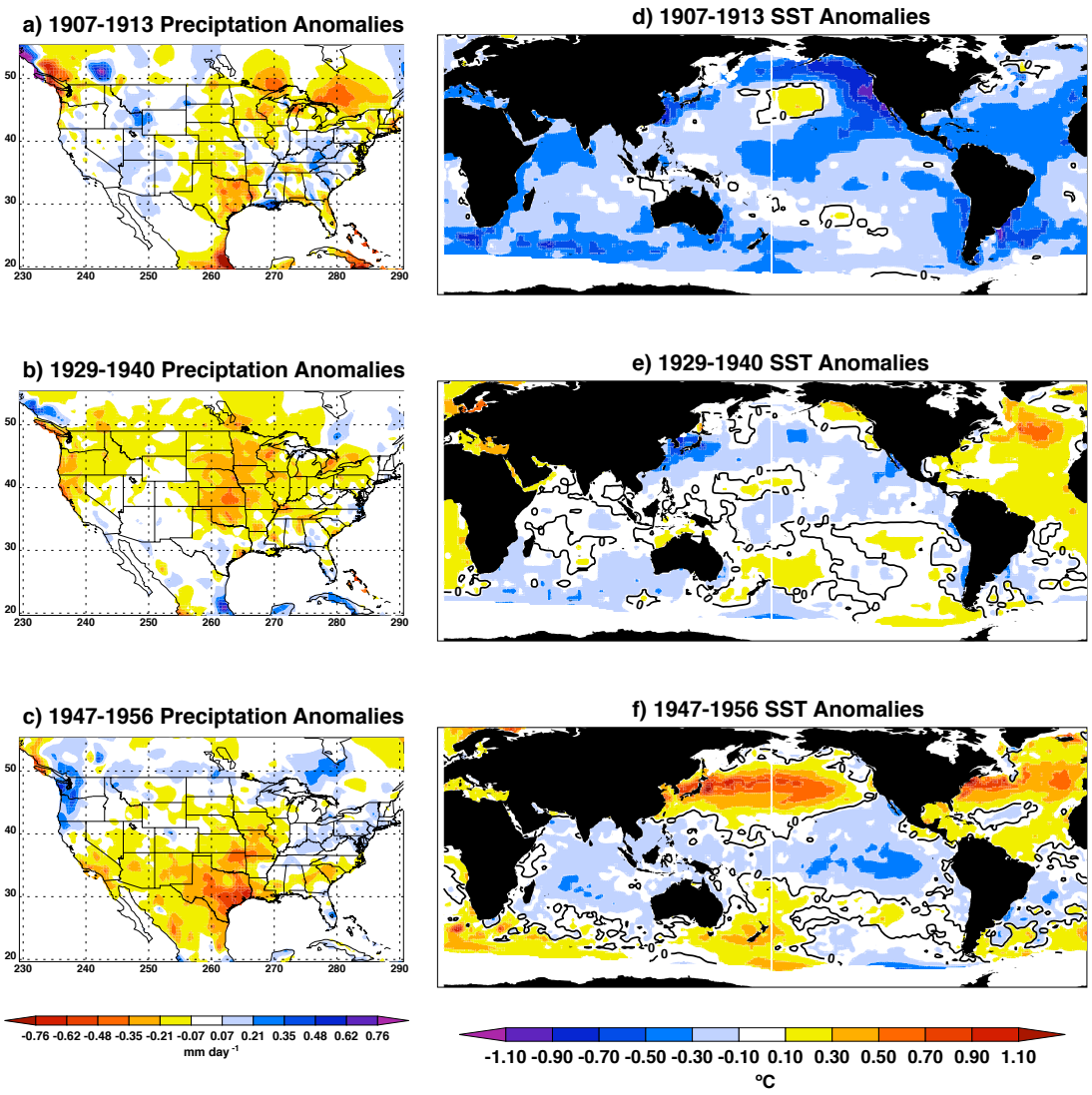


Figure 6.31. *Composite annual precipitation anomalies (left column) and sea surface temperature anomalies (right column) associated with the three long-term Great Plains drought periods that occurred during the observed 20th Century. Precipitation anomalies are from the CRU data set and SST anomalies are from the HadISST data set.*

America, and warm conditions in the Atlantic Ocean (Figure 6.31e). During the 1950s drought period SST anomalies exhibited a classic La Niña pattern (see Figure 5 from Alexander et al. (2002)) with cool conditions in the equatorial Pacific and the Indian Ocean, warm conditions in the North Pacific, but with cool conditions off the coast of North America, and warm conditions in the North Atlantic (Figure 6.31f).

Despite many differences in the global pattern of SST anomalies, drought conditions did persist over the Great Plains region during each of these time periods. The La Niña-like conditions in the tropical Pacific described in Seager et al. 2005 are the common thread for all three drought periods and are thought to be one of the leading causes of long-term droughts over this region (see Chapter 2). It is possible that the SST anomalies associated with other ocean basins such as the North Atlantic and North Pacific may influence the magnitude and spatial extent of dryness over the Great Plains region.

The next step is to see if the long-term droughts simulated by the three models, as identified in the previous section, are also associated with persistent, cool, La Niña-like SST anomalies in the equatorial Pacific. To do this we created composite maps of global SST anomalies for each drought period identified in Table 1.

6.4.2a CM 2.0 and HadCM3

Figures 6.32-6.34 show the composite SST anomalies associated with the long-term droughts from CM 2.0 while Figures 6.35 and 6.36 show similar spatial maps, but for HadCM3. Cool SST anomalies in the tropical Pacific are present in all the long-term drought periods simulated in the integrations from CM 2.0 and HadCM3. SST anomalies in other parts of the globe vary, during drought periods, but cool conditions are always present in the tropical Pacific. This is similar to what has been observed, possibly indicating that in CM 2.0 and HadCM3 cool conditions in the tropical Pacific are a necessary forcing of Great Plains drought. It is difficult to make any connection between global SST anomalies and the spatial extent and magnitude of drought over the Great

Plains. There are many different and interacting factors that contribute to long-term drought conditions over the Great Plains that can influence the spatial patterns and intensity of these droughts. Some of these other forcings include the position of the Bermuda High in the Atlantic Ocean and land-atmosphere interactions.

6.4.2b CCSM3

Figures 6.37 - 6.44 show the composite global SST anomalies associated with the long-term droughts produced by the CCSM3 model. In CCSM3, drought conditions over the Great Plains tend to be associated with one of three different types of global SST anomaly patterns. The three categories of SST anomalies are as follows:

- ***Type 1*** - Cool conditions persisting in all ocean basins with large negative anomalies in the tropical Pacific, the tropical Atlantic and the Indian Ocean. In this category of SST anomalies, small regions in the North Pacific and North Atlantic exhibit positive anomalies. These SST anomaly patterns are similar to those seen in during the 1907-1913 drought (Figures 37d, 38b, 39d, 40e, 40f, 41e, 42d, 42e, 43d and, 44c).
- ***Type 2*** - Warm conditions persisting in all ocean basis during the drought period, even in the equatorial Pacific. Small regions in the North Pacific and North Atlantic tend to exhibit cool conditions. In some sense, this pattern of SST anomalies is exactly out of phase with Type 1 SST anomalies (Figures 37f, 39f, 38g, 41h and, 43f).
- ***Type 3*** - SST anomalies of this type tend to be symmetric about the equator in the Pacific, with either cool or warm conditions in a narrow band at the

equatorial Pacific, and SST anomalies of opposite sign in the subtropical regions of both the North and South Pacific. In the polar regions of these two ocean basins, SST anomalies again switch sign and are in phase with the equatorial pacific. Both the Indian Ocean and the North Pacific tend to be out of phase with the anomalies in the equatorial Pacific. Of course exception do occur (Figures 37e, 39e, 40g, 40h, 41f, 42f, 43e and, 44d).

There appears to be no systematic relationship between Great Plains drought and tropical Pacific SST anomalies in CCSM3. Drought conditions over the Great Plains in CCSM3 are associated with a wide range of global SST anomalies. It also appears that cool conditions in the tropical Pacific are not a necessary for dry conditions to persist over the Great Plains for long periods of time. The spatial coverage, magnitude, and length of each long-term drought over the Great Plains does not appear to be a function of global SST anomalies. As mentioned previously, other factors may contribute to long-term drought over the Great Plains may play an important role in this model, including, the position of the Bermuda High and local lock-in mechanisms that involve feedbacks between soil moisture and precipitation.

In this section we have focused on examining the role that external forcing mechanisms from the tropical Pacific play in influencing Great Plains precipitation in the models. In the next section, we focus our attention on land-atmosphere feedback mechanisms that may cause Great Plains precipitation anomalies to lock-into place thereby resulting in persistent drought conditions.

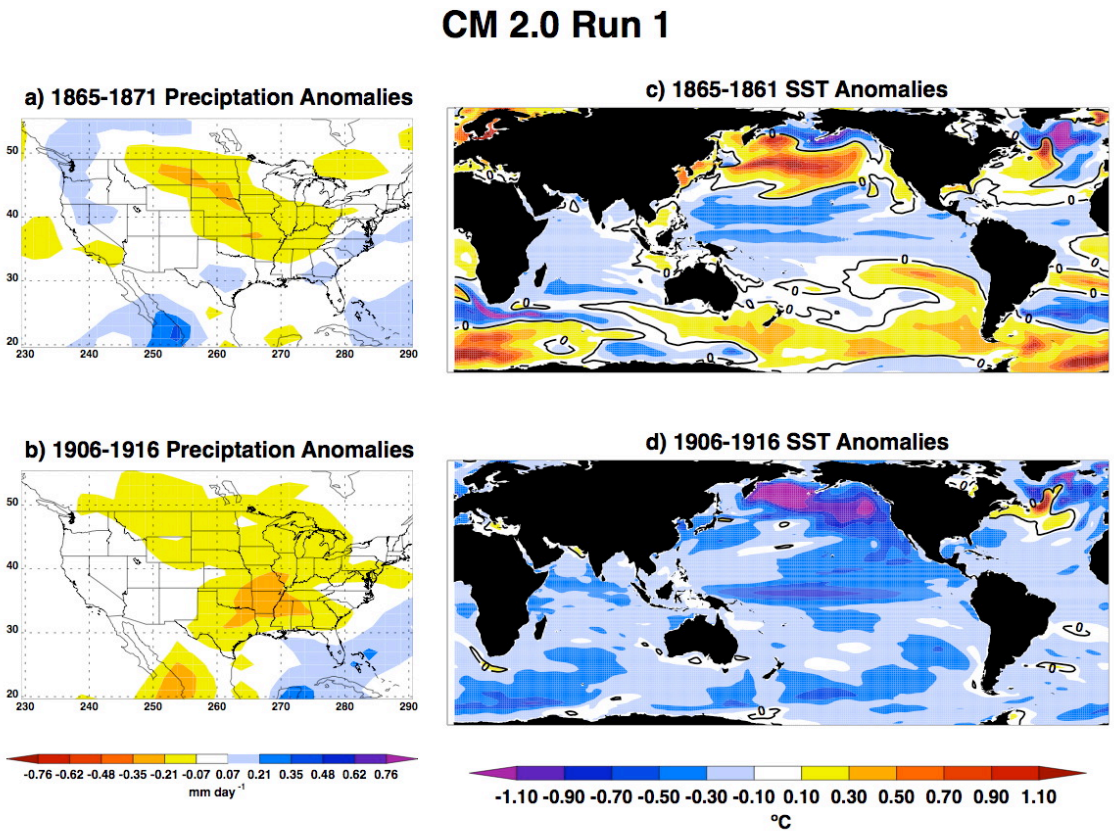


Figure 6.32. *Same as Figure 6.28 only for CM 2.0 Run 1.*

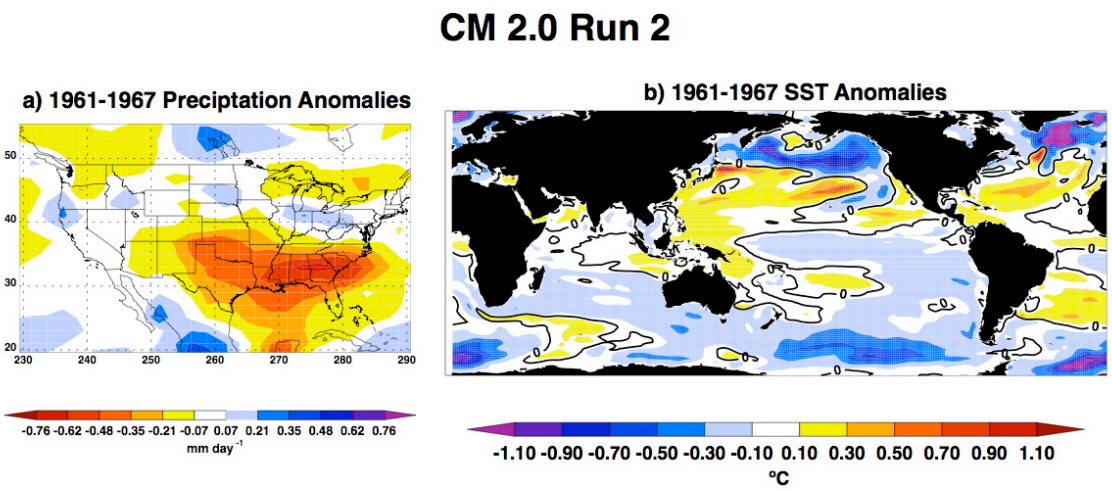


Figure 6.33. *Same as Figure 6.28 only for CM 2.0 Run 2.*

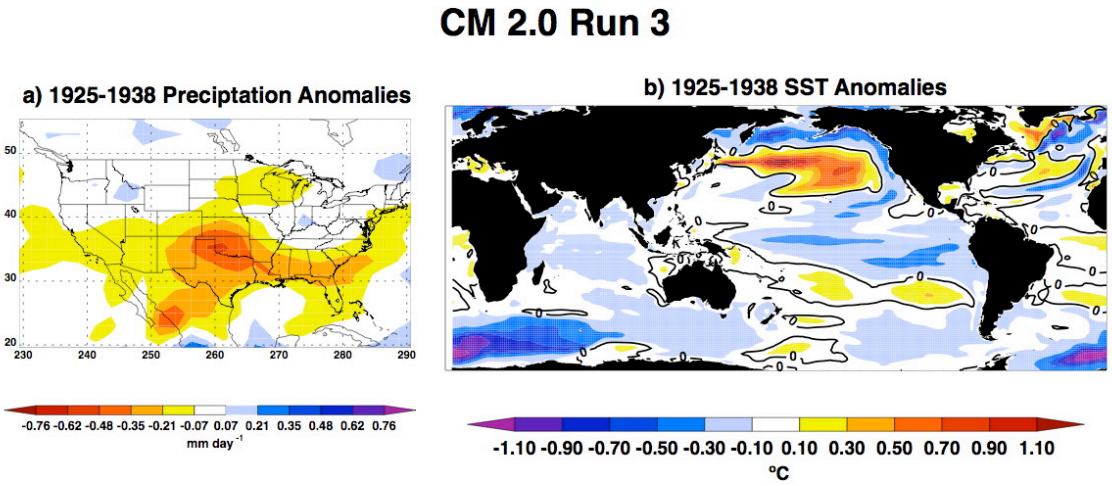


Figure 6.34. *Same as Figure 6.28 only for CM 2.0 Run 2.*

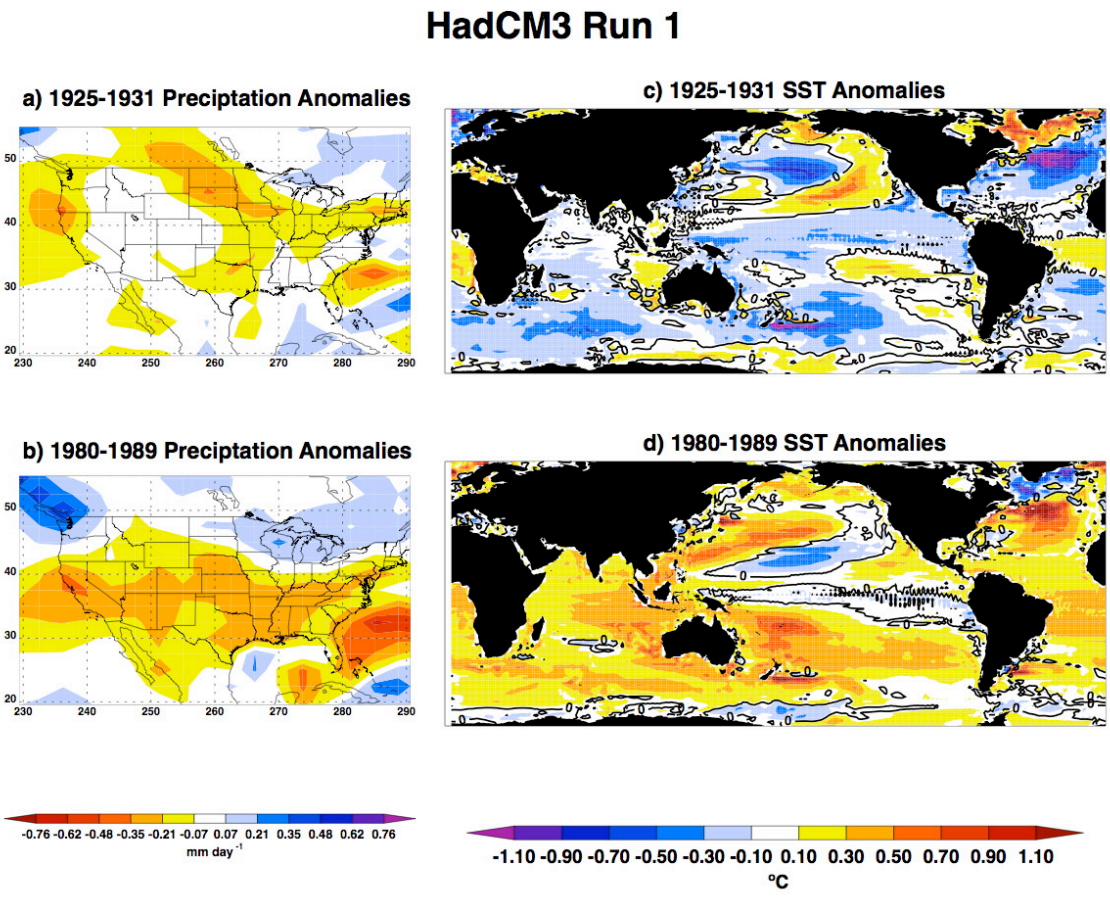


Figure 6.35. *Same as Figure 6.28 only for HadCM3 Run 1.*

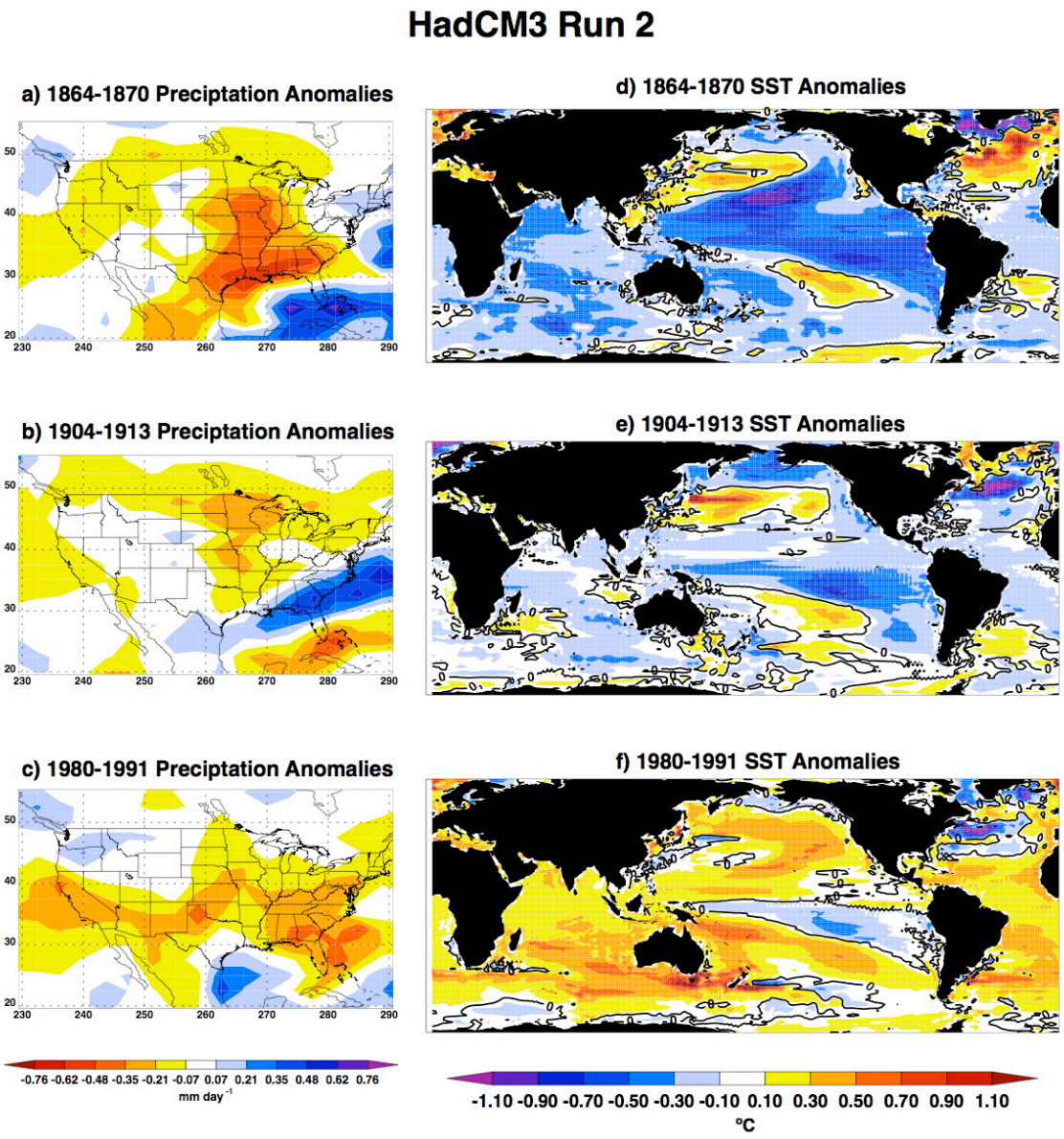


Figure 6.36. *Same as Figure 6.28 only for HadCM3 Run 2.*

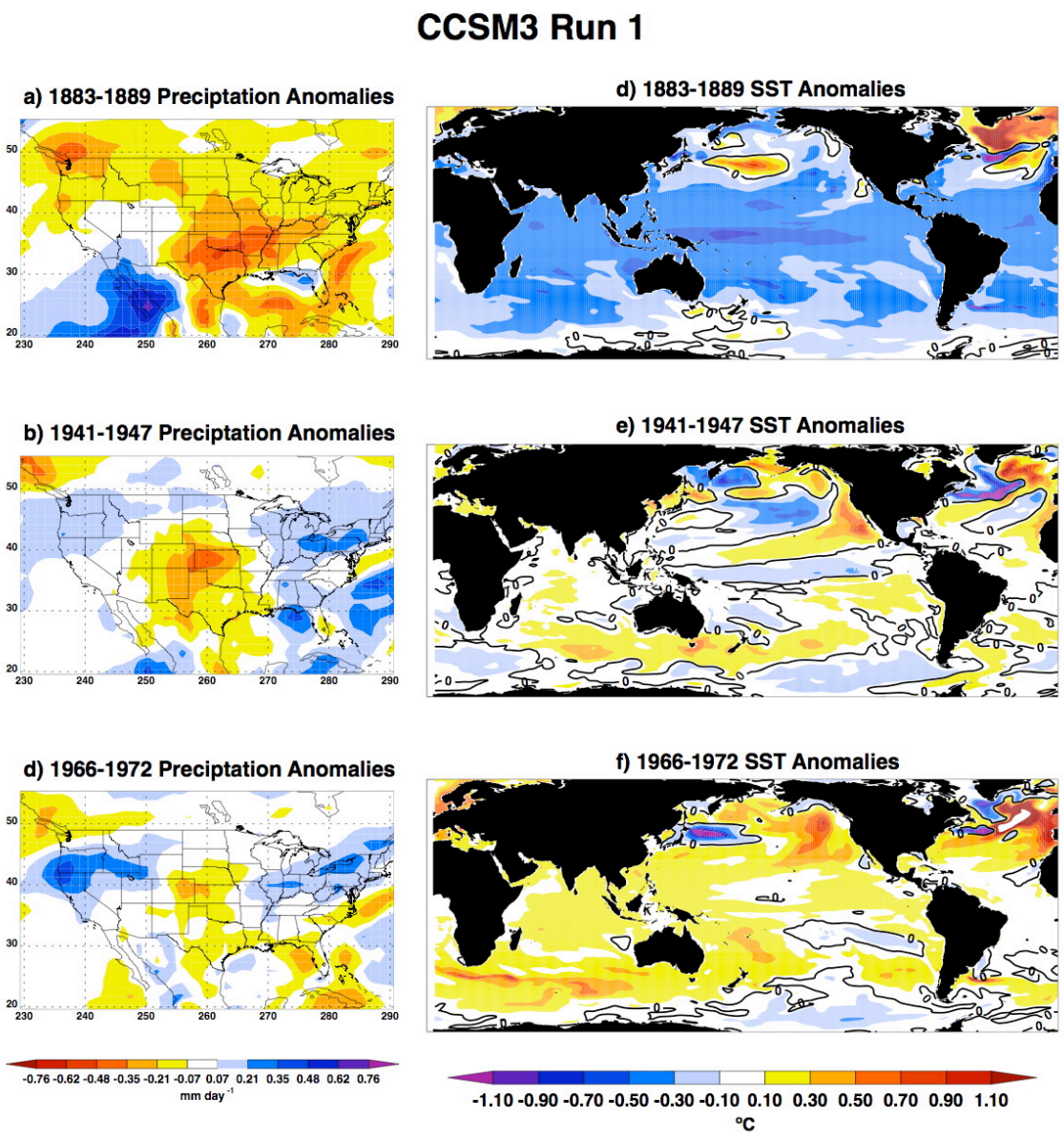


Figure 6.37. *Same as Figure 6.28 only for CCSM3 Run 1.*

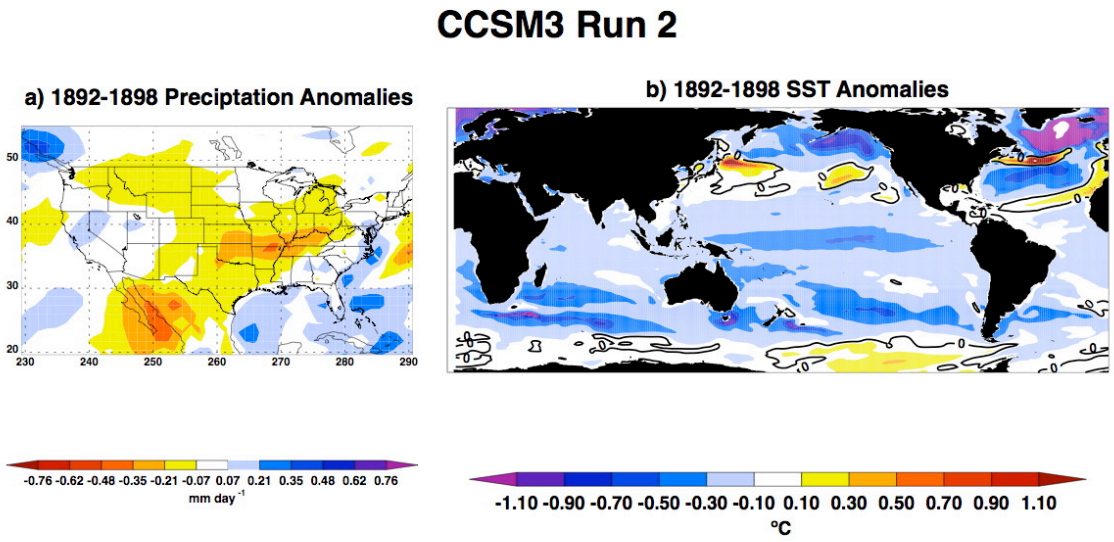


Figure 6.38. *Same as Figure 6.28 only for CCSM3 Run 2.*

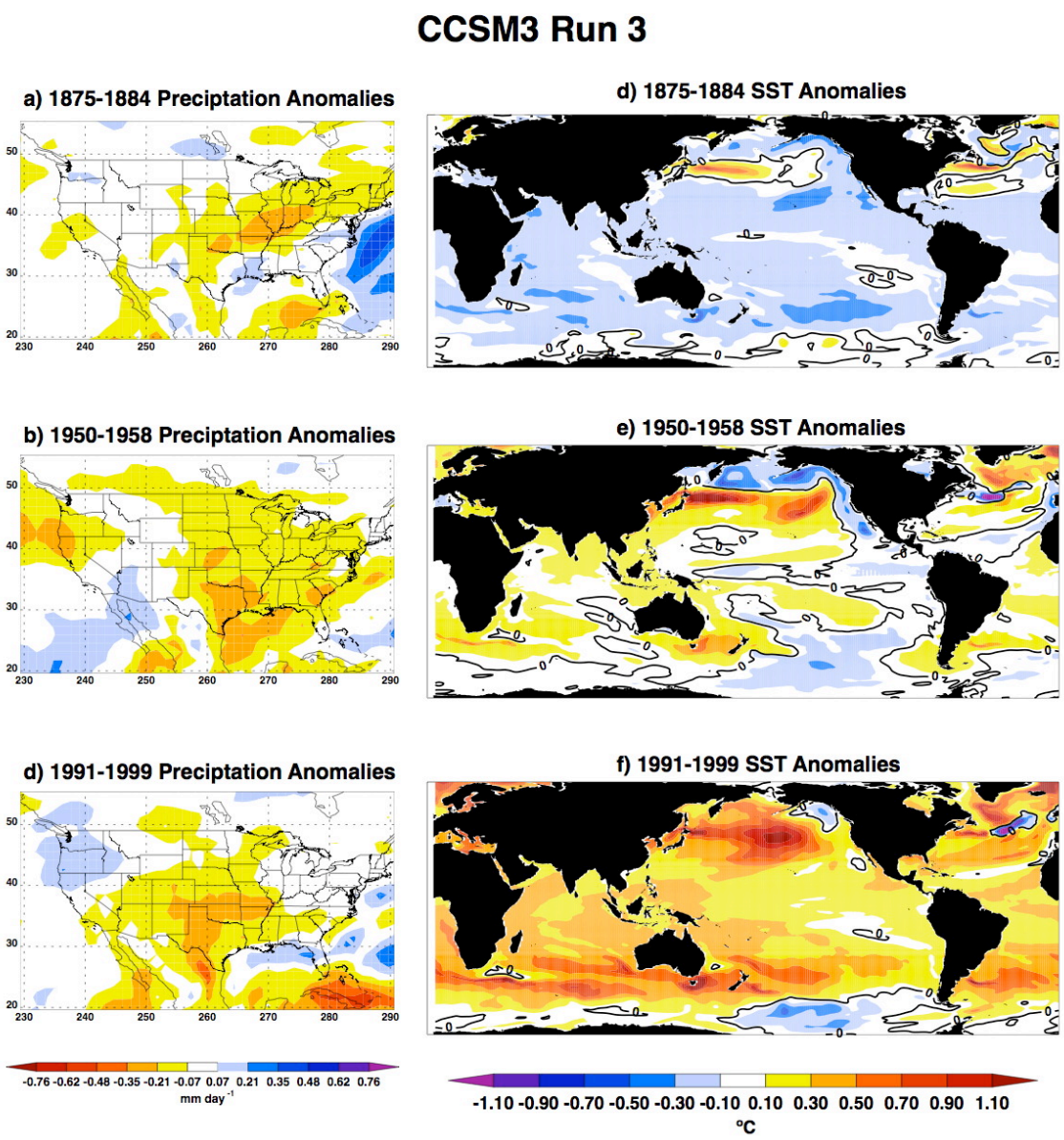


Figure 6.39. *Same as Figure 6.28 only for CCSM3 Run 3*

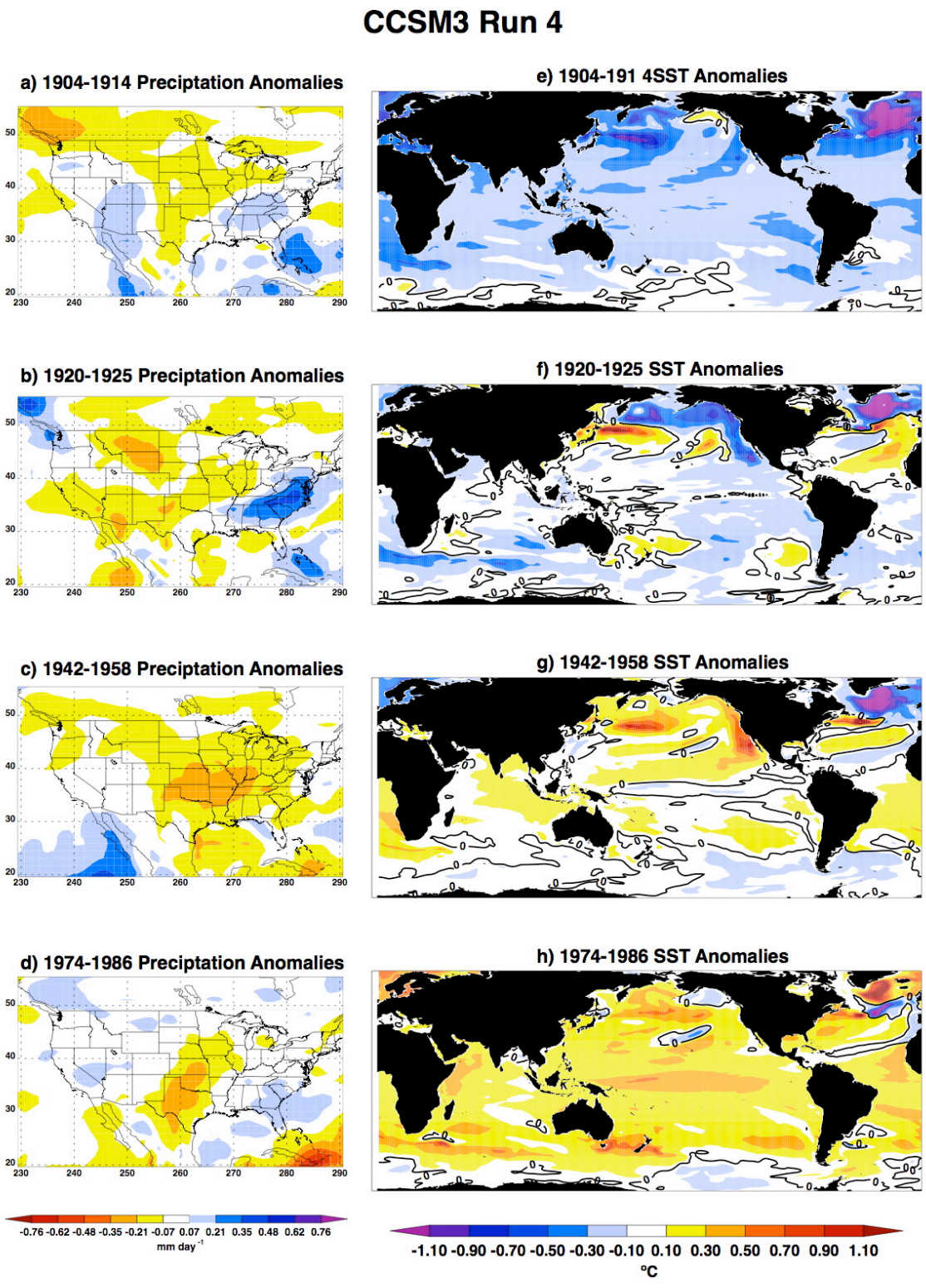


Figure 6.40. *Same as Figure 6.28 only for CCSM3 Run 4.*

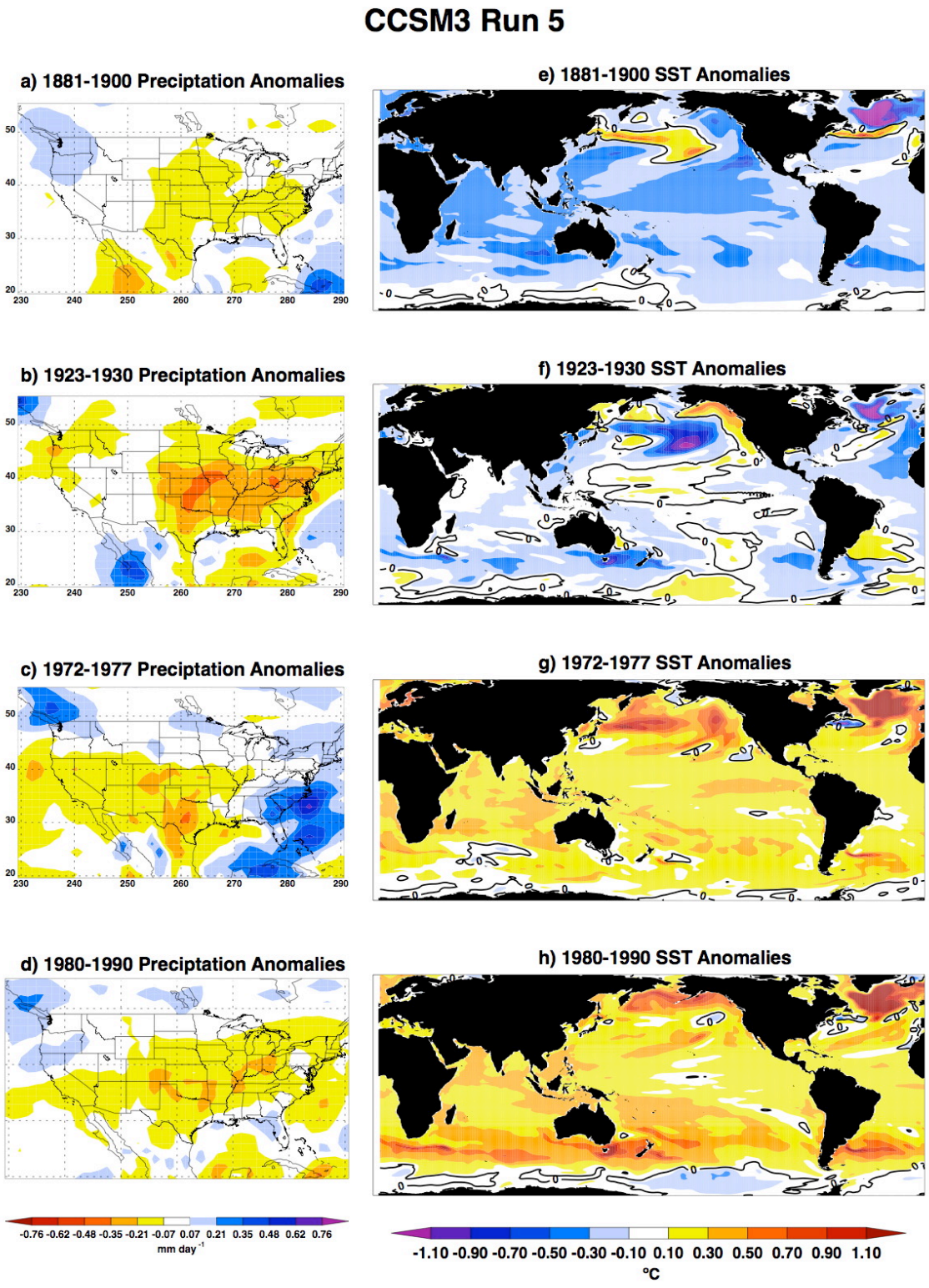


Figure 6.41. *Same as Figure 6.28 only for CCSM3 Run 5.*

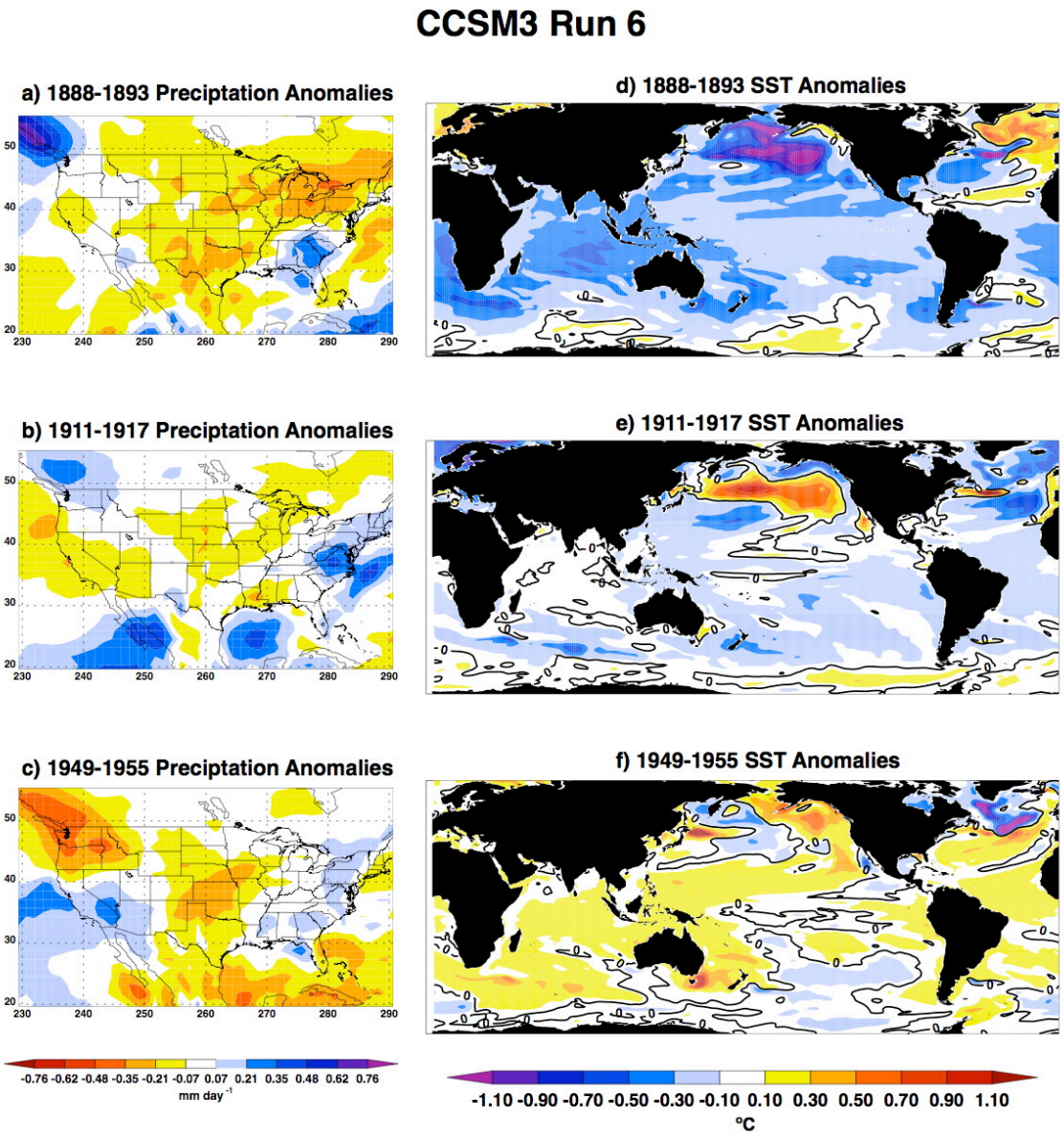


Figure 6.42. *Same as Figure 6.28 only for CCSM3 Run 6.*

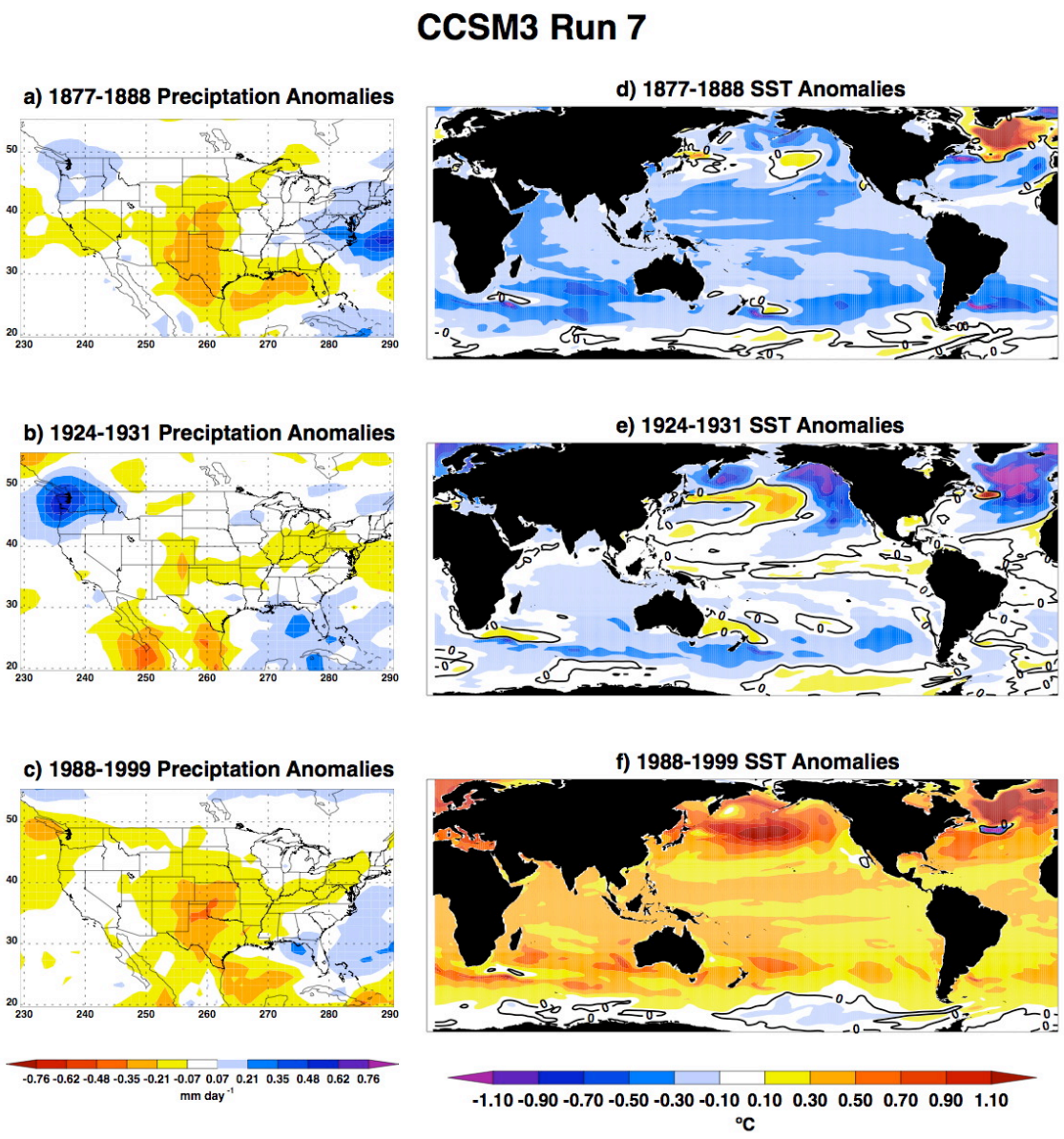


Figure 6.43. *Same as Figure 6.28 only for CCSM3 Run 7.*

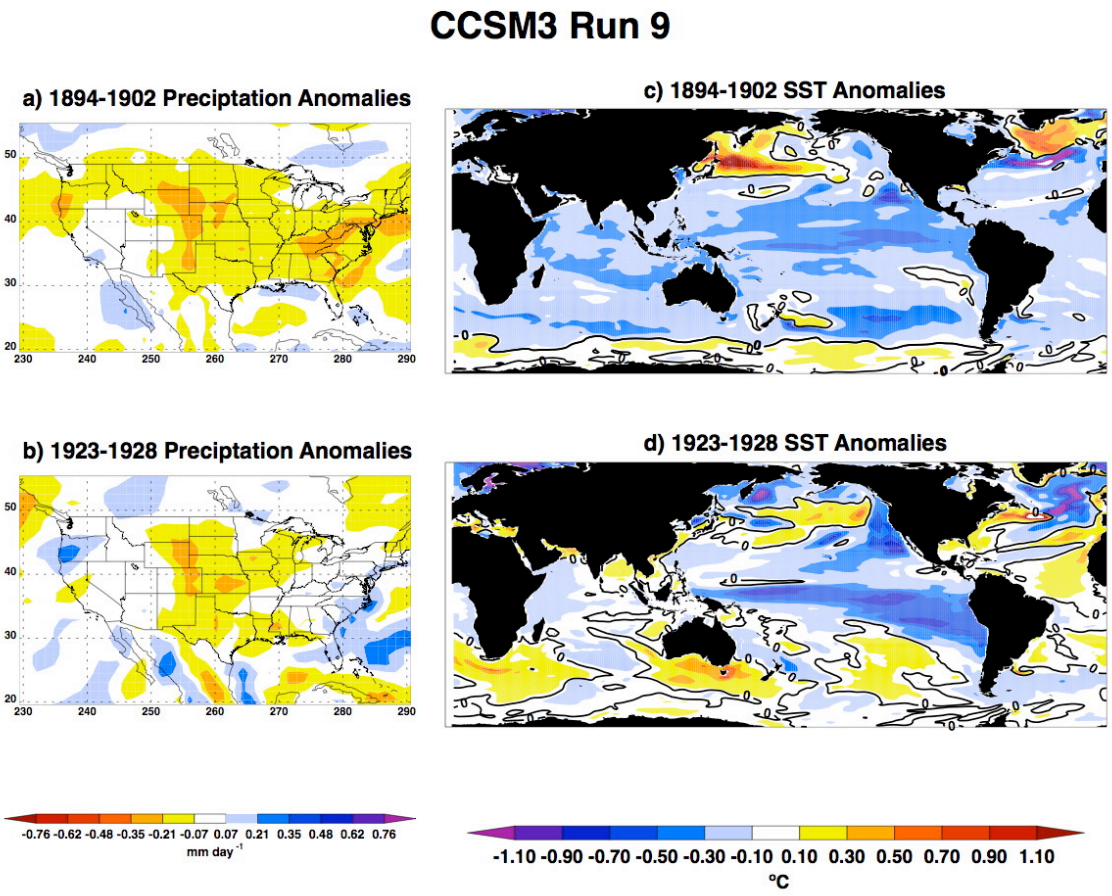


Figure 6.44. *Same as Figure 6.28 only for CCSM3 Run 9.*

6.5 Land-Atmosphere Interactions

As also discussed in Chapter 2, land-atmosphere interactions and feedbacks between soil moisture concentrations and precipitation can act as a bridging mechanism between winter precipitation anomalies and summer rainfall deficits. Also, interactions between the land surface and the atmosphere can act to reinforce the atmospheric conditions associated with drought, such as anomalous high-pressure ridges.

In this section we analyze the coupling between the land surface and the atmosphere in the models. Remember that large scale observations of many hydrologic variables such as evapotranspiration and soil moisture content are not available so we use a macroscopic soil moisture model forced with observed meteorological parameters from the 20th century as our "best representation" of what occurred.

To investigate the relationship between the land surface and the atmosphere in each model, we look at the linear relationships that exist between precipitation, evapotranspiration, and soil moisture over the Great Plains. Since evapotranspiration is the main mechanism by which the land surface influences the atmosphere above, we expect the coupling between the land-surface and the atmosphere to be strongest during the wet season months when the amount of water and energy available at the surface is largest.

In the following sections we will be examining both the magnitude and the strength of the linear relationships between these variables. The magnitude of the linear relationship is represented by the regression coefficient, denoted by **a** in the figures. The regression coefficient represents the slope of the least squares fit line (the red line plotted

on each of the following scatter plots). By looking at the magnitude of the relationship we are interested in seeing how large the variations in the independent variable (the variable plotted on the y-axis of the scatter plots) are compared to the variations in the dependent variable (the variable plotted on the x-axis of the scatter plots). For the case of precipitation versus evapotranspiration, the magnitude of the relationship tells us how large changes in evapotranspiration are compared to changes in precipitation. The strength of the linear relationship, on the other hand, is represented by the correlation coefficient, denoted by an **r** in the figures. The correlation coefficient is a measure of the scatter or the error about the least squares fit line and therefore represents the quality or the reliability of the linear relationship. If there is a large amount of scatter about the least squares fit line, then the correlation coefficient will be small and the linear relationship between those variables is weak. The correlation coefficient can be small even if the regression coefficient is large and vice versa.

6.5.1 Precipitation and Evapotranspiration

Figure 6.45 shows scatter plots of evapotranspiration versus precipitation for the Great Plains region from VIC, CM 2.0, CCSM3, and HadCM3. The regression and correlation coefficients are also marked on each figure. In VIC, the soil moisture model run by Adredias et al. (2005),there exists a positive relationship between precipitation and evapotranspiration over the Great Plains, on monthly timescales. This implies that increases in monthly precipitation rates tend to be associated with increases in monthly evapotranspiration rates. During wet season months, precipitation explains approximately 25.7% of the variance in evapotranspiration, and a 1 mm month^{-1} change

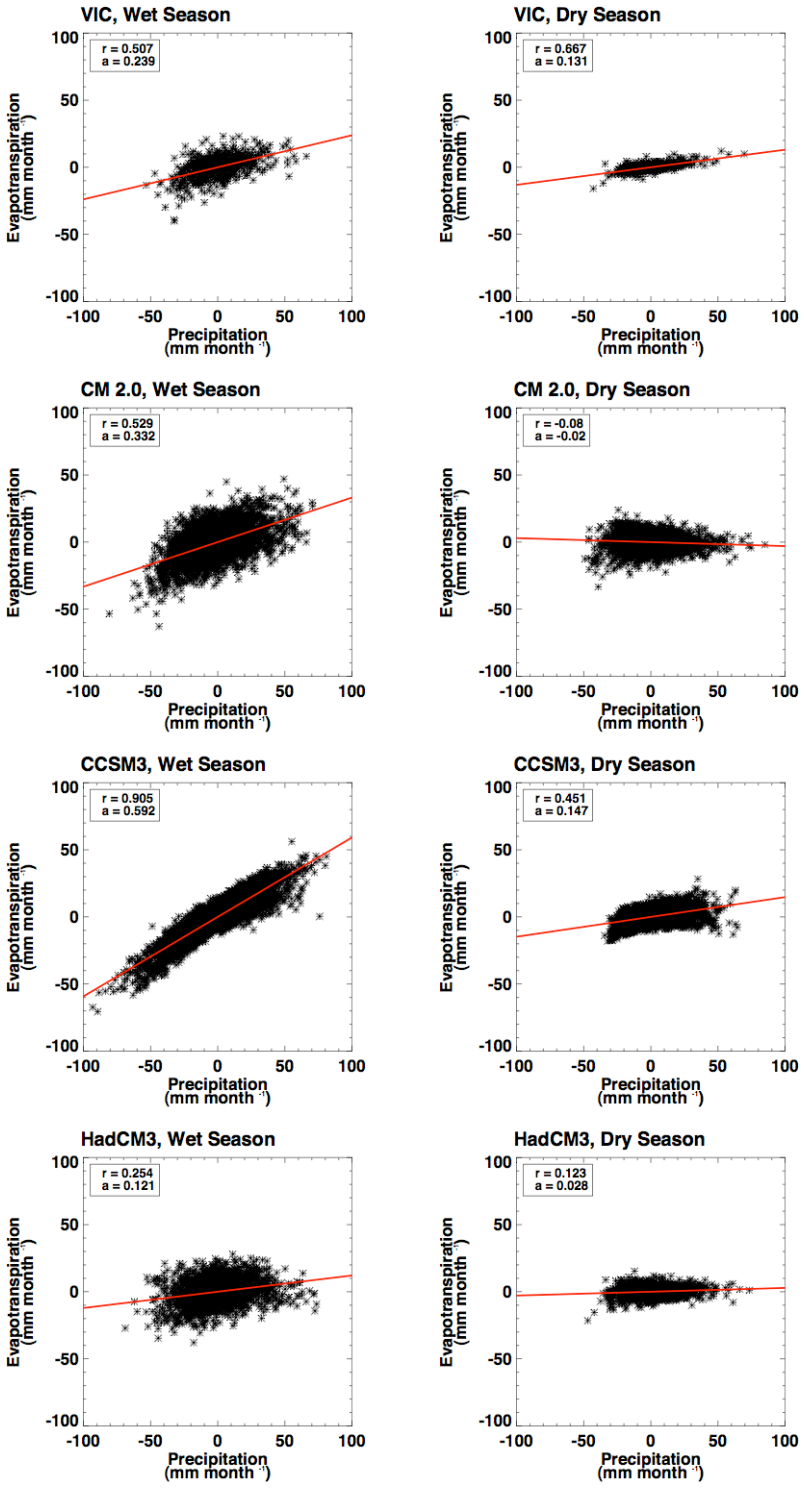


Figure 6.45. *Scatter plots of monthly anomalies precipitation versus evapotranspiration for VIC, CM 2.0, CCSM3, HadCM3 for the wet season months (April-September) and dry season months (October - March). The red line denotes the "least squares fit line". Also marked on each figure is the regression coefficient, denoted by an a, and the correlation coefficient, denoted by an r. We have combined information from all the simulations performed by each*

in precipitation corresponds to a 0.239 mm month $^{-1}$ change in evapotranspiration over the Great Plains. During the dry season, there still exists a positive relationship between these two variables, although the magnitude of the linear relationship is weaker. Remember that evapotranspiration rates are a function of both the amount of water and the amount of energy available at the surface. Therefore we expect changes in evapotranspiration to be small during the dry season when both surface water and downwelling radiation are minimal.

In all three models, during the wet season, precipitation and evapotranspiration are positively correlated with each other. The linear relationship between these variables is largest in CCSM3, where precipitation explains 81.9% of the variance in evapotranspiration and a 1 mm month^{-1} change in precipitation corresponds to a 0.592 mm month^{-1} change in evapotranspiration. The magnitude of the relationship between precipitation and evapotranspiration in CCSM3 may indicate that over the Great Plains, the land surface and the atmosphere are too strongly coupled. Previous studies have shown that the CAM, the atmospheric component of CCSM3, tends to overestimate the amount of light to moderate rainfall that reaches the surface and underestimates the amount of heavy or convective rainfall that reaches the surface (DeMott et al., 2007). What this actually means is that in the CAM, it tends to drizzle over the entire grid box for long periods of time, rather than having heavy, but short lived, precipitation events occurring over just part of the grid box. This light to moderate rainfall is easily intercepted by the vegetation at the surface and tends to be immediately re-evaporated into the atmosphere.

CM 2.0 also exhibits a strong linear relationship between precipitation and evapotranspiration during the wet season months, but in HadCM3, there exists almost no linear relationship between these two variables. In fact, in HadCM3 precipitation only explains 6.4% of the variance in evapotranspiration and a 1 mm month^{-1} change in precipitation only corresponds to a 0.121 mm month^{-1} change in evapotranspiration. This points to a lack of interaction between the land surface and the atmosphere in HadCM3 and that precipitation may be a function of moisture convergence, not local evapotranspiration.

During the dry season months, the relationship between precipitation and evapotranspiration is greatly reduced, with CM 2.0 and HadCM3 exhibiting no linear relationship between these variables and CCSM3 exhibiting a weak, positive relationship that is similar to the relationship seen in VIC.

6.5.2 Soil Moisture and Evapotranspiration

Figure 6.46 shows the scatter plots for monthly soil moisture anomalies versus evapotranspiration. Soil moisture and evapotranspiration are also positively correlated with each other over the Great Plains. This indicates that increases in surface soil moisture content correspond to increases in evaporation and that increases in the soil moisture content of the root-zone of the vegetation correspond with increases in transpiration. In VIC, during the wet season months, changes in soil moisture accounts for approximately 61.3% of the variance in evapotranspiration. The linear relationship between soil moisture and evapotranspiration is larger than the relationship between precipitation and evapotranspiration, where a 1 mm month^{-1} change in soil moisture

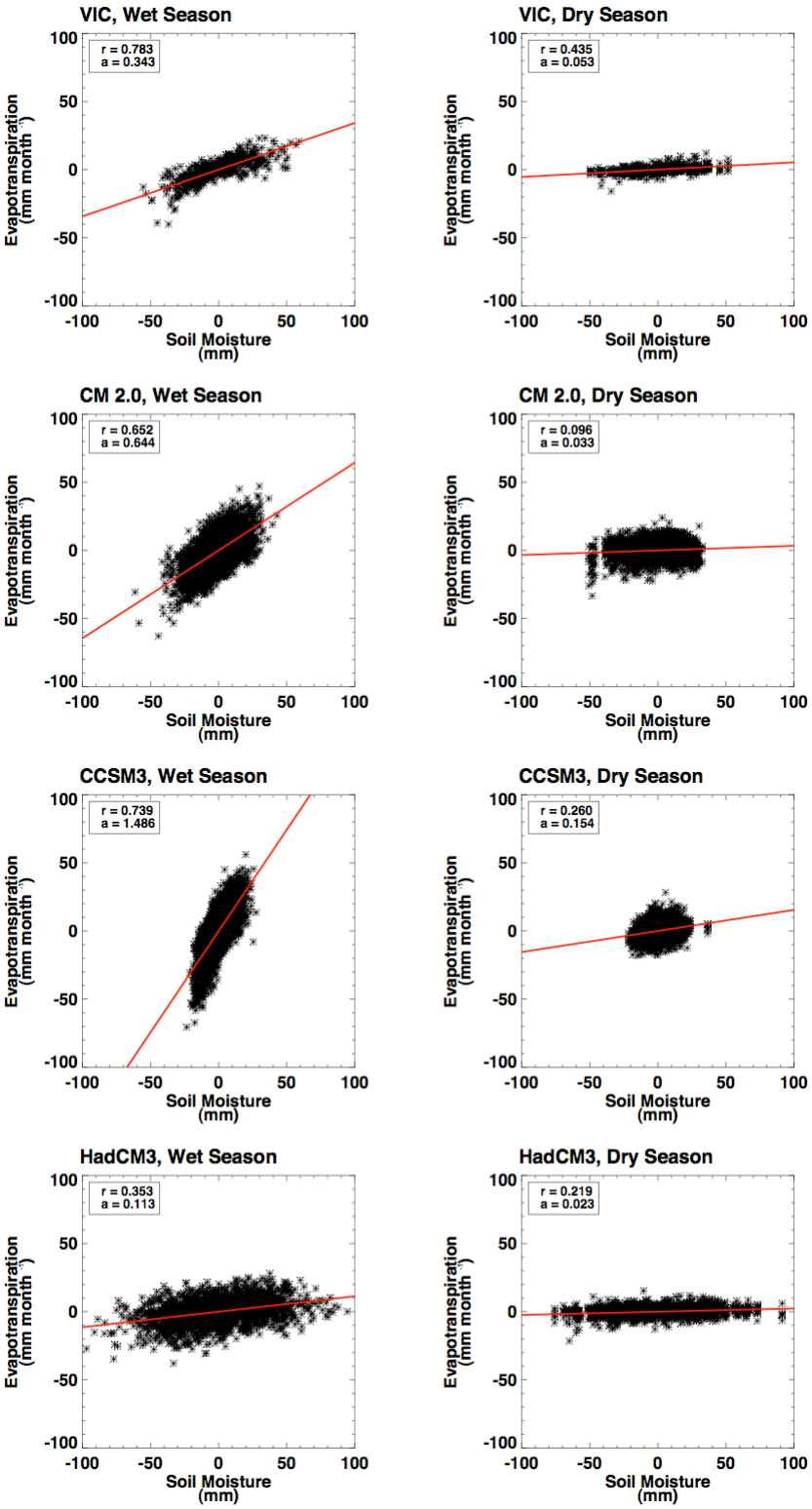


Figure 6.46. *Same as Figure 6.45 only for soil moisture anomalies versus evapotranspiration.*

content corresponds with a 0.343 mm month^{-1} change in evapotranspiration. Again, during the dry season months, there exists almost no linear relationship between evapotranspiration and soil moisture content with the lack of downwelling radiation at the surface being the most likely inhibitor of evapotranspiration during these months.

In the models, the varied relationship between evapotranspiration and soil moisture is similar to that of precipitation and evapotranspiration. The linear relationship between evapotranspiration and soil moisture is again largest in CCSM3 with changes in soil moisture content accounting for approximately 58.6% of the variance in evapotranspiration and a 1 mm month^{-1} change in soil moisture content accounting for a 1.486 mm month^{-1} change in evapotranspiration. It may seem strange that changes in evapotranspiration are much larger than changes in soil moisture content, but all this indicates is that other factors, such as precipitation are influencing evapotranspiration.

The linear relationship between soil moisture and evapotranspiration is also large in CM 2.0, but the relationship in HadCM3 is minimal and comparable to the relationship between precipitation and evapotranspiration in this model.

During the dry season, the relationship between soil moisture and evapotranspiration in the models also weakens, with soil moisture explaining very little of the variability in evapotranspiration in any of the models.

6.5.3 Precipitation and Soil Moisture

Remember that soil moisture content over the Great Plains is influenced by three variables: precipitation, evapotranspiration, and runoff. While runoff and evapotranspiration act to diminish soil moisture supplies, precipitation acts to increase the

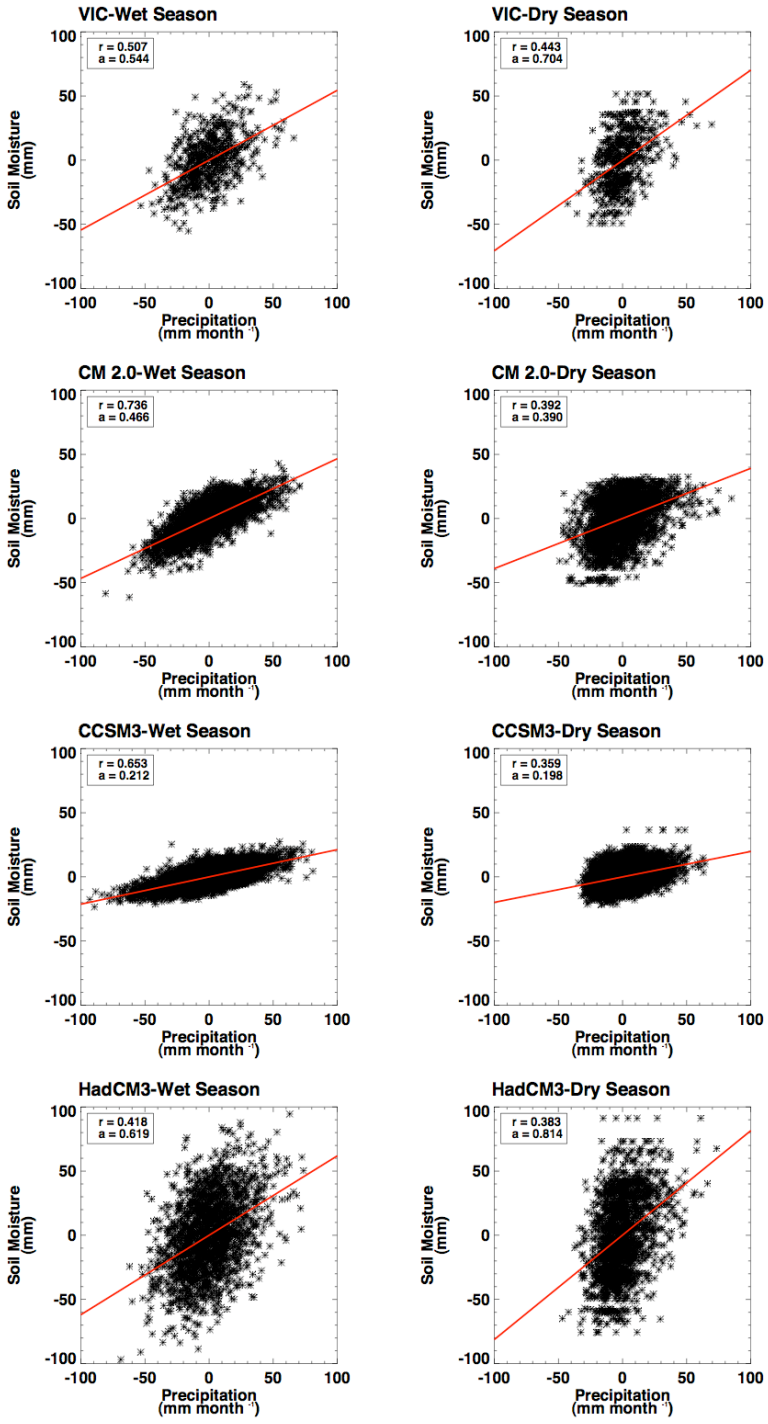


Figure 6.47*. Same as Figure 6.45 only for soil moisture anomalies versus precipitation.*

amount of water within the soils. Therefore, we expect that precipitation anomalies will also exhibit a positive relationship with soil moisture concentrations. Figure 6.47 show the scatter plots of precipitation versus soil moisture anomalies for all the data sets. In VIC, a 1 mm month-1 change in precipitation results in a 0.544 mm month^{-1} change in soil moisture content. In this model, precipitation explains 25.7% of the variance in soil moisture. Overall, the magnitude of the relationship between precipitation and soil moisture is larger than the relationship between precipitation and evapotranspiration and soil moisture and evapotranspiration.

The magnitude of the relationship between precipitation and soil moisture content over the Great Plains region is also large in CM 2.0 and HadCM3, but as mentioned previously, there exists almost no linear relationship between preciptation and soil moisture in CCSM. One possible explanation for this is that a large portion of the precipitation that reaches the surface being intercepted by vegetation and re-evaporated immediately, not interacting with the surface soil.

Interestingly, during the dry season, the relationship between precipitation and soil moisture content remains large in all of the data sets. This implies, that during the dry season months, changes in precipitation rates cause soil moisture concentrations to also change. As discussed in Chapter 2, it is possible that negative precipitation anomalies that occur during the dry season months cause reductions in soil moisture concentrations which then translate into reduced evapotranspiration rates during the summer months and can lead to reductions in wet season rainfall amounts. It is clear from Figure 6.47 that during the dry season months, precipitation and soil moisture are

strongly related in VIC, CM 2.0, and HadCM3, but the relationship between these variables is small in CCSM3. Since precipitation appears to have a minimal impact on soil moisture content, the question remains what role does the soil moisture have on the memory of precipitation anomalies in CCSM3. If precipitation does not influence soil moisture content do winter precipitation anomalies translate into summer precipitation anomalies in this model? And, do soil moisture anomalies help to maintain wet season precipitation anomalies from year to year? These questions are not answered in this thesis are are left for future study.

6.5.4 Discussion of Land-Atmosphere Interactions

Both CCSM3 and CM 2.0 exhibit strong coupling between the the land surface and the atmosphere via interactions between precipitation, evapotranspiration, and soil moisture content. It is possible that the interactions between the land surface and the atmosphere will help to perpetuate drought conditions over the Great Plains from year to year in these two models. In HadCM3, on the other hand, there appears to be very little relationship between the land surface and the atmosphere indicating that land-atmosphere interactions may not play an influential role in perpetuating long-term droughts over the Great Plains in this model.

The results found in this study are supported by the findings from the GLACE (Global Land-Atmosphere Coupling Experiment) study (Koster et al. 2004, 2006a, b). In the GLACE study, the coupling strength between the land surface and the atmosphere was evaluated in 16 different climate models. Every climate model used in the study was asked to perform two modeling experiments. In the first experiment, soil moisture

concentrations were allowed to vary as predicted by the model throughout the course of the simulation, but in the second experiment, subsurface soil moisture conditions were forced to be the same in all the models. The study then compared results from the two simulations from each model to see if prescribing surface properties such as soil moisture, influenced atmospheric parameters such as precipitation. Results from the GLACE study point to strong land-atmosphere coupling in the CCSM3 and CM2.0, but weak coupling between the land surface and the atmosphere in HadCM3.

Lawrence and Slingo (2005) have studied the land surface of HadCM3 in detail and they argue that the cause of the weak soil moisture - precipitation feedback in HadAM3 (the atmospheric component of HadCM3) is related to one of two factors, either how the boundary-layer adjusts to changes in surface forcing (i.e. how the boundary layer adjusts to changes in latent and sensible heat fluxes), or how moist convection responds to boundary layer conditions (i.e. the relationship between the stability of the boundary layer and the timing and initiation of moist convection). Their tests show that the diurnal evolution of moist static energy in the boundary layer is largely independent of soil moisture conditions, and therefore moist convection during the summer is not influenced by surface properties such as soil moisture.

Whatever the cause, our results indicate that coupling between the land surface and the atmosphere is too strong in CCSM3 and too weak in HadCM3. In CCSM3, it is possible that land-atmosphere coupling causes precipitation rates over the Great Plains to respond too strongly to small changes in surface conditions

Interestingly, HadCM3 represents the variability of precipitation over the Great Plains at least as well as the other models, despite the fact that the surface and the atmosphere appear to be fairly decoupled.

6.7 Summary

In this chapter we have attempted to answer the following questions: Do the models simulate long-term drought conditions over the Great Plains and do these droughts occur for the same reasons in the models as they do in the observations? The main conclusions are as follows.

- In all of the simulations, the Great Plains region experiences at least one long-term drought period during the 20th century. Simulated droughts persist for similar periods of time as was observed and typically extend for 7-11 years.
- There is a tendency for CM 2.0 to under-represent how frequently long-term droughts occur over the Great Plains during the 20th century, with only 1-2 long-term droughts occurring in each integration performed by this model. Deep soils act as a long-term reserve for warm season precipitation anomalies and act to increase the month to month memory in soil moisture concentrations. Also, deep soil moisture stores have been shown to contribute to the persistence of drought conditions over the Great Plains during consecutive wet season. Since the reservoir for soil moisture is small in CM 2.0 (total column soil moisture content only averages ~120 mm, see Chapter 4), it is possible that there is not enough memory in the deep soils to influence precipitation rates from year to year.

- The spatial patterns of long-term drought are similar between the simulations and observations. In CM 2.0 and HadCM3, the southern part of the Great Plains is mostly heavily impacted by negative precipitation anomalies which is one indication that the tropical Pacific may influence Great Plains drought in the model.
- Dry conditions over the Great Plains are typically associated with an anomalous upper level anti-cyclone, subsidence, strong surface heating, anomalous moisture flux divergence out of the region, reduced soil moisture concentrations, and low evapotranspiration rates. Low evaporation and strong surface heating at the surface will help enhance the upper level anti-cyclone by expanding the column of air above the Great Plains and increasing the upper level geopotential height anomalies. These interactions help perpetuate the atmospheric anomalies associated with drought conditions.
- Dry conditions over the Great Plains in the observations are generally associated anomalously offshore flow near the Gulf of Mexico which reduces the amount of moisture that is fluxed into the region. This is generally not the case in CM 2.0 & CCSM3 but does hold true for HadCM3.
- In the observations, cool La Niña-like conditions in the tropical Pacific are associated with long-term drought conditions over the Great Plains, and may be one of the primary driving mechanisms that cause dry conditions to persist. In both CM 2.0 and HadCM3, all of long-term drought periods simulated by these models have also been shown to be associated with cool conditions in the tropical Pacific. In CCSM3, on the other hand, there appears to be no systematic relationship between SST anomalies

in the tropical Pacific and Great Plains drought. Both both warm and cool conditions in the equatorial Pacific have been found to occur during long-term Great Plains drought simulated in CCSM3. This may in part be due to the fact that the relationship between ENSO and Great Plains precipitation is minimal at best in this model. Other factors such as position of the Bermuda High, and interactions between the land surface and the atmosphere may be causing long-term droughts in this model.

- Feedbacks between the land surface and the atmosphere have been shown to be an important component in long-term droughts. Soil moisture - rainfall feedbacks can cause precipitation anomalies to lock into place over the Great Plains region. The land surface and the atmosphere are strongly coupled in CCSM3 and CM2.0, but HadCM3 shows a distinct lack of coupling between these two reservoirs. Although precipitation and evapotranspiration are excessively correlated with each other in CCSM3, there is little relationship between precipitation and soil moisture so the question still remains, if precipitation does not really impact soil moisture, can soil moisture anomalies act as a bridging mechanism between winter and summer precipitation anomalies?

Overall, the models all exhibit different strengths and weaknesses when it comes to simulating drought conditions over Great Plains. For example, in HadCM3 and CCSM3 the frequency of occurrence of long-term drought conditions, the intensity of the simulated droughts, and the spatial patterns associated with the droughts are similar to the observations. CM 2.0 tends to underestimate how frequently long-term drought conditions occurred over the Great Plains, but the intensity and the spatial patterns of the

droughts simulated by this model are also similar to the observations. While CM 2.0 and HadCM3 both show some indication that cool conditions in the tropical Pacific may influence Great Plains drought, there is no systematic relationship between tropical Pacific SST variability and drought in CCSM3. Both HadCM3 and CCSM3 have trouble representing the coupling that occurs between the land surface and the atmosphere. While CCSM3 greatly overestimates the coupling between these two reservoirs, HadCM3 tends to underestimate land-atmosphere coupling. It has yet to be determined what impact this has on long-term drought.

The varied strengths and weaknesses of these models causes their simulated representations of Great plains drought to be different. We argue that CM 2.0 and HadCM3 are better suited for studies involving the future of drought over the Great Plains region. Both of these models exhibit fewer problems representing the hydrology of the Great Plains than CCSM3.

Chapter 7

Conclusions

The Great Plains region of the United States was influenced by a number of multi-year droughts during the twentieth century. Most notable were the "Dust Bowl" drought of the 1930s and the Great Plains drought of the 1950s. In this study we evaluate the ability of three of the Coupled Global Climate Models (CGCMs) used in the Fourth Assessment Report (AR4) of the IPCC to simulate Great Plains droughts with the same frequency and intensity as was observed during the twentieth century. The models chosen for this study are: GFDL CM 2.0, NCAR CCSM3, and UKMO HadCM3. Results from this study are intended to help assess whether or not these climate models are credible for use in the assessment of future drought over the Great Plains region of the United States.

- The models capture the climatology of the hydrologic cycle of the Great Plains with reasonable fidelity. Both CM 2.0 and HadCM3 do a good job capturing the timing of the seasonal cycle of precipitation, although the amplitude is somewhat overestimated in each model. CCSM3 has some difficulty representing the seasonal cycle of precipitation. In this model, precipitation exhibits a large, unrealistic decrease from July to August which suggests that the mechanisms that

maintain Great Plains precipitation into the late summer are not present in CCSM3.

- Total Column Soil Moisture content differs significantly between the three models and from the VIC soil moisture model. It has proven difficult to determine the actual cause of these differences, but possible explanations include: differences in the depth of the soil column being considered, differences in the hydraulic properties of the soils including texture and porosity, and differences in the root-depths of the vegetation in the Great Plains region. These parameters are prescribed as input to the models.
- In general, all the models overestimate the variability in annual mean Great Plains precipitation, but this is especially true for CM 2.0. Precipitation anomalies tend to be more extreme in the models than the observations.
- Although persistent dry periods do occur in each simulation, simple probability tests indicate that it is possible for these persisted dry periods to occur by chance. This implies that external forcing mechanisms and internal feedback processes may not be required for long-lasting dry events to occur in the models.
- In all simulations of the climate of the 20th century, the Great Plains region experiences at least one long-term drought period. Typically, the spatial and temporal extent of the simulated droughts are similar to the observed droughts of the twentieth century. In both the models and the observations, dry conditions over the Great Plains are often associated with an upper level anticyclone, strong surface warming, large-scale moisture flux divergence, and reduced soil moisture

concentrations.

- Tropical Pacific SST variability may drive persistent droughts over the Great Plains region in CM 2.0 and HadCM3. In both of these models, long-term droughts are associated with cool, La Niña-like conditions in the tropical Pacific. The connection between tropical Pacific SST variability and Great Plains drought is much less obvious in CCSM3; where both cool and warm conditions in the tropical Pacific are associated with drought in this model.
- Strong coupling between the land surface and the atmosphere is found in CCSM3. Most of the Great Plains precipitation that falls to the surface in this model is immediately re-evaporated into the atmosphere. It is possible that, in the model, feedbacks between the land surface and the atmosphere dominate the drought signal over the Great Plains. In HadCM3, on the other hand, the land surface and the atmosphere appeared to be fairly decoupled. It is possible that land-atmosphere feedbacks do not play a significant role in the persistence of Great Plains drought in HadCM3.

We have shown that models all have some difficulty representing the observed variability of Great Plains precipitation, especially when it comes to simulating long-term Great Plains drought. Given that only three long-term droughts occurred during the twentieth century, it is difficult to determine statistically if the models simulate long-term drought with the same frequency as observed. That being said, our analysis suggests that

CM 2.0 is best suited for studies involving the future of drought over the Great Plains region than CCSM3 and HadCM3. CM 2.0 and HadCM3 better represent the climatology and variability of Great Plains precipitation than CCSM3. Also, in CM 2.0, long-term Great Plains drought seem to happen through mechanisms similar to those observed. These mechanisms include both the external forcing from tropical Pacific SST variability and local feedbacks between the land surface and the atmosphere. In CCSM3, on the other hand, the land surface and the atmosphere appear to be coupled to an excessive degree, and the role of tropical Pacific SST variability in Great Plains drought in not yet apparent.

The models are extremely complex and represent many important aspects of the climate system, which is even more complex. Determining why the models represent Great Plains precipitation variability in different ways has been a daunting task that has required me to delve into model documentation, model center technical notes, and even at times source code that has been provided by the modeling groups. After all of this work, I still do not have a clear understanding of why these models are so different. Some problems, such as trying to understand the differences between precipitation parameterizations in these models and how those differences might influence Great Plains precipitation, were always well out of my reach. Even seemingly simple problems such as trying to understand why total column soil moisture content varies between the models were almost impossible to solve because variables like soil moisture depend on everything else in the model. While investigating this issue I often faced the problem that it was difficult to determine exactly how land surface parameters such as soil type and

texture are prescribed in the models. Model documentation often references archaic data archives for vegetation and soil types that were created in the early 1980s.

Despite these difficulties, I have compiled a list of things I believe could be updated or changed in the models to help improve their representation of long-term drought over the Great Plains. My suggestions are as follows:

- In large-scale models such as these, boundary-layer processes are often poorly represented. This can lead to problems involving the timing and the initiation of convection. To improve simulated precipitation over the Great Plains, the relationships between surface moisture conditions, evapotranspiration, and the buildup of moist static energy in the lowest layer of the atmosphere need to be better parameterized. Also, enhancing the vertical resolution of the model may help to better represent boundary layer processes. Overall, coupling of the boundary layer to precipitation processes needs to be improved.
- GCMs have difficulty representing the variations of precipitation intensity. Improving precipitation parameterizations, in general, will help the models to better represent the seasonal cycle and variability of Great Plains precipitation.
- In the real world, during extreme dry conditions (without the help of irrigation) vegetation will often dry up and turn brown. In the most severe cases, vegetation may die altogether and leave behind only bare soil. Dry, dead vegetation, and bare soils have different radiative properties from green, healthy vegetation. Also, dead vegetation does not pump water out of the surface. Vegetation state can play an important role in influencing Great Plains precipitation, and may cause

droughts to persist for longer periods of time. Currently, surface parameters such as vegetation type and albedo are prescribed in the models, and no matter how dry it gets over the Great Plains, the vegetation will remain radiatively healthy and green. Allowing vegetation to react to changes in weather and climate conditions may improve the representation of drought in the models.

- As mentioned previously, the "Dust Bowl" drought of the 1930s was so named after the severe dust storms that characterized the central plains during this time period. Studies have shown that enhanced atmospheric dust concentrations over the Great Plains region at this time resulted in reductions in net surface radiation which acted to reduce surface evaporation fluxes and thereby led to a negative precipitation feedback (Cook et al., 2008) Including the effects of dust loading during dry periods may enhance the ability of the models to represent long-term Great Plains drought.

Appendix A

ENSO Variability in the Models

In this Appendix we provide an assessment of the ability of the CGCMs to represent the El Niño - Southern Oscillation phenomenon. We are primarily interested in looking at how well the models represent the magnitude of ENSO events and the return period for the positive and negative phases of ENSO. Previous studies by Oldenborgh et al. (2005) and Joseph and Nigam (2006) have also examined ENSO variability in these models, only in more detail. In this section we provide a simple analysis of ENSO that is suitable for our needs.

We use the Niño 3.4 index as our marker for ENSO variability. The domain for the Niño 3.4 index is defined as the area between 5ºS-5ºN, 120ºW-170ºW and is shown in Figure A.1. We chose to use the Niño 3.4 index over other ENSO indices because the Niño 3.4 region is centrally located in the Pacific and so is able to better capture all

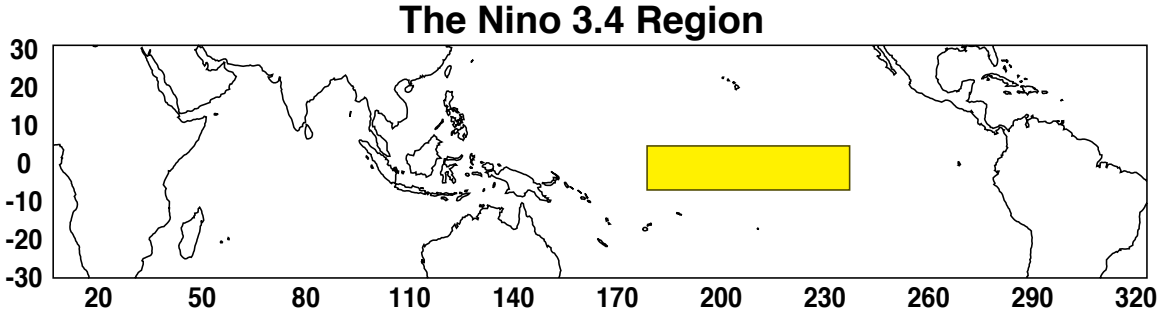


Figure A.1. *The Nino 3.4 region is defined by the area that lies between 5ºS-5ºN and 120ºW - 170ºW). This area is shaded in yellow on the figure.*

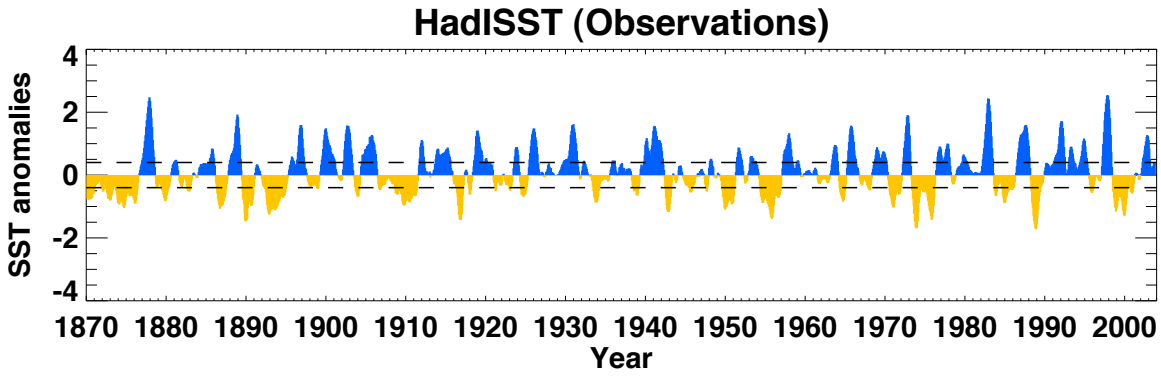


Figure A.2. *Time series of the Nino 3.4 index from the HadISST observational data set.*

ENSO events compared to lets say the Niño 3 region. It also turns out the the Niño 3.4 anomalies are more normally distributed than other SST ENSO indices, such that it is more symmetric and less problematic ENSO index. (Trenberth, 1997; Burgers and Stephenson, 1999; Hannachi et al., 2003; Pezzulli et al., 2005).

We calculate the Niño 3.4 index using the methods outlined in Trenberth (1997). First we average the monthly mean SST values over the Niño 3.4 region of the equatorial Pacific. Then SST anomalies for this region were created by removing the climatology of SST values determined from the base period of 1950-79. Last we apply a five month running average to the time series of SST anomalies. Figure A.2 shows the time series of the Niño 3.4 index calculated with the HadISST observational data set. Positive SST anomalies indicate when ENSO is in its positive phase (blue) while negative SST anomalies indicate when ENSO is in its negative phase (yellow). Dashed lines delineate where the index exceeds ±0.4ºC. An El Niño event is said to occur when the Niño 3.4 index exceeds 0.4ºC for 6 months or longer and a La Niña event is said to occur when the Niño 3.4 index is less than -0.4ºC for six months or longer (Trenberth, 1997). In the

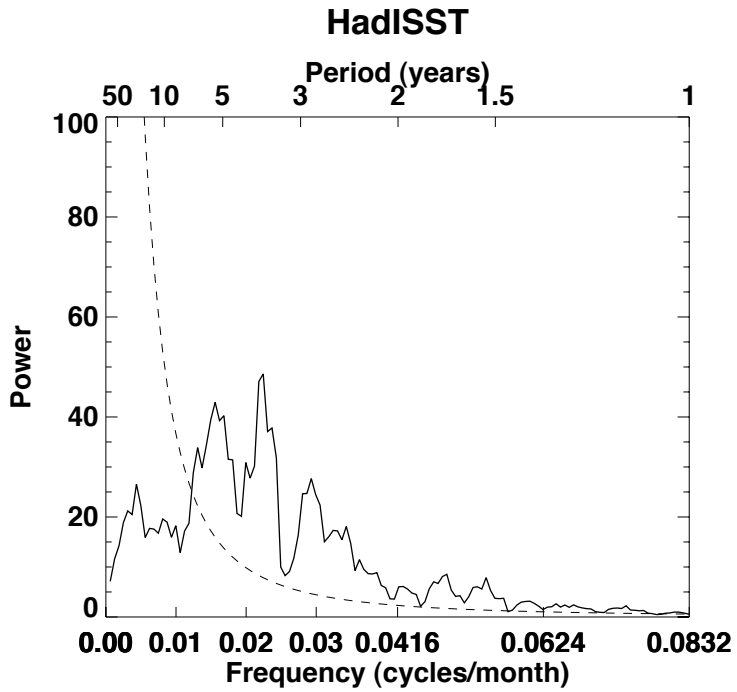


Figure A.3. *Fourier power spectrum of the Nino 3.4 SST index (solid). The dashed line represents the 95% confidence spectrum. Any part of the power spectrum curve that lies above the 95% confidence spectrum exhibit statistically significant power at that frequency or period.*

observational record, which extends from 1870-2003, a total of 30 El Niño events and 25 La Niña events occurred. We can also see from figure two that El Niño events tend to be more extreme than La Niña events (i.e. the Niño 3.4 index tends to be larger for El Niño events than La Niña events).

Figure A.3 shows the Fourier power spectrum of the Niño 3.4 SST index. From this figure we see that most of the power lies within the 2-6 year band. The observed power spectrum exhibits a tri-modal structure with significant peaks at 5.4, 3.7. and 3.8 years indicating enhanced variability at those time periods. This indicates that the return period of ENSO events is on the order of 2-6 years in the observations.

Figures A.4-A.6 show the time series of the Niño 3.4 index calculated from each simulation and Figure A.7 shows the Fourier power spectrums of the simulated Niño 3.4

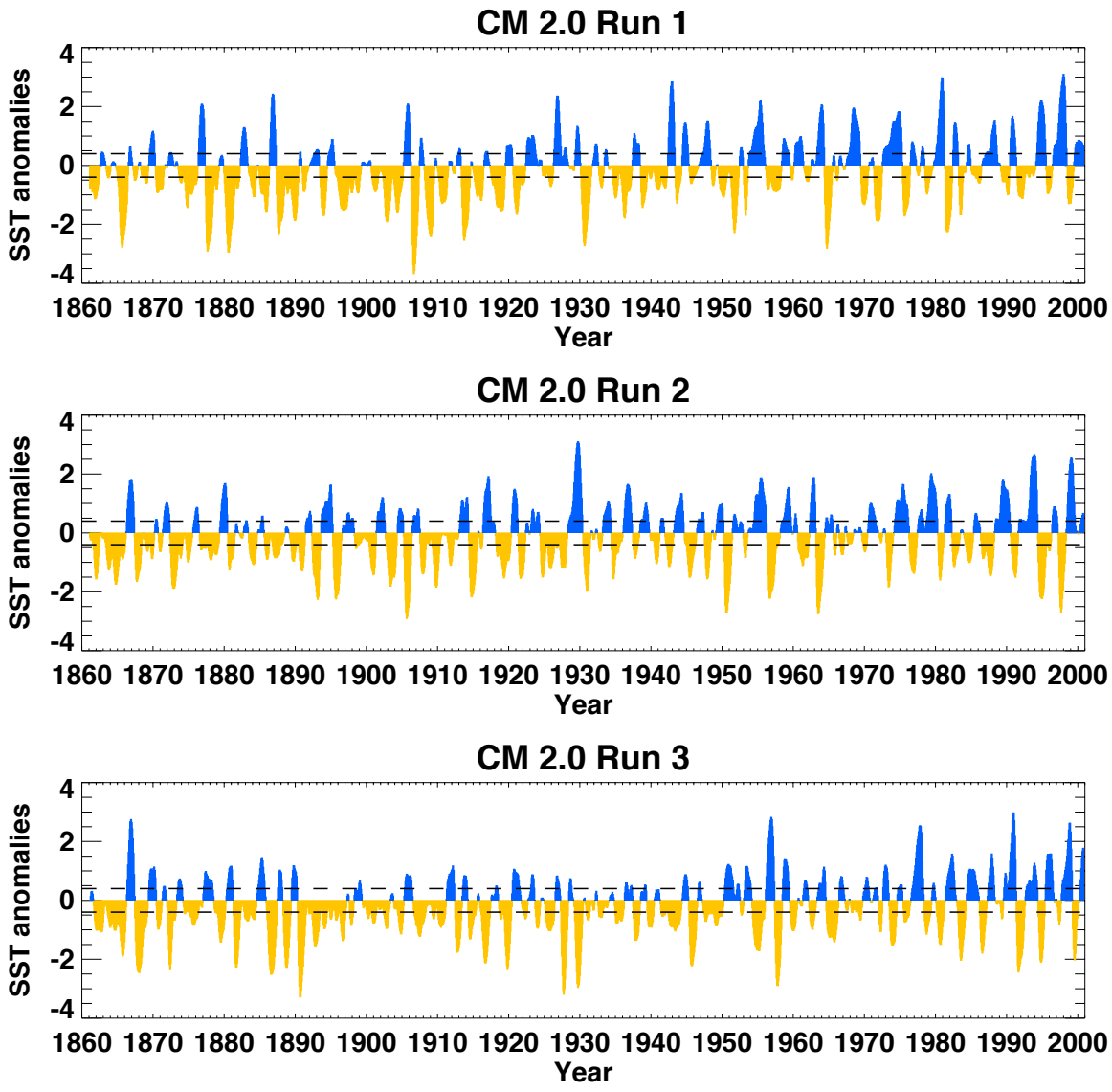


Figure A.4. *Same as Figure A.2, but for CM 2.0*

index time series. From Figure A.4 we see that ENSO events occur too frequently in CM 2.0 and than the SST anomalies associated with each ENSO event tend to be much larger than was observed. The Fourier spectrum diagrams (Figure A.7) from CM 2.0 show us that most of the power lies within the 3.5-2 year band for all three model integrations indicating that the return period for ENSO events is too short in this model.

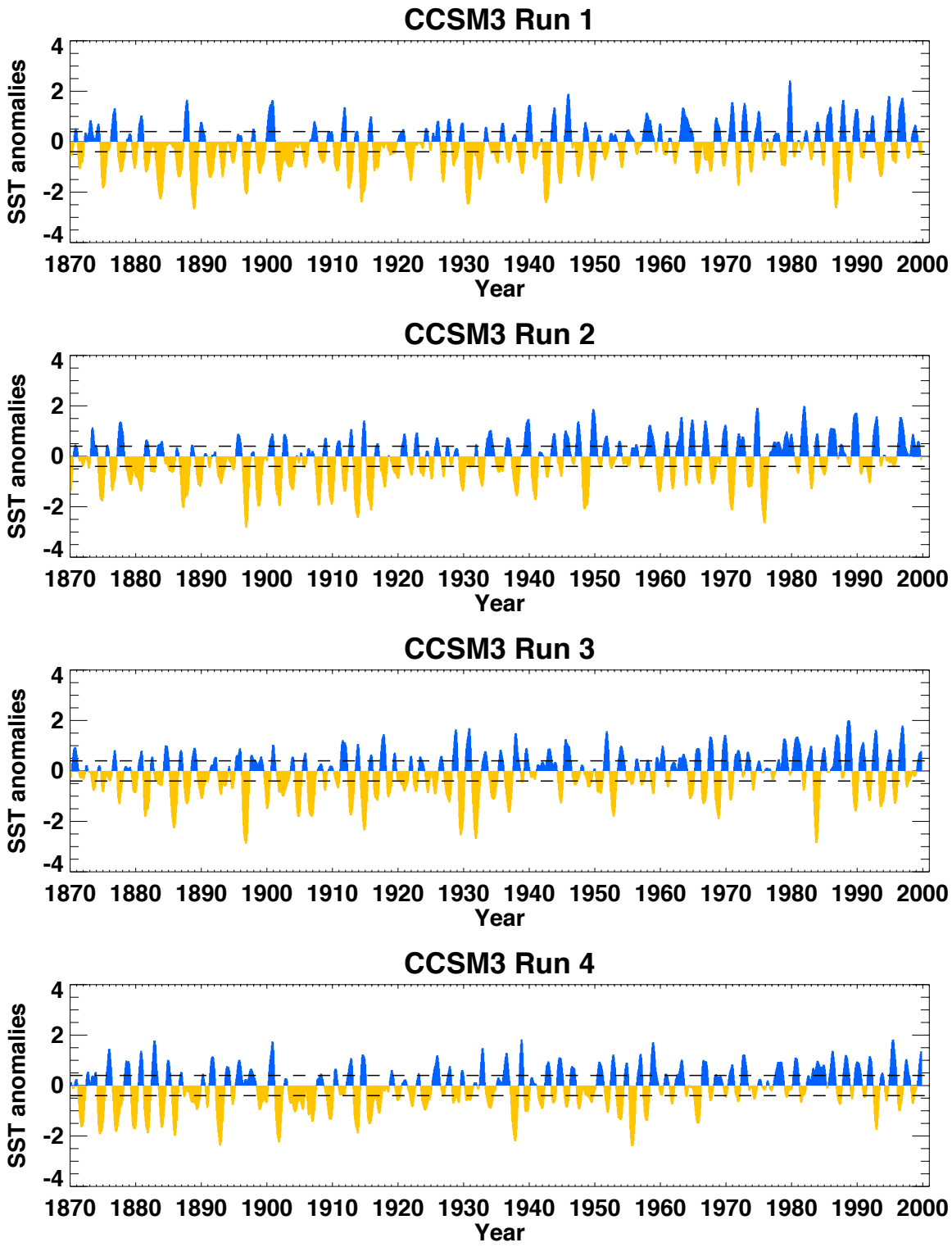


Figure A.5. *Same as Figure A.2, but for CCSM3.*

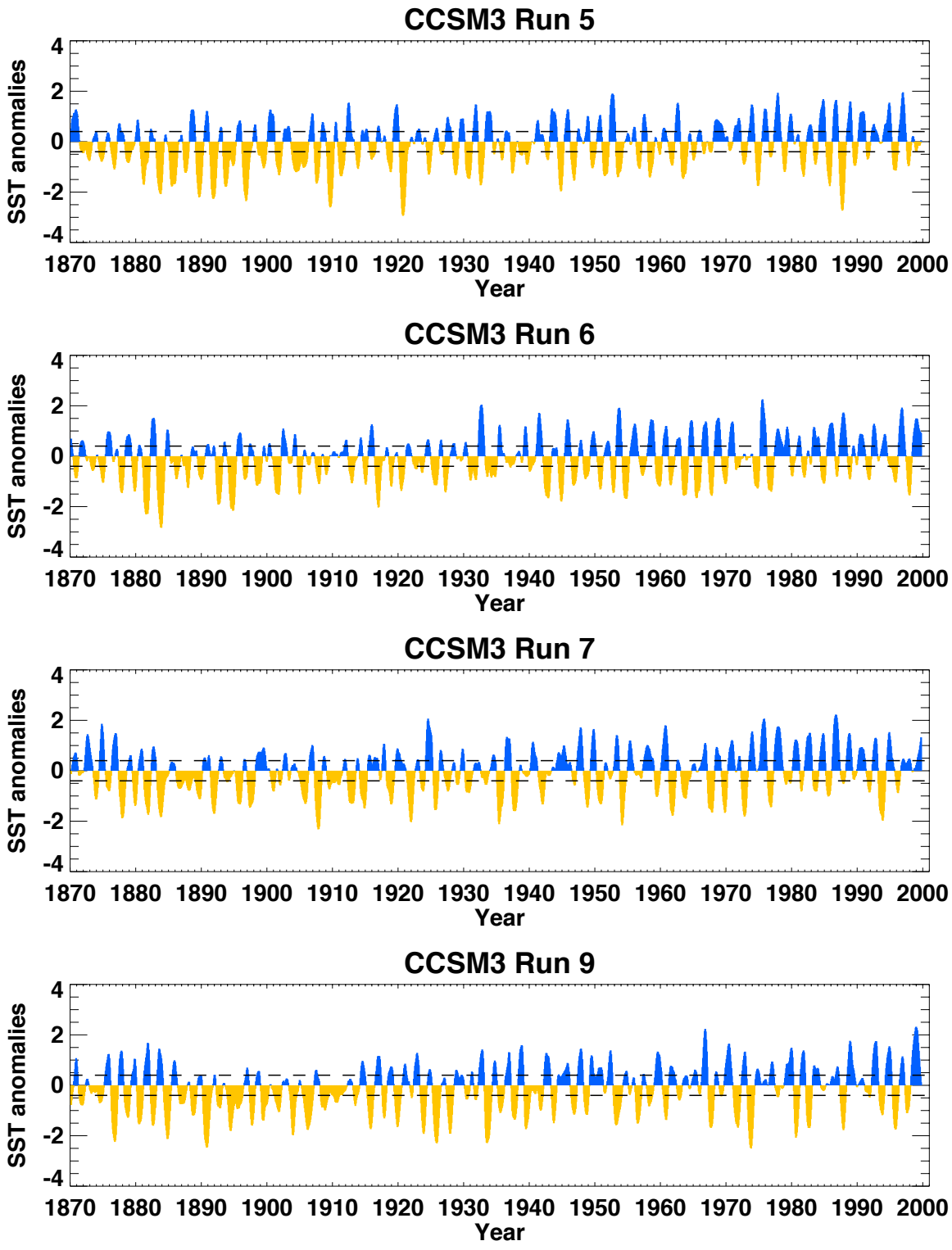


Figure A.5. *continued*

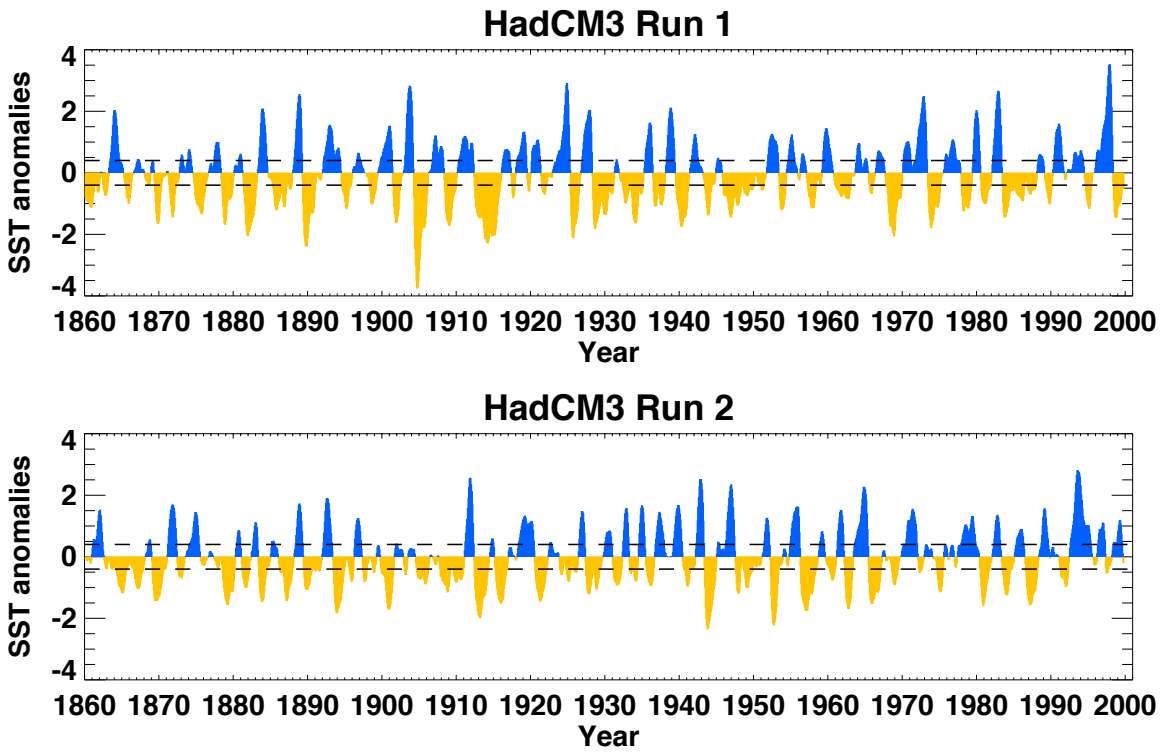


Figure A.6. *Same as Figure A.2, but for HadCM3*

Figure A.5 shows the Niño 3.4 time series for the eight integrations produced with CCSM3. It is readily apparent from this figure that CCSM3 greatly overestimates the frequency and intensity of ENSO events, but especially La Niña events. Most of the power lies within the 3-1.5 year band for all simulations from CCSM3, with a single significant peak occurring at approximately 2 years. These results support the findings from the Niño 3.4 time series figures that CCSM3 greatly overestimates the frequency of strong ENSO events.

From Figure A.6 and the Fourier power spectrum diagrams we see that HadCM3 does the best job capturing the observed variability in ENSO. Although ENSO events do appear to occur too frequently in this model, the time series plots from HadCM3 best capture what is see in the observations. In this model, most of the power lies in the 5-2

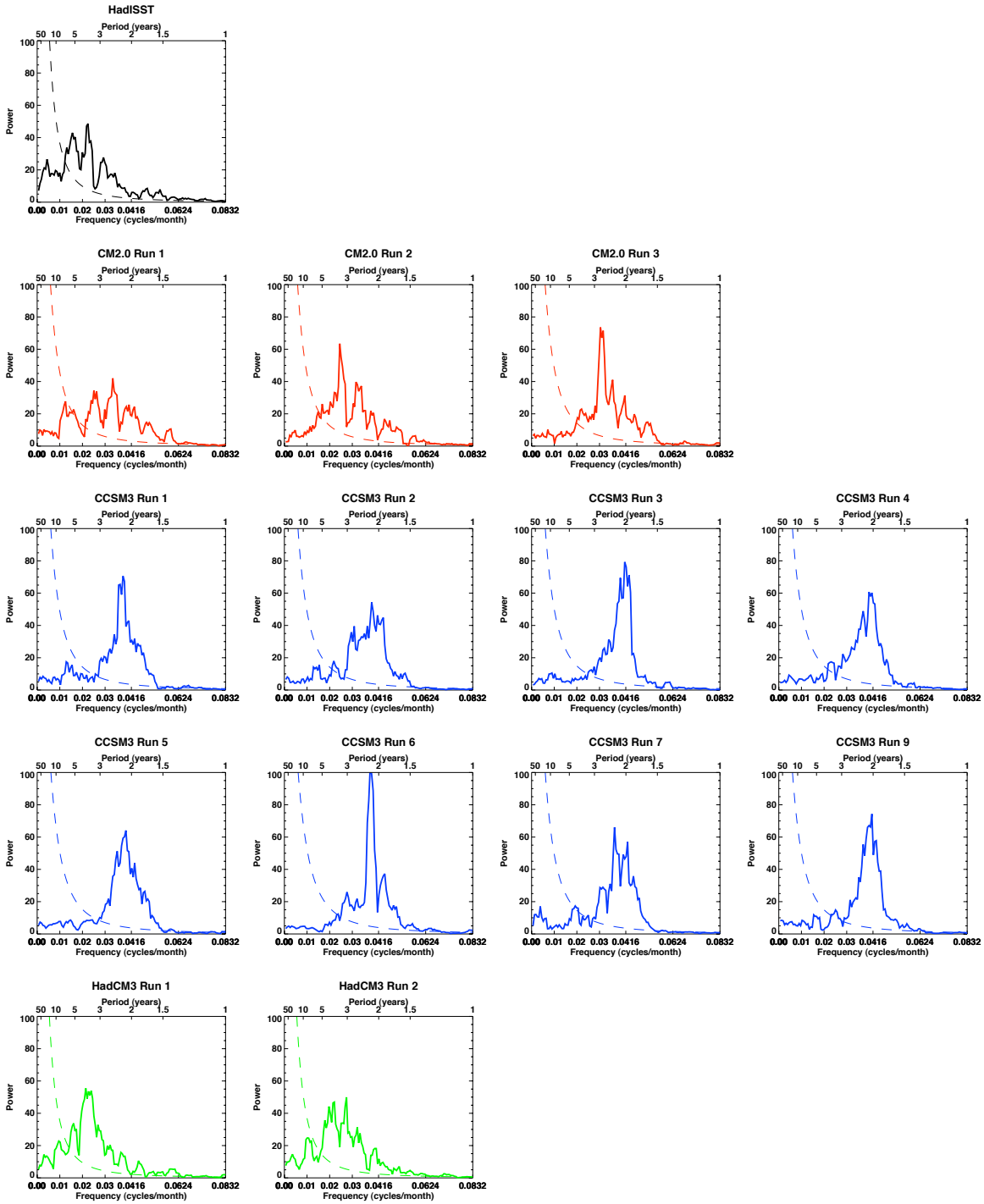


Figure A.7. *Same as Figure A.3, but includes the Fourier power spectrums from CM 2.0 (red), CCSM3 (blue) and HadCM3 (green)*

year band, and the power spectrum exhibits a similar tri-modal pattern as in the observations.

From these results we can conclude that all three models do simulate ENSO, but typically the frequency of occurrence of ENSO events and the magnitude of those events is too extreme in the models. Of the three models, HadCM3 does the best job capturing the observed variability in ENSO while CCSM3 does the worst job.

References

Airey, M. and M. Hulme, 1995: Evaluating climate model simulations of preciptation: Methods, problems and performance. *Prog. Phys. Geog.,* **19**, 427- 448.

Alexander, M. A., I. Blade, M. Newman, J. R. Lazante, N.-C. Lau, and J. D. Scott, 2002: The atmospheric bridge: The influence of ENSO on air–sea interaction over the global oceans. *J. Climate,* **15,** 2205–2231.

Andreadis, K. M., E. A. Clark, A. W. Wood, A. F. Hamlet, and D. P. Lettenmaier, 2005: Twentieth-Century Drought in the Conterminous United States. *J. Hydrometeor*., **6**, 985-1001.

Arakawa, A. and W. H. Schubert, 1974: Interaction of a Cumulus Cloud Ensemble with Large-Scale Environment. *J. Atmo. Sci.*, **31**, 674-701.

Benson, L. K., K. Petersen, and J. Stein, 2007: Anasazi (pre-Columbian Native American) migrations during the middle 12th and late-13th century, where they drought induced? *Climatic Change*, **83**, 187-213.

Beven, K. J., and M. J. Kirkby, 1979: A physically based variable contributing area model of basin hydrology. *Hydrol. Sci. Bull.,* **24,** 43–69.

Bonan, G. B., K. W. Oleson, M. Vertenstein, and S. Levis, 2002a: The Land Surface Climatology of the Community Land Model Coupled to the NCAR Community Climate Model. *J. Climate*, **15**, 3123-3149.

Bonan, G.B., S. Levis, L. Kergoat, and K. W. Olsen, 2002b: Landscapes and patches of plant functional types: An integrating concept for climate and ecosystem models. *Global Biogeo. Cycles*, **16**, 5.1-5.18.

Bonner, W.D., 1968: Climatology of the Low Level Jet. *Mon. Wea. Rev*., **96**, 833-850.

Borchert, J. R., 1950: The climate of the central North American grassland. *Ann. Assoc. Amer. Geogr.,* **40,** 1–39.

Borchert, J. R., 1971: The dust bowl in the 1970s. *Ann. Assoc. Amer. Geogr.,* **61,** 1–22.

Boville, B.A., and C.S. Bretherton, 2003: Heating and kinetic energy dissipation in the NCAR Community Atmosphere Model. *J. Climate*, **16**, 3877-3887.

Bradley, R. S., and P. D. Jones (Eds), 1992: Climate Since 1500. Routledge, London, 693 pp.

Bretherton, C. S., M. Widmann, and V. P. Dymnikov, 1999: The Effective Number of Spatial Degrees of Freedom of a Time-Varying Field. *J. Climate*, **12**, 1990-2009.

Brubaker, K. L., D. Entekhabi, and P. S. Eagleson, 1993: Estimation of Continental Precipitation Recycling. *J. Climate*, **6**, 1077-1089.

Brubaker, K. L., and D. Entekhabi, 1996: Analysis of feedback mechanisms in land - atmosphere interaction. *Water. Res. Research*, **32**, 1343-1357.

Bryson, R. A., 1966: Air masses, streamlines, and the boreal forest. *Geogr. Bull.,* **8,** 228 - 269.

Bryson, R. A., and F. K. Hare, 1974: *The Climates of North America.* Vol.II, *World Survey of Climate,* Elsevier, 420 pp.

Charney, J., 1975: Dynamics of deserts and droughts in the Sahel, *Q. J. R.Meteorol. Soc*., **101**, 193 - 202.

Charney, J. G., W. J. Quirk, S. H. Chow, and J. Kornfield, 1977: A comparative study of the effects of albedo change on drought in semi-arid regions. *J. Atmos. Sci.,* **34,** 1366 - 1385.

Cherkauer, K. A., and D. P. Lettenmaier, 2003: Simulation of spatial variability in snow and frozen soil. *J. Geophys. Res.,* **108,** 8858, doi:10.1029/2003JD003575.

Collins, W. D., 2001: Parameterization of generalized cloud overlap for radiative calculations in general circulation models. *J. Atmos. Sci.*, **58**, 3224-3242.

Collins, W. D., and Coauthors, 2004: Description of the NCAR Community Atmosphere Model (CAM3). Tech. Rep. NCAR/TN-464 STR, National Center for Atmospheric Research, Boulder, CO, 226 pp.

Collins, W. D., and Coauthors, 2006a: The formulation and atmospheric simulation of the Community Atmosphere Model version 3 (CAM3). *J. Climate,* **19,** 2144–2161.

Collins, W. D., and Coauthors, 2006b: The Community Climate System Model Version 3 (CCSM3). 19, J. Climate, 2122-2143.

Cook, E. R., D. M. Meko, D. W. Stahle, and M. K. Cleaveland, 1999: Drought reconstructions for the continental United States. *J. Climate*, **12**, 1145-1162.

Cook, E.R., C. A. Woodhouse, C. M. Eakin, D. M. Meko, D. W. Stahle, 2004: Long-term aridity changes in the western United States. *Science,* **306**, 1015–1018.

Cook, E. R., R. Seager, M. A. Cane, D. W. Stahle, 2007: North American drought: Reconstruction, causes, and consequences. *Earth-Science Rev.*, **81**, 93-132

Cook, B. I., R. L. Miller, and R. Seager, 2008: Dust and sea surface temperature forcing of 1930s "Dust Bowl" drought. *Geophys. Res. Lett.*, **35**,

Cox, P. M., C. Huntingford, and R. J. Harding, 1998: A canopy conductance and photosynthesis model for use in a GCM land surface scheme. *J. Hydrology*, **212**, 79-94.

Cox, P. M., R. A. Betts, C. B. Bunton, R. L. H. Essery, P. R. Rowntree. and J. Smith, 1999: The impact of new land surface physics on the GCM simulation of climate and climate sensitivity. *Climate Dynamics*, **15**, 183-203.

Danabasoglu, G., Large, W., Tribbia, J., Gent, P. and Briegleb, B., 2005: Diurnal ocean-atmosphere coupling, *J. of Climate,* **18**.

Delworth, T. L, and Coauthors, 2006: GFDL's CM2 Global Coupled Climate Models. Part I: Formulation and Simulation Characteristics. *J. Climate*, **19**, 643-674.

DeMott, C. A., D. A. Randall, and M. Khairoutdinov, 2007: Convective Precipitation Variability as a Tool for General Circulation Model Analysis. *J. Climate*, **20**, 91-112.

Dirmeyer, P. A., A. J. Dolman, and N. Sato, 1999: The pilot phase of the global soil wetness project, *Bull. Am. Meteorol. Soc*., **80**, 851-878.

Doesken, N. J., and W. P. Stanton, 1991: Colorado: Floods and droughts. National Water Summary, 1988–89—Floods and droughts: Hydrologic perspectives on water issues. USGS Water-Supply Paper 2375, 591 pp. [Available from USGS Information Services, Box 25286, Denver Federal Center, Denver, CO 80225.]

Eagan, T., 2006: The Worst Hard Time. Houghton Miffin Company, New York, New York, USA., 340 pp.

Edwards J. M. and A. Slingo, 1996: Studies with a flexible new radiation code. I: choosing a configuration for a large-scale model. *Q. J. R. Meteorol. Soc.*, **122**: 689-719.

Eltahir, E. A., 1998: A soil moisture-rainfall feedback mechanism 1. Theory and observations. *Water Resour. Res.*, **34**, 765-776.

Entekhabi, D., I. Rodriguez-Iturbe, and F. Castelli, 1996: Mutual interaction of soil moisture state and atmospheric processes. *J. Hydrology*, **184**, 3-17.

Freidenreich, S. M., and V. Ramaswamy, 2005: Refinement of the Geophysical Fluid Dynamics Laboratory solar benchmark computations and an improved parameterization for climate models. *J. Geophys. Res.*, **110**, D17105, doi: 10.1029/2004JD005471.

Fritts, H. C., 1991: Reconstructing Large-Scale Climatic Patterns from Tree-Right Data. *University of Arizona Press*, Tucson, AZ. 286 pp.

Fye, F., D.W. Stahle, and E.R.Cook, 2003: Paleoclimatic analogs to 20th century moisture regimes across the USA. *Bull. Amer. Meteor. Soc.*, **84**, 901–909.

Gent P. and J.C. McWilliams, 1990: Isopycnal mixing in ocean circulation models. *J. Phys. Oceanogr.* **20**: 150-155.

Georgakakos, K. P, and D. E. Smith, 2001: Soil moisture tendencies into the next century for the conterminous United States. *J. Geophys. Res.*, **106**, 27367-27382.

GFDL GAMDT, 2004: The new GFDL global atmosphere and land model AM2-LM2: Evaluation with prescribed SST simulations, *J. Climate*, **17**, 4641-4673.

Gordon, C., C. Cooper, C. A. Senior, H. Banks, J. M. Gregory, T. C. Johns, J. F. B. Mitchell, and R. A. Wood, 2000: The simulation of SST, sea ice extens and ocean heat transport in a version of the Hadnly Centre coupled model without flux adjustments. *Climate Dynamics,* **16**, 147-168.

Gregory, D. and D. Morris, 1996: The sensitivity of climate simulations to the specification of mixed phase clouds. *Clim. Dyn.,* **12**, 641-651.

Gregory D. and P. R. Rowntree,1990: A mass Flux convection scheme with representation of cloud ensemble characteristics and stability dependent closure. *Mon. Weather. Rev.,* **118**, 1483-1506.

Gregory D., R. Kershaw, and P. M. Inness, 1997: Parametrization of momentum transport by convection. II: tests in single-column and general circulation models. *Q. J. R. Meteorol. Soc.,* **123**, 1153-1183.

Griffies, S. M., 1998: The Gent-McWilliams skew flux. *Journal of Physical Oceanography,* **28**, 831-841.

Griffies, S. M. , A. Gnanadesikan, R. C. Pacanowski, V. D. Larichev, J. K. Dukowicz, R. D. Smith,1998: Isoneutral diffusion in a z-coordinate ocean model. *J. Phys. Oceanogr*. **28**: 805-830.

Griffies, S. M., 2003: An introduction to ocean climate modeling. In *Global Climate*, Rodó, X., and F. A. Comín, eds., Berlin: Springer-Verlag, 55-79.

Griffies, S. M., M. J. Harrison, R. C. Pacanowski, and A. Rosati, 2004: A Technical Guide to MOM4, NOAA/Geophysical Fluid Dynamics Laboratory, Princeton, USA, 337 pp.

Griffies, S.M., A. Gnanadesikan, K.W. Dixon, J.P. Dunne, R. Gerdes, M.J. Harrison, I.M. Held, A. Rosati, J. Russell, B.L. Samuels, M.J. Spelman, M. Winton, and R. Zhang, 2005: Formulation of an ocean model for global climate simulations, *Ocean Sci.,* **1**, 45-79.

Guttman, N.B., 1999: Accepting the Standardized Precipitation Index: A calculation algorithm. *Journal of the American Water Resources Association*, **35**, 311-322.

Hack, J. J., 1994: Parameterization of moist convection in the National Center for Atmospheric Research Community Climate Model (CCM2), *J. Geophys. Res*., **99**, 5551-5568.

Heim, R. R., Jr., 2002: A Review of Twentieth-Century Drought Indices Used in the United States. *Bull. Amer. Meteor. Soc.*, **83**, 1149-1165.

Helfand, H. M., and S. D. Schubert, 1995: Climatology of the simulated Great Plains low-level jet and its contribution to the moisture budget of the United States. *J. Climate,* **8,** 784–806.

Herweijer, C., R. Seager, E. R. Cook, 2006: North American droughts of the mid to late nineteenth century: a history, simulation and implication for Medieval drought. *The Holocene* **16**, 159–171.

Herweijer, C., R. Seager, E. R. Cook, and J. Emile-Geay, 2007: North American Droughts of the Last Millennium from a Gridded Network of Tree-Ring Data. *J. Climate*, **20**, 1353-1376.

Herweijer, C., and R. Seager, 2008: The global footprint of persistent extra-tropical drought in the instrumental era. *Int. J. Climatolo.*, Early View.

Higgins, R. W., Y. Yao, E. S. Yarosh, J. E. Janowiak, and K. C. Mo, 1997: Influence of the Great Plains low-level jet on summertime precipitation and moisture transport over the central United States. *J. Climate,* **10,** 481–507.

Hirschboeck, K. K., 1991: Climate and floods. National Water Summary, 1988–89 Floods and droughts: Hydrologic perspectives on water issues. USGS Water-Supply Paper 2375, 591 pp. [Available from USGS Information Services, Box 25286, Denver Federal Center, Denver, CO 80225.]

Hoerling, M. P., A. Kumar, and M. Zhong, 1997: El Nino, La Nina, and the Nonlinearity of their Teleconnections. *J. Climate*, **10**, 1769-1786.

Hoerling, M. P. and A. Kumar, 2002: Atmospheric Response Patterns Associated with Tropical Forcing. *J. Climate*, **15**, 2184-2203.

Hoerling, M. P. and A. Kumar, 2003: The Perfect Ocean for Drought. *Science*, **31**, 691-694.

Holtslag, A. A. M., and B. A. Boville, 1993: Local versus nonlocal boundary-layer diffusion in a global climate model, *J. Climate*, **6**, 1825-1842.

Holton, J. R., 2004: An Introduction to Dynamic Meterology. *Elsevier Academic Press*, 529 pp.

Holzman, B., 1937: Sources of moisture for precipitation in the United States, *U.S. Dep. Agric. Tech. Bull. 589*, 41 pp.

Horel, J. D., and J. M. Wallace, 1981: Planetary-scale atmospheric phenomena associated with the interannual variability of sea surface temperature in the equatorial Pacific. *Mon. Wea. Rev.,* **109,** 813–829.

Horton, R. E., 1943: Hydrologic interrelations between lands and oceans, *Eos Trans. AGU*, *24*, 753 - 764.

Hoskins, B. J. and D. J. Karoly, 1981: the Steady Linear Response of a Spherical Atmosphere to Thermal and Orographic Forcing. *J. Atmos. Sci.*, **38**, 1179-1196.

Hostetler, S. W., 1994: Hydrologic and Atmospheric Models - The (Continuing) Problem of Discordant Scales. *Climatic Change*, **27**, 345-350.

Huang, J., H. M. Van den Dool, and K. P. Georgakakos, 1996 Analysis of model calculated soil moisture over the United States (1931-1993) and applications to long-range temperature forecasts, *J. Climate*, **9**,1350-1362.

Hughes, M., A. Hall, and R. G. Fovell, 2008: Blocking in areas of complex topography, and its influence on rainfall distribution. *J. Atmos. Sci*., in press.

Hughes, P., 1976: Drought: The land Killer. *American Weather Stories*, U.S. Dept. of Commerce, NOAA-EDS, 77-87.

IPCC, 2007: Climate Change 2007: The Physical Science Basis. Contribution of Working Group I to the Fourth Assessment Report of the Intergovernmental Panel on Climate Change. [Solomon, S., D. Quin, M. Manning, Z. Chen, M. Marquis, K. B. Averyt, M. Tignor and H. L. Miller (eds)]. Cambridge University Press, Cambridge, United Kingdom and New York, NY, USA.

IPCC, 2008: Climate Change and Water. IPCC Technical Paper VI. [Batest, B., Z. W. Kundzewicz, S. Wu and J. Palutikof (eds)]. Cambridge University Press, Cambridge, United Kingdom and New York, NY, USA.

Jensen, J. C., 1935: The relation between surface evaporation from lakes and ponds to precipitation from local thunderstorms in the drought area. *Bull. Am. Meteorol. Soc*., *16*, 142–145.

Jones, T.L, G. M Brown, L. M. Raab, J. L. McVickar, W. G. Spaulding, D. J. Kennett, A. York, and P. L. Walker, 1999: Environmental imperatives reconsidered - Demographic crises in western North America during the Medieval Climatic Anomaly. *Curr. Anthro*., **40**, 137-170.

Joseph, R. and S. Nigam, 2006: ENSO Evolution and Teleconnections in IPCC's Twentieth - Century Climate Simulations: Realistic Representation? *J. Climate*, **19**, 4360-4376.

Kalnay, E., and Coauthors, 1996: The NCEP/NCAR 40-Year Reanalysis Project. *Bull. Amer. Meteor. Soc.,* **77,** 437–471.

Koster, R. D., and Coauthors, 2004: Regions of strong coupling between soil moisture and precipitation. *Science*, **305**, 1138-1140.

Koster, R. D., and Coauthors, 2006a: GLACE: The Global Land-Atmosphere Coupling Experiment. Part I: Overview. *J. Hydrometeor*., **7**, 590-610.

Koster, R. D., and Coauthors, 2006b: GLACE: The Global Land-Atmosphere Coupling Experiment. Part II: Analysis. *J. Hydrometeor*., **7**, 590-610.

Kraus, E. B. and J. S. Turner, 1967: A one dimensional model of the seasonal thermocline II. The general theory and its consequences. *Tellus*, **19**, 98-105

Lawrence, D. M. and J. M. Slingo, 2005: Weak Land-Atmosphere Coupling Strength in HadAM3: The Role of Soil Moisture Variability. *J. Hydrometeor*., **6**, 670-680.

Lawson, M.P. and C. W. Stockton, 1981: Desert myth and climatic reality. *Ann. Assoc. Amer. Geograph.*, **71**, 527-535.

Large, W. G., J. C. McWilliams, and S. C. Doney, 1994: Oceanic Vertical Mixing - A Review and a Model with a Nonlocal Boundary-Layer Parameterization. *Rev. Geophysics*, **32**, 363-403.

Liang, X., D. P. Lettenmaier, E. F. Wood, and S. J. Burges, 1994: A simple hydrologically based model of land surface water and energy fluxes for GSMs. *J. Geophys. Res.,* **99,** 14415–14428.

Liang, X., D. P. Lettenmaier, E. F. Wood, and S. J. Burges, 1996: One-dimensional statistical dynamic representation of subgrid spatial variability of precipitation in the two-layer variable infiltration capacity model. *J. Geophys. Res.,* **101,** 21403 - 21422.

Livesey, R. E., and W. Y. Chen, 1983, Statistical field significance and its determination by Monte Carlo techniques, Mon. Weather Rev., 111, 46 – 59.

Livezey, R., and T. Smith, 1999: Covariability of aspects of North American climate with global sea surface temperatures on interannual to interdecadal timescales. *J. Climate,* **12,** 289 - 302.

Lock, A., R. Brown, M. R. Bush, G. M. Martin, and R. N. B. Smith, 2000: A new boundary layer mixing scheme. Part I: Scheme description and single-column model tests. *Mon. Wea. Rev.,* **128,** 3187–3199.

Matthews, E., 1983, Global vegetation and land use: new high resolution data bases for climate studies. *J. Clim. and App. Met.*, **22**, 474 - 487.

Mattice, W. A., 1935a: Dust storms, November 1933 to May 1934, *Mon. Weather. Rev.*, **63**, 53-55.

Mattice, W. A., 1935b: Dust Storms, *Mon. Weather. Rev*., **63**, 113-115.

Maurer, E. P., A. W. Wood, J. C. Adam, and D. P. Lettenmaier, 2002: A Long-Term Hydrologically Based Dataset of Land Surface Fluxes and States for the Conterminous United States. *J. Climate*, **15**, 3237-3251.

McKee, T.B., N.J. Doesken, and J. Kleist, 1993. The relationship of drought frequency and duration ot time scales. Eighth Conference on Applied Climatology, American Meteorological Society, Jan 17-23, 1993, Anaheim CA, pp. 179-186.

Mock, C. J., 1996: Climate Controls and Spatial Variations in Precipitation in the Western United States. *J. Climate*, **9**, 1111-1125.

Moorthi, S. and M. J. Suarez, 1992: Relaxed Arakawa-Schubert. A Parameterization of Moist Convection for General Circulation Models. *Mon. Wea. Rev.*, **120**, 978-1002.

Meehl, G.A., C. Covy, T. Delworth, M. Latif, B. McAvaney, J. F. B. Mitchell, R. J. Stouffer, and K. E. Taylor, 2007: The WCRP CMIP3 Multimodel Dataset. *Bull. Amer. Meteor. Soc.*, **88**, 1383-1394.

Milly, P.C.D, and A.B. Shmakin, 2002: Global modeling of land water and energy balances, Part I: The land dynamics (LaD) model, *J. Hydromet.*, **3**, 283-299.

Mitchell, K. E., and Coauthors, 2004: The multi-institution North American Land Data Assimilation System (NLDAS): Utilizing multiple GCIP products and partners in a continental distributed hydrological modeling system. *J. Geophys. Res.,* **109,** D07S90, doi:10.1029/2003JD003823.

Mitchell T. D. and P. D. Jones, 2005: An Improved Method of Constructing a Database of Monthly Climate Observations and Associated High-Resolution Grids. *Int. J. Climatol.*, **25**, 693-712.

Namias, J., 1955: Some meteorological aspects of drought with special reference to the summers of 1952–54 over the United States. *Mon. Wea. Rev.,* **83,** 199–205.

Namias, J, 1960: Factors in the Initiation, Perpetuation and Termination of Drought. *Association of Scientific Hydrology Commission on Surface Waters Publication*, **51**, 81-94.

Namias, J., 1983: Some causes of United States drought. *J. Climate Appl. Meteor.,* **22,** 30–39.

National Assessment Synthesis Team, 2001: Climate change impacts on the United States: the potential consequences of climate variability and change. Cambridge University Press, Cambridge, United Kingdom and New York, NY, USA.

New, M., M. Hulme, and P. Jones, 1999: Representing Twentieth-Century Space-Time Climate Variability. Part I: Development of a 1961-90 Mean Monthly Terrestrial Climatology. *J. Climate*, **12**, 829-856.

New, M., M. Hulme, and P. Jones, 2000: Representing Twentieth-Century Space-Time Climate Variability. Part II: Development of 1901-96 Monthly Grids of Terrestrial Surface Climate. *J. Climate*, **13**, 2217-2238.

Oglesby, R. J., and D. J. Erickson III, 1989: Soil moisture and persistence of North American drought. *J. Climate,* **2,** 1362–1380.

Oglesby, R. J., 1991: Springtime soil moisture, natural climatic variability, and North American drought as simulated by the NCAR Community Climate Model 1. *J. Climate*, **4**, 890–897.

Pacanowski, R. C., and S. G. Philander, 1981: Parametrisation of vertical mixing in numerical models of tropical oceans. *J. Phys. Oceanogr.,* **11**, 1443-1451.

Pal, S. J, and E. A. B. Eltahir, 2001: Pathways Relating Soil Moisture Conditions to Future Summer Rainfall within a Model of the Land-Atmosphere System. J. Climate, 14, 1227-1224.

Palmer, W. C., 1965: Meteorological drought. U.S. Department of Commerce, Weather Bureau Res. Paper 45, 58 pp.

Palmer, W.C. 1968: Keeping track of crop moisture conditions, nationwide: The new Crop Moisture Index. *Weatherwise,* **21**,156–161.

Pope, V. D., M. L. Gallani, P. R. Rowntree, and R. A. Stratton, 2000: The impact of new physical parameterizations in the Hadley Centre climate model: HadAM3, *Climate Dynamics,* **16**, 123-146.

Rasmusson, E. M., and T. H. Carpenter, 1983: The relationship between eastern equatorial Pacific sea surface temperature and rainfall over India and Sri Lanka. *Mon. Wea. Rev.,* **110,** 354–384.

Rayner, N. A., D. E. Parker, E. B. Horton, C. K. Folland, L. V. Alexander, D. P. Rowell, E. C. Kent, and A. Kaplan, 2003: Global analyses of SST, sea ice and night marine air temperature since the late nineteenth century. *J. Geophys. Res.,* **108,** 4407, doi:10.1029/2002JD002670.

Roads, J. O., S.-C. Chen, A. K. Guetter, and K. P. Georgakakos,1994: Large-scale aspects of the United States hydrologic cycle, *Bull. Am.Meteorol. Soc.*, **75**, 1589-1610.

Robock, A., K. Y. Vinnikov, G. Srinivasan, J. K. Entin, S. E. Hollinger, N. A. Speranskaya, S. Liu, and A. Namkhai, 2002: The Global Soil Moisture Data Bank. *Bull. Amer. Meteor. Soc,* **81**, 1281-1299.

Ropelewski, C., and M. Halpert, 1986: North American precipitation and temperature patterns associated with El Nino/Southern Oscillation (ENSO). *Mon. Wea. Rev.,* **114,** 2352–2362.

Rotstayn, B., F. Ryan, and J. Katzfey, 2000: A scheme for calculation of the liquid fraction in mixed-phase clouds in large-scale models. *Mon. Wea. Rev.,* **128,** 1070 –1088.

Ruiz-Barradas, A., and S. Nigam, 2006a: Great Plains Hydroclimate Variability: The View from North American Regional Reanalysis. *J. Climate*, **19**, 3004-3010.

Ruiz-Barradas, A., and S. Nigam, 2006b: IPCC's Twentieth-Century Climate Simulations: Varied Representations of North American Hydroclimate Variability. *J. Climate*, **19**, 4041-4058.

Schubert, S. D., M. J. Suarez, P. J. Pegion, R. D. Koster, and J. T. Bacmeister, 2004a: Causes of Long-Term Drought in the U.S. Great Plains. *J. Climate*, **17**, 485-503.

Schubert, S. D., M. J. Suarez, P. J. Pegion, R. D. Koster, and J. T. Bacmeister, 2004b: On the Cause of the 1930s Dust Bowl. *Science*, **303**, 1855-1859.

Schwarzkopf, M. D., and V. Ramaswamy, 2008: Evolution of stratospheric temperature in the 20th Century. *Geophys. Res. Lett.*, **35**, L03705, doi:10.1029/2007GL032489.

Seager, R., N. Harnik, Y. Kushnir, W. Robinson, and J. Miller, 2003: Mechanisms of Hemispherically Symmetric Climate Variability. *J. Climate*, **16**, 2960-2978.

Seager, R., Y. Kushnir, C. Herweijer, N. Naik, and J. Velez, 2005a: Modeling of Tropical Forcing of Persistent Droughts and Pluvials over Western North America: 1856-2000. *J. Climate*, **18**, 4065-4088.

Seager, R., N. Harnik, W. A. Robinson, Y Kushnir, M. Ting, H. -P. Huang and J. Velez, 2005b: Mechanisms of ENSO-forcing of hemispheric symmetric precipitation variability. *Q. J. R. Meteorol. Soc*., 131, 1501-1527.

Seager, R., and Coauthors, 2007a: Model Projections of an Imminent Transition to a More Arid Climate in Southwestern North America. *Science*, **316**, 1181-1184.

Seager, R., 2007b: The Turn of the Century North American Drought: Global Context, Dynamics, and Past Analogs. *J. Climate*, **20**, 5527-5552.

Seager, R., Y. Kushnir, M. Ting, M. Cane, N. Naik, and J. Miller, 2008: Would Advance Knowledge of 1930s SSTs Have Allowed Prediction of the Dust Bowl Drought? *J. Climate*, **21**, 3261-3281.

Shao, Y., and A. Henderson-Sellers, 1996: Validation of soil moisture simulation in landsurface parameterisation schemes with HAPEX data, Global Planet. *Change*, **13**, 11–46, Special Issue.

Smith, R. N. B., 1990: A Scheme for predicting layer clouds and their water content in a general circulation model. *Q. J. R. Meteorol. Soc*. **116**, 435-460.

Smith, R. N. B.,1993: Experience and developments with the layer cloud and boundary layer mixing schemes in the UK Meteorological Office Unified Model. In: Proc ECMWF/GCSS workshop on parametrization of the cloud-topped boundary layer, 8-11 June 1993, ECMWF, Reading, England.

Smith, R. D., and P. R. Gent, 2002: Reference manual for the Parallel Ocean Program (POP), ocean component of the Community Climate System Model (CCSM2.0 and 3.0). Tech. Rep. LA-UR-02-2484, Los Alamos National Laboratory. [Available online at http://www.ccsm.ucar.edu/models/ccsm3.0/pop.]

Stahle, D. W., E. R. Cook, M. K. Cleaveland, M. D. Therrell, D. M. Meko, H. D. Grissino- Mayer, E. Watson, and B .H. Luckman, 2000: Tree-ring data document 16th century megadrought over North America. *Eos* **81**, 121.

Steinbeck, J., 1939: The Grapes of Wrath. Penguin Books Ltd, Harmondsworth, Middlesex, England, 464 pp.

Stockton, C. W. and D. M. Meko, 1975; A long-term history of drought occurrence in western United States as inferred from tree rings. *Weatherwise*, **28**, 244-249.

Tiedtke, M., 1993: Representation of clouds in large-scale models. *Mon. Wea. Rev.,* **121,** 3040 –3061.

Ting, M., and H. Wang, 1997: Summertime U.S. precipitation variability and its relation to Pacific sea surface temperature. *J. Climate,* **10,** 1853–1873.

Trenberth, K. E., and G. W. Branstator, 1992: Issues in Establishing Causes of the 1988 Drought over North America. *J. Climate*, **5**, 159-172.

Trenberth, K. E., 1997: The Definition of El Nino. *Bull. Amer. Meteor. Soc.,* **12**, 2771-2777.

Trenberth, K. E. G. W. Branstator, D. Karoly, A. Kumar, N.-C. Lau, and C. Ropelewski, 1998: Progress during TOGA in understanding and modeling global teleconnections associated with tropical sea surface temperatures. *J. Geophys. Res.,* **103,** 14291 - 14324.

Tsiros, E., E. Kanellou, C. Domenikiotis, and N. R. Dalezios, and van Den Dool, H. M, 1983: A Possible Explanation of the Observed Persistence of Monty Mean Circulation Anomalies, *Mon. Wea. Rev.*, **111**, 539-544.

Vinnikov, K. Y., A. Robock, N. A. Speranskaya, and C. A. Schlosser, 1996: Scales of temporal and spatial variability of midlatitude soil moisture. *J. Geophys. Res*., **101**, 7163-7174.

Visbeck, M., J. Marshall, T., Haine, M. Spall, 1997: On the specification of eddy transfer coefficients in coarse resolution ocean circulation models. *J. Phys. Oceanogr.*, **27** 381-402.

von Storch, H. and F. W. Zwiers, 2001: Statistical analysis in climate research. Cambridge University Press, Cambridge, United Kingdom and New York, NY, USA, 468 pp.

Wallace, J. M. and D. S. Gutzler, 1981: Teleconnections in the Geopotential Height Field during the Northern Hemisphere Winter. *Mon. Wea. Rev.* **109**, 784-812.

Weaver, S. J. and S. Nigam, 2008: Variability of the Great Plains Low-Level Jet: Large-Scale Circulation Context and Hydroclimate Impacts., *J. Climate*, **21**, 1532-1551.

Wilhite, D. A., and M. H. Glantz, 1985: Understanding the Drought Phenomenon: The Role of Definitions. *Water Internat.*, **10**, 11-120.

Wilks, D. S., 1995: Statistical Methods in the Atmospheric Sciences. Academic Press, San Diego, California, USA, 464 pp.

Wilson, M. F., A. Henderson-Sellers, 1985: A Global Archive of Land Cover and Soils Data for use in General Circulation Climate Models. *J. Climatology*, **5**, 119-143.

Woodhouse, C. A., and J. T. Overpeck, 1998: 2000 Years of Drought Variability in the Central United States. *Bull. Amer. Meteor. Soc.*, **79**, 2693-2714.

Wright, D. K., 1997: A new eddy mixing parametrisation and ocean general circulation model. *Int WOCE Newsl,* **26**: 27-29.

Zhang, G. J., and N. A. McFarlane, 1995: Sensitivity of climate simulations to the parameterization of cumulus convection in the Canadian Climate Centre general circulation model, *Atmos. Ocean,* **33**, 407-446.

Zhao, W., and M. A. K. Khalil, 1993: The Relationship between Precipitation and Temperature over the Contiguous United States. *J. Climate*, **6**, 1232-1236.